The tsunami history of southwest Thailand – Recurrence, magnitude and impact of palaeo-tsunamis inferred from onshore deposits

Inaugural-Dissertation

zur

Erlangung des Doktorgrades

der Mathematisch-Naturwissenschaftlichen Fakultät

der Universität zu Köln

vorgelegt von

Dominik Brill

aus Fulda

Köln 2012

Berichterstatter/Gutachter: Prof. Dr. Helmut Brückner

                                Prof. Dr. Olaf Bubenzer

Tag der mündlichen Prüfung: 5. November 2012

Abstract

The Indian Ocean tsunami (IOT) of December 2004 has uncovered a till then widely unacquainted tsunami risk for the west coast of southern Thailand. To limit loss of life and damage due to potential future events, data about the frequency and magnitude of tsunamis in Thailand over a longer time period is needed. Since modern and historical tsunami recording in the Bay of Bengal is limited to the last 300 years, details about the long-term hazard have to be drawn from geological evidence of prehistoric tsunami flooding by (i) identifying new palaeotsunamis, (ii) dating and (iii) correlating spatially distinct evidence, and (iv) establishing the magnitude and the intensity of these events. For this, sediments from near-shore geoarchives in the coastal areas of Phang-nga province and Phuket (Thailand) have been sampled and analysed sedimentologically (granulometry, geochemistry, mineralogy, fauna, sedimentation modelling) and chronologically (optically stimulated luminescence and radiocarbon dating).

Evidence of multiple prehistoric coastal flooding events in the form of allochthonous sand beds was identified in the coastal plain of Ban Bang Sak. The layers are assigned to high-energy events of marine origin, either tsunamis or tropical storms, by means of the sediment characteristics. The distinction between tsunamites and tempestites is mainly based on comparison of the palaeoevent beds with the local deposit of the IOT 2004, which revealed similarities regarding spatial extent and sediment properties. Furthermore, the radiocarbon age of the youngest palaeoevent correlates with contemporaneous tsunami evidence from India and Sumatra. Hence, the youngest event, dated to 500-700 cal BP, is related to a basin-wide tsunami, while several older events that took place between 2000 and 1180 cal BP preliminary are treated as tsunami candidates.

Since the application of radiocarbon for dating tsunamites on Phra Thong Island is limited by the scarcity of datable macro-remains and the contamination by young roots, here, the potential of optical dating (OSL) is evaluated by applying the method to a suite of tsunamigenic and littoral deposits for which independent age control is available. Small aliquots of coarse-grained quartz were used for measurements, and processed statistically by means of appropriate age models. Cross-checking with independent radiocarbon data showed good agreement for littoral deposits and only insignificant residuals of less than 40 years for the poorly bleached deposits of the IOT 2004. These results legitimate the use of OSL to determine ages of palaeotsunamis in the same setting. Therefore, the established luminescence procedure was applied as a tool to correlate the spatially distinct sand sheets of prehistoric tsunamis that are preserved in the swales of Phra Thong's beach-ridge plain. At least three palaeoevents – being 490–550, 925–1035 and 1740–2000 years old – are distinguished and correlated between the swales of Phra Thong (as an indicator for inundation distances), as well as within the Bay of Bengal (as an indicator for the impact areas).

For the interpretation of onshore tsunami deposits in terms of magnitude and impact on coastal systems, the boundary conditions at the time of prehistoric tsunami events have to be taken into ac-

count. Pre-existing sea-level curves for the Malay-Thai Peninsula postulate a mid-Holocene maximum of 1-5 m above present sea level, whereas the exact timing and magnitude of the Holocene highstand in Thailand remained to be defined. By the use of fixed biological and geomorphological sea-level indicators a Holocene maximum of +2.6 m in the south and +1.5-2.0 m in the north of the study area is assessed for c. 5500 years ago. In addition, Holocene changes of palaeogeography and their influence on local tsunami records are studied. While the patterns of palaeotsunamis recorded on Phra Thong and at Ban Bang Sak can be explained by the onset of back-barrier swamp formation, the existence of only one prehistoric tsunami deposit at Pakarang Cape is in conflict with the persistence of a back-reef lagoon, which provided favourable conditions for preservation over millennia.

Although the IOT 2004 had a strong short-term impact on infrastructure, housing, ecosystems and coastal morphology in Thailand, the damaged systems have almost completely recovered after less than 10 years. For prehistoric tsunamis, the long-term impact is assessed based on variations of the sedimentary environments before and after the events. It can be shown that all recorded palaeotsunamis had only insignificant impact on the ecosystems and the geomorphology of Phra Thong Island, Ban Bang Sak and Pakarang Cape.

To deduce transport processes and hydrodynamic parameters of tsunami events from the onshore deposits found at Ban Bang Sak, as an estimate of palaeotsunami magnitude, two different approaches are applied. (i) The maximum offshore sediment source is determined using granulometry, geochemistry, mineralogy, and foraminifera of tsunamites and reference samples from various marine and terrestrial environments. (ii) By means of sedimentation modelling, onshore flow velocities and flow depths of the associated tsunami waves are estimated. The approach is evaluated by means of the IOT 2004, for which modelled flow velocities and onshore flow depths, as well as the deduced sediment source are in good agreement with quotations based on survivor videos and post-tsunami field surveys. For the 500-700 year old predecessor with modelled flow velocities and flow depths of 4.1-5.9 m/s and 7.0 m, respectively, a magnitude similar to the IOT 2004 is reconstructed. The deposits of the three tsunami candidates dated to 1180-2000 cal BP partly indicate source areas equal to the IOT 2004, suggesting events of comparable size, and partly indicate a much shallower sediment source, pointing to a storm origin or tsunamis of a lesser magnitude.

In conclusion, a recurrence interval of 500-600 years for tsunamis in southwest Thailand is estimated on the basis of sedimentary evidence. Since all tsunamis recorded in Thailand are triggered by mega-ruptures of the Sunda Arc with similar magnitude and geometry as the 2004 earthquake, which have not only local but basin-wide impact, the data from Thailand provide valuable information for the assessment of future tsunami risk in other countries around the northern Indian Ocean, as well.

Kurzzusammenfassung

Der Indian Ocean Tsunami (IOT) von Dezember 2004 offenbarte eine bis dahin weitgehend unbekannte Tsunamigefährdung der Westküste Südthailands. Um die Anzahl der Opfer und potentielle Schäden durch zukünftige Tsunamis zu minimieren, ist eine möglichst detaillierte Datengrundlage über die Auftrittshäufigkeit und die Magnitude von Tsunamis in Thailand erforderlich. Da moderne und historische Aufzeichnungen über Tsunamis im Golf von Bengalen auf die letzten 300 Jahre beschränkt sind, müssen Einzelheiten über das längerfristige Gefahrenpotential aus geologischen Befunden abgeleitet werden indem man (i) neue Ereignisse identifiziert, die räumlich isolierten Befunde (ii) datiert und (iii) korreliert, sowie (iv) die Magnitude und die Auswirkung der Ereignisse rekonstruiert. Zu diesem Zweck wurden küstennahe Geoarchive auf Phuket und in der Phang-nga Provinz (Thailand) sondiert und hinsichtlich sedimentologischer (Körnung, Geochemie, Mineralogie, Fauna, Sedimentationsmodelle) und geochronologischer (optisch stimulierte Lumineszenz und Radiokohlenstoffdatierung) Kriterien analysiert.

Anzeiger für prähistorische Überflutungsereignisse in Form allochthoner Sandlagen wurden in der Küstenebene von Ban Bang Sak identifiziert. Diese Ablagerungen werden auf Grundlage ihrer sedimentären Eigenschaften hochenergetischen Überflutungsereignissen marinen Ursprungs, Tsunami oder Sturm, zugeordnet. Die Abgrenzung zwischen Tsunamiten und Tempestiten stützt sich im vorliegenden Fall vorwiegend auf den Vergleich zwischen Paläolagen und der lokalen Ausprägung der IOT 2004 Ablagerungen, wobei Ähnlichkeiten hinsichtlich sedimentärer Eigenschaften und räumlicher Erstreckung festgestellt wurden. Darüber hinaus liegen für das jüngste Vorgängerereignis, das auf 500-700 Jahre BP datiert wurde, zeitgleiche Tsunamibefunde aus Indien und Sumatra vor, weshalb es einem ozeanweiten Tsunami zugeordnet wird, während mehrere ältere Ereignisse, die sich zwischen 2000 und 1180 Jahre BP ereigneten, ohne zusätzliche Argumente zunächst nur als Tsunamikandidaten behandelt werden können.

Da die Anwendbarkeit der ^{14}C-Methode zur Datierung von Tsunamiablagerungen auf der Insel Phra Thong durch die Verfügbarkeit datierbarer Makroreste und durch rezente Durchwurzelung limitiert ist, wurde in diesem Fall das Potential der optischen Datierung (OSL) an Tsunamiablagerungen und Litoralsanden, für die unabhängige Altersdaten vorliegen, evaluiert. Grobkornquartz wurde in kleinen Teilproben gemessen und statistisch mittels geeigneter Altersmodelle ausgewertet. Die Überprüfung mit unabhängigen ^{14}C-Altern ergab eine gute Übereinstimmung für die Litoralsedimente und unwesentliche Residuen von weniger als 40 Jahren für die unvollständig gebleichten IOT 2004 Proben. Auf dieser Grundlage wurde OSL als Instrument zur Korrelation räumlich isolierter Paläotsunamibefunde auf Phra Thong verwendet. Mindestens drei Paläoereignisse – mit Altern von 490-550, 925-1035 und 1740-2000 Jahren – wurden unterschieden und räumlich korreliert, was die Abschätzung von lokalen Überflutungsdistanzen und beckenweiten Einflussradien der zugehörigen Tsunamis ermöglichte.

Für die Interpretation der identifizierten Tsunamiablagerungen hinsichtlich der Magnitude und der Auswirkungen der ablagernden Ereignisse auf die Küste, wurden die Rahmenbedingungen zum Zeitpunkt der prähistorischen Tsunamis berücksichtigt. Bestehende Meeresspiegelkurven postulieren einen holozänen Hochstand von 1-5 m, wobei die exakte Höhe und der exakte Zeitpunkt des Maximums in Thailand unklar bleiben. Auf Grundlage biologischer und geomorphologischer Indikatoren wurde für 5500 Jahre BP ein Meeresspiegelhochstand von +2,6 m im Süden und +1,5-2,0 m im Norden des Untersuchungsgebietes rekonstruiert. Zusätzlich wurden die holozänen Küstenveränderungen und ihr Einfluss auf die Erhaltung von Tsunamibefunden untersucht. Während die Tsunamibefunde, die auf Phra Thong und bei Ban Bang Sak überliefert sind, durch die beginnende Formung von Küstensümpfen erklärt werden können, steht das Vorhandensein von nur einem einzigen Paläotsunamibefund bei Pakarang im Gegensatz zur Langlebigkeit des zugehörigen Geoarchivs.

Obwohl der IOT 2004 in Thailand kurzzeitig enorme Auswirkungen auf Infrastruktur, Gebäude, Ökosysteme und Küstenmorphologie hatte, war die Erholung der betroffenen Systeme nach weniger als 10 Jahren bereits fast vollständig abgeschlossen. Die Langzeitauswirkungen prähistorischer Tsunamis wurden durch den Abgleich der Sedimentationsmilieus direkt vor und nach diesen Ereignissen untersucht. Es zeigt sich, dass alle erhaltenen Paläotsunamis lediglich insignifikanten Einfluss auf die Ökologie und Geomorphologie von Phra Thong, Ban Bang Sak und Pakarang ausübten.

Um Transportprozesse und hydrodynamische Parameter aus Tsunamiablagerungen abzuleiten – als Indikatoren für die Magnitude – wurden zwei unterschiedliche Herangehensweisen gewählt. (i) Das seewärtige Limit der Sedimentaufnahme durch den Tsunami wurde auf Grundlage der granulometrischen, geochemischen, mineralogischen und faunistischen Zusammensetzung der Tsunamite im Vergleich zu marinen und terrestrischen Referenzproben bestimmt. (ii) Mittels Sedimentationsmodellierung wurden die Strömungsgeschwindigkeiten und Fließtiefen der zugehörigen Tsunamiwellen geschätzt. Nach Eichung an Sedimenten des IOT 2004, konnte im Falle eines 500-700 Jahre alten Vorgängerereignisses mit modellierten Fließgeschwindigkeiten und -tiefen von 4,1-5,9 m/s und 7,0 m auf eine vergleichbare Magnitude wie 2004 geschlossen werden. Für drei auf 1180-2000 Jahre BP datierte Tsunamikandidaten ergaben sich teilweise ähnliche Sedimentquellen wie für den IOT 2004, was auf ähnliche Magnituden der Ereignisse hindeutet, und teilweise deutlich flachere Herkunftsgebiete, die sich eher durch Stürme oder Tsunamis mit geringerer Magnitude als 2004 erklären lassen.

Auf Basis der sedimentären Befunde wurde ein Wiederkehrintervall von 500-600 Jahren für Tsunamis in Südwestthailand ermittelt. Da alle in Thailand zu findenden Tsunamiablagerungen auf Tsunamis zurückgehen, die durch Erdbeben mit vergleichbarer Magnitude und Geometrie wie 2004 erzeugt wurden und deshalb ozeanweite Auswirkungen hatten, liefern die Daten aus Thailand auch wichtige Informationen bezüglich des langfristigen Tsunamirisikos in anderen Anrainerstaaten des Indischen Ozeans.

Acknowledgements

Table of Contents

List of Figures

List of Tables

Chapter 1

1 Introduction

1.1 The roll of palaeotsunami research for the assessment of coastal risk

Extreme geological, climatic and hydrologic events caused large numbers of casualties and frequently devastated human infrastructure during the past thousands of years. The likelihood that such a *"potentially damaging event will occur within a particular region during a specified period of time"* (Korup and Clague, 2009) is defined as **natural hazard**. While extreme physical events took place over millions of years affecting only flora and fauna, the importance of modern natural hazard research is fundamentally based on their impact on human societies (Alcantara-Ayala, 2002). This impact or **disaster** is defined as "*severe alterations in the normal functioning of a community or a society due to hazardous physical events interacting with vulnerable social conditions, leading to widespread adverse human, material, economic, or environmental effects that require immediate emergency response to satisfy critical human needs and that may require external support for recovery*" (IPCC, 2012). Especially hazards to coastal areas continuously increase in importance, since a high percentage of the global population is already threatened by coastal flooding events and, due to the rising sea level and the rapidly growing world population, even more people will be affected in the near future (Small et al., 2000; IPCC, 2007). **Coastal hazards** can be discriminated into **rapid-onset hazards** that last over periods of minutes to several days, such as major cyclones, storm surges, and tsunamis, and **slow-onset hazards** which develop over longer time periods, such as long-term coastal erosion and sea-level rise (Gornitz, 2005). While sea-level rise and storms are widely discussed and studied in the course of global warming and climate change (IPCC, 2007, 2012), the hazard due to tsunamis gained importance in the scientific and public interest after the Indian Ocean Tsunami (IOT) of December 2004 (Engel and Brückner, 2011). While during the 1990s tsunamis killed less than 4000 people and caused economic losses of 1 billon US\$ (IOC, 2008), the total death toll of the IOT 2004 alone reached more than 225,000 casualties and the overall economic damage amounted to several billions US\$ (Brückner and Brill, 2009). The actuality of the topic was lately emphasized by the tsunamis in Chile 2010 and Japan 2011, with more than 300 and 19,000 casualties, respectively (CNN World, 2010; Spiegel-Online, 2012). The disastrous effects of these recent tsunamis demonstrate a lack of awareness and preparedness in respect of the local tsunami risk (UNESCO, 2007). And even five years after the catastrophic Indian Ocean Tsunami in December 2004 the vulnerability of most affected areas had not been reduced significantly (Ziegler et al., 2009).

The long-term probability of damage due to natural hazards for a specific area is given by its **risk**, i.e. the likelihood of disasters over a specified time period, quantitatively expressed by the formula risk = hazard x vulnerability (Nadim and Glade, 2006). While **vulnerability** describes the predisposition of natural and social systems to be negatively affected, hazard is determined by the **frequency** and the **magnitude** of potential **extreme events** with impact on the area (IPCC, 2012). For the coastlines of southwest Thailand the tsunami risk was demonstrated for the first time by the IOT 2004 that caused more than 8300 casualties and economical damage of more than two billion US$ (Brückner and Brill, 2009). While the vulnerability of the area was, and still is, object to intensive research (e.g. Calgaro and Lloyd, 2008), there is still insufficient information about the frequency and magnitude of strong tsunamis generated along the Sunda Arc prior to 2004 (Bondevik, 2008).
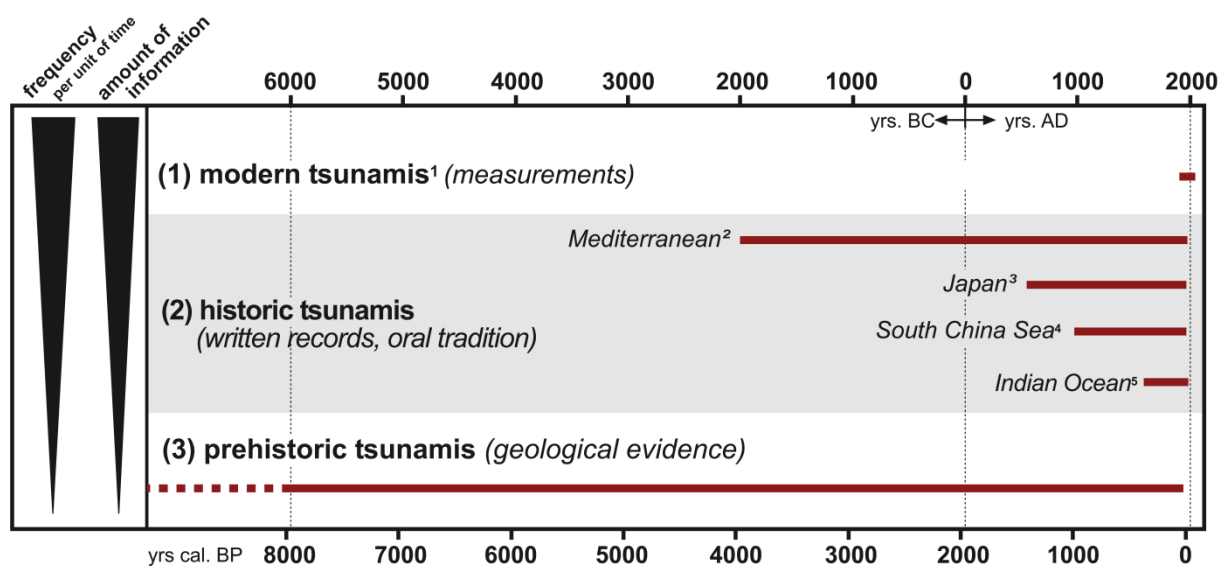
Figure 1.1: Availability and quality of the different types of tsunami data: modern events, historical events (selected regions) and prehistoric events. [1]Scheffers and Kelletat, 2003; [2]Soloviev et al., 2000; [3]Cartwright and Nakamura, 2008; [4]Lau et al., 2010; [5]Dominey-Howes et al., 2007.

To quantify the tsunami hazard of a region, frequency and magnitude statistics on the basis of **modern events** that have been documented via measurements, and **historic events** that provide information in the form of written records and oral tradition can be used (fig. 1.1). Since these time series are often too short to record long-term recurrence intervals and to capture the complete range of event magnitudes, **prehistoric events** preserved in the geological record may offer the opportunity to enhance the dataset for hazard evaluation (Rhodes, 2006; Korup and Clague, 2009). While historical tsunami records for the Indian Ocean cover only the last 400 years (Murty and Rafiq, 1991; Kumar and Achyuthan, 2006; Dominey-Howes et al., 2007; Alam et al., 2012), documenting only three pre-2004 tsunamis in the Andaman Sea which had no effects along the coasts of Thailand (e.g. Bilham et al., 2005), geological evidence of tsunami impacts (dislocated boulders and allochthonous sand sheets) and triggering earthquakes (uplifted or subsided corals and palaeosols) goes back thousands of years and

indicates the repeated occurrence of mega-events comparable with the IOT 2004 (e.g. Jankaew et al., 2008; Monecke et al., 2008; Sieh et al., 2008; Dura et al., 2011).

More detailed information on the long-term tsunami hazard of southwest Thailand is crucial for the improvement of risk assessment and the development of mitigation strategies, preparedness, as well as recovery and rehabilitation strategies (Patwardhan and Sharma, 2005; Sieh, 2006; UNESCO, 2007). In consequence, this work concentrates on the enhancement of statistically usable tsunami data in the form of geological tsunami imprints. To "read" the geological evidence in terms of their informative value for tsunami recurrence and impact, the tsunami events have to be (i) identified, (ii) dated and correlated with evidence at other locations, and (iii) quantified in terms of their magnitude and intensity (Sugawara et al., 2008).

1.2 Aims of the study

This study was integrated in the bilateral Thai-German research cooperation TRIAS *("Tracing Tsunami Impacts onshore and offshore in the Andaman Sea Region")* funded by the Deutsche Forschungsgemeinschaft (DFG, reference number: PAK 228) and the National Research Council of Thailand (NRCT). Within this program, the subproject *"Tracing tsunami impacts in coastal geo- and bio-archives along the west coast of Thailand"* (TRIAS-COAST, ref. no.: BR 877/27-1, -2; KE 190/26-1), designed by Prof. Dr. Helmut Brückner and Prof. Dr. Dieter Kelletat, deals with the improvement of the regional tsunami history by searching nearshore geo- and bio-archives of southwest Thailand for the impacts of modern and prehistoric tsunamis (fig. 1.2).
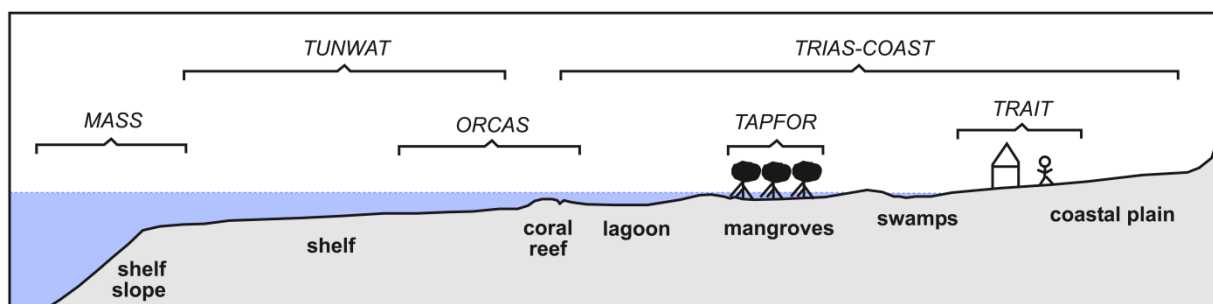
Figure 1.2: *The roll of subproject TRIAS-COAST within the TRIAS research design. MASS = Morphodynamics and slope stability of the Andaman Sea shelf; TUNWAT = Tsunami Deposits in Near-shore and Coastal Waters of Thailand; ORCAS = Pelagic-Benthic Coupling near Andaman Sea Coral Reefs; TAPFOR = Tsunami Attenuation Performance of Coastal Forests; TRAIT = Tsunami Risk, Vulnerability and Resilience in the Phang-nga Province, Thailand.*

This dissertation focuses on the application of sedimentary evidence to enhance the knowledge about the frequency and the magnitude of past tsunamis, since the determination of tsunami recurrence, potential tsunami magnitudes (wave height, flow velocity, etc.) and impact scenarios (inundation areas) from geological evidence is one of the tasks recommend-

ed by the UNESCO (2007) for an effective hazard and risk assessment. To evaluate the research hypotheses that the geoarchives of the study area are suited to reconstruct the recurrence, magnitude and impact of palaeotsunamis in southwest Thailand, the study followed the goals of palaeotsunami research formulated by Sugawara et al. (2008).

Hypothesis 1 – The coastal sediment record of southwest Thailand is an appropriate archive to improve the database of prehistoric tsunamis in the Indian Ocean.

Goal I: Identification of new palaeotsunamis

The number of locations with well constrained palaeotsunami evidence along the coastlines of the Indian Ocean and especially Thailand is small. The identification of further tsunami deposits – by discriminating them from sediments of other processes, especially strong storms – constitutes the basis of an improved tsunami history.

Hypothesis 2 – Sedimentary imprints of tsunamis can be used to establish recurrence intervals for local and regional events.

Goal II: Dating of palaeotsunamis

To establish a chronology of tsunami events and to estimate their recurrence rates, it is essential to precisely date newly identified tsunami evidence as well as poorly dated tsunamites from locations already described in literature, such as Phra Thong Island (Jankaew et al., 2008).

Goal III: Correlation of spatially distinct tsunami evidence

Based on its age, spatially distinct tsunami evidence identified in this study should be correlated locally (e.g. with deposits in other swales), to reconstruct inundation distances, and regionally with tsunami and earthquake imprints from Thailand and other countries around the Indian Ocean, to establish spatial patterns of impact (e.g. Løvholt et al., 2012).

Hypothesis 3 – Tsunami deposits allow for the evaluation of magnitude and impact of past tsunamis in southwest Thailand.

Goal IV: Establishing the magnitude and the intensity of tsunami events

While the tsunami magnitude is an objective measure of the strength of tsunamis, the intensity of an event describes its impact on natural and social systems. Since the characteristics of tsunami deposits are significantly influenced by local factors (e.g. Shanmugam, 2012), the reconstruction of deviating boundary conditions, especially sea level and palaeogeography, is an important aspect when interpreting sedimentary tsunami evidence in terms of the size and impact of associated events. This leads to the following sub-goals:

Goal IV.1: Reconstruction of <u>Holocene sea-level</u> oscillations in SW Thailand

To deduce the relative magnitudes of prehistoric tsunamis from parameters such as inundation distance or run-up height, these parameters have to be related to the water level at the time of impact. While reconstruction of tide levels is not possible, long-term fluctuations of the mean sea level can be established using geological evidence.

Goal IV.2: Reconstruction of local changes in coastal <u>palaeogeography</u>

Changes in the palaeogeography, especially shifts in the shoreline position, have a similar effect on the interpretation of relative magnitude parameters as sea level.

Goal IV.3: Evaluating the <u>impact</u> of tsunamis on the coastal evolution of Thailand

The IOT 2004 had a significant effect on the geomorphological and ecological evolution of affected coastal areas, at least locally and temporally (e.g. Brown, 2005; Cochard et al., 2008). In the Mediterranean, lasting effects of prehistoric tsunamis on coastal evolution are suggested (May, 2010; May et al., 2012). In some cases even the development of human societies may have been affected (e.g. Bruins et al., 2008; Scheffers et al., 2009; Goff et al., 2012). The influence of past tsunamis on ecosystems and coastal geomorphology in Thailand may help to estimate the impact of future events.

Goal IV.4: Estimating the <u>magnitude</u> of palaeotsunamis

The size or strength of the IOT 2004 could be documented by contemporaneous measurements by satellites, videos and tide gauges, as well as post-tsunami field surveys. In case of palaeotsunamis, magnitude information, at least relative magnitudes compared to the IOT 2004, may be deduced from their sedimentary imprints (e.g. Nanayama et al., 2003; Jaffe and Gelfenbaum, 2007).

1.3   Research design and outline of the study

The research design presented in figure 1.3 provides the methodological techniques and the timetable to achieve the goals formulated in chapter 1.2: In <u>step 1</u>, data has been collected at different locations – selected on the basis of information about the topography and the inundation area of the IOT 2004 – by various fieldwork techniques (coring, trenching, GPS survey), and the processing of these data in the laboratory (sediment analyses, dating by OSL and AMS-^{14}C, sedimentation modelling). The results allow for the identification and characterisation of event deposits (storm and tsunami) and the establishment of Holocene sea-level curves and palaeogeographical scenarios. In <u>step 2</u>, these results are interpreted in their local contexts in terms of type of event (storm or tsunami), chronology, magnitude and impact on coastal systems. Initially, both steps were applied to a variety of locations and environments with a low spatial resolution (<u>phase 1</u>); subsequently, the most promising locations were studied systematically with a higher spatial resolution (<u>phase 2</u>). <u>Step 3</u> led to a final synopsis of all in-

vestigated sites and – based on historical and geological data from literature – integration in the broader context of basin-wide tsunami recurrence and spatial impact patterns.
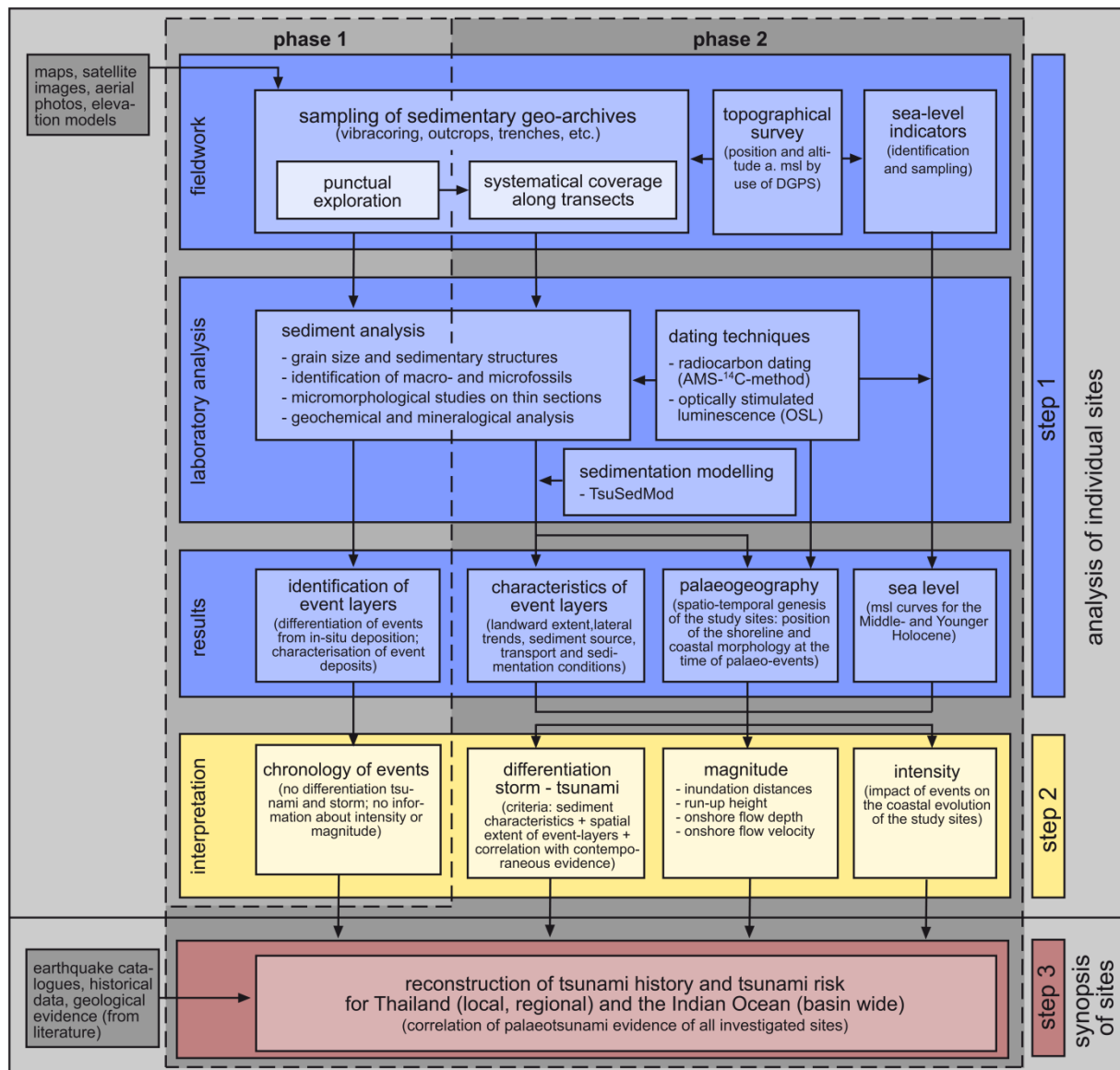
Figure 1.3: *Research design of the study.*

Before the results of the project are presented in *Chapters 4-11*, a general introduction into the state of the art in tsunami research, including the topics "tsunami hydrodynamics" and "tsunami deposits", as well as into the most important physical aspects of the study area will be given in *Chapter 2* and *Chapter 3*. The first case study documents tsunami deposits of the IOT 2004 and several prehistoric events from the coastal plain of Ban Bang Sak, focussing on goal I, the identification of tsunamites and their discrimination from storm deposits (*Chapter 4*). *Chapter 5* introduces the optically stimulated luminescence technique (OSL) as an alternative tool to date tsunami deposits (goal II). The evaluation of this method on deposits of the IOT 2004 from Phra Thong Island proves its potential for determining reliable ages for tsunami-laid sand sheets in southwest Thailand. Thus, the procedure established in Chapter 5 is

applied to a suit of spatially distinct palaeotsunami deposits from Phra Thong Island in *Chapter 6*. By using the OSL ages for spatial correlation of the deposits (goal III), minimum inundation distances (local scale) and basin-wide impact patterns (regional to supra-regional scale) can be presented for three palaeotsunami events.

In order to estimate the magnitudes and impacts of palaeotsunamis, at first the boundary conditions at the time these events hit the coastline have to be reconstructed: *Chapter 7* deals with the construction of regional sea-level curves for the last 6000 years (goal IV.1), using beach-ridge heights of Phra Thong Island for the northern part of the study area and fixed biological markers from Phuket and the Phang-nga Bay for the southern part. In *Chapter 8,* the palaeo-geographical evolution (goal IV.2) of Phra Thong Island, Ban Bang Sak and Pakarang Cape, the three locations with well constrained palaeotsunami evidence, is discussed. The contribution of tsunami impact to long-term coastal evolution is the topic of *Chapter 9* (goal IV.3). Afterwards, *Chapter 10* takes on the information about sea levels and palaeogeography to interpret modelled hydrodynamic parameters (flow velocity, flow depth) and sediment transport (transport distance, source area of the sediment) that are used to estimate the magnitude (goal IV.4) of palaeotsunamis from Ban Bang Sak. Finally, in *Chapter 11* the most important results of the study are summarised and their implications for the wider context of risk assessment and risk mitigation are discussed.

Chapter 2

2 Tsunami research: State of the art

2.1 Tsunamis – generation, propagation and inundation

The term tsunami is the Japanese expression for "harbour wave". Tsunamis are defined as water waves with extreme wavelengths generated by sudden displacements of the seafloor or disruptions of any body of standing water (Helal and Mehanna, 2008). The expressions "seismic sea waves" and "tidal waves" that are occasionally used synonymously with tsunamis should be avoided, since tsunamis are not related to tides and can be generated by other mechanisms than earthquakes.

Triggering events

Tsunamis can be generated by any significant disturbance of the water column, either bottom-up impulses such as earthquakes and submarine slides, as well as top-down impulses such as landslides and meteorites that hit the water body from above (Dawson and Stewart, 2007). In general, four different kinds of generating mechanisms can be distinguished:

(1) Submarine earthquakes. Earthquakes directly below or near the ocean floor are the most frequent mechanism of tsunami generation. Within the last 200 years 90% of all recorded tsunamis were triggered by submarine earthquakes (Sugawara et al., 2008). However, not all submarine earthquakes with high energy release cause tsunamis. Fundamental characteristics of "tsunami earthquakes" are a shallow focus of less than 70 km depth, large vertical slip and a large rupture area, slow movement of the vertical rupture, and huge water depths of more than 3000 m (IOC, 2008; Sugawara et al., 2008). The IOT 2004, the strongest earthquake-generated tsunami since the beginning of automatic recording, was characterised by a focal depth of only 10 km, a fault length of 1500 km and a maximum vertical displacement of 15 m over a time period of 50 minutes (Lay et al., 2005; Geist et al., 2006).

(2) Landslides. Gravitational mass movements with appropriate volumes that occur either underwater or propagate from coastal areas into deep water bodies are capable to trigger tsunamis, since they result in significant disturbances of the sea bottom. Submarine slides can be triggered by earthquakes, volcanic eruptions or the breakdown of gas-hydrates that break up the stability of sediments at steep slopes, e.g. the shelf edge (IOC, 2008; Sugawara et al., 2008). The most prominent example is the submarine Storegga Slide, a gigantic slump at the Norwegian shelf edge that resulted in a tsunami with impact in Nor-

way, Scotland and Britain approximately 8000 years ago (Dawson et al., 1988; Long et al., 1989). More recently, a submarine slide triggered the 1998 Papua New Guinea tsunami (Synolakis et al., 2002). Prominent examples for flank collapses at steep coastlines, caused either by earthquakes or volcanic eruptions, are the tens to hundreds km³ big flank failures on Hawaii (Moore, 2000) and the Canary Islands (Krastel et al., 2001) that are supposed to have triggered gigantic tsunamis in the Pleistocene. Generally, slide-generated tsunamis have less energy, shorter wave lengths and smaller impact radii than seismic tsunamis (Sugawara et al., 2008).

(3) Volcanic eruptions. Although to date no exact physical models for the generation of tsunamis by submarine volcano eruptions exist, the eruptions of Krakatau in 1883 AD (Latter, 1981) and Santorin c. 1500 BC (Minoura et al., 2000; Bruins et al., 2008) demonstrated the tsunami-triggering potential of volcanic events. Responsible is probably a combination of submarine caldera formation, pyroclastic flows, and interaction between seawater and magma (Sugawara et al., 2008).

(4) Meteorite impacts. Comparable rare but exceptionally strong events are tsunamis triggered by meteorite impacts. The most prominent example is the 65 Million years BP impact at the K/T boundary that created a tsunami with enormous wave heights in the Gulf of Mexico (Schulte et al., 2010).

Propagation in deep water

Tsunamis are commonly generated as a series of waves with extreme wave lengths of several hundred kilometres, periods of several minutes to one hour between successive wave crests, and amplitudes of only a few decimetres in deep water (IOC, 2008; fig. 2.1). Different from wind generated waves, tsunamis always behave as shallow water waves, since the water depth even in deep ocean basins is small compared to their gigantic wave lengths (Helal and Mehanna, 2008). This implies that the propagation speed of wave crests (v) is controlled solely by water depth ($v = \sqrt{g * h}$, with gravity acceleration g and water depth h). Thus, tsunamis in deep water travel with speeds of up to 800 km/h and the direction of propagation is guided by bathymetrical structures (IOC, 2008; Sugawara et al., 2008). In contrast, the current velocity (u) – i.e. the orbital velocity of the water particles – that is constant throughout the water column decreases with water depth ($u = \pm\eta * \sqrt{g/h}$, with water elevation above still-water level η) resulting in currents of only a few centimetres per second in deep water (Sugawara et al., 2008).

Shoaling in shallow waters and inundation at the coast

Since the propagation of tsunamis is controlled by water depth, the waves are subject to a significant transformation when they enter shallow seas: due to interaction with the sea bottom,

the propagation speed (v) and the wave length of tsunamis decrease, while the wave height and the current velocity (u) increase with decreasing water depth (IOC, 2008; Sugawara et al., 2008). When tsunamis finally reach a coastline – after several minutes in case of local tsunamis, a few hours in case of regional events (Titov et al., 2005), and up to one day in case of teletsunamis like the 1700 AD Cascadia tsunami (Satake and Atwater, 2007) – wave heights can amount to several decametres and current velocities to several meters per second. Due to amplification effects by local bathymetry such as bays, river inlets and reefs, as well as harbour resonance in small basins, the height and speed of tsunami waves at the shoreline may vary significantly over short distances (IOC, 2008). After crossing the shoreline – tsunamis either arrive in the form of trough leading waves with initial recession or crest leading waves (Helal and Mehanna, 2008) – the waves may inundate up to several kilometres inland (inundation distance) and may reach heights above sea level of several decametres (run-up height), before they again recede to the sea (backwash). Run-up heights of more than 500 m as observed during the landslide-triggered tsunami in Lituya Bay (Weiss et al., 2009) are exceptional cases. Since successive wave crests of the tsunami wave train may ride on each other when inundation of the following wave is prior to complete recession of the previous one, the first wave is not always the highest (Sugawara et al., 2008).
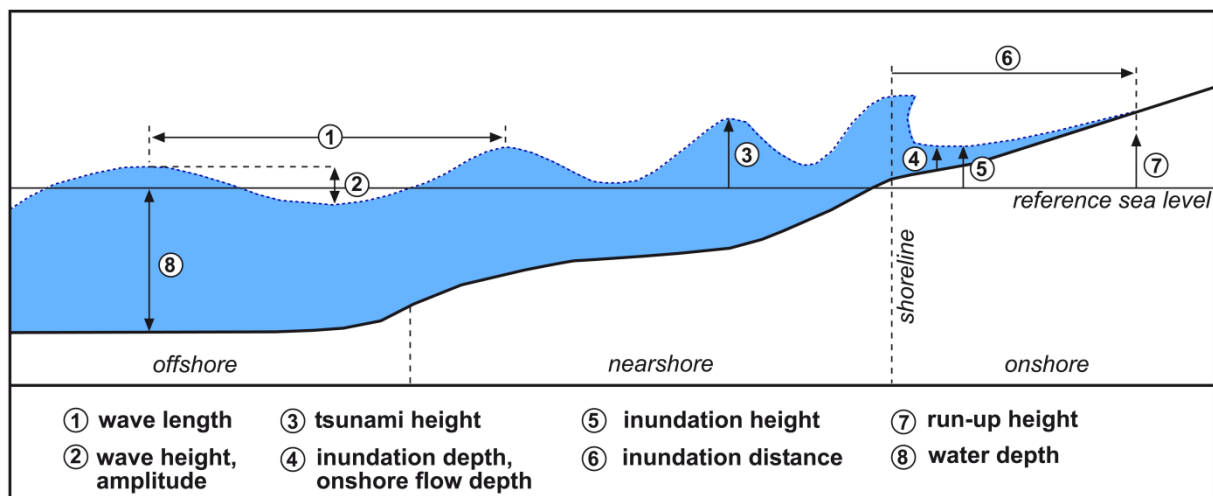
Figure 2.1: *Terminology of determining parameters of tsunami waves relevant for this study (after Sugawara et al., 2008 and Bryant, 2001).*

2.2   Tsunami deposits

Types of tsunami deposits

Tsunamis are capable to trigger sediment movement in two generally different ways. When the tsunami wave exceeds a critical current velocity, unconsolidated sediment is eroded. This sediment is transported in suspension and as traction load until the current falls below a critical transport velocity. Sediments that are actively transported by tsunami waves – either

landward (onshore deposits) or seaward (offshore deposits) – are called "tsunami deposits" (Dawson and Stewart, 2007). In addition, tsunamis can trigger submarine slides of material at instable slopes that moves downhill in the form of turbidity currents. Both, actively transported deposits and tsunami induced gravity movements are summarised with the term "tsunamiite" (Shiki and Yamazaki, 2008) or "tsunamite" (Shanmugam, 2006). Common for all of these tsunami-induced deposits are the characteristic properties of "event deposits", i.e. episodic occurrence and unusually high-energetic transport processes compared to the autochthonous background deposition. They can be classified by the geoarchives they are finally accumulated in (Bourgeois, 2009; fig. 2.2):

(1) Homogenites. Tsunami-induced turbidity currents form "homogenites" at the foot of steep, submarine slopes, most frequently in front of the shelf edge (Dawson, 1999). Cita et al. (1984), for example, describe homogenites caused by the 3500 BP Santorini tsunami in a water depth of 4000 m in the Ionian Sea.

(2) Onshore tsunami deposits. A major part of tsunami-transported sediment is eroded offshore and in the coastal zone, and deposited in onshore sediment traps during tsunami inundation. These onshore tsunami deposits are characterised by allochthonous material of marine origin that is deposited in terrestrial, limnic or brackish environments (Dawson and Stewart, 2007). Most frequent are sandy layers that are deposited in bodies of standing water such as lakes, lagoons, and bays (e.g. Minoura et al., 1994; Donato et al., 2008; Vött et al., 2008), or in terrestrial archives such as mires, swales and mangroves (e.g. Atwater and Moore, 1992; Cisternas et al., 2005). Although the formation of sublayers is predominantly related to the impact of successive waves, the number of sublayers is not always equal to the number of waves (Fujiwara and Kamataki, 2008; fig. 2.3).Where coarser material is available, even boulders and blocks can be moved inland. Commonly, boulder sized deposits are transported inland from reefs and cliffs at the shoreline over comparatively short vertical and horizontal distances (e.g. Mastronuzzi and Sansò, 2004; Goto et al., 2010a; Spiske and Bahlburg, 2011; Engel and May, 2012).

(3) Offshore tsunami deposits. Parts of the sediments taken up by tsunamis are transported in seaward direction by backwash currents. These offshore tsunami deposits are characterised by allochthonous sediment from near-shore and terrestrial environments that is deposited deposits characteristic for deeper water (Dawson and Stewart, 2007). Due to the impact of storm waves, the preservation potential in shallow water is relative low (Bourgeois, 2009) and only deposits in water depths of at least 50 m will commonly be preserved (Weiss and Bahlburg, 2006). For example, Smedile et al. (2011) describe palaeo-tsunami deposits with ages of several millennia in a water depth of 72 m in the Mediterranean. However, modern examples of offshore tsunami deposits from the shelf off SW Thailand that originate from the IOT 2004 were restricted to water depths of less than 50 m. They

showed run-up and backwash features, and contained mud, sand and small boulders (Feld-ens et al., 2009; Sugawara et al., 2009; Sakuna et al., accepted).
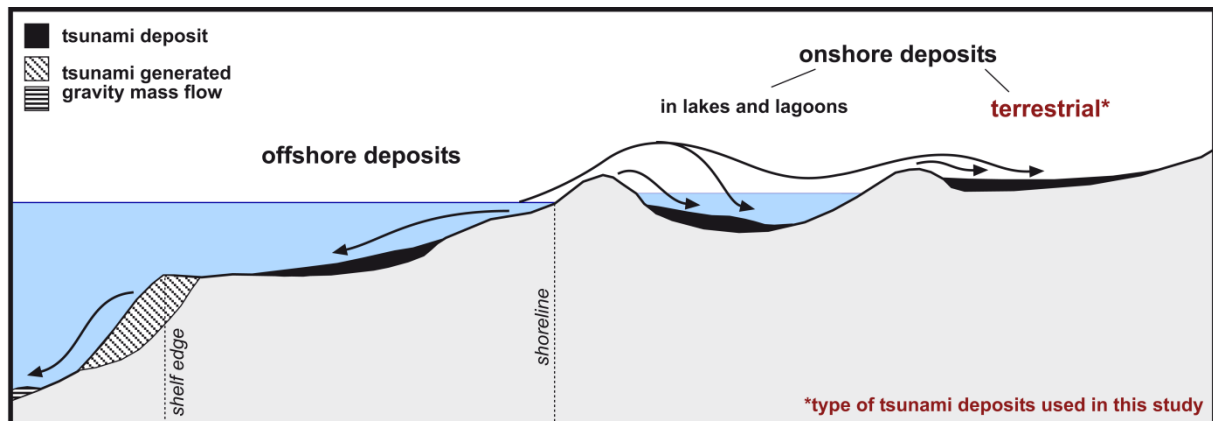
Figure 2.2: *The main types of tsunami deposits and archives (after Dawson and Stewart, 2007). Due to the scarcity of natural lakes and lagoons in SW Thailand, this study concentrates on tsunami-laid onshore deposits in terrestrial geoarchives.*

Generally, favourable geoarchives are those, where post-depositional disturbances are absent and the properties of event deposits significantly contrast with the background sedimentation. This is especially true for low-energy environments with fine grained sedimentation such as lakes and lagoons. However, due to the natural conditions in the coastal areas of southwest Thailand, where the scarcity of natural lakes and lagoons excluded the analyses of deposits in water bodies and where boulders are rare, the study concentrates on sandy onshore deposits archived in terrestrial environments, mostly coastal plains with successions of beach ridges and swales.
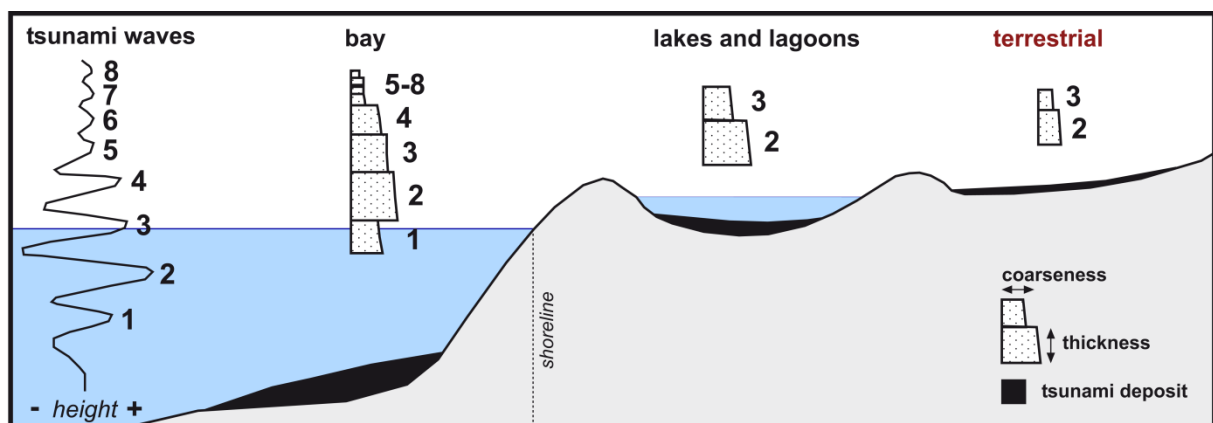
Figure 2.3: *Information content of onshore tsunami deposits from different geoarchives (slightly modified from Fujiwara and Kamataki, 2008).*

Sediment characteristics of tsunami deposits

The oldest observations on modern tsunami deposits reach back as far as the 19th century, e.g. in Japan (Bourgeois, 2009), and sedimentary evidence of prehistoric tsunamis was described for the first time by Atwater (1987) in Washington State and Dawson et al. (1988) in Scot-

land. However, the knowledge of processes and signatures relevant in tsunami sedimentology increased drastically due to studying recent tsunami events within the last 20 years, such as the 1992 Flores tsunami (Shi et al., 1995), the 1998 Papua New Guinea tsunami (Gelfenbaum and Jaffe, 2003), the 2011 Japan tsunami (e.g. Goto et al., 2011), and especially the IOT 2004 (e.g. Szczuciński et al., 2005; Hawkes et al., 2007; Hori et al., 2007; Kelletat et al., 2007; Kozak et al., 2008; Choowong et al., 2008c; Morton et al., 2008; Srinivasalu et al., 2008; Kunz et al., 2010; Switzer et al., 2012). For the deposits of these modern events the tsunamigenic origin is certain, and the effect of post-depositional disturbances is at a minimum. Additionally, the big amount of information about triggering events and tsunami hydrodynamics from seismic recording, satellite altimetry, tide gauges, survivor videos and immediate post-tsunami field surveys provides the opportunity to relate sediment characteristics to flow and transport processes within the tsunami waves. The general structure of an ideal tsunami deposit that forms from changing current velocities and directions due to the interplay of inflow and backwash, if sufficient sediment is available in the source area and erosion of sediment by subsequent waves is neglected (Fujiwara and Kamataki, 2008; Naruse et al., 2010), is documented in figure 2.4a. Since these conditions are rarely realistic for the formation of onshore tsunami deposits, they commonly show bedding structures modified by erosion during backwash and following waves (fig. 2.4b).
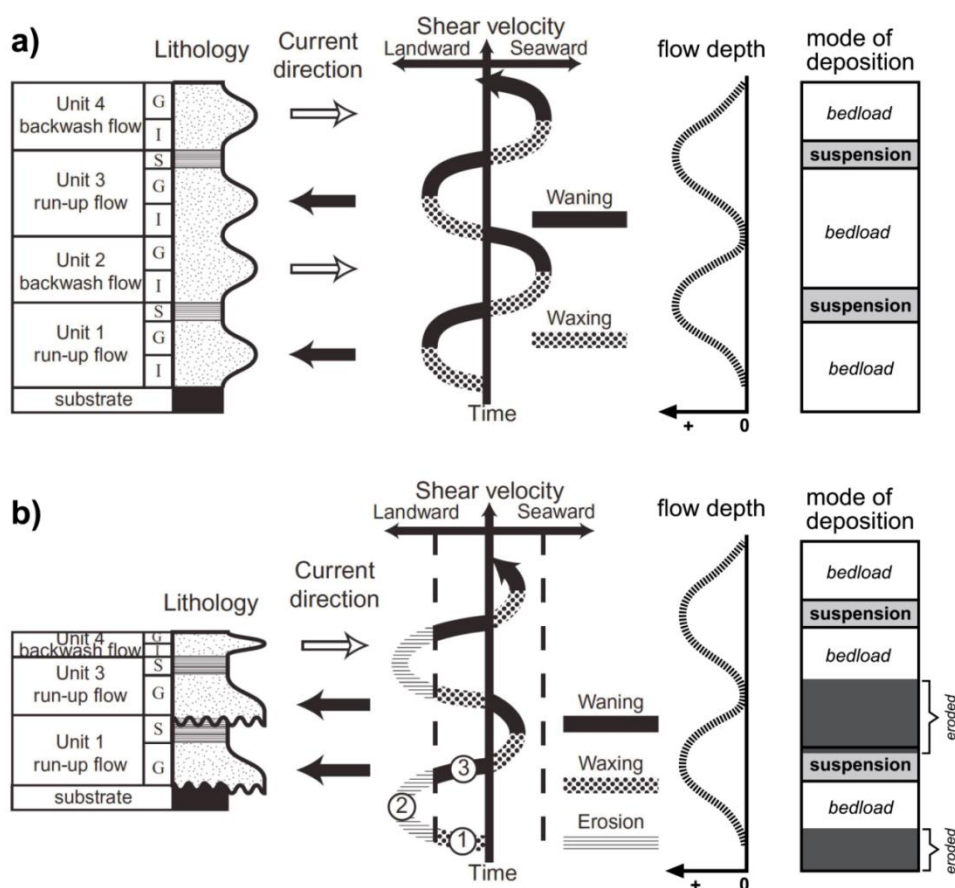
Figure 2.4: *Relationship between the structure of tsunami deposits and hydrodynamic processes. (a) Ideal tsunami deposit; (b) real tsunami deposit, affected by erosion (modified after Naruse et al., 2010).*

Due to the specific transport and sedimentation processes in tsunami waves the following signatures are typical in onshore tsunami deposits:

(i) Sedimentary features. The specific sedimentary features of onshore tsunami deposits are the effect of the highly energetic hydrodynamics connected with extreme wave events (Shanmugam, 2012). High initial current velocities are capable to erode the underlying substrate and, thus, can form sharp, erosive bases and incorporate rip-up clasts into the basal sections of tsunami deposits. The decrease and increase of flow velocity during flooding causes changes between bedload and suspension-dominated deposition, resulting in normally and inversely graded sublayers (Fujiwara, 2008; Choowong et al., 2008b, c; Moore et al., 2006, 2011). The stagnant stage at the end of wave run-up can produce fine laminated silt and mud caps (Fujiwara and Kamataki, 2008; Goto et al., 2008; Switzer et al., 2012). The switchover between inflow and backwash currents produces characteristic bidirectional flow structures, inland and seaward. During backwash terrestrial macro remains such as wood, plant fragments and anthropogenic artefacts are incorporated (Nanayama et al., 2000; Fujiwara, 2008; Choowong et al., 2008b). Lateral trends in thickness, mean grain size and sorting reflect the decreasing flow depth and speed with increasing distance from the shoreline (e.g. Nishimura and Miyaji, 1995; Bahlburg and Weiss, 2007; Fujino et al., 2010).

(ii) Geochemical signature. The geochemistry of tsunami deposits reflects the environmental conditions at the source areas of the sediments. Since tsunami-transported onshore deposits typically have a marine origin and a terrestrial, limnic or brackish sink, they contrast from the background sedimentation by their marine signature (Chagué-Goff, 2010; Chagué-Goff et al., 2011, 2012). Characteristic are elevated concentrations of sea-water salts such as sodium, magnesium, and chlorine (Minoura et al., 1994; Szczuciński et al., 2005; Vött et al., 2009). Locally, elevated heavy metal concentrations (e.g. Pb, Cd, Cu) are reported, e.g. for IOT 2004 deposits from Thailand and India (Szczuciński et al., 2005; Srinivasalu et al., 2008).

(iii) Macro- and microfauna. Similar to the geochemistry, the faunal composition of tsunami deposits reflects the environmental conditions of the source areas (Mamo et al., 2009; Ruiz et al., 2010). Since tsunamis may entrain sediment over distances of several tens of kilometres, the fauna is commonly a mixture of individuals originating from all affected environments, i.e. marine, brackish, limnic and terrestrial (Dawson et al., 1996a; Nagendra et al., 2005; Nanayama and Shigeno, 2006); sediment from a marine source can further be related to different water depths based on foraminifera or diatoms (Sawai et al., 2009; Uchida et al., 2010). The taphonomy of shells (Donato et al., 2008) and microfossils (Ruiz et al., 2010; Pilarczyk and Reinhardt, 2012), e.g. angular breaks and articulated valves, may be indicative for the high energetic transport processes.

(iv) Mineralogy. The mineralogical composition is indicative solely for the source area of tsunami deposits. Since there is no typical marine mineralogy, it is controlled by local geology. Although the feature locally may be useful to define sediment sources (e.g. Switzer et al., 2005) or hydrodynamic processes (Jagodzínski et al., 2009), it is not a general tsunami indicator.

However, although the features described above reflect characteristic properties of tsunamis, especially the highly energetic flow conditions and the switchover between run-up and back-wash, there is no "typical tsunami deposit". Instead, the local deposits are strongly influenced by site-specific factors, such as topography, bathymetry, sediment sources and sediment availability (Peters and Jaffe, 2010; Engel and Brückner, 2011; Shanmugam, 2012). Furthermore, while some of the features mentioned above – especially grain size, sedimentary structures and mineralogy – are rather stable and commonly resist even over long time periods, others are sensitive to post-depositional processes such as solution or bioturbation. Especially geochemistry is significantly altered after short time periods in most terrestrial geoarchives (Szczuciński et al., 2006; Szczuciński, 2012) and is only preserved as a proxy for palaeotsunamis in lakes or lagoons (e.g. Minoura et al., 1994; Vött et al., 2009). In tropical climates even foraminifera and diatoms are dissolved rapidly under terrestrial conditions (Jankaew et al., 2008; Sawai et al., 2009).

Discrimination between storm- and tsunami deposits

While the characteristics of tsunami deposits are unique enough to distinguish them from most other types of sediments, the discrimination between tsunamites and storm deposits remains a major challenge. This is due to the fact that both types of deposits originate from similar source areas and are moved by similar, highly energetic flow processes (Sugawara et al., 2008). Therefore, mere indicators of a marine sediment origin, such as geochemistry or marine fauna, are not appropriate to discriminate between tempestites and tsunamites (Chagué-Goff et al., 2011, 2012). In almost the same manner features that result from highly energetic hydrodynamic processes, such as erosive surfaces, rip-up clasts, normally and inversely graded layers and flow structures, can occur in both types of sediment. Nevertheless, at the beginning of palaeotsunami research several indicators that were supposed to be unique features for either storm or tsunami deposits were suggested by different authors (e.g. Morton et al., 2007; Switzer and Jones, 2008). These facies models were based on the hydrodynamic differences between storm waves and tsunamis, such as the number of waves (few for tsunamis, hundreds for storms) and the current direction (repeated turnover of landward and seaward flow for tsunamis). However, in the course of an increasing number of case studies on recent tsunami and storm deposits, especially after Hurricane Katrina and the IOT 2004, all these criteria appeared to be present in both kinds of deposits (Peter and Jaffe, 2010; Engel and Brückner, 2011; Shanmugam, 2012); all indicators that tend to favour a tsunami origin have meanwhile

been detected in storm deposits and the other way round. For example, lamination, formerly related explicitly to multiple storm wave impact, was observed in tsunami deposits as well (e.g. Switzer et al., 2012), and a small number of graded layers, supposedly typical for tsunamites, was also proved to occur in tempestites (Engel and Brückner, 2011).

The reason for the presence of all typical tsunami features in storm deposits is that besides hydrodynamic processes site specific factors such as morphology and sediment source play a major role in the formation of event deposits (Umitsu et al., 2007; Scheucher and Vortisch, 2011). Features related to the magnitude of events, such as maximum depth of eroded sediment, inundation width, run-up height or flow depth that potentially can reach higher values in case of tsunamis, are only of a relative value, since they are influenced significantly by the local conditions (e.g. Borrero, 2005; Papadopoulos et al., 2006; Peterson et al., 2010). It is therefore necessary to interpret evidence of extreme wave events in its local context rather than looking for universal tsunami indicators (Engel et al., 2010). Only a combination of features, interpreted in its local context, allows for the discrimination between tempestites and tsunamites.

Promising strategies to identify palaeotsunamis include the analyses of modern references for both storm- and tsunami deposits (Nanayama et al., 2000; Goff et al., 2004; Tuttle et al., 2004; Kortekaas and Dawson, 2007), if these are available, or the determination of local maximum offshore sediment sources below the storm wave base (Switzer et al., 2005; Uchida et al., 2010). Additionally, the probability of storm and tsunami occurrence due to local and regional climatic and geographical factors should be considered. This can be supported by numerical simulations of storms and tsunamis, as well as the associated depositional processes (e.g. Witter et al., 2008; Paris et al., 2010; Priest et al., 2010).

Chapter 3

3 The study area

3.1 Geographical setting of southwest Thailand

The study area comprises the west coast of southern Thailand between 9° and 7°30′ N (fig. 3.1). It is located at the eastern limit of the Andaman Sea, a marginal sea of the Indian Ocean with an area of 800,000 km² (Rodolfo, 1969). The water bodies of the Indian Ocean (the area between India and southeast Asia is also called Bay of Bengal) and the Andaman Sea are separated by the morphological barrier of the volcanic island arc at the Sunda subduction zone, where the Australian-Indian Plate and the Sunda and Burma Microplates converge with a mean velocity of 4-5 cm per year (Lay et al., 2005). The topographic elevations of this arc emerge in form of the Andaman and Nicobar Islands. East of the island arc, the Andaman Sea reaches maximum water depths of more than 4000 m, before it passes into a shallow shelf sea with water depths < 200 m offshore Thailand. The broad and shallow shelf starts up to 260 km west of the shoreline, the 100 m contour 40 km offshore Phuket (Rodolfo, 1969).

As being part of the Malay-Thai Peninsula, southwest Thailand is bordered by the Gulf of Thailand to the east and the Andaman Sea to the west (fig. 3.1). In contrast to the wide and flat coastal plains of the gulf coast, which are dominated by lagoons, coastal lakes, cheniers and marshes, the western side of the peninsula is characterised by north-south striking mountain chains that extend close to the Andaman Sea and generally form steep and rocky coasts (Sinsakul, 1992). Along the **west coast of Phang-nga province**, between Phra Thong Island in the north and the northern spit of Phuket in the south (fig. 3.1b), the coastal geomorphology is dominated by barrier islands, beach-ridge plains and wide intertidal flats with mangroves that alternate with rocky headlands (Sinsakul, 1992). The offshore morphology to the west is flat and gently sloping at an angle of 0.09° (Di Geronimo et al., 2009), reaching only 20 m water depth at a distance of 12 km from the coast (Szczuciński et al., 2006). The coasts of **Phuket** (fig. 3.1b, e) are predominantly formed by steep granite headlands alternating with small, sandy pocket beaches and steep alluvial plains (Dheeradilok, 1995). Along the sheltered eastern coast, coral reefs and mangroves are an additional element of the coastal zone. And the shallow shelf area east of Phuket, called **Phang-nga Bay** (fig. 3.1b, f), is geologically constituted by islands of Permian limestone (Watkinson et al., 2008). The spatial pattern of these islands as well as the form of single islands follows the structurally predetermined N-S direction (Tjia, 1996; Watkinson et al., 2008). Long-lasting tropical karstification transformed the limestone into karst towers with steep slopes to the surrounding sea. Because of the input of river sediments from the north, the inner parts of the Phang-nga Bay are characterised by

forms of coastal progradation such as deltas and tidal flats, mostly covered by *Rhizophora*-dominated mangrove forests. With diminishing input of fresh water and suspended sediment, coral reefs become a frequent feature in the south of the Phang-nga Bay (Department of Mineral Resources, 2002).
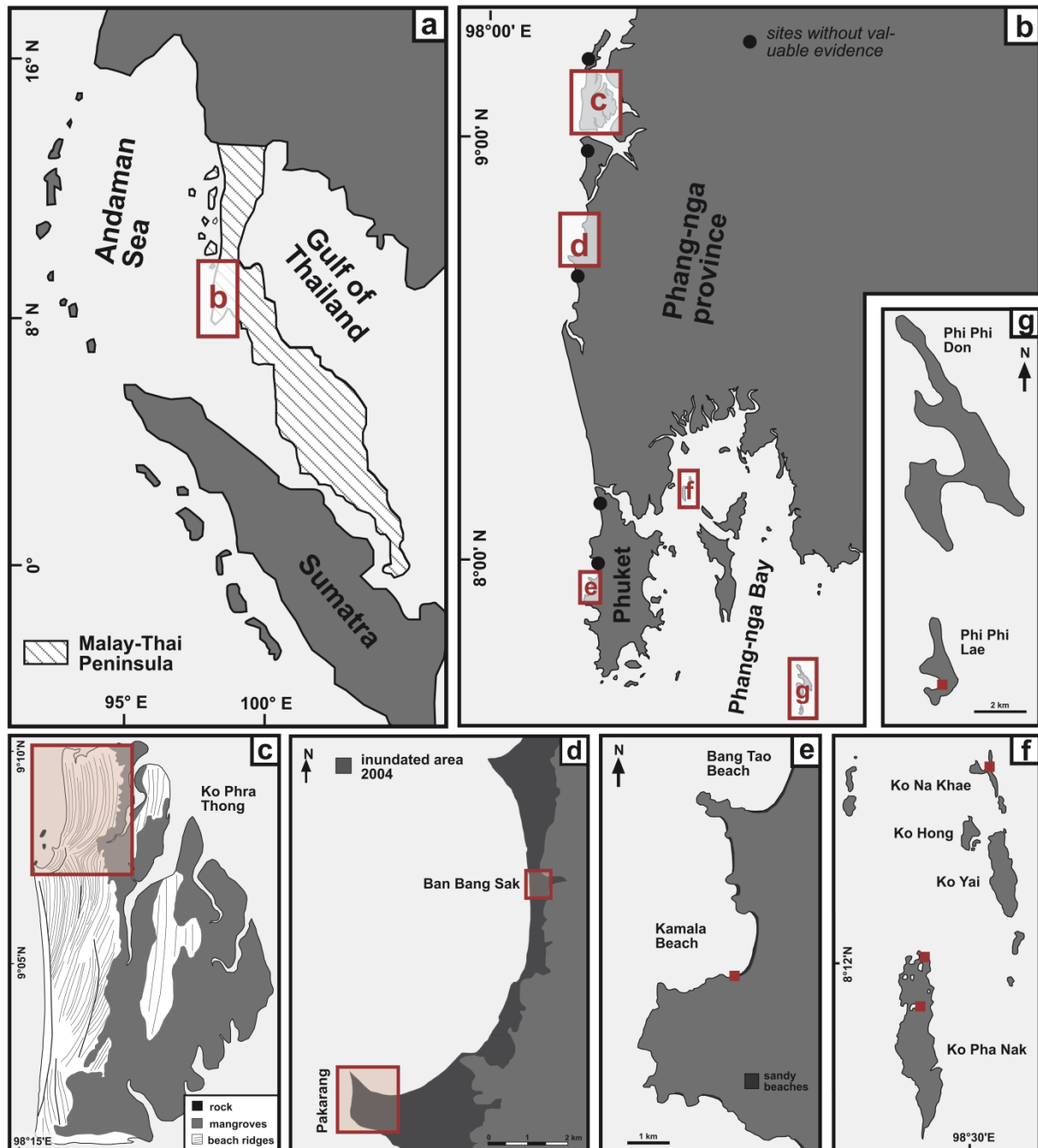
Figure 3.1: *Geographical position of the study area and locations of all study sites. (a) Malay-Thai Peninsula, (b) SW Thailand, (c) Phra Thong Island, (d) Ban Bang Sak and Pakarang, (e) Kamala Beach, Phuket, (f) Ko Pha Nak and Ko Na Khae, Phang-nga Bay, (g) Phi Phi Islands. Red squares in c-g indicate sampling locations.*

The locations intensively investigated in the course of this study, either due to evidence of palaeotsunamis or due to suitable sea-level indicators, are (i) Phra Thong Island, (ii) Ban Bang Sak, (iii) Pakarang Cape, (iv) Kamala Beach, Phuket, (v) the Phi Phi Islands, as well as

(vi) Ko Pha Nak and Ko Na Khae (fig. 3.1). While the first five sites were severely affected by the waves of the IOT 2004, the protected islands Pha Nak and Na Khae were only reached by low, refracted waves. Further sites – a mangrove forest and an artificial lagoon on Phuket, the islands Ra, Kho Khao and Hong, as well as the coastal plain at Ban Bang Niang – were visited once during the first field trip but did not provide worthwhile geoarchives. The characteristics of the investigated sites are described in the following.

(i) Phra Thong Island (Ko Phra Thong) is located 125 km north of Phuket (fig. 3.1d, c). Separated from the mainland by tidal channels, it extends 15 km in a north-south direction and 8 km from east to west. The island is formed by sequences of almost shore-parallel beach ridges and intervening swales. While the ridge plain is predominantly covered by mangroves and dense vegetation in the eastern part of the island, the western section is dominated by grassy ridges. During the IOT 2004 Phra Thong was flooded by waves higher 10 m that inundated more than 2 km inland and left behind a sand sheet of several centimetres thickness (Jankaew et al., 2008).

(ii) Ban Bang Sak. The coastal morphology of Ban Bang Sak, located c. 25 km south of Ko Phra Thong (fig. 3.1b, d), is determined by a succession of shore-parallel beach ridges and swales, which constitute a 300-600 m wide sandy plain. To the east, the coastal zone is bordered by the steep slope of the pre-Holocene bedrock; only where small rivers discharge into the sea, Holocene sediments extend further inland and form gently dipping alluvial plains. In December 2004, all low lying areas along this section of the Thai coast were flooded by 7-11 m high waves that caused severe destruction to buildings and infrastructure (amongst others the total destruction of Ban Sak School), erosion of beaches, and inland transport of sediment (Szczuciński et al., 2006; Kelletat et al., 2007; Goto et al., 2008).

(iii) Pakarang Cape is the headland south of Ban Bang Sak, only 13 km north of the tourist centre Khao Lak (fig. 3.1d). Pakarang is a sedimentary cape that developed behind a Holocene coral reef. Today, the dead reef forms an intertidal platform at the western side of the cape. The adjacent coastal plain is flat without significant geomorphology except for some artificial lakes of former tin mining activity. It is covered with young trees and scattered houses, most of them hotels. Pakarang is the most prominent example for the morphological impact of the IOT 2004 in Thailand: field surveys and the comparison of satellite images directly before and after the event demonstrated coastal erosion of at least 30 meters (Neubauer et al., 2011), deposition of tsunamigenic sand in the coastal plain (Szczuciński et al., 2006), movement of coral boulders on the intertidal platform of the former reef (Goto et al., 2007, 2009, 2010a) and mangrove destruction along river inlets (Yanagisawa et al., 2009) by up to 9 m high waves (Goto et al., 2007).

(iv) Kamala Beach is one of Phuket's west exposed pocket beaches (fig. 3.1e). It is bordered by granite headlands to the south (Laem Son) and to the north. The waves of the IOT 2004

reached heights of 9 m (Kelletat et al., 2007) and generated onshore tsunami deposits several centimetres thick (Choowong et al., 2008c).

(v) The Phi Phi Islands lie at the southern margin of the Phang-nga Bay (fig. 3.1g), where the water is 20–30 m deep immediately at the shoreline. In consequence, the wave impact from the Andaman Sea is stronger than in the protected parts of the bay, which results in more extended beaches and tombolo formation on Phi Phi Don. The islands were flooded by IOT 2004 waves up to 9 m high and inundating more than 400 m inland (Hawkes et al., 2007). Besides deposition of onshore tsunami sediment, the waves caused minor damage to coral colonies (Department of Marine and Coastal Resources, 2005; Kelletat et al., 2007).

(vi) Ko Pha Nak and Ko Na Khae (fig. 3.1f) are towerkarst islands in the shallow (only 5-10 m water depth) central part of Phang-nga Bay with steep, nearly vertical coasts. Both islands show several "hongs", water filled karst depressions within the island that are connected with the sea by submarine caves, and narrow sand beaches in front of the cliff-like limestone walls. Since the islands are uninhibited, no impact of the IOT 2004 is documented.

3.2   The probability of seismically induced tsunamis

Globally, more than 80% of all reported tsunamis have been generated in subduction zones (Sugawara et al., 2008). This is true for the Indian Ocean as well, where most recorded tsunamis have their origin in one of the seismically active subduction zones offshore Pakistan/Iran or along the Sunda Arc (fig. 3.2): (I) Makran Zone, (II) Myanmar-North-Andaman Zone, (II) North-Sumatra-Andaman Zone, (IV) Nias Zone, (V) Sumatra-Mentawai Zone, and (VI) Java Zone (Okal and Synolakis, 2008). The segmentation of the Sunda Arc in five zones is based on tectonic features on the down diving plate. These features define areas of predominantly aseismic slip or strain release by many small ruptures between the five zones and, thereby, inhibit joint ruptures of neighbouring segments (Newcomb and McCann, 1987; Briggs et al., 2006). The potential of subduction zones to trigger tsunamis is determined by all factors that influence the magnitude and the frequency of tsunami waves. This includes the seismic moment of the earthquake, which is dependent on the vertical slip and the rupture length, the directivity of the source area that is reflected in the direction of wave propagation, the water depth at the source area, the convergence rate of the tectonic plates, the rigidity of the crust, which is age dependent, the relationship between seismic and aseismic stress release, and the stress transfer between neighbouring segments during strong ruptures (Chlieh et al., 2008; Okal and Synolakis, 2008; McCloskey et al., 2008). As a result, all subduction zones except the North-Sumatra-Andaman Zone trigger tsunamis that are not a threat for Thailand:
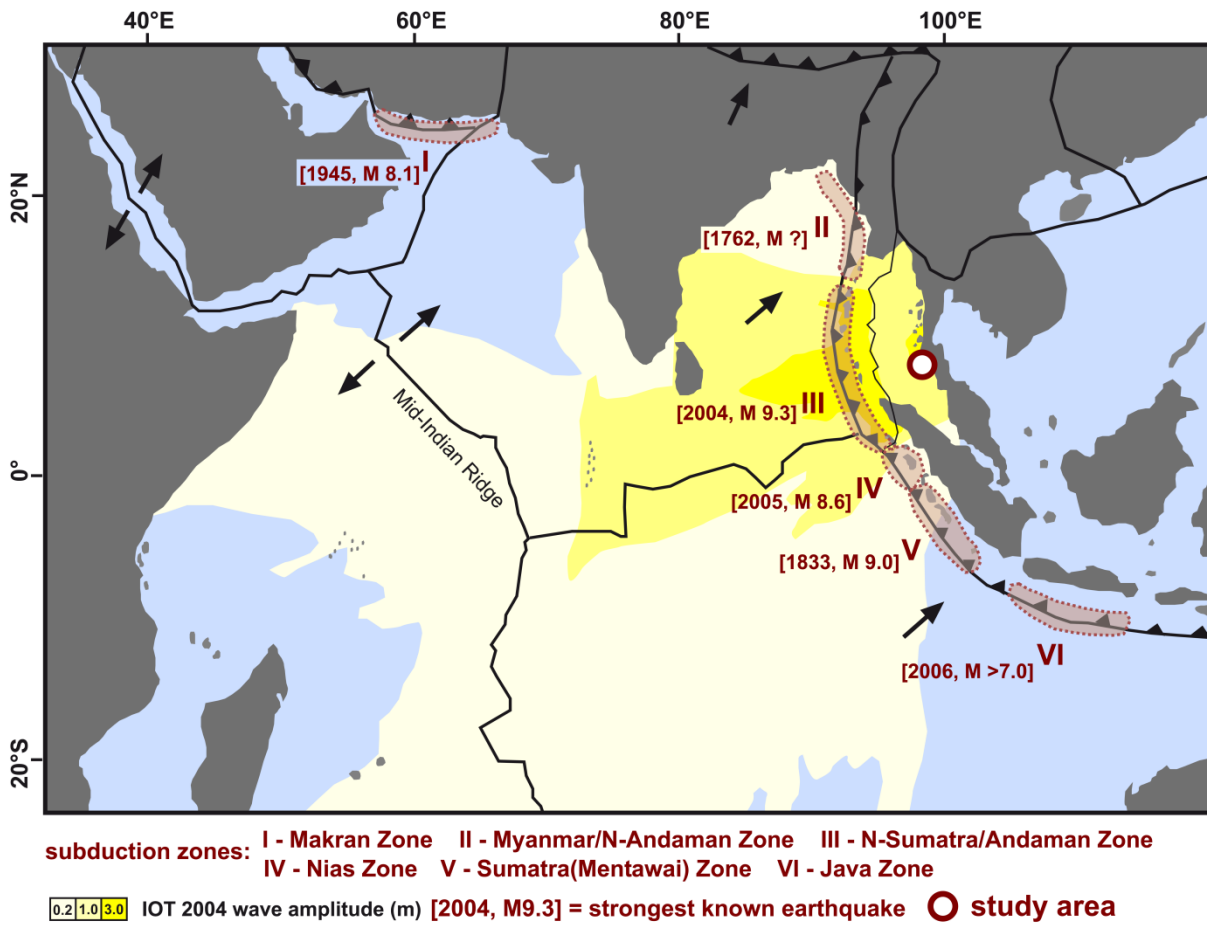
Figure 3.2: *Main tectonic structures of the Indian Ocean. Potential source areas of seismic tsunamis (subduction zones) and the strongest known earthquakes of each segment are presented following Okal and Synolakis (2008) and Lay et al. (2005). The wave pattern of the IOT 2004 is plotted according to Subarya et al. (2006).*

(I) Makran Zone. A strong historical earthquake that triggered a tsunami with regional impact in Oman and on the Seychelles happened in 1945 AD (Shah-hosseini et al., 2011). Further ruptures occurred in 1851-1864 AD, 1765 AD and 1483 AD. But even modelled worst case scenarios of the resulting tsunamis had no impact on the Bay of Bengal (Okal and Synolakis, 2008).

(II) Myanmar-North-Andaman Zone. Only a single well constrained historical earthquake is reported from this segment (April 2, 1762 AD). It generated a tsunami that had a historically documented impact on Myanmar and Bangladesh. Modelling of the event also suggests slight impact in eastern India and Sri Lanka (Cummins, 2007). However, models of all thinkable future events, even worst case scenarios, show insignificant tsunami heights for Thailand (Okal and Synolakis, 2008), because the general physiographic conditions may lead to strong earthquakes but do not favour the generation of mega tsunamis comparable to the IOT 2004 further south (Gupta and Gahalaut, 2009; Kundu and Gahalaut, 2010; Khan, 2012).

(IV) Nias Zone. Strong historical ruptures connected with several metres of uplift and subsidence (Briggs et al., 2006), as well as local tsunami inundation along several 100 kilometres of the northern Sumatra coast occurred in 2005 AD (M_w8.6), 1907 AD (M_w7.8), and 1861 AD (M_w8.5) (Newcomb and McCann, 1987; Lay et al., 2005; Kanamori et al., 2010). None of them affected the coast of Thailand.

(V) Sumatra-Mentawai Zone. The biggest earthquake in historical times with 550 km rupture length, 13 m vertical slip and a magnitude of M_w9.0 occurred in November 1833 AD (Lay et al., 2005; Okal and Synolakis, 2008). The associated tsunami had documented impact at the west coast of Sumatra, and on the Seychelles (Newcomb and McCann, 1987); inundation on Madagascar, the Mascarenas, in South Africa, Somalia, and Oman, locally four times stronger than 2004, is suggested by numeric modelling. However, even modelled worst case scenarios have no impact on the Thai coast (Okal and Synolakis, 2008). Further historical tsunamis generated at the Mentawai segment, e.g. by the M_w8.4 earthquake in 1797 AD, caused only flooding on Sumatra and its offshore islands (Newcomb and McCann, 1987).

(VI) Java Zone. Due to the old age of the oceanic crust south of Java, the subduction zone is supposed to be less tsunamigenic. Historical ruptures in 2006 AD, 1994 AD, 1840 AD and 1859 AD caused only small tsunamis on Java and along northern Australia (Newcomb and McCann, 1987; Dawson et al., 1996b). Models of worst case ruptures and tsunamis definitely exclude consequences for Thailand.

Tsunamis that are a threat for the coast of SW Thailand are generated exclusively along the North-Sumatra-Andaman Zone (Okal and Synolakis, 2008). Tectonically, it can be divided into three segments that either rupture separately or together (Lay et al., 2005): the North Sumatra Segment (420 km), the Nicobar Segment (325 km), and the Andaman Segment (570 km). The only example for a mega-rupture of all three segments is the earthquake of December 2004 with a rupture length of 1300-1600 km (fig. 3.3), 15-20 m vertical slip, and a magnitude of M_w9.1-9.3 (Lay et al., 2005; Subarya et al., 2006). Uplift and subsidence of up to 5 m were observed from the Simeulue Islands offshore Sumatra to the Andaman Islands (Bilham et al., 2005; Briggs et al., 2006; Kayanne et al., 2007; Som et al., 2009; Narayana, 2011). The associated tsunami was triggered in the southern 600-800 km of the rupture area (Lay et al., 2005) and significantly affected coastal areas on Sumatra, in Thailand, in India, on Sri Lanka, the Maldives, the Andaman and Nicobar Islands, as well as in eastern Africa (Okal and Synolakis, 2008). While waves >10 m were recorded in southwest Thailand (Tsuji et al., 2006), as far as 20,000 km away amplitudes of several decimetres were observed (Titov et al., 2005).

Historically, only three other ruptures in the North-Sumatra-Andaman Zone have been recorded (fig. 3.3): the June 26, 1941 AD earthquake with a magnitude of M_w7.9 affected only the Andaman Segment. Although it was accompanied by subsidence and uplift on the Andaman Islands, the amplitude of the associated tsunami which was recorded by tide gauges in

India was too small to cause inundation at the Thai coast (Bilham et al., 2005). Similarly, the December 1881 AD and October 1847 AD ruptures were restricted to the Andaman Segment and had magnitudes < M_w8.0. The associated tsunamis that were recorded by tide gauges around the Bay of Bengal were not accompanied by significant flooding or sediment movement (Bilham et al., 2005). These observations are supported by numerical models, which predict that maximum tsunami waves of 2 m at the Thai coast can be generated by partial ruptures of the Andaman and Nicobar segments, i.e. by earthquakes of magnitude M_w8.5 or smaller (Løvholt et al., 2006). However, geological evidence of prehistoric events in the form of strong uplift and subsidence (Rajendran et al., 2008; Meltzner et al., 2010, Malik et al., 2011; Grand Pre et al., 2012), as well as onshore tsunami deposits (e.g. Jankaew et al., 2008; Monecke et al., 2008; Dahanayake and Kulasena, 2008; Fujino et al., 2009; Rajendran et al., 2011; Nair et al., 2011) documents that the IOT 2004 was not a one-time phenomenon.
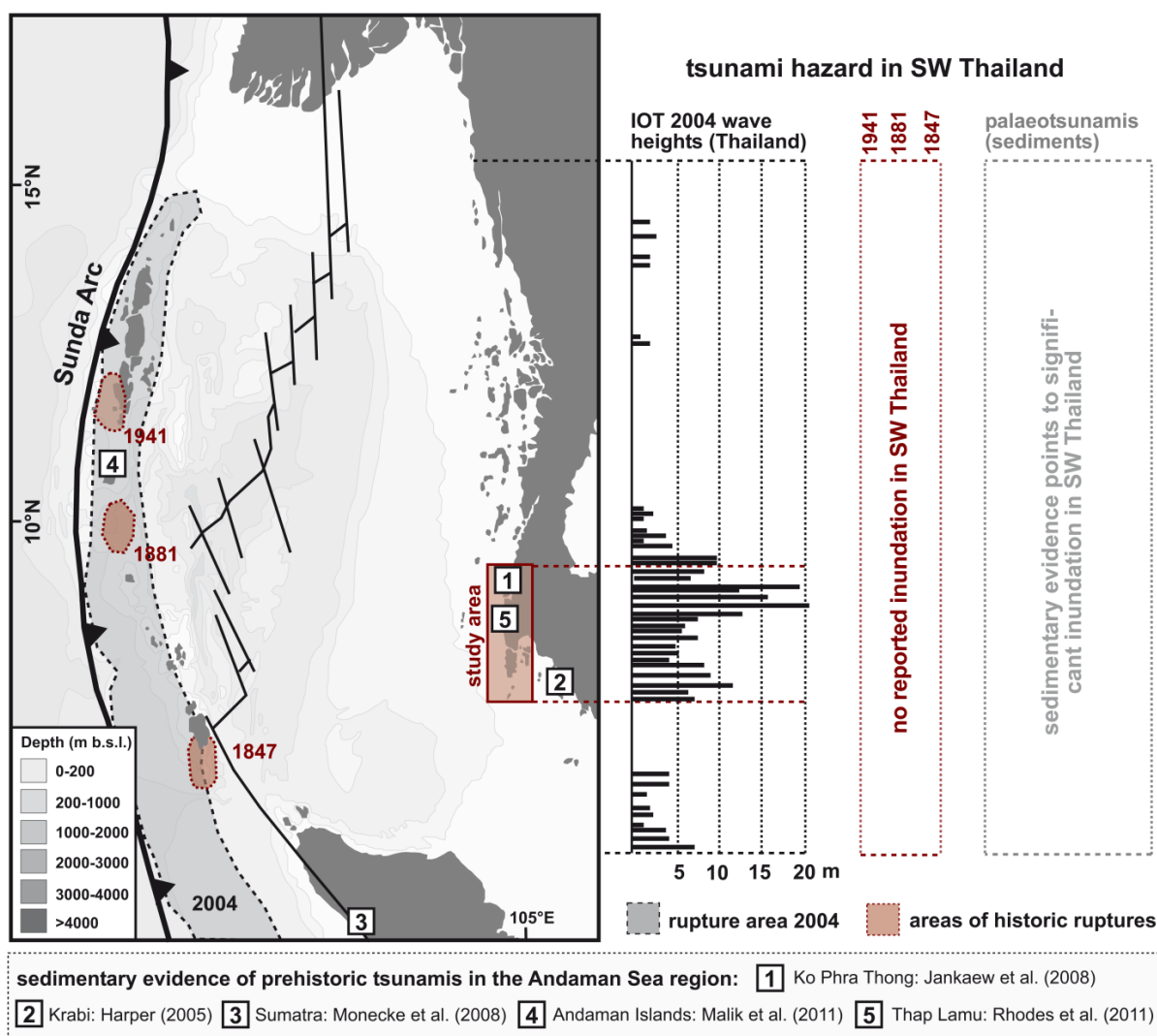
Figure 3.3: Tsunami risk in the Andaman Sea. Rupture areas of the IOT 2004 according to Subarya et al., (2006) and historic earthquakes in 1941 AD, 1881 AD and 1847 AD following Ortiz and Bilham (2003) and Bilham et al. (2005). While the IOT 2004 caused significant inundation and run-up along the Thai coast (Tsuji et al., 2006; Satake et al., 2006), no significant tsunami waves are reported for the historic events (Bilham et al., 2005). However, geological findings demonstrate that the IOT 2004 was not a one-time phenomenon.

However, historical events provide no sufficient statistical basis to determine recurrence intervals of mega-ruptures in the North-Sumatra-Andaman Zone. Alternatively, the rate of stress accumulation by plate convergence is used to estimate return periods of mega-ruptures, leading to 230-600 years, if the release of stress is only due to mega-ruptures (minimum value), or 460-1200 years, if 50% of stress is released by aseismic slip and small ruptures (Bilham et al., 2005; Subarya et al., 2006;). Løvholt et al. (2006) suggest a 400 year recurrence period as a reasonable value. This value is approximately supported by geological evidence of prehistoric earthquakes (Rajendran et al., 2008; Meltzner et al., 2010). The average recurrence interval of smaller earthquakes on the basis of convergence rates is estimated to be 270 years for $M_w8.5$ ruptures, with a higher frequency of 200 years in the south and a longer return period of 400 years in the north, and 114-200 years for earthquakes of M_w8 or smaller (Løvholt et al., 2006).

An additional source of tsunamis that has not been studied sufficiently yet might be submarine landslides at the shelf slope triggered by earthquakes or venting of gas-hydrates (Jintasaeranee et al., 2008; Krastel, 2011). Although there is evidence of several submarine slope failures, they could not be linked successfully to tsunamis yet (Brune et al., 2010).

3.3   The probability of tropical cyclones

The Bay of Bengal is located in a sub-humid, tropical climate characterised by heavy rainfall during the summer monsoon and a dry season from December to February. In the transitional periods from April to May and September to November tropical storms may occur, since the sea surface temperatures exceed 27 °C (Brown et al., 1996) and the Coriolis force is strong enough for cyclone generation (Pielke and Pielke, 1997). Besides tsunamis, tropical storms are the second type of rapid-onset hazard threatening the world's coastlines. Especially in connection with storm surges "tropical cyclones kill more people and cause more insured losses than any other natural disaster" (Murnane and Liu, 2004). According to Murty et al. (1986) the most deadly storm surges – "changes in water level generated by storms passing over the sea" (Murty et al., 1986) – worldwide occur in the Bay of Bengal, where they caused more than 400,000 casualties in the 1960s alone. More than half of it died during the disastrous 1970 storm surge in Bangladesh (Flierl and Robinson, 1972). Especially where local factors such as a large shelf area, a focusing shape of the coastline, or high tidal ranges amplify the surge height, extreme water levels may be generated (Flierl and Robinson, 1972). However, in SW Thailand, where normal coastal dynamics are controlled by moderate waves with heights of 2-3 m and tides in a range of 1.5–3.5 m (Choowong et al., 2008a), not a single storm surge was observed during the last 150 years of weather recording (Phantuwongraj and Choowong, 2011).

The reason for this lack of storm surges is the general pathway of tropical cyclones in the Bay of Bengal (fig. 3.4). Storm track data since 1891 document that the general movement of cyclones is directed towards the coasts of India and Bangladesh; less frequently the pathways cross Sri Lanka and Myanmar (Singh, 2000; India Meteorological Department, 2007). In contrast, not a single cyclone crossed the coast of SW Thailand (Murty et al., 1986). The tropical storm that made landfall closest to the study area was cyclone Nargis in 2008, which hit the coast of Myanmar and caused more than 100,000 casualties and economic losses of 10 billion US$, especially in the Irrawaddy Delta (Fritz et al., 2009a; Shen et al., 2010). However, making landfall 800 km to the north, southwest Thailand was not affected by this event. Furthermore, typhoons generated over the Pacific Ocean rarely cross the border between the Gulf of Thailand and the Andaman Sea, and the few exceptions loose most of their energy while crossing the landmass of southern Thailand (Singh, 2000). Thus, typhoons seem to affect only the east coast of Thailand, where they frequently cause economic damage as well as erosion and deposition in the low lying coastal areas (Phantuwongraj and Choowong, 2011). The most destructive storms that crossed the land barrier between the Gulf of Thailand and the Andaman Sea within the last century were Typhoon Gay in 1989, Typhoon Harriet in 1962 that caused a storm surge with 900 casualties along the Gulf of Thailand, and Typhoon Linda in 1997 (Phantuwongraj and Choowong, 2011). All of them had no significant impact on infrastructure and ecosystems along the west coast of Thailand (UN Department of Humanitarian Affairs, 1989).
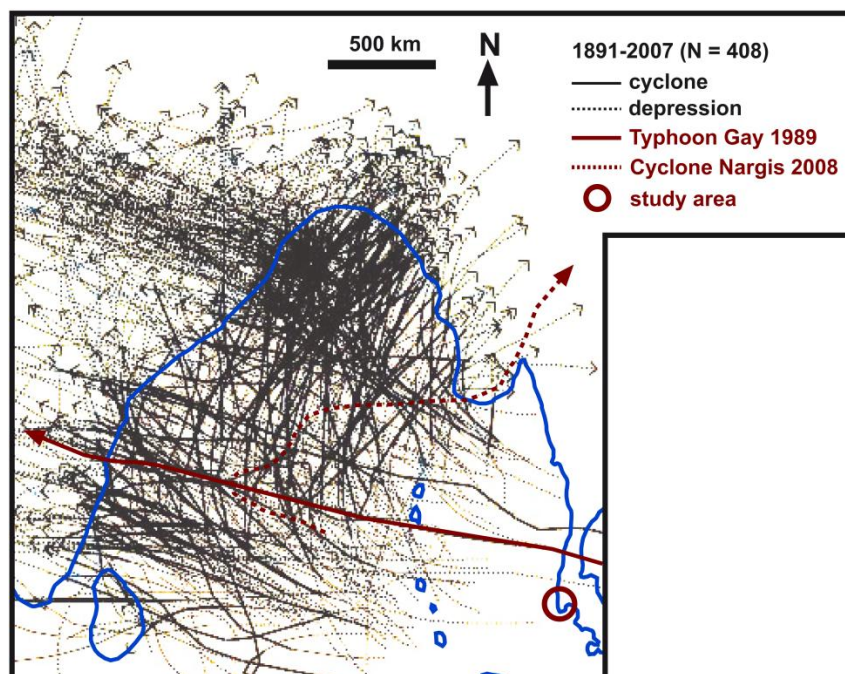
Figure 3.4: *Storm tracks in the Bay of Bengal. The general pathway of tropical cyclones is directed to the coasts of Sri Lanka, India, Bangladesh and Myanmar (based on recorded storms between 1891 and 2007: India Meteorological Department, 2007). Examples for storms with landfall comparatively close to the study area are Cyclone Nargis in March 2008 (Shen et al., 2010) and Typhoon Gay in 1989 (Joint Typhoon Warning Center, 1989).*

Chapter 4

4 Potential predecessors of the 2004 Indian Ocean Tsunami – Sedimentary evidence of extreme wave events at Ban Bang Sak, SW Thailand[1]

Abstract: Where historical records are short and/or fragmentary, geological evidence is an important tool to reconstruct the recurrence rate of extreme wave events (tsunamis and/or storms). This is particularly true for those coastal zones around the Indian Ocean, where predecessors of similar magnitude as the 2004 Indian Ocean Tsunami (IOT) have not been reported by written sources. In this context, the sedimentary record of the Holocene coastal plain of Ban Bang Sak (Phang-nga province, Thailand) provides evidence of multiple prehistoric coastal flooding events in the form of allochthonous sand beds, which were radiocarbon dated to 700–500, 1350–1180, and younger than 2000 cal BP. The layers were assigned to high-energy events of marine origin, which could be either tsunamis or tropical storms, by means of granulometry, geochemistry, vertical structure, and macrofossil content. Although no landfall of a strong storm has occurred in the last 150 years of meteorological data recording, cyclones cannot be ruled out for the last centuries and millennia. However, discrimination between tsunami and storm origin was mainly based on the comparison of the palaeoevent beds with the local deposit of the IOT, which revealed similar characteristics in regard to spatial extend and sediment properties. Furthermore, the youngest palaeoevent correlates with contemporaneous deposits from Thailand and more distant coasts. Hence, we relate it to a basin wide tsunami which took place 700-500 years ago. For the sediments of older extreme events, deposited between 2000 and 1180 cal BP, we found no unambiguous counterparts at other sites; nevertheless, at least for now, they are treated as tsunami candidates.

Keywords: Tsunami; Palaeotsunami; Tsunami deposit; Holocene; Thailand; Sedimentology

4.1 Introduction

In December 2004, the Indian Ocean Tsunami (IOT), generated by a 1300 km long fault rupture along the Sunda Arc (Lay et al., 2005; Stein and Okal, 2007), flooded wide coastal areas around the Indian Ocean with disastrous impacts on coastal communities and infrastructure in both near-field and far-field locations. Different from other tsunami risk regions with long

---

tsunami records (Soloviev et al., 2000 for the Mediterranean; Nanayama et al., 2003 for Japan; Lau et al., 2010 for NE South China Sea), historical tsunami catalogues for the Indian Ocean are primarily restricted to the last 400 years and therefore providing little information about the long-time hazard of the region. Where available, the rare historical data for longer timescales are imprecise and questionable (Murty and Rafiq, 1991; Kumar and Achyuthan, 2006; Rastogi and Jaiswal, 2006; Dominey-Howes et al., 2007). Thus, in most affected regions, the disaster struck completely unexpected.

Geological archives which often extend back thousands of years and might give insights into the recurrence rate of prehistoric tsunamis, provide the opportunity to enhance the historic record (Atwater, 1987; Dawson et al., 1988; Goff et al., 2001; Nanayama et al., 2003; Pinegina et al., 2003; Cisternas et al., 2005; Engel et al., 2010; May, 2010). Thus, the IOT 2004 not only offered the possibility to study the characteristics of modern tsunami deposits (Richmond et al., 2006; Szczuciński et al., 2006, 2007; Bahlburg and Weiss, 2007; Hori et al., 2007; Srinivasalu et al., 2007; Morton et al., 2008; Paris et al., 2009) but also initiated the search for palaeotsunamis along the coasts around the Indian Ocean (Rajendran et al., 2006; Dahanayakeand Kulasena, 2008; Jankaew et al., 2008; Monecke et al., 2008). However, due to the low preservation potential under tropical climates (Szczuciński et al., 2007; Szczuciński, 2010) and the scarcity of natural low-energy environments with high resolution archives of extreme events (storm and/or tsunami), such as lagoons, lakes and marshes, a precisely dated calendar of Holocene tsunamis for the Indian Ocean remains to be defined.

For the coast of Thailand, where the waves of the IOT were second in height only to northern Sumatra, palaeotsunami information is rare. The only well documented evidence so far originates from the island Phra Thong, where several sand sheets, inferred to be tsunamigenic, have been deposited in the swales of a wide beach-ridge plain (Jankaew et al., 2008; Fujino et al., 2009). In this paper, we present data from Ban Bang Sak (Phang-nga province) and offer additional evidence of potential palaeotsunamis along the west coast of Thailand.

4.2 Physical setting

The coastal plain of Ban Bang Sak is located on the west coast of southern Thailand, 80 km north of Phuket and 30 km south of Phra Thong (fig. 4.1a). SW Thailand is part of the Malay-Thai Peninsula, bordered by the Gulf of Thailand to the east and the Andaman Sea to the west. In contrast to the wide and flat coastal plain of the gulf coast, which is dominated by lagoons, coastal lakes, cheniers and marshes, the western side of the peninsula is dominated by mountain chains extending close to the Andaman Sea. Hence in this area, the coastal morphology is characterised by steep, rocky headlands and eroded cliffs. Especially along the coast of Phuket, these capes are only interrupted by narrow pocket beaches and alluvial plains (Dheeradilok, 1995), whereas Holocene sediments in form of intertidal flats, sandy beaches

and barrier islands occupy wider areas further north in the Phang-nga province (Sinsakul, 1992; fig. 4.1b). The offshore morphology to the west of the study area is generally flat and gently sloping, reaching only 20 m water depth at a distance of 12 km from the coast (Szczuciński et al., 2006). Moreover, the near-shore bathymetry, which is of importance for the propagation of tsunami waves, shows no irregularities west of Ban Bang Sak and is constantly dipping with 0.09° (Di Geronimo et al., 2009).
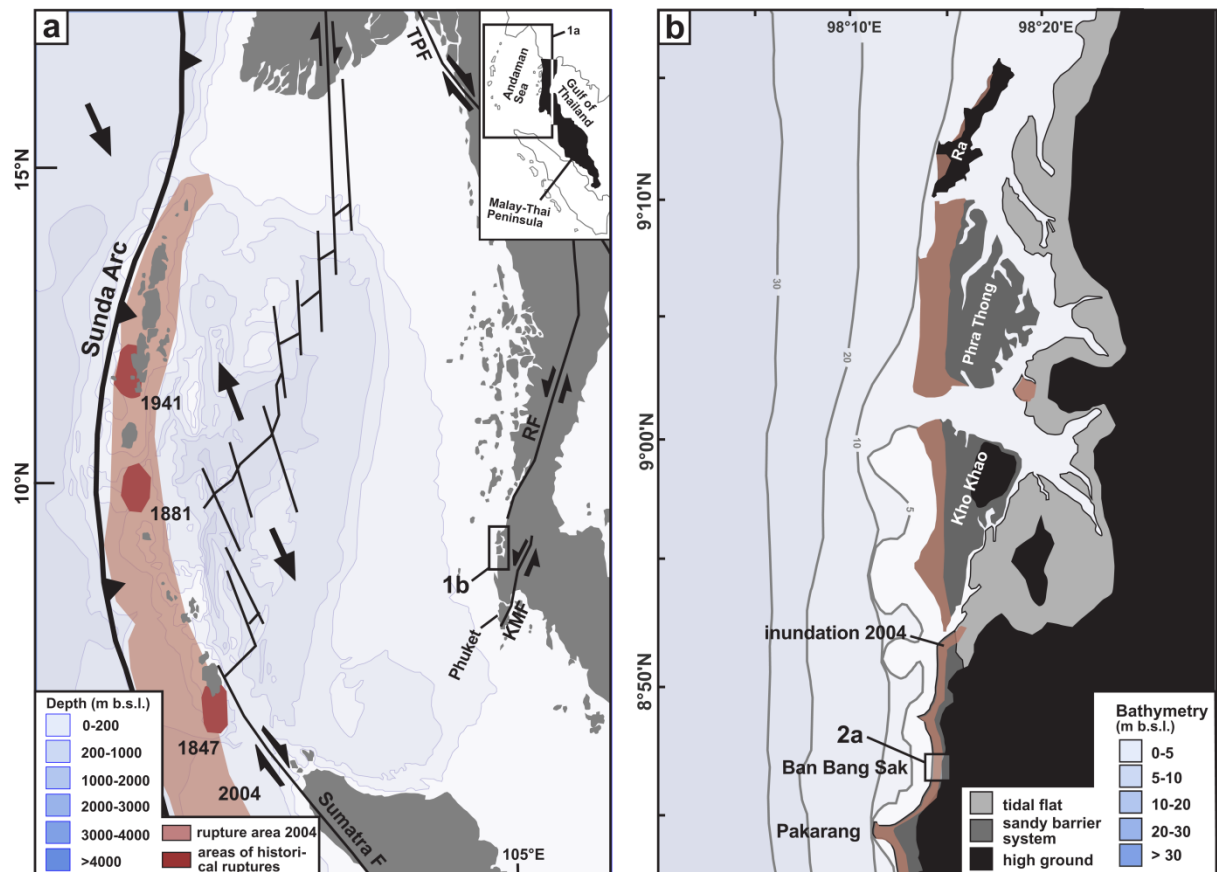
Figure 4.1: Geographical and tectonic setting of the study area. (a) Plate boundaries and tectonic faults in the Andaman Sea region (after Watkinson et al., 2008; KMF=Klong Marui Fault, RF = Ranong Fault, TPF = Three Pagodas Fault) with rupture areas of the 2004 megathrust (Subarya et al., 2006) and historical earthquakes (Ortiz and Bilham, 2003; Bilham et al., 2005) along the Andaman-Nicobar segment of the Sunda Arc. (b) West coast of southern Thailand between Khao Lak and Ra Island. The location of Ban Bang Sak, the inundation area of the IOT (Fujino et al., 2009), as well as coastal environments (Sinsakul, 1992) are indicated.

In a tectonic context, the Malay-Thai Peninsula is part of the relatively stable Sunda Plate (Tjia, 1996), where tectonic movement is limited to small rates of uplift on the west coast and slight subsidence in the east (Dheeradilok, 1995). The main tectonic structures of the region, the NE-SW trending Ranong and Klong Marui faults, have exhibited little tectonic activity during the Holocene (Watkinson et al., 2008). Seismically active zones are found to the west of the study area. The Sunda Arc subduction zone, where the Australian−Indian Plate and the Sunda and Burma Microplates converge with a mean velocity of 4-5 cm per year (Lay et al., 2005), is a major source of earthquakes. As observed in December 2004, giant submarine

earthquakes generated by ruptures of the plate boundary are capable of producing tsunami waves strong enough to reach the Thai coast. While basin wide tsunamis along the Sunda fault are commonly generated by megathrust earthquakes similar to the December 2004 event (Lay et al., 2005; Subarya et al., 2006), all historical ruptures were restricted to smaller segments of the subduction zone, hence releasing much less energy. Historical earthquakes noted for the Andaman-Nicobar segment (Bilham et al., 2005; fig. 4.1a), where tsunamis are generated, which can potentially reach the study area, did not affect the Thai coast significantly (Okal and Synolakis, 2008). Based on earthquake statistics and subduction rates Løvholt et al. (2006) postulated a mean recurrence interval of at least 300-400 years for a rupture of the Sunda fault similar to that of 2004 and 200 years for magnitude 8.5 earthquakes along the Andaman and Nicobar segment, which still might cause tsunamis reaching the coast of Thailand. Evidence of co-seismic movement in form of uplifted coral terraces along the Andaman and Nicobar Islands dated to 600 cal BP and 1000 cal BP by Rajendran et al. (2008) supports this recurrence interval of mega ruptures. However, in the absence of historical data, this assumption can only be validated by means of sedimentary evidence.

Climatically, SW Thailand is located in the sub-humid tropics with heavy rainfall during the summer monsoon and a dry period from December to February. Normal coastal dynamics are controlled by moderate waves with heights >2 m and tides in a range of 1.5-3.5 m. Higher waves are common during the summer monsoon (Choowong et al., 2008a). Furthermore, north of 5° N, where the Coriolis force is still strong enough (Pielke and Pielke, 1997), the inter-monsoon periods from April to May and September to November are characterised by the occurrence of tropical storms. However, typhoons generated in the South China Sea commonly loose energy when they cross the Malay-Thai Peninsula and the cyclone tracks in the Bay of Bengal are predominantly directed to the coasts of India, Bangladesh and Myanmar (Singh et al., 2000). In contrast, the west coast of the Malay-Thai Peninsula has not been affected by the landfall of tropical storms within the last 150 years (Murty and Flather, 2004). Nevertheless, due to rare events such as cyclone Nargis in 2008 that hit the coastline of southern Myanmar only 800 km north of the study area and flooded wide areas of the Irrawaddy delta (Fritz et al., 2009a), we cannot definitely rule out the occurrence of tropical storms with landfall in the research area for the past centuries or millennia.

4.3   Methods

The stratigraphical data presented in this paper were obtained from vibracores taken with an Atlas Copcomk1 corer and a hydraulic lifter. Penetration reached maximum depths of 9 m below the ground surface (b.s.) using core diameters of 6, 5 and 3.6 cm. Open sediment cores were photographed, described and sampled directly in the field. To establish an on-site facies stratigraphy the sediment was characterised in terms of colour, sedimentary structure and

macrofossils. Grain size, sorting and carbonate content were estimated following Ad-hoc-Arbeitsgruppe Boden (2005). Subsequently, each sedimentary stratum was sampled for further laboratory analyses. Additionally, closed sediment cores in plastic tubes were recovered from important stratigraphical sections and surface sediment samples were taken to provide a reference for recent environments. A differential GPS (Leica SR 530) with an accuracy of less than 3 cm was used to measure the position and elevation of each coring site as well as to reconstruct the topography of the study area.

To characterise the transport and sedimentation conditions, which formed the event deposits, as well as the source area of the material, we determined granulometric parameters (Morton et al., 2007) and the geochemical composition (Minoura et al., 1994; Szczuciński et al., 2007). Grain-size analyses were performed on dried fine-sediment samples (>2 mm) after treatment with H_2O_2 to remove organic matter using a laser particle sizer (Beckmann Coulter LS13320 Mikro). For the calculation of grain-size statistics after Folk and Ward (1957), the GRADISTAT software was applied (Blott and Pye, 2001). Geochemical data include loss on ignition (LOI), determined by oven-drying at 105 °C for 12 h and ignition in a muffle furnace at 550 °C for 4 h (Beck et al., 1995). $CaCO_3$ was measured gas-volumetrically after the Scheibler method. Flame atomic absorption spectrometry (Perkin Elmer A-Analyst 300) was used to determine the element concentrations of calcium (Ca), magnesium (Mg), iron (Fe), sodium (Na) and potassium (K) after digesting samples with concentrated HCl (37%). To establish a chronological framework, we dated macrofossil and plant remains by means of AMS-[14]C. Measurements were carried out at the radiocarbon laboratory of the University of Georgia at Athens (USA). Calendar ages were calculated from conventional radiocarbon years by means of the OxCal 4.01 software using the IntCal09 and Marine09 calibration curves of Reimer et al. (2009). For marine species we considered a regional marine reservoir effect of ΔR=−2 as recommended by Southon et al. (2002). All ages are presented in 2 σ sidereal years.

4.4 Evidence of extreme wave events in near-shore geo-archives of Ban Bang Sak

4.4.1 The Holocene stratigraphy of coastal sediments

The coastal geomorphology of Ban Bang Sak consists of a succession of shore-parallel beach ridges and swales, which form a 300 m wide sandy plain (fig. 4.2). 24 vibracores taken along three transects perpendicular and parallel to the coastline allowed the definition of the general stratigraphy of the coastal sediment succession. For all cores, four main sediment units with comparable sedimentary and geochemical characteristics were distinguished (units 1-4; unit 4 was divided into subunits 4a, 4b and 4c). These units made up the stratigraphy of all 24 sediment cores. Based on their succession from base to ground surface, two main types of stratigraphy, representative for the whole transect, were identified (fig. 4.3). Succession A (represented by BBS 12) documents the characteristic internal structure of the beach ridges (ridges

I, II and III in fig. 4.2); succession B (represented by BBS 1) is a representative for the area of the swales (swales I and II in fig. 4.2). All other cores of the transect show a similar stratigraphy as either BBS 12 (cores on ridges) or BBS 1 (cores in swales).
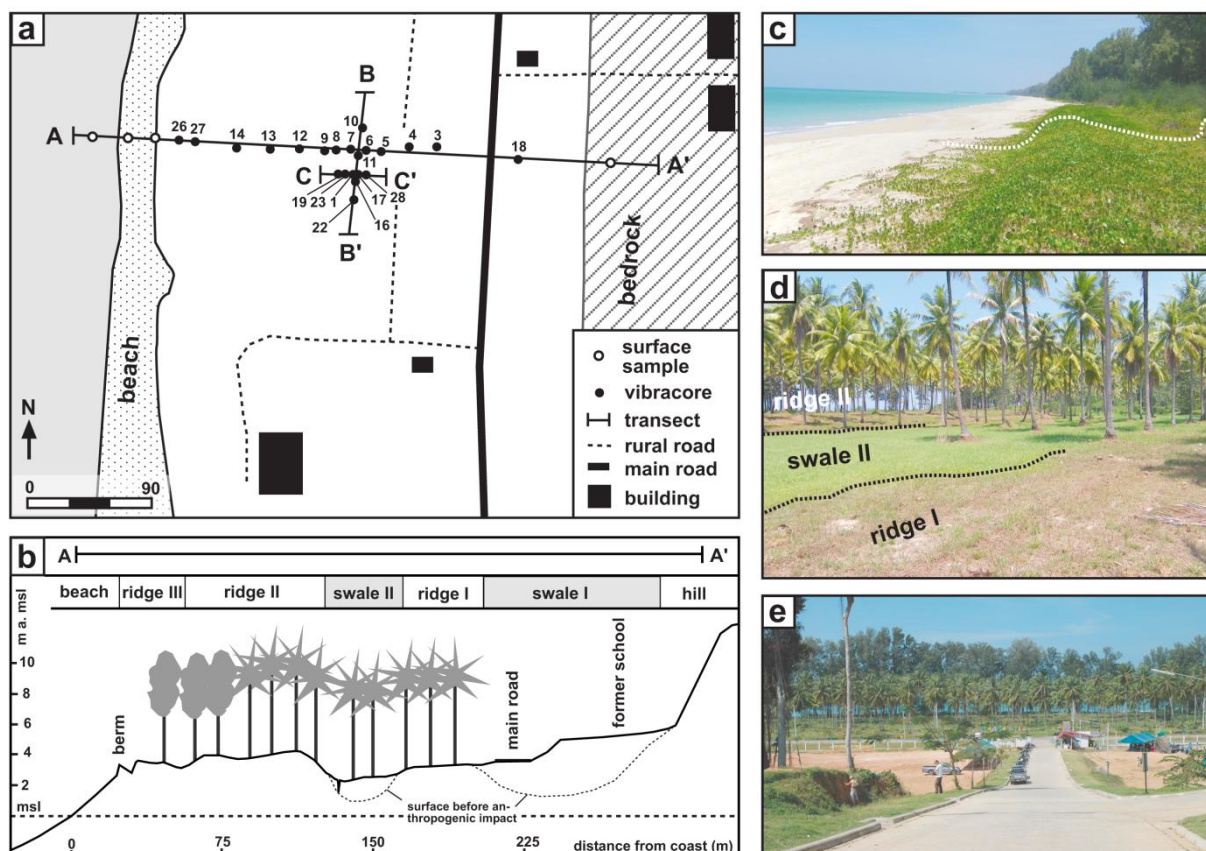
Figure 4.2: The coastal plain of Ban Bang Sak. (a) Schematic overview of the research area with positions of transects and sampling sites. (b) Topographic profile along transect A. (c) The littoral zone with beach berm and erosive scarp of the IOT. (d) View from ridge I towards the NW. The differences in vegetation cover clarify the separation into swales and ridges. (e) View from the hill at the eastern limit of the coastal plain towards the sea.

Unit 1: The deepest part of the key profiles BBS 1 and 12 as well as of all other longer cores was composed of clayey silt with low amounts of medium sand. The deposits showed little variation regarding grain size (mean = 10-22 μm, sorting = 5.5-9 μm) and chemical composition (Ca/Fe = 0-1, Na = 0-1 g/kg, Fe = 30-85 g/kg) with generally high contents of Fe, total absence of carbonate and low concentrations of water soluble salts (Na, Ca, Mg) and organic matter (0-0.6 mass-%). The colour was yellowish brown to reddish brown, occasionally white, dark brown or violet. The whole unit lacked fossils as well as organic material; macro remains were present in the form of some angular stones (quartz) and weathered rock fragments. The material was generally solid. However, in some cores, the uppermost decimetres appeared soft and showed horizontal lamination (e.g. BBS 7, 9 and 11). The only interruptions in the monotonous substrate were two thin sand sheets in BBS 12 that differed significantly from the surrounding material (described as layers C in Chapter 4.4.2).
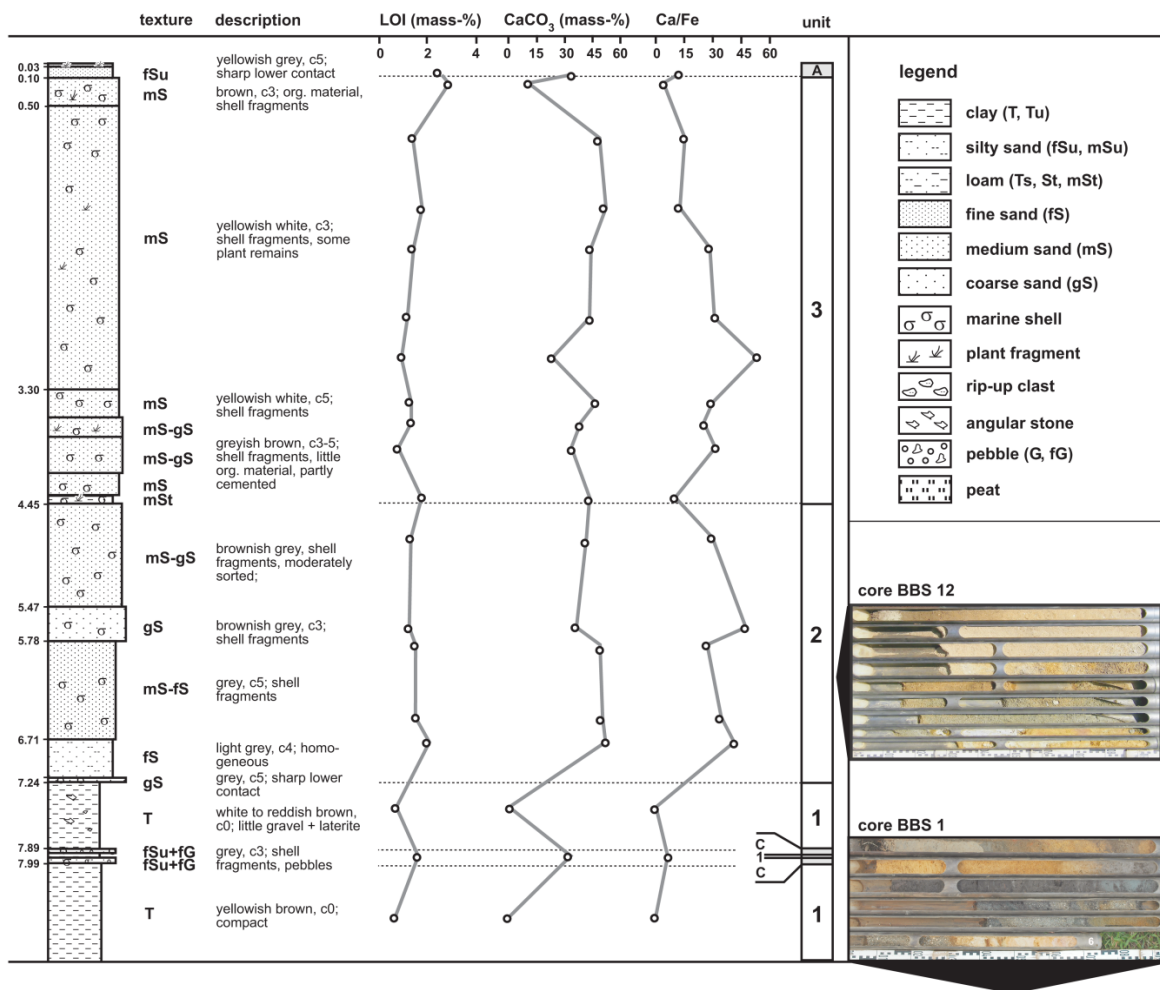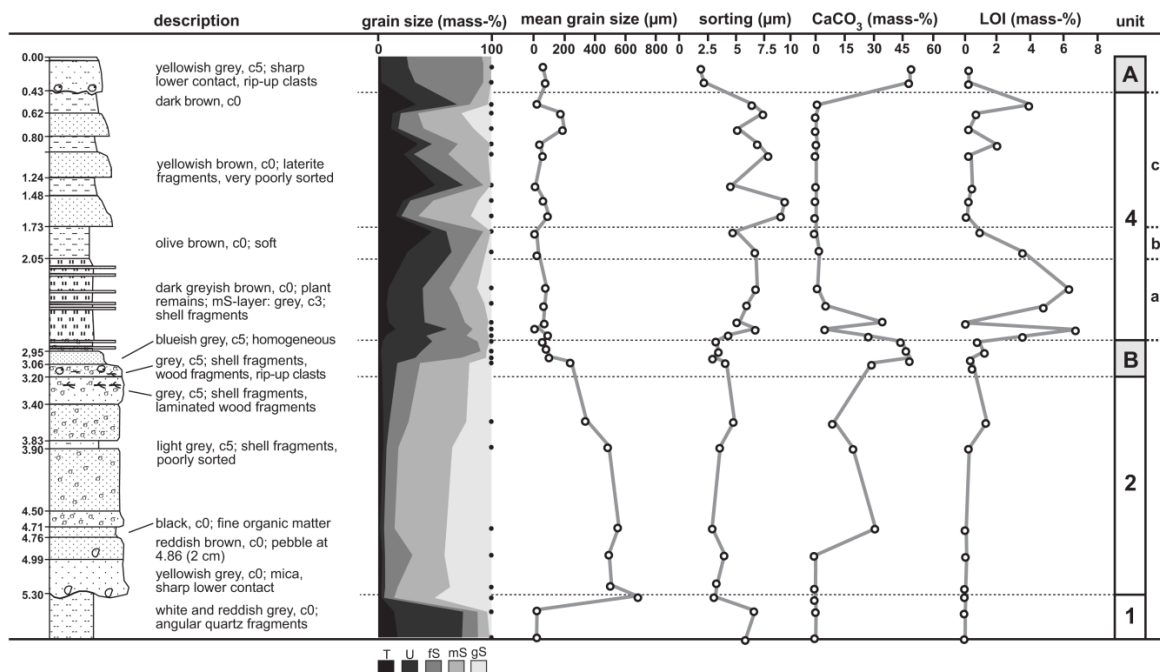
Figure 4.3: *The sedimentary record of the coastal plain. Vibracore profiles of BBS 12 (a: beach ridge) and BBS 1 (b: swale) document the typical stratigraphy of the study area.*

Unit 2: In both reference cores, a sharp contact with significant changes in colour and substrate separated the yellowish silt of unit 1 from much coarser (mean = 240-670 μm) and better sorted (sorting = 3-5 μm) grey coloured sand that contained high amounts of valves and fragments of marine shells. The substrate consisted of repeated alternations of coarser and finer sections. While the sand in BBS 12 showed a tendency from fine to coarse towards the top of unit 2, an overall fining trend was detected in BBS 1. At the basal contact of BBS 1, big rounded quartz pebbles were observed; in the upper part plant remains and wood fragments occurred occasionally. Parallel to these changes in substrate, the concentrations of carbonate (10-55 mass-%), soluble salts (Ca/Fe = 25-50, Na = 0.5-3 g/kg) and organic matter (0.5-2 mass-%) increased, while the Fe content decreased to 2-12 g/kg.

Unit 3: In BBS 12 the upper part of unit 2 formed a gradational transition from greyish brown to yellowish white sand, dominated by the medium and coarse fraction (mean = 350-500 μm, sorting = 3-4 μm). While this substrate comprised nearly the whole core section between unit 2 and the ground surface in BBS 12, it was absent in BBS 1 (fig. 4.3). Fragments and valves of marine molluscs with rounded edges and traces of abrasion were present throughout the unit. At the base, sand grains and shell fragments were cemented by a calcareous agent. Chemical changes compared to unit 2 were only minor: the contents of carbonate (25-50 mass-%), organic matter (0.5-2 mass-%) and iron (2-12 g/kg) remained more or less stable. The concentrations of soluble salts declined slightly (Na = 1-3 g/kg, Mg decreased from 2-5 g/kg to 1-2 g/kg). Differing from this general trend, a change in colour from yellowish white to dark brown at 60 cm b.s. was accompanied by enrichment in organics and decalcification (carbonate decreased to 10 mass-%). The uppermost 10 cm in BBS 12 was formed by a sheet of fine sand with sedimentary properties totally different from those of unit 3 (described as layer A in Chapter 4.4.2).

Unit 4: While unit 2 was replaced by the sand of unit 3 in BBS 12, it was covered by a succession of varying deposits in BBS 1. The sediments were free of carbonate and fossils and were restricted to the swale areas. Due to these common characteristics, they were summarised in unit 4 (fig. 4.3). In BBS 1 the lower boundary of unit 4 was formed by a 25 cm thick sand layer that differed significantly from the surrounding material (described as layer B in Chapter 4.4.2). This sand sheet was followed by a nearly 1 m thick section of dark brown, peaty silt (subunit 4a) with gradational contacts to the surrounding material. While the grain size was smaller (mean = 26-60 μm) and the sorting poorer (sorting = 4-7 μm) than in unit 2, the concentration of carbonate dropped to zero (except in some very thin sand laminae). In accordance with significantly elevated contents of fine organic matter (from 0.5-2 to 5-7 mass-%), large amounts of wood and plant fragments were embedded in the peaty substrate. Subunit 4a was followed by a 30 cm thick stratum of soft, olive brown, clayey silt (mean = 5-20 μm, sorting = 5-7 μm) that was defined as subunit 4b. The lower transition was gradational and accompanied by a successive decline in organics (1-3.5 mass-%). A sharp contact existed

at 1.70 m b.s., where the mud of subunit 4b was replaced by alternating layers of unsorted sand (mean = 70-200 µm, sorting = 7-9 µm) and slightly better sorted loamy clay (mean = 8-40 µm, sorting = 5 µm), which were classified as subunit 4c. These reddish brown deposits contained less organic material (0-0.5 mass-%) compared to subunits 4a and 4b and abundant fragments of laterite and angular quartz. It was covered by a 40 cm thick, allochthonous sheet of fine sand (layer A in Chapter 4.4.2).
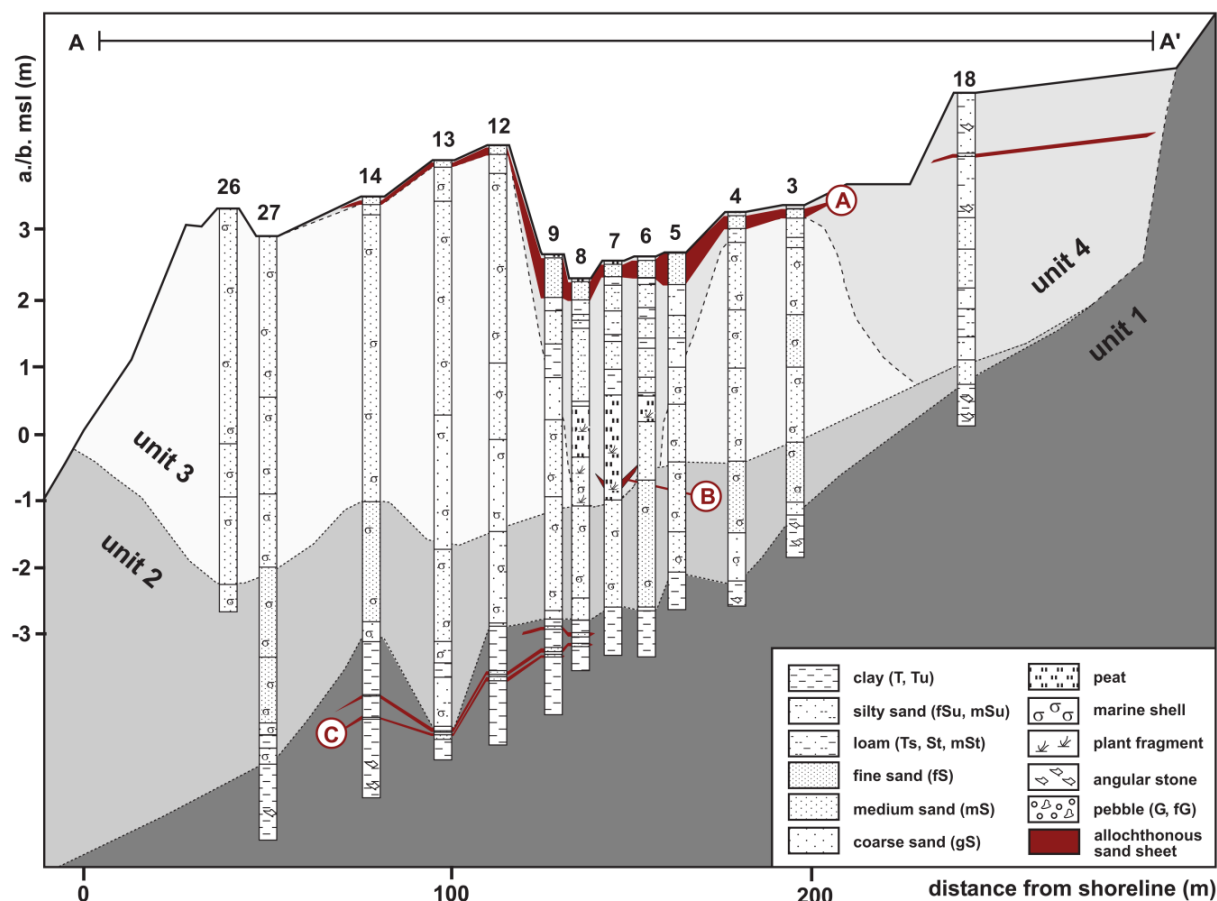
Figure 4.4: Cross section through the sedimentary succession of the coastal plain at Ban Bang Sak.

Figure 4.4 shows the spatial distribution of units 1–4 along a cross section through the coastal plain (transect A in fig. 4.2). The slightly seaward dipping surface of Unit 1 proceeded from 5 m below sea level (b.s.l.) in BBS 27 to 0.80 m above sea level (a.s.l.) in BBS 18, before it outcropped at the eastern edge of the plain and formed the steep hill slope. The regular inclination of unit 1 was only interrupted 70 m east of the coastline, where a bar-like structure emerged. Unit 2 also extended throughout the whole transect, although it thinned towards its eastern limit (a minimum of 40 cm in BBS 18). The maximum elevation decreased from the east (1.10 m a.s.l. in BBS 18) to the west (2.5 m b.s.l. in BBS 27). Unit 3 appeared in lenses of several meters thickness, building up the beach ridges. It was completely missing in the swales. A maximum thickness of 3.5 m was reached below ridge I, whereas a 6 m thick section from 2 m b.s.l. to 4 m a.s.l. formed ridges II and III. In contrast, Unit 4 was exclusively

found in the swales but was absent in the ridges. In swale II it accounted for 3.5 m of the sediment, from 1 m b.s.l. to 2.5 m a.s.l. In swale I it amounted to more than 4 m and thus completely masked the former morphological depression (fig. 4.2b).

4.4.2 Allochthonous sand sheets

As described in Chapter 4.4.1, the deposits of units 1-4 were repeatedly interrupted by thin sheets of sand showing completely different sedimentary characteristics. These sand sheets represent abrupt changes in the depositional circumstances. Hence, we refer to them as allochthonous sand sheets. Related to their position within the coastal stratigraphy, layers A, B and C were distinguished (fig. 4.4): Layer A was located directly below the present surface, covered solely by a thin initial soil. Layer B was found at a depth of 3 m b.s. in swale II. Embedded in unit 1 several layers C were identified.

4.4.2.1 Layer A

Figure 4.4 shows the spatial extent of layer A in a cross section perpendicular to the coast (transect A in fig. 4.2). Initially recognised in BBS 14, the deposit was traced up to the easternmost coring site (BBS 18) at 250 m east of the shore. With the exception of a narrow strip 70 m east of the shoreline, layer A continuously covered the surface of the transect. Although highly variable, the bed thickness revealed no clear thinning trend in an easterly direction. The thickest deposits occurred in swale II (up to 61 cm). The deposit thinned across the ridges (e.g. 3-8 cm atop ridge II). Towards the limit of sedimentation in swale I, it accounted for less than 1 cm.

For BBS 1, the typical characteristics of layer A are documented in fig. 4.5. Macroscopically, the 26 cm thick layer appeared homogeneous, forming a sharp basal contact. While the colour changed from dark brown to yellowish grey, the loamy substrate of the underlying soil (mean = 30 μm, sorting = 6.2 μm) was replaced by coarser and better sorted sand (mean = 50-120 μm, sorting = 1.5-5 μm). The internal structure was formed by two normally graded sublayers generally dominated by rather homogeneous silty fine sand (mean = 55-65 μm, sorting = 1.5-3 μm). The lower sublayer showed a slightly coarser base consisting of fine sand with small fragments of marine shells (mean = 117 μm, sorting = 5 μm). The transition from layer A to the underlying substrate was also reflected by the geochemical parameters. The carbonate content increased from zero to 40-50 mass-%, that of sodium from 4 to 5-6 g/kg, and the Ca/Mg ratio from 6 to 25. Within the deposit, all parameters remained more or less constant. The sedimentary and geochemical characteristics of layer A were comparable in all cores of the transect. However, differences occurred in the number and structure of sublayers, which

varied between one massive sublayer on the ridges and a maximum of three graded sublayers in swale II (tab. 4.1).
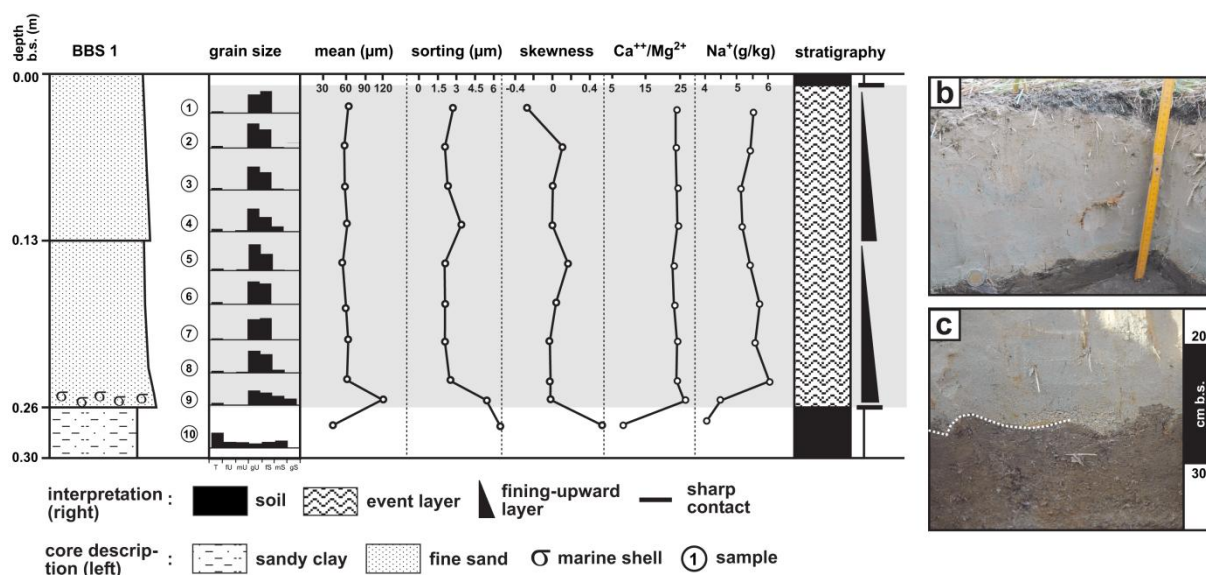
Figure 4.5: Layer A in BBS 1. (a) In the profile, the tsunamite of 2004 contrasts significantly with the underlying soil. Grain-size analyses reveal a division of three graded sublayers. (b) Photograph of layer A (26 cm thick). (c) Detailed photograph of the sharp basal contact. At the base of the tsunamigenic sand sheet coarser-grained sand with shell fragments is visible.

4.4.2.2 Layer B

Layer B was limited to the area of swale II (fig. 4.4). Its dimensions in a shore-perpendicular direction are documented in figure 4.6 (transect C in fig. 4.2). The deposit was restricted to a 15 m wide section between 135 and 150 m east of the present shoreline. Following this section of swale II in a coast-parallel direction (transect B in fig. 4.2) it was traced, although discontinuously, for more than 40 m from BBS 10 in the north to BBS 16 in the south. The lower limit of layer B was found at 0.30-1.30 m b.s.l., between unit 2 and the peat of subunit 4a, or completely embedded in subunit 4a. The total thickness of layer B varied from 3 cm in BBS 23 to 43 cm in BBS 17. A lateral trend – either parallel or perpendicular to the coastline – was not detected.

The characteristics of layer B are exemplified using BBS 17, and are depicted in figure 4.7. The sharp contact to subunit 4a was prominent in terms of substrate (grey sand instead of peaty soil) and geochemistry. The concentrations of carbonate (from 0 to 30-50 mass-%) and sodium (from 0.7 to 3.5-5.5 g/kg), as well as the Ca/Fe ratio (from 0 to 21) increased significantly, while the iron content dropped from 52 to 5.5 g/kg. Layer B was composed of a 6 cm thick stratum of medium sand (mean = 423 μm) with abundant fragments of indefinable marine shells at the base of the bed, followed by 37 cm of bluish fine sand (mean = 80-100 μm). The whole bed revealed a fining-upward trend with a gradational contact to subunit 4a above. Mixing of fine sand and peaty silt in this transition zone was accompanied by a decline in

sorting (from 2.3 to 6.1 µm) and Ca/Fe ratio (from 20 to 10), while the iron concentration increased from 5.5 to 8.6 g/kg. Additionally, rip-up clasts of brownish silt were found. In contrast to BBS 17, other cores did not show a separation into a coarser base and a finer top. In BBS 7, 8 and 23 a vertical trend was missing. In BBS 10 and 16 the layer had a massive structure. Similar to thickness, no lateral fining trend towards the eastern limit of sedimentation occurred (tab. 4.1).

To get age estimation for layer B, wood and plant fragments from the sediment below and above were dated (fig. 4.6 and tab. 4.2). Wood fragments, incorporated in the peat directly above layer B, yielded ages of 626–512 cal BP (UGAMS-4954), 505–320 cal BP (UGAMS-8032) and 501–319 cal BP (UGAMS-8037). From wood fragments in the sand below, an age of 695–570 cal BP (UGAMS-4955) was obtained.

Table 4.1*: Sediment characteristics of event layers A, B and C.*

Core	Event	Thickness (cm)	Vertical structure	Contact	Macro content	Grain size (mean; µm)	Distance from coastline (m)
BBS 14	A	4	1 fining-upward sequence	Sharp	Marine molluscs	156.8	74
BBS 13	A	3	1 fining-upward sequence	Sharp	Marine molluscs		97
BBS 12	A	8	1 fining-upward sequence	Sharp	Marine molluscs	172	114
BBS 9	A	61	3 fining-upward sequences	Sharp	Marine molluscs	(1) 92.5 (2) 91.2 (3) 86.4	129
BBS 8	A	21	2 fining-upward sequences	Sharp	Marine molluscs		136
BBS 19	A	28	2 fining-upward sequences	Sharp	Marine molluscs		136
BBS 23	A	30	2 fining-upward sequences	Sharp	Marine molluscs		140
BBS 1	A	26	2 fining-upward sequences	Sharp	Marine molluscs	(1) 131 (2) 90.3	145
BBS 7	A	26	2 fining-upward sequences	Sharp	Marine molluscs		145
BBS 17	A	20	2 fining-upward sequences	Sharp	Marine molluscs		146
BBS 10	A	37	2 fining-upward sequences	Sharp	Marine molluscs		150
BBS 16	A	52	2 fining-upward sequences	Sharp	Marine molluscs		150
BBS 21	A	40	2 fining-upward sequences	Sharp	Marine molluscs		150
BBS 22	A	30	2 fining-upward sequences	Sharp	Marine molluscs		150
BBS 6	A	32	2 fining-upward sequences	Sharp	Marine molluscs	(1) 146.8 (2) 83.70	154
BBS 5	A	54	3 fining-upward sequences	Sharp	Marine molluscs		162
BBS 4	A	23	2 fining-upward sequences	Sharp	Marine molluscs		178
BBS 3	A	22	2 fining-upward sequences	Sharp	Marine molluscs	(1) 113.7 (2) 78.30	194
BBS 18	A	2		Disturbed			243
BBS 8	B	5		Unsharp		368	136
BBS 23	B	3		Sharp	Mud-clasts		140
BBS 1	B	25	1 fining-upward sequence	Sharp	Marine molluscs	271 to 80	145
BBS 7	B	4		Unsharp		232	145
BBS 17	B	43	1 fining-upward sequence	Lower: sharp	Marine molluscs, mud-clasts	413 to 100	146
BBS 10	B	11	Massive	Sharp	Marine molluscs, plant remains, mud-clasts	368.5	150
BBS 11	B	14	Massive	Sharp		384	150
BBS 16	B	17	Massive	Upper: sharp	Marine molluscs		150
BBS 6	B	19	1 fining-upward sequence	Sharp	Marine molluscs		154
BBS 8	C1	5	2 fining-upward sequences	Sharp	Marine molluscs	(1) 119 to 867 (2) 119 to 837	136
	C2	3	1 fining-upward sequence	Sharp	Marine molluscs	113 to 617	
BBS 9	C1	2	Massive		Marine molluscs	792.4	129
	C2	3	1 fining-upward sequence	Sharp	Marine molluscs,	106 to 579	
	C3	5	1 fining-upward sequence	Sharp	Marine molluscs, Angular broken pebbles Angular broken pebbles	116 to 779	
BBS 12	C1	2	1 fining-upward sequence	Sharp	Marine molluscs, pebbles	75.5 to 797	114
	C2	2		Sharp	Marine molluscs, pebbles		
BBS 13	C1	2		Sharp	Marine molluscs, pebbles	84	90
	C2	8		Sharp	Marine molluscs, pebbles	74	
BBS 14	C1	1	Massive	Sharp	Marine molluscs	125 to 983	74
	C2	1	Massive	Sharp	Marine molluscs		
BBS 21	C1	6	Massive	Sharp	Marine molluscs	572.6	150
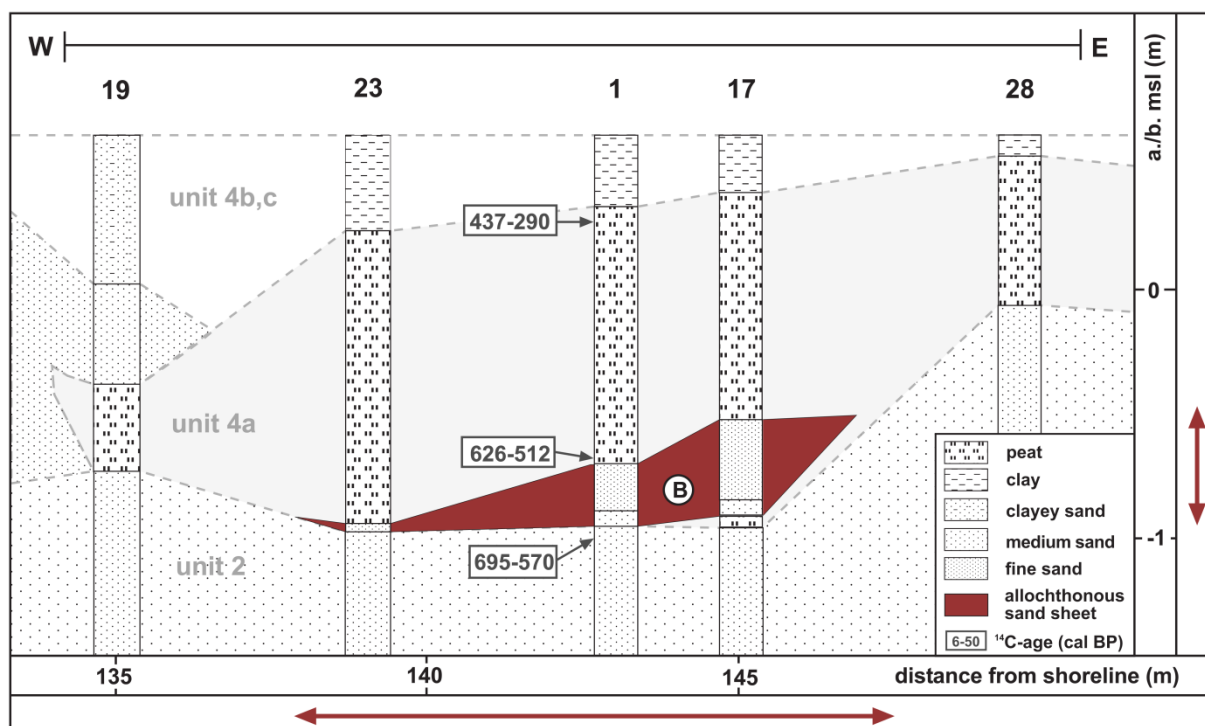
Figure 4.6: *Spatial extent of layer B perpendicular to the shoreline. The radiocarbon age intervals are given with 2 sigma error.*
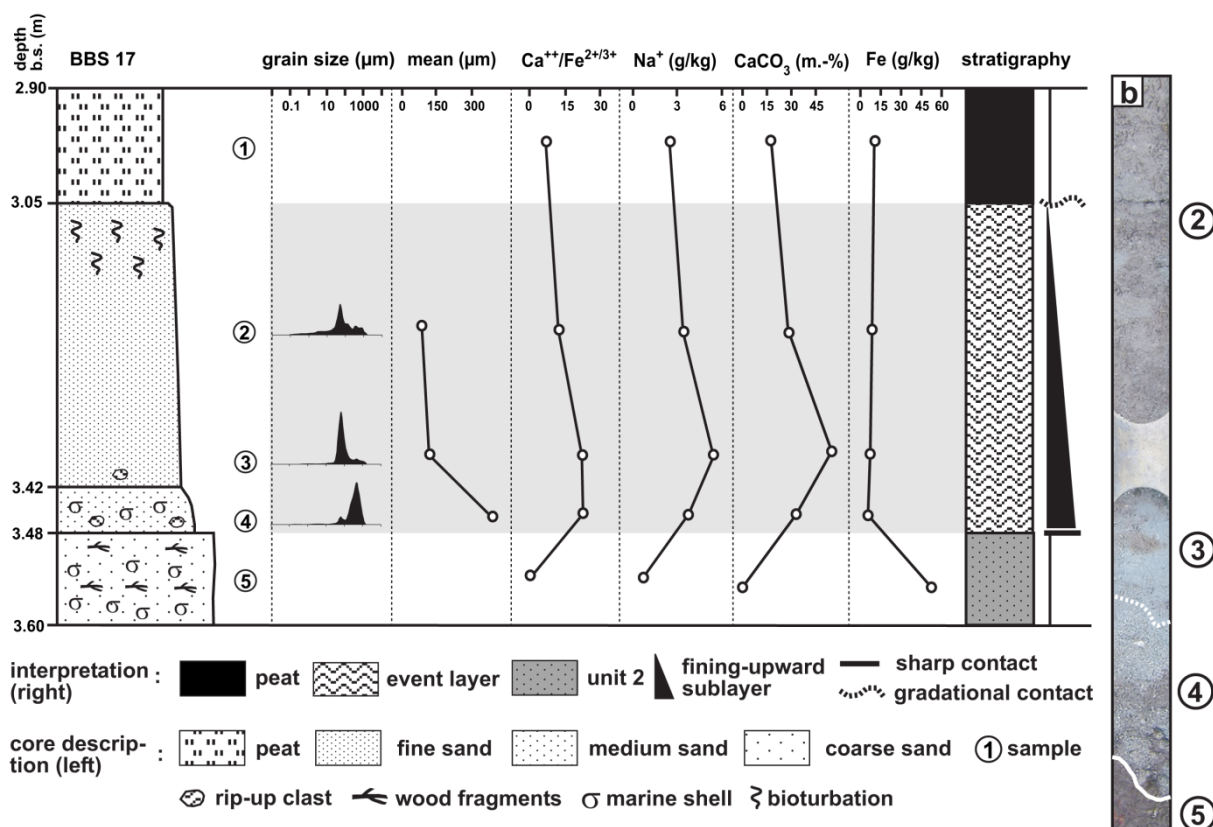
Figure 4.7: *Layer B in BBS 17. (a) The profile documents the contrast between sand sheet B and the confining sediments. Grain-size analyses reveal a single fining-upward sublayer with a coarse base (sample 4) and a finer upper unit (samples 2 and 3). (b) Photograph of layer B (for scale compare a).*

4.4.2.3 Layers C

Up to three allochthonous sheets of grey sand were found embedded in unit 1 (fig. 4.4). These layers are summarised as layers C (C1, C2 and C3), which varied in number at the different coring sites. All three layers C were present in BBS 9, two layers were identified in BBS 14, 13, 12 and 8, while BBS 21 and 28 contained only one layer C. At other coring sites no comparable deposits were found. Due to their discontinuity, a correlation of the distinct layers C between coring sites was not possible. Figure 4.8 shows their position in a shore perpendicular transect (combination of transects A and C in fig. 4.2). In a lateral direction they were traced between 70 and 160 m east of the present shoreline. Their depth ranged from 5 to 9 m b.s. or 2.70 to 4.50 m b.s.l.

Table 4.2: Radiocarbon data for Ban Bang Sak. All samples were measured in the Center for Applied Isotope Studies, University of Georgia, Athens (Lab Code = UGAMS).

Sample	Depth (m b.s.)	Lab code	Material	$\delta^{13}C$ (‰)	^{14}C (years BP)	2σ sidereal years (years cal BP)	2σ sidereal years (years cal AD/BC)
BBS 1b/1	2.16	UGAMS-4953	Wood[a]	−28.70	290 ± 25	437–290	1513–1660 AD
BBS 1/18	2.71	UGAMS-4954	Wood[a]	−28.90	530 ± 25	626–512	1324–1438 AD
BBS 1b/2	3.22	UGAMS-4955	Wood[a]	−28.60	720 ± 25	695–570	1256–1381 AD
BBS 1b/3	4.14	UGAMS-4956	Plant fragm.[a]	−24.50	890 ± 25	907–735	1044–1215 AD
BBS 5/17	4.85	UGAMS-8030	Plant fragm.[a]	−27.30	1320 ± 25	1298–1181	653–770 AD
BBS 7/7	2.30	UGAMS-8031	Wood[a]	−28.10	60 ± 25	256–31	1694–1919 AD
BBS 7/11	3.35	UGAMS-8032	Wood[a]	−28.10	380 ± 25	505–320	1446–1630 AD
BBS 8/16	5.35	UGAMS-8033	Shell[b]	−0.90	2840 ± 25	2700–2490	751–541 BC
BBS 8/19	5.52	UGAMS-8034	Plant fragm.[a]	−31.00	1400 ± 25	1346–1286	604–665 AD
BBS 9/15	5.90	UGAMS-8035	Charcoal[a]	−26.80	3680 ± 25	4090–3925	2141–1976 BC
BBS 9/17	6.04	UGAMS-8036	Shell[a]	−0.70	2310 ± 25	2001–1839	52 BC–112 AD
BBS 10/2	2.65	UGAMS-8037	Wood[a]	−27.60	370 ± 25	501–319	1449–1632 AD
BBS 12/18	7.90	UGAMS-8038	Shell[b]	−2.00	2660 ± 25	2440–2290	491–341 BC
BBS 13/18	7.55	UGAMS-8039	Shell[b]	−0.90	4110 ± 30	4282–4060	2333–2111 BC
BBS 14/17	7.39	UGAMS-8041	Shell[b]	0.40	4300 ± 30	4520–4321	2571–2372 BC
BBS 21/5	5.20	UGAMS-8042	Shell[b]	−0.10	2300 ± 25	1988–1830	40 BC121 AD

[a] Calibrated ages calculated with IntCal09 (Reimer et al., 2009).
[b] Calibrated ages calculated with Marine09 (Reimer et al., 2009). A reservoir effect of ΔR = −2 was adapted from Southon et al. (2002).
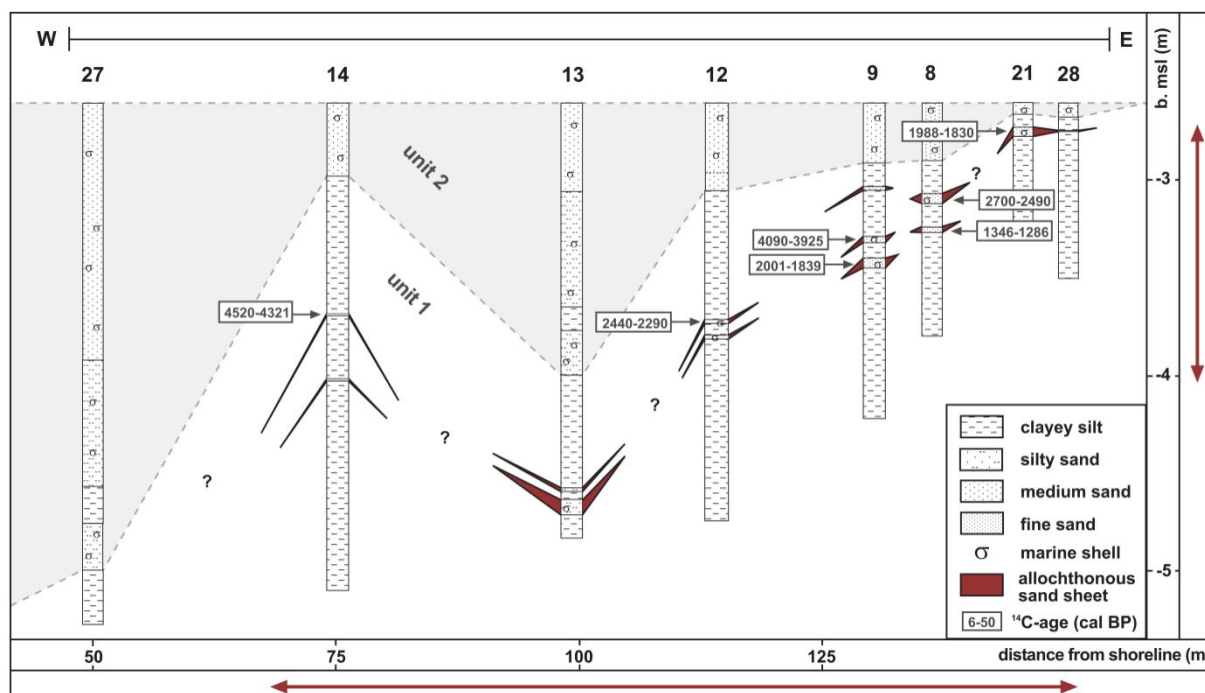
Figure 4.8: Spatial extension of event layers C perpendicular to the shoreline (transect A in fig. 4.2a).

Typical characteristics of layers C are presented for BBS 8 in figure 4.9. Here, embedded in the fine sediment of unit 1, two separate beds were identified. The lower of them (layer C2, 3 cm thick) was composed of grey sand, forming a sharp contrast to the confining silt (fig. 4.9c). Concentrations of carbonate (from 0 to 30 mass-%), sodium (from 0.8 to 3 g/kg) and the Ca/Fe ratio (from 0 to 5.8) increased. It contained a mixture of marine shell valves and fragments with angular and rounded breaks (e.g. *Tellina* sp., *Cerastoderma* sp., *Calyptraea extinctorium*, *Dentalium* sp.). A fining-upward trend from medium sand (mean = 617 μm) to fine sand (mean = 113 μm) was detected. About 12 cm above C2, the second bed (layer C1) was found, revealing similar characteristics. However, unlike C2, it consisted of two normal graded sublayers, starting with medium sand and shells at the base (mean = 830 μm and 870 μm), gradually changing to fine sand (mean = 119 μm) to the top. In all other cores layers C revealed similar properties, although their thicknesses varied between 1 and 6 cm (without lateral trends), and the structure varied between two graded sublayers and one graded or massive bed (tab. 4.1).
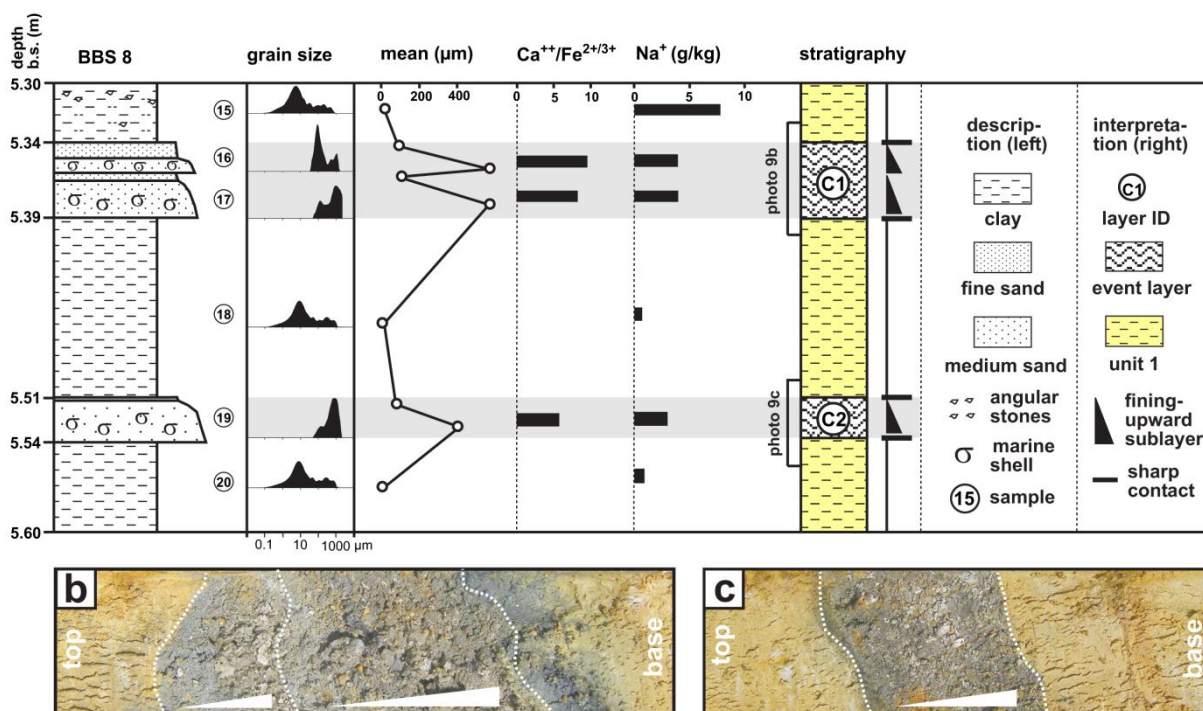
Figure 4.9: Layers C in BBS 8. (a) The stratigraphical profile shows two distinct layers (C1 and C2). The upper one is composed of two fining-upward sublayers, while the lower layer contains only one normally graded sublayer. (b) Detailed photograph of layer C1. (c) Detailed photograph of layer C2.

Due to the lack of datable material in the confining deposits, only a single minimum age of 1298–1181 cal BP (UGAMS-8030) from plant remains at the base of unit 2 in BBS 5 could be obtained. All other radiocarbon ages were determined on material from inside the sand sheets (fig. 4.10, tab. 4.2). A shell in the upper layer C of BBS 14 with 4520–4321 cal BP (UGAMS-8041) and a piece of charcoal inside the middle layer of BBS 9 (layer C2) with 4090–3925 cal BP (UGAMS-8039) gave the oldest age estimates. Four marine shells from

layers C in cores BBS 12, 9, 8 and 21 were dated to ages between 2700 and 1830 cal BP (UGAMS-8033, -8036, -8038 and -8042). The youngest maximum age of 1346–1286 cal BP originates from the lower sand sheet (C2) in BBS 8 (UGAMS-8034).

4.5 Discussion

4.5.1 Depositional environments of units 1-4

Based on their sedimentary and geochemical characteristics and a comparison with reference samples from recent deposits, depositional environments for units 1-4 were defined. Since they form the sedimentary framework of the event deposits A, B and C, their interpretation allows inferences concerning palaeogeographical circumstances.

Unit 1 (pre-transgressive terrestrial): Generally, the poor sorting and the small grain sizes of the deposits reflect either sedimentation under low-energy conditions or intensive weathering. The yellowish brown colour, the total absence of fossils as well as the geochemical composition with high iron contents and low concentrations of carbonate and soluble salts point to terrestrial conditions, dominated by intensive weathering and oxidation processes. While the lower part of unit 1 – characterised by the occurrence of weathered stone fragments, compaction and a lack of stratification – represents the weathered saprolite, the laminated and soft silt at the top of unit 1, containing layers C, are interpreted as deposits of shallow, ephemeral ponds of standing water.

Unit 2 (marine to shallow marine): The grey colour and the increased amounts of carbonate and soluble salts indicate sedimentation below sea level (Szczuciński et al., 2007; Chagué-Goff, 2010). The marine shells, showing no signs of reworking, are indicative of submarine conditions. Thus, a vertical succession of environments is supposed: the coarse sand with pebbles and big shells at the base, together with the sharp contact to unit 2, is interpreted as facies of the Holocene marine transgression. The following strata of alternating, moderately sorted fine and medium sand reflect a regressive succession from open water conditions to rather shallow marine environments with abundant wood and plant fragments, interpreted to originate from an onshore source.

Unit 3 (littoral): The faunal and geochemical findings indicate a marine influence similar to unit 2. Considering the slightly higher energy conditions, indicated by the coarse-sand-dominated substrate, and the abrasion marks of the fossils, as well as the yellowish white colour, which points to deposition above water level, unit 3 is interpreted as a beach facies. The lens-like geometry of the deposits and the evidence of lithification (beachrock) support this conclusion.

Unit 4 (terrestrial): The general characteristics of unit 4, the absence of fossils and carbonate, as well as their location inside the swales, point to terrestrial environments. However, the subunits differ significantly: The peaty silt of subunit 4a is interpreted to reflect accumulation in a sheltered (indicated by the fine, unsorted sediment) and wet (the lack of oxygen prevents the destruction of organic matter) environment. A minor marine influence is indicated by several thin sand laminae with small shell fragments. We refer to it as a coastal swamp environment that formed due to the sheltered conditions within the swales after they had been separated from the sea by beach-ridge formation. The unsorted clayey silt of subunit 4b points to a low-energy environment as well. Due to the similarity with a limnic reference sample from an artificial pond (ca. 100 m south of the study area) it is supposed to be a deposit of a shallow, probably temporary lake that developed behind the beach ridges after the swamp formation. Subunit 4c is composed of reddish loamy sand and clay, the colour indicating intensive oxidation and weathering. The inhomogeneous substrate and abundant laterite fragments, originating from the pre-Holocene bedrock, point to an anthropogenic deposit that was dumped inside the wet swales to create dryer conditions.

4.5.2   The origin of the allochthonous sand sheets

Layer A is known to be deposited by the waves of the IOT 2004. In contrast, the origin of layers B and C remains unclear; they might have been produced by several processes (Kortekaas and Dawson, 2007; Switzer and Jones, 2008; Engel et al., 2010). Besides coastal flooding events such as prehistoric tsunamis and tropical storms, river runoff and sheet floods, induced by heavy rain, are capable to produce allochthonous sand layers as well.

4.5.2.1 The source of the sand in layers B and C

One important clue to the determination of generating events is the origin of the dislocated material. First of all, the abundance of marine fossils in layers B and C (e.g. *Tellina* sp., *Cerastoderma* sp, *Calyptraea extinctorium*, *Dentalium* sp.) provides evidence for their marine origin (fig. 4.10b). Additional information is offered by the geochemical composition of the sand sheets, which may enable discrimination between marine and terrestrial sources as well (Minoura et al., 1994; Szczuciński et al., 2007). Under tropical conditions with heavy rain and high temperatures $CaCO_3$ and water soluble salts are rapidly leached from subaerial sediments (Szczuciński et al., 2007; Szczuciński, 2010). In contrast, marine sediments deposited below water level contain high values of carbonate from calcareous organisms and high contents of salts (e.g. Na, Mg) from the sea water (Chagué-Goff, 2010). Figure 4.10a documents the increased contents of $CaCO_3$, Na and Ca/Fe in layers A, B and C (Na_{mean} = 3.6 g/kg, Ca/Fe_{mean} = 13) compared to the confining material of units 1-4 (Na_{mean} = 1.1 g/kg, Ca/Fe = 1.6). Although the concentrations in the sand sheets are lower than those in marine reference samples (Na_{mean}

= 8 g/kg, Ca/Fe$_{mean}$ = 45), they show a clear marine influence, while the confining material resembles the terrestrial reference samples (Na$_{mean}$ = 0.7, Ca/Fe$_{mean}$ = 0.2). The reduced concentrations compared to recent marine deposits might reflect the influence of weathering on the marine material after it was deposited onshore, a process which was observed for the deposits of the IOT after only 5 years (Szczuciński, 2010).
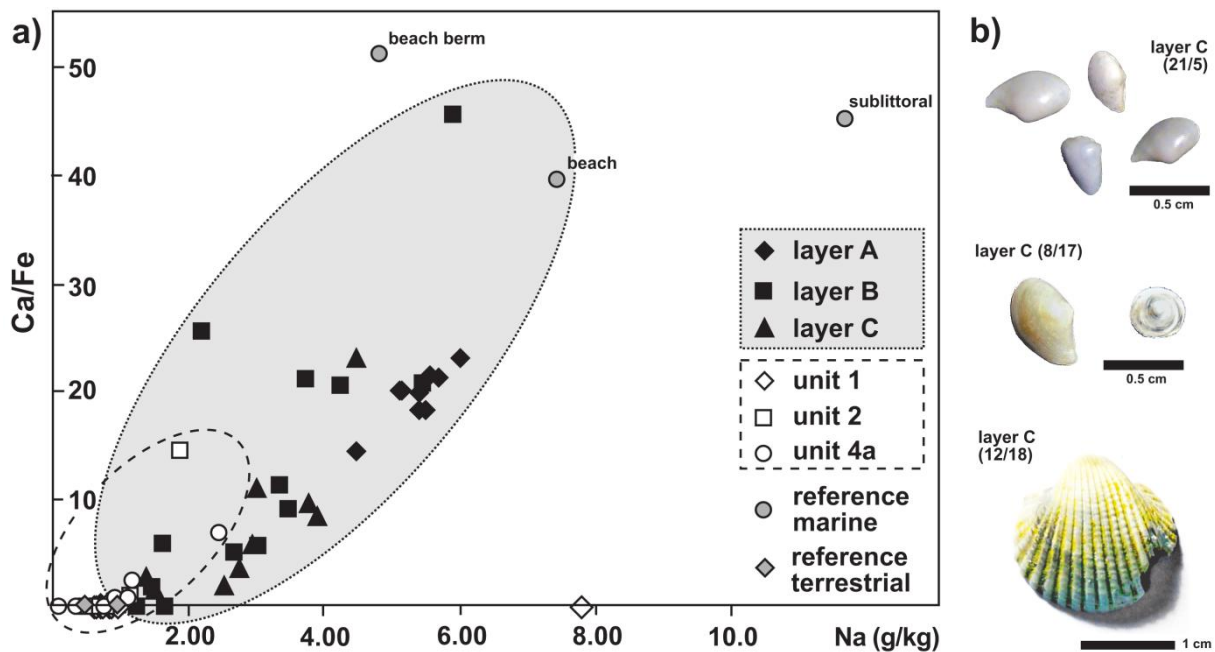
Figure 4.10: *Indicators for a marine origin of layers A, B and C. (a) Diagram of Ca/Fe ratio versus sodium content. The geochemical composition of the event deposits indicates a significant marine influence, while the surrounding material (units 1, 2 and 4a) resembles the terrestrial reference samples. (b) Marine shells from event layers C. BBS 21/5 = Tellina sp., BBS 8/17 = Tellina sp. and Calyptraea extinctorium, BBS 12/18 = Cerastoderma sp.*

More precise information about the water depth of the source area is given by the grain-size data (Switzer et al., 2005). The presence of a very fine sand component (80 μm and 106-116 μm) in layers B and C, which is absent from reference samples of near-shore (berm, beach and sublittoral) and terrestrial sediments (lake, bedrock, swamp; fig. 4.11), points to an offshore source of the deposits, where sediments even finer than observed in the sublittoral reference sample (2 m water depth) exist (Di Geronimo et al., 2009). Since both layers are embedded in terrestrial or beach sediments, their offshore origin can only be explained by (1) storm, (2) tsunami, or (3) short-term sea-level fluctuations. The general appearance of the layers – sharp contacts, rip-up clasts and thicknesses of only a few centimetres, indicating high-energy flow conditions – as well as the sea-level history of the region (Horton et al., 2005) rule out the latter explanation. Thus, only strong storms or tsunamis remain as potential generating mechanisms of layers B and C.
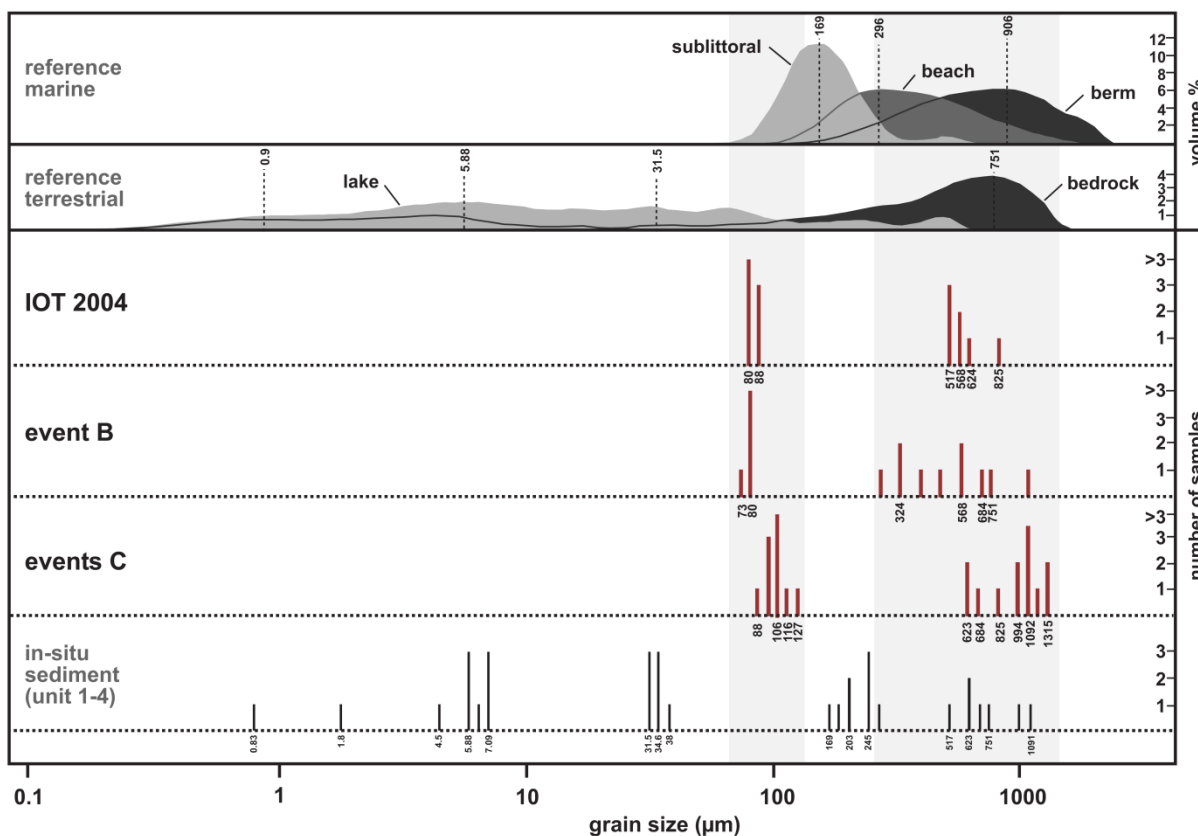
Figure 4.11: *Comparison of the grain-size modes of the palaeoevent deposits B and C with those of the IOT sediment (frequency distribution of grain-size modes of all analysed samples, numbers below the bars indicate the value of each grain-size mode). All three event layers show a similar composition of a coarse-grained component and fine-grained material, marked in light grey. While the coarse fraction is found in marine and terrestrial reference materials as well as in the surrounding in-situ sediments, neither of them can be the source of the very fine-sand component.*

4.5.2.2 Discrimination between tsunami and storm origin

Although the study area is probably not affected by landfall of tropical storms strong enough to leave onshore deposits (cf. Chapter 4.2 and Jankaew et al. (2008) for discussion), we cannot definitively exclude strong storm impact for the past millennia. This has to be taken into account when discussing the origin of layers B and C. Although comparative studies between tsunami and storm deposits suggest that there might be sedimentary criteria to discriminate between both types of sediment (Tuttle et al., 2004; Morton et al., 2007; Switzer and Jones, 2008), modern examples show that all features can be present in both, tempestites and tsunamites (Peters and Jaffe, 2010). Thus, characteristics such as the occurrence of rip-up clasts, a small number of graded or massive sublayers and sharp erosive contacts, which were observed in our event layers and generally favour deposition by tsunamis (Morton et al., 2007; Switzer and Jones, 2008), are no exclusive arguments against a storm origin. Rip-up clasts and erosive contacts with the underlying sediment afford high inundation velocities, which are more common for tsunami waves, but have been observed in hurricane deposits as well

(Wang and Horwitz, 2007). A small number of normally graded sublayers points to the formation by few waves with long periods as it is characteristic for tsunamis, while small period storm waves are more likely to result in laminated beds (Tuttle et al., 2004; Switzer and Jones, 2008). Nevertheless, storm beds can consist of one massive or graded layer, too (Kortekaas and Dawson, 2007). Therefore, discrimination between storm and tsunami deposits solely based on single signatures is not possible. It is only by interpreting the sedimentary signatures in their site-specific context that the origin of layers of extreme wave events can be determined. Especially the consideration of modern analogues for local storm and tsunami deposits at the same site might provide promising information about discrimination criteria (Nanayama et al., 2000; Goff et al., 2004; Kortekaas and Dawson, 2007).

Although remains of historical storms, which inundated the coastal zone are missing in the study area (Phantuwongraj and Choowong, 2011), at least the sand sheet of the IOT 2004 can serve as a recent example in an attempt to discriminate between storm and tsunami origin of the palaeoevent deposits at Ban Bang Sak. As mentioned above, significant signatures of layer A, that represent typical features of a local tsunami deposit are – besides its marine geochemical and faunal imprint – a sharp basal contact to the underlying soil, the occurrence of muddy rip-up clasts and a small number of 1-3 graded sublayers. The erosional base and the intra clasts are indicative of high-energy flow conditions in the first tsunami wave, capable to erode the pre-tsunami surface even after having crossed the barrier of 3-4 m high beach ridges. Normal grading of the deposits generally reflects sedimentation of suspended material from the water column of inundating waves during the decline of flow velocity. The occurrence of up to three graded sublayers probably reflects deposition by the three incoming tsunami waves that were observed at the coast of Khao Lak (Szczuciński et al., 2006). Similar run-up sediments of up to three waves were also documented at other locations along the Thai coast (Hawkes et al., 2007; Hori et al., 2007; Choowong et al., 2008b; Fujino et al., 2010; Naruse et al., 2010). Others observed only one fining-upward layer or massive beds (Szczuciński et al., 2006; Hawkes et al., 2007). The variable number of sublayers at Ban Bang Sak probably results from erosion by subsequent waves. Since all those features are present in layers B and C as well (except for rip-up clasts in layers C) similar mechanisms of transport and sedimentation as discussed for the deposits of the IOT can be expected. This conclusion is supported by similarities between the prehistoric and modern event layers regarding grain-size composition and sorting (fig. 4.11). Each of the three deposits (layers A, B and C) is characterised by a bimodal grain-size composition with a variable coarse (300-1300 μm) and fine component (80-120 μm). While the former might originate from several environments present in the littoral and near-shore zone of the study area (especially the beach and the beach ridges), the fine component is absent in all other deposits of the setting and indicates a second sediment source further offshore for all three event layers (Chapter 4.5.2.1). All event deposits are moderately to poorly sorted (sorting = 1.5-3.2 μm).

Differences were observed in thickness and spatial distribution of the event layers. While the IOT deposit was laterally continuous and its thickness varied between 3 and 61 cm, layers B and C exhibited distinct lateral extents and, in case of layers C, significantly thinner beds of only 1-6 cm. However, this discrepancy does not necessarily point to their formation by different depositional events (i.e. by tropical storms); they may also be the result of different morphological settings during deposition and also of different levels of conservation. While the IOT sand sheet and event layer B were deposited under similar conditions in a ridge and swale environment, the topographic situation during accumulation of layers C was found to have been different. In contrast to the ridge and swale topography that controlled the deposition of layers A and B, the gently inclining and flat pre-event surface of layers C did not allow for variable deposition in morphological depressions (where the greatest thickness of layers A and B was observed) and on mounds.

The spatial discontinuity of the palaeolayers compared to the IOT deposit can be explained by intensive post-depositional alteration in tropical climates. Szczuciński (2010) showed for IOT deposits in SW Thailand that after only five years of erosion and weathering – due to bioturbation, soil formation and anthropogenic impact – thin tsunami layers (less than 10 cm) at many locations have already disappeared or cannot be distinguished from the surrounding material anymore. Therefore, it is likely that only the thickest parts of the 2004 sand sheet, which are concentrated in swale II, will be preserved in the future geological record; thus, it will show a similar extension as found for layer B. Furthermore, in terms of the applied techniques, the inferiority of coring compared with trenching can complicate the identification of layers B and C. Although geometrical similarity alone is not a validating argument, in some cases (dependent on local factors) tsunamis and strong storms show differences in their spatial distribution (Morton et al., 2007). Thus, the nearly identical geometrical extension of the tsunami reference and event layer B provides another piece of information favouring it as a tsunamite. In contrast, the different geometry of layers C does not necessarily reflect a different mechanism of deposition, since the local circumstances were different as well.

Another important indicator often consulted to distinguish between storm and tsunami is the inland distribution of event deposits, since the potential inundation and run-up of storm waves is expected to be smaller compared to tsunamis (Tuttle et al., 2004; Kortekaas and Dawson, 2007). However, in the case of Ban Bang Sak, where coastal flooding is limited by the width of the steep coastal plain to only 300 m, storms are capable to flood the area covered by layers B and C as well. Thus, inland extend of the deposits is no useful discrimination criterion at the study site.

In summary, layers B and C resemble the IOT deposits in their faunal, granulometric and geochemical composition. If we account for differences in palaeotopography, post-depositional changes, as well as misinterpretations due to the coring technique, the sedimentary structures,

as well as the spatial extent of the palaeoevent deposits can be explained best by transport mechanisms similar to those of the 2004 tsunami. Thus, the sedimentary evidence, especially in combination with the regional climatic background, favours a tsunamigenic origin of layers B and C over a storm origin.
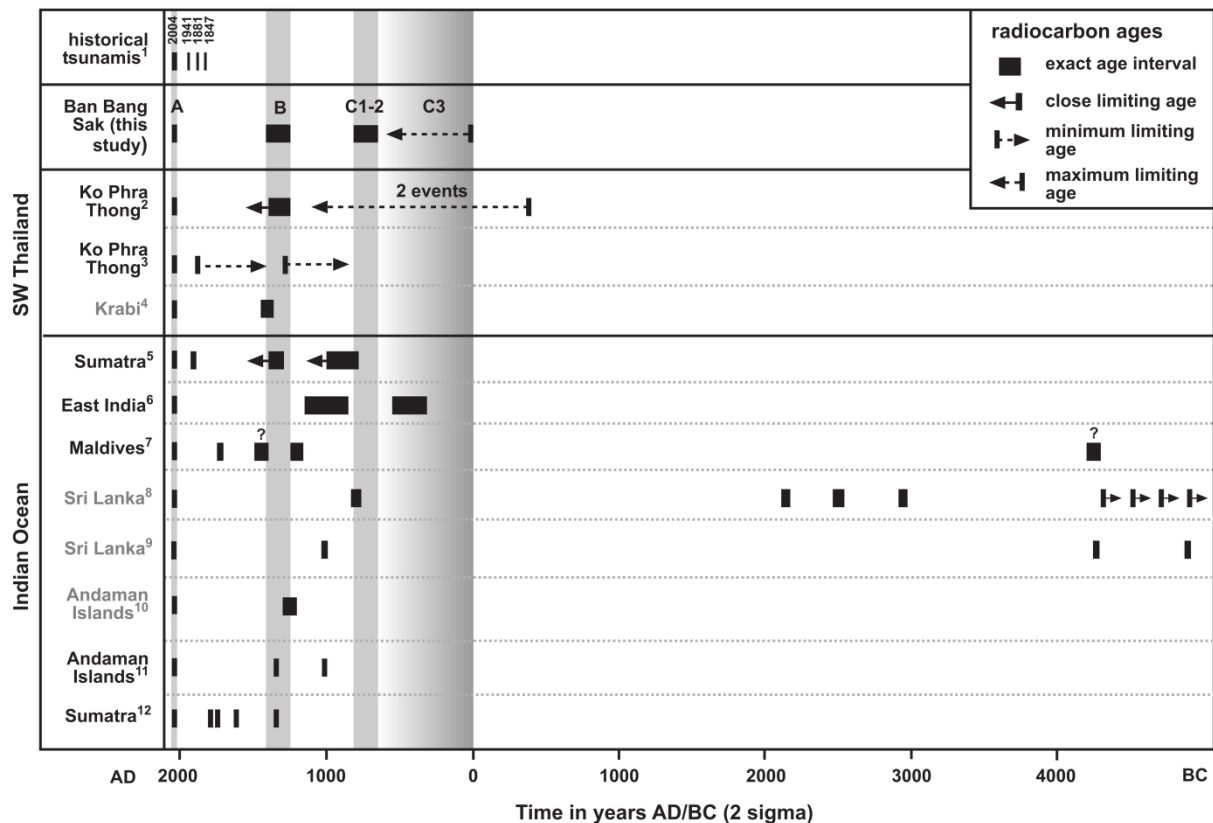
Figure 4.12: Correlation of the event chronology of Ban Bang Sak with historical and geological evidence of potential palaeotsunamis from literature (published articles and conference abstracts). [1]Historical tsunamis generated along the Andaman–Nicobar segment (Ortiz and Bilham, 2003; Bilham et al., 2005), [2]ridge-swale topography (Jankaew et al., 2008), [3]ridge-swale topography (Fujino et al., 2009), [4]onshore deposit in a cave (Harper, 2005), [5]ridge-swale topography (Monecke et al., 2008), [6]onshore deposits within an archaeological site (Rajendran et al., 2006), [7]subaquatic caves below the storm wave level (Mörner, 2007), [8]lagoon (Jackson et al., 2008), [9]ridge-swale topography/lagoon/marsh (Ranasinghage et al., 2010), [10]ridge-swale topography (Malik et al., 2010), [11]uplifted coastal terraces (Rajendran et al., 2008), [12]uplifted coastal terraces (Sieh et al., 2008).

4.5.3 Chronology of extreme wave events

The crucial point for the reconstruction of recurrence intervals of extreme wave events is the precise dating of the geological evidence. This will enable us (1) to establish a local event chronology for Ban Bang Sak, and (2) to estimate event type and magnitude by correlating local data with evidence from other risk areas.

(1) The age of palaeoevent B of Ban Bang Sak is confined by four radiocarbon dates. Since significant age overestimation caused by reworking of older material is not likely, due to their embedding in undisturbed peat, the dates are treated as close limiting ages. Thus, the

event took place before 620-500 cal BP (composition of three dates: 626-512 cal BP, 505-320 cal BP and 501-319 cal BP) and shortly after 700-570 cal BP, which gives a time range of 700-500 cal BP (1250-1440 AD) for the potential tsunami impact. Interpretation of the dating results for layers C is more complicated (fig. 4.8). Dated plant fragments from marine deposits (Unit 2) above the sand sheets provide a single minimum age of 1300–1180 cal BP. However, the maximum ages provided by material from inside the event layers scatter between 4520 and 1290 cal BP and reveal age inversions for BBS 8 and BBS 9. This implies that (i) most of these ages are too old and do not represent the time of deposition but reworking of older material by the extreme events, and (ii) a correlation of the beds between different cores based on dating results is not possible. In this case, the youngest radiocarbon date of the oldest layer C (C3 in BBS 9: 2000-1840 cal BP) provides the best estimate for a maximum age of all layers C, while the age of the second layer (C2 in BBS 8: 1350-1290 cal BP) further limits the maximum ages of C1 and C2. Thus, all three events C took place before 1300–1180 cal BP, but after 2000-1840 cal BP, i.e. in the period 2000-1180 cal BP (50 BC-770 AD), whereas the radiocarbon dates of the second layer C in BBS 8 indicate that the two younger events occurred after 1350-1290 cal BP and thus are related to the period 1350-1180 cal BP (600-770 AD).

(2) Since the IOT had a significant impact on distant coasts in a range of several thousands of kilometres, potential predecessors might be characterised by a similar geographical distribution of affected areas. Thus, correlation with (A) historical data and (B) geological evidence of palaeotsunamis from other locations within the inundation zone of the IOT is an important tool to discriminate between local, regional and ocean wide tsunamis (fig. 4.12). A wide geographical distribution of contemporary event layers would point to a large tsunami as generating mechanism. In contrast, event deposits restricted to a limited area or only one single site have to be interpreted as local palaeoevents in the form of local tsunamis or tropical storms.

(a) Although historical tsunamis strong enough to leave onshore deposits are not reported for the Thai coast, there might have been events striking the study area without being documented in the historical record. The earthquake record of the Indian Ocean notes several ruptures of the Sunda Arc for the last 250 years, but only three of them affected the Andaman-Nicobar segment (Ortiz and Bilham, 2003; Bilham et al., 2005) and thus might have been potential sources of tsunamis in the Andaman Sea (Okal and Synolakis, 2008). However, due to their young ages, none of these earthquakes is considered to coincide with event deposits at Ban Bang Sak (fig. 4.12).

(b) Depositional evidence of palaeoevents was studied in nearly all countries affected by the IOT and in a great variety of geo-archives. Figure 4.12 summarises dated evidence of potential palaeotsunamis (deposits) and seismologic events (uplift and subsidence) from the coasts of Thailand, India, Sumatra, Sri Lanka, the Andaman Islands

and the Maldives. These dates are compared with the ages of event deposits in this study. For event layer B, which was dated to 1250-1440 AD, contemporaneous tsunami evidence is reported from Ko Phra Thong (1250-1400 AD; Jankaew et al., 2008) and Krabi (1410-1425 AD; Harper, 2005) in western Thailand, as well as from northern Sumatra (1290-1400 AD; Monecke et al., 2008). Potential tsunami deposits from the Maldives (1510-1590 AD and 1170-1250 AD; Mörner, 2007) and the Andaman Islands (1200-1300 AD; Malik et al., 2010) could match with layer B of Ban Bang Sak as well. Furthermore, the deposit can be correlated with a potential rupture of the Sunda Arc around 1300-1400 AD (indicated by uplifted coastal terraces and micro atolls; Rajendran et al., 2008; Sieh et al., 2008; Meltzner et al., 2010). Possible analogues for layers C, which were deposited between 50 BC and 770 AD, are quoted from the Thai island Phra Thong by Jankaew et al. (2008; two events younger than 400-200 BC). Furthermore, findings from Sri Lanka (Jackson et al., 2008) match with the younger layers C dated to 600-770 AD, and evidence from the east coast of India (321-564 AD; Rajendran et al., 2006) matches deposit C3, which has an age younger than 50 BC. For tsunami sediments from Phra Thong reported by Fujino et al. (2009; one sand sheet older than 1300 AD) and northern Sumatra (younger than 780-990 AD; Monecke et al., 2008) the correlation with layers C1 or C2 is less explicit.

The coincidence of the deposition of layer B with geological tsunami evidence from other locations along the coast of Thailand, as well as from more distant sites, is another argument towards interpreting it as the deposit of a palaeotsunami with geographically wide-spread impact rather than a tropical storm. Same as layer B, layers C can be correlated with possible counterparts from Phra Thong, Sri Lanka and India. However, due to the inaccurate age data of layers C at Ban Bang Sak, the correlation is rather poor; it does, therefore, not provide an argument for the tsunamigenic origin of layers C. Additionally, the short time interval of only 180 years for the deposition of beds C1 and C2 may point to the assumption that at least one of them is not the result of tsunami impact.

4.6 Conclusions

Geological evidence is an important tool to reconstruct the recurrence probability of large tsunamis along the coasts of the Indian Ocean, despite the generally low preservation potential of event deposits in most coastal areas of the region. In this context, the sedimentary record of the Ban Bang Sak coastal plain provides new information about potential predecessors of the IOT 2004:

(1) The coastal sediments at Ban Bang Sak contain allochthonous sand sheets at three different depth levels that significantly contrast with the confining material. While the uppermost

layer was deposited by the tsunami of 2004 (layer A), layer B at a depth of 3 m b.s. and three layers C at depths of 5-7 m b.s. represent prehistoric events.

(2) For all of the four palaeoevent deposits B, C1, C2 and C3 geochemical and faunal characteristics prove their marine origin. Grain-size distribution, sedimentary structure and sharp contacts to the underlying deposits document the high-energy flow conditions necessary to create them. Thus, they must have been generated by extreme wave events, either storm or tsunami.

(3) The chronology of these palaeoevents, based on radiocarbon dating, covers the last 2000 years. The oldest event (layer C3) was dated to be younger than 2000 cal BP, layers C2 and C1 must have followed between 1350 and 1180 cal BP. The youngest potential predecessor event of the IOT took place between 700 and 500 cal BP.

(4) To discriminate between tempestites and tsunamites we focused on the comparison of the palaeoevents with the modern tsunami deposit of the IOT, as well as on correlation with palaeotsunami deposits from other locations around the Indian Ocean. The aggregate of all sedimentary characteristics documents a strong similarity between the modern tsunami deposit and the prehistoric event layers. However, while event B coincides precisely with evidence of prehistoric tsunamis in Thailand, Sumatra and the Andaman Islands, the layers C from Ban Bang Sak do not have unambiguous counterparts at other locations of the region.

(5) The results of our study, combined with the generally low potential for landfalls of tropical storms in the research area, clearly favour tsunami over storm origin for the youngest palaeoevent of Ban Bang Sak. We assign it to a basin wide palaeotsunami 700-500 years ago. Further evidence of extreme wave events between 2000 and 1200 years ago could be the result of palaeotsunamis as well as tropical storms; until clarification by further studies, these deposits may be regarded as potential predecessors of the IOT.

Chapter 5

5 OSL dating of tsunami deposits from Phra Thong Island, Thailand[2]

Abstract: *To evaluate the potential of optical dating (OSL) in establishing a proper tsunami chronology for Phra Thong Island (SW Thailand), the method was applied to a suite of tsunamigenic and littoral sandy deposits, for which independent age control was available. Small aliquots of coarse-grained quartz were used for measurements, and processed statistically by means of appropriate age models. Based on the equivalent dose distributions, the well bleached littoral deposits were analysed with the central age model (CAM); the tsunamigenic samples revealed poor bleaching, thus, the minimum age model (MAM) was applied. The cross-check with independent age data showed good agreement between luminescence ages and the existing radiocarbon chronology for the littoral deposits. The poorly bleached deposits of the 2004 Indian Ocean tsunami revealed residuals of less than 40 years, which are insignificant for older deposits and demonstrate the general suitability of the dating technique for tsunamites on Phra Thong. Afterwards, the approach was extended to tsunamigenic and littoral sediments of unknown age. Since those revealed properties similar to their reference deposits, the procedures of statistical D_e determination were adopted. The resulting ages were in agreement with the stratigraphical position and (largely) with the wider chronological context.*

Keywords: *OSL; Quartz; Age Model; Tsunami deposit; Holocene; Thailand*

5.1 Introduction

Dating sandy tsunami deposits is of great importance for the prediction of hazard frequencies, especially in areas with poor historical record. To determine ages for the sedimentary remains of prehistoric events, radiocarbon dating is usually applied. Since the ^{14}C-method predominantly provides limiting ages – by dating the strata above and below the event layers – and because it is often affected by relocation of material or contamination by roots, lately the optically stimulated luminescence technique (OSL) was used to cross-check or substitute radiocarbon data (Huntley and Clague, 1996). The need for OSL dating on Phra Thong Island (Ko Phra Thong) rests in the so far dissatisfying radiocarbon chronology of the event deposits. Limiting ages achieved from bulk samples of the confining peat proved to be too young due

---

[2] Chapter 5 is based on: <u>Brill, D.</u>, Klasen, N., Brückner, H., Jankaew, K., Scheffers, A., Kelletat, D., Scheffers, S., 2012. OSL dating of tsunami deposits from Phra Thong Island, Thailand. Quaternary Geochronology 10, 224-229.

to the contamination with young roots, and organic macro-remains such as seeds or leafs are extremely rare (Jankaew et al., 2008).

To evaluate the potential of OSL for improving the event chronology of Ko Phra Thong, the method was applied to a sediment suite, for which independent age control was available (deposits of the 2004 Indian Ocean Tsunami (IOT) and radiocarbon-dated littoral sand). Afterwards, the validated procedure was adopted to date deposits of unknown age (palaeotsunamis and littoral sediment). More age data for prehistoric tsunami deposits and a detailed discussion of their chronological relevance will be presented in an additional paper (Brill et al., 2012b).
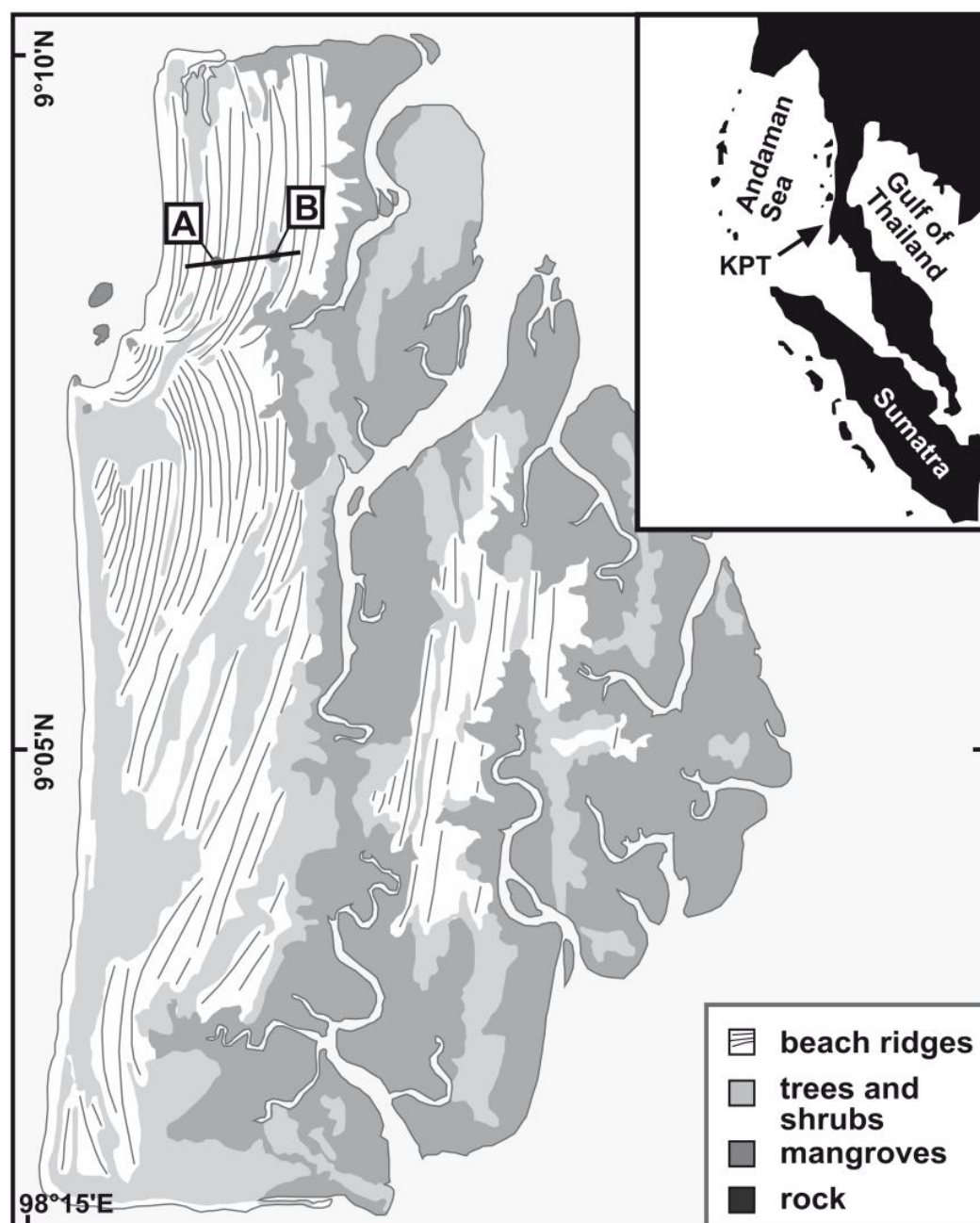
Figure 5.1: *Geographical setting of Ko Phra Thong.*

5.2   Study site

The island of Phra Thong is situated at the Andaman Sea coast of southern Thailand. Separated from the mainland by tidal channels it extends up to 15 km in a north-south direction and 8 km from east to west. The island is formed by sequences of almost shore-parallel beach ridges that reach altitudes of 3-5 m above mean sea level; the intervening swales are on average about 1m lower. In the eastern part, these structures are predominantly covered by mangroves and dense vegetation, while grassy ridges and wet swales build up an open beach ridge plain in the western part of the island (fig. 5.1).

In December 2004 this western section of Phra Thong was heavily affected by the IOT. Waves of >10 m height inundated more than 2 km inland and left behind a 5-20 cm thick sheet of sand (Jankaew et al., 2008). While these deposits are poorly preserved on the ridges and can hardly be distinguished any more from the pre-existing sediments, the wet, peaty swales exhibit favourable conditions for the accumulation and preservation of tsunami deposits. Therefore, not only the tsunamite of 2004, but also several older sand sheets, which are inferred to be tsunamigenic (see Jankaew et al., 2008 for discussion), are preserved between the peat and peaty soils of the swales.

5.3   Samples and methodology

5.3.1   Field work

For OSL sampling, two swales and the adjacent beach ridges at distances of 700 m and 1300 m from the shoreline were chosen (swales A and B in fig. 5.1). Confined by strata of peat or peaty soil, two (swale A) and three (swale B) allochthonous sand sheets were archived in these depressions (fig. 5.2). The uppermost layer (S1) was deposited by the IOT 2004; the older ones (S2 and S3) resulted from prehistoric tsunami events. The intra-swale deposits were confined by intertidal sand below the swales (M) and laterally by beach ridges. Samples for light sensitive analyses were taken in opaque plastic tubes from the tsunamites (KPT 2i/1 and 2i/2 from S1, KPT 2k/1 and 2k/2 from S2) and the surrounding littoral sand (KPT 2j/1 and 2j/2 from M, KPT 12a/1 and 12a/2 from the landward ridge) of swale A, as well as the palaeotsunamis (KPT 20/1 from S2, KPT 20/2 form S3) and the swale base (KPT 20/3 from M) in swale B. Samples for radionuclide analyses were collected from each stratigraphical unit separately, to account for the inhomogeneous substrate (fig. 5.2): the tsunami layers, the confining peaty strata (KPT 2k+1, 2k-1, 20/1+1, 20/1-1 and 20/2-1), the intertidal sand at the swale bases and the beach ridge.
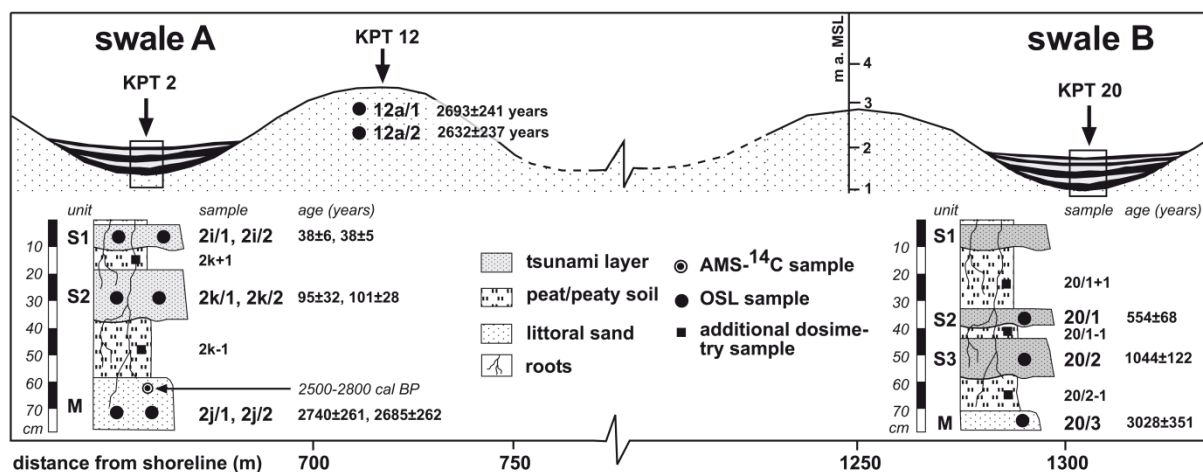
Figure 5.2: *Stratigraphy of the sampling sites with the positions of OSL samples. Radiocarbon data adopted from Jankaew et al. (2008). S1 = IOT 2004 deposit, S2-3 =palaeotsunami deposits, M = marine deposits.*

5.3.2 Sample preparation and equipment

The processing for the palaeodose determination was carried out in subdued red light. All samples were dry sieved to separate grain-size fractions between 100 and 250 μm and treated with HCl, H_2O_2 and sodium oxalate. To extract pure quartz, the sediment was separated with heavy liquid (2.62 and 2.68 g/cm^3) and finally etched with concentrated HF (40%). Measurements were performed on a Risø TL/OSL DA 20 with a ^{90}Sr/^{90}Y beta source delivering 0.0965 Gy/s at the sample position. Luminescence signals were detected through a Hoya U340 filter (7.5 mm) after blue LED stimulation at 125 °C for 50 s. Small aliquots of 1 or 2 mm were fixed on steel discs using silicon oil. The measurement procedure followed the SAR protocol of Murray and Wintle (2003) with three regenerative doses, zero measurement, repetition of the first regenerative dose, and test doses of ~25% of the natural signal or 0.5 Gy as a minimum. After the last regeneration cycle, IR stimulation was applied to check for feldspar contamination (Stokes, 1992). The dose rate (tab. 5.1) was calculated from K, Th and U concentrations, which were estimated by high resolution gamma spectrometry, and cosmic radiation (based on geographical position, thickness and density of the sediment cover) using the ADELE software (Kulig, 2005); for the effect of in-situ water content and organic carbon (LOI) similar stopping powers were assumed (Madsen et al., 2005). In case of inhomogeneous stratigraphy (strata < 60 cm thick) the dose rate was calculated by means of a layer model (Kulig, 2005). Significant radioactive disequilibria were not observed.

5.3.3 Laboratory experiments

The effect of thermal pre-treatment was analysed using preheat-plateau and thermal transfer tests (Rhodes and Bailey, 1997) with increasing preheat temperatures of 160-280 °C. The

general applicability of the samples for OSL dating was tested by analysing recuperation (acceptable if < 80 mGy), recycling ratio (acceptable if 0.9-1.1), and dose recovery (acceptable if < 5% discrepancy) with laboratory doses in the range of the natural dose (Wintle and Murray, 2006). Linear modulated OSL measurements were performed to separate signal components with different bleaching sensitivities (Bulur et al., 2000).

Table 5.1: Dosimetry data of swales A and B. K = potassium, Th = thorium, U = uranium, W = water content, LOI = loss on ignition, D = dose rate.

Sample	Depth (cm)	K (%)	Th (ppm)	U (ppm)	W (%)	LOI (%)	D (Gy/ka)
KPT 2i/1	8	0.82±0.03	95.5±3.8	13.2±0.5	15	1.6	6.47±1.1
KPT 2i/2	8	0.31±0.01	49.7±2.7	7.3±0.11	16	1.7	2.78±0.4
KPT 2k+1	14	0.35±0.01	27.2±1.1	4.9±0.20	28	4.0	
KPT 2k/1	33	0.13±0.01	8.5±0.32	1.9±0.08	15	0.5	1.70±0.3
KPT 2k/2	33	0.07±0.01	12.4±0.5	2.9±0.09	15	0.5	1.47±0.4
KPT 2k-1	50	0.52±0.02	54.3±2.1	8.5±0.32	23	3.0	
KPT 2j/1	80	0.15±0.01	17.7±0.4	4.1±0.13	23	0.3	1.71±0.2
KPT 2j/2	80	0.15±0.01	16.6±0.7	3.8±0.05	24	0.3	1.69±0.2
KPT 12a/1	90	0.03±0.01	2.76±0.2	0.8±0.05	12	0.4	1.03±0.1
KPT 12a/2	90	0.03±0.01	2.89±0.2	0.9±0.03	12	0.4	1.03±0.1
KPT 20/1+1	30	0.65±0.07	75.8±3.0	13.3±0.6	45	11.6	
KPT 20/1	41	0.50±0.07	86.8±3.5	13.5±0.6	17	0.9	8.19±0.4
KPT 20/1-1	45	0.63±0.07	83.3±3.3	12.1±0.5	21	5.5	
KPT 20/2	50	0.71±0.17	155±6.2	19.7±0.8	18	0.8	12.0±0.6
KPT 20/2-1	60	0.80±0.05	26.9±1.1	5.1±0.22	31	4.8	
KPT 20/3	90	0.52±0.02	9.1±0.48	2.3±0.10	17	0.3	1.67±0.3

5.3.4 Equivalent dose determination

Equivalent doses (D_e) were extracted from shine-down curves using the late background technique (LBG) with intervals of 0-1 s (signal) and 40-50 s (background), as well as the early background approach (EBG) of Ballarini et al. (2007) with intervals of 0-0.4 s (signal) and 0.4-1.4 s (background) (fig. 5.3); for EBG a signal-background ratio of 1:2.5 was adopted from Cunningham and Wallinga (2010). For poorly bleached sediments EBG is supposed to give better results, due to a bigger percentage of the fast component, which is bleached more quickly than the medium and the slow component (Ballarini et al., 2003).

Mean equivalent doses were determined by the central age model (CAM) and the minimum age model (MAM) of Galbraith et al. (1999). The expected scatter (σ_b) calculated by means of Gaussian error propagation [Geyh, 2005; $\sigma_b = (\text{internal scatter}^2 + \text{micro-dosimetry}^2)^{0.5}$] with internal scatter determined by dose recovery tests and micro-dosimetry taken from the well bleached samples KPT 2j (11%) for littoral deposits and KPT 20/1 (6.2%) for tsunamigenic deposits, gave values of 7.3-7.6% for the tsunamites and 10.3-11.3% for littoral sediment. Since the adopted micro-dosimetry values are not necessarily valid for all samples of the same type and the determined σ_b values seem inappropriately low (e.g. Arnold and Roberts, 2009),

the average over-dispersions of well bleached littoral samples (15%, based on KPT 2i/1-2, 12a/1-2, 20/3) and well bleached tsunamites (11%, based on KPT 20/1-2) were used instead.

5.4 Results

5.4.1 Luminescence properties

The shine-down curves revealed relatively high signal intensities for all samples; LM-OSL measurements demonstrated a dominating fast component (fig. 5.3). The preheat tests showed stable plateaus with acceptable recycling ratios and low thermal transfer (fig. 5.4). Based on this, preheat temperatures of 220 °C (KPT 2i, 12a, 20/1-3) and 240 °C (KPT 2k and 2j) were selected. Concerning the recycling ratio and recuperation, only 7% of the tsunamigenic and 20% of the littoral aliquots had to be excluded. Dose recovery worked out well for all samples with an average ratio between measured and given dose of 1.02 ± 0.01.
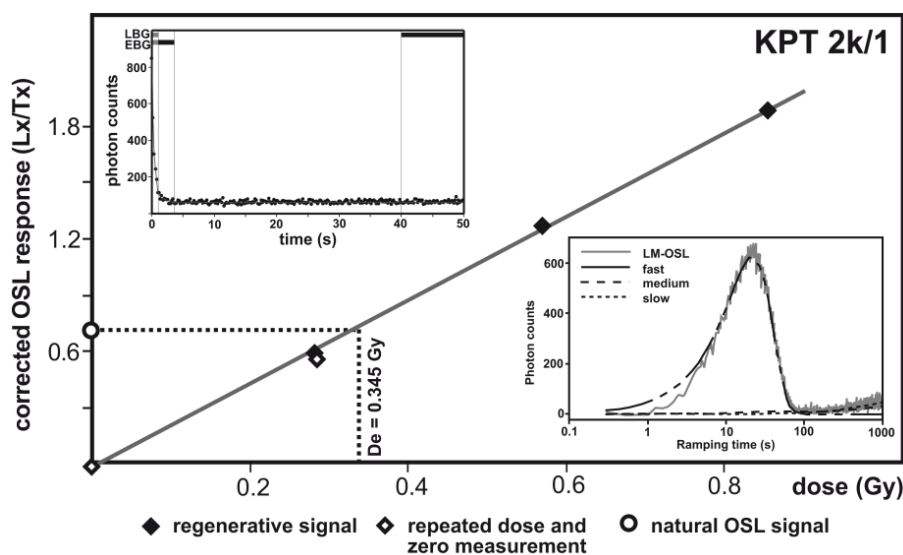
Figure 5.3: *Typical luminescence signal of KPT 2k/1 (2 mm aliquots). Shine-down curve with LBG and EBG integrals, linear SAR growth curve, and linear modulated luminescence response.*

5.4.2 Equivalent dose distributions

Both approaches of D_e determination – EBG and LBG – produced values with acceptable signal-background ratios and precision. Thus, due to the potential benefits of EBG for poorly bleached deposits (Cunningham and Wallinga, 2010) it was preferred for the D_e calculation. The associated D_e values (tab. 5.2 and fig. 5.5) showed an approximately normal distribution in case of the littoral deposits (KPT 12a/1-2, 2j/1-2 and 20/3) with only slight skewness (0.3-1.8), and moderate values of scatter (RSD < 20%) and over-dispersion (11-22%). In contrast, the tsunami layers in swale A (KPT 2i/1-2 and 2k/1-2) revealed higher skewness (0.6-3) and

scatter (RSD = 40-120%, over-dispersion = 36-79%); only those in swale B (KPT 20/1 and 20/2) were slightly skewed (0.7) and scattered (over-dispersion = 11%).
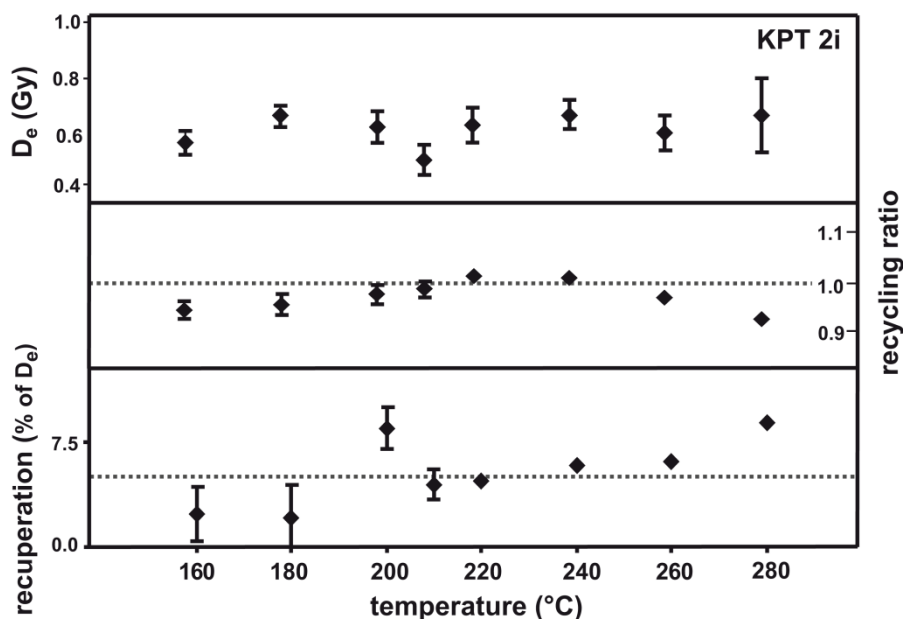
Figure 5.4: *Preheat test for KPT 2i. Equivalent doses (top), recycling ratios (middle), and recuperation (down) plotted against increasing preheat temperatures.*

5.4.3 Age model results

While the ages (in years before AD 2009) of samples from the same stratigraphical unit (e.g. KPT 2i/1 and 2i/2) were relatively conformable within each method and therefore reproducible, the results of different age models partially differed significantly (tab. 5.2 and fig. 5.5). Considering the dating uncertainty, CAM and MAM provided the same ages for the littoral deposits and the palaeotsunamites in swale B. In case of the tsunamigenic sand sheets in swale A, the ages derived with CAM were significantly older compared to MAM.

5.5 Discussion of luminescence ages

The selection of the most appropriate age model for each type of sediment was based on the D_e distribution and its statistical parameters (tab. 5.2 and fig. 5.5), using CAM for well bleached samples and MAM for poorly bleached deposits. With 40-100 aliquots that passed SAR acceptance criteria (cf. chapter 5.3.3) per sample, the results should be statistically significant, even for heterogeneously bleached material (Rodnight, 2008); the small diameter of the aliquots should be suitable to detect incomplete bleaching (Wallinga, 2002). To evaluate the reliability of the luminescence ages, the results of tsunamigenic (KPT 2i/1-2) and littoral (KPT 2j/1-2 and 12a/1-2) reference deposits in swale A were cross-checked with independent

age control provided by the IOT 2004 and radiocarbon data of Jankaew et al. (2008) (Chapter 5.5.1).

Table 5.2: Mean D_e and ages for all samples. N = number of accepted aliquots, Ovd = over-dispersion, σ_b = expected scatter, Sk = skewness, CAM = central age model, MAM = minimum age model.

Sample	Ø	N	Ovd	Sk	σ_b	CAM		MAM	
	mm		%		%	D_e (Gy)	age (a)	D_e	age (a)
KPT 2i/1	1	105	56.2	2.9	11.0	0.59±0.1	72±15	0.31±0.03	38±6
KPT 2i/2	1	108	36.3	0.6	11.0	0.49±0.1	60±14	0.31±0.02	38±5
KPT 2k/1	2	57	75.7	2.9	11.0	0.39±0.1	246±80	0.15±0.04	95±32
KPT 2k/2	2	81	78.9	3.0	11.0	0.45±0.1	284±85	0.16±0.03	101±28
KPT 2j/1	1	56	14.2	0.3	15.0	4.68±0.1	2740±261	4.67±0.1	2728±261
KPT 2j/2	1	83	10.5	0.6	15.0	4.47±0.1	2685±262	4.46±0.1	2678±262
KPT 12a/1	1	48	20.8	0.7	15.0	2.76±0.1	2693±241	2.33±0.1	2249±214
KPT 12a/2	1	38	22.1	1.6	15.0	2.72±0.1	2632±237	2.55±0.1	2432±225
KPT 20/1	1	57	6.2	0.7	11.0	4.48±0.2	557±69	4.45±0.2	554±68
KPT 20/2	1	40	11.1	0.7	11.0	14.1±0.5	1177±139	12.5±0.4	1044±122
KPT 20/3	1	42	11.2	1.8	15.0	5.07±0.1	3028±351	5.07±0.1	3028±351

5.5.1 Reference deposits in swale A

Considering the normal distributed D_e values of the littoral deposits in swale A as an indicator for complete bleaching (Wallinga, 2002), CAM – yielding ages of 2425-3000 years (KPT 2j/1-2) and 2390-2930 years (KPT 12a/1-2) – should be the most reasonable choice to determine burial doses. The swale base (KPT 2j/1-2) has been radiocarbon-dated to 2500-2800 cal BP (fig. 5.2) by Jankaew et al. (2008). Since the adjacent landward ridge must be slightly older, an age of at least 2500-2800 cal BP is expected for KPT 12a/1-2. Thus, if analysed with CAM, the OSL ages of littoral deposits are in very good agreement with independent radiocarbon data (fig. 5.5).

The positively skewed and over-dispersed D_e distribution of the IOT 2004 deposit indicates incomplete resetting of the luminescence signal (Wallinga, 2002). Thus, MAM should provide the most reliable results. Since IOT 2004 samples KPT 2i/1 and 2i/2 were dated early in AD 2009, their correct age is four years. Although this is overestimated by both model approaches (fig. 5.5), with maximum offsets of only 53-83 years based on CAM, the residual is similar to that of IOT 2004 deposits in India (< 50 years, Murari et al., 2007) and tsunamites of other locations (e.g. 60-120 years for the Lisbon 1755 tsunami, Cunha et al., 2010). The residuals of 28-40 years determined by MAM, are even less significant, especially compared to the dating error of palaeoevents with ages > 500 years.
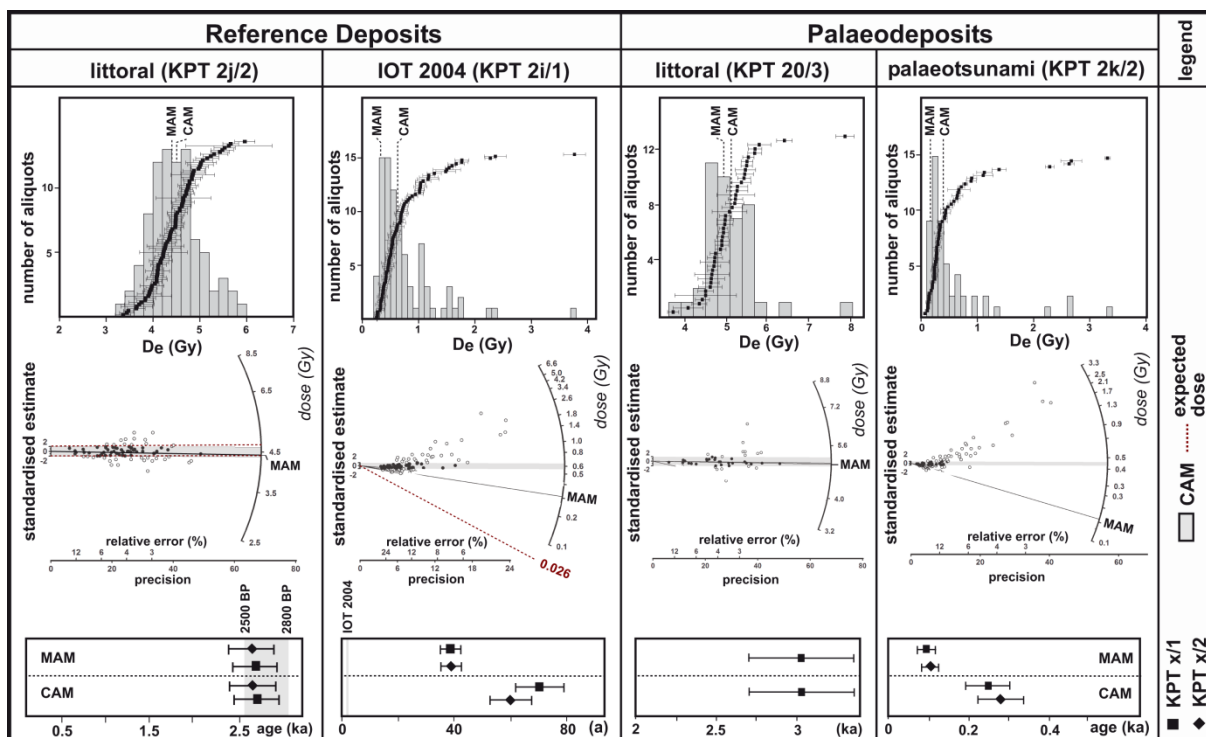
Figure 5.5: *Typical D_e distributions and ages (determined with different age models and compared to expected ages) of all sediment types.*

5.5.2 Palaeodeposits of unknown age

The intertidal sand at the base of swale B (KPT 20/3) is characterised by normally distributed D_e values, similar to the littoral sediments of swale A (fig. 5.5). Thus, as shown for the reference deposits, the CAM-based age of 3030 ± 350 years should provide a reliable estimate. The palaeotsunami deposit in swale A (KPT 2k/1-2) reveals a D_e distribution similar to the modern tsunamites, reflecting significant effects of incomplete bleaching (fig. 5.5). Therefore, MAM (98 ± 30 years) should give the most reliable results as demonstrated for the tsunami-genic reference deposits of the IOT 2004. In contrast, the D_e distributions of the palaeotsuna-mi layers in swale B (KPT 20/1 and 20/2) are only slightly skewed and over-dispersed and resemble those of the littoral sediments. This discrepancy can be explained by the much older ages of the prehistoric tsunamites in swale B, since similar residuals like those observed for the IOT 2004 are small compared to the dating error of 500-1000 year old deposits. However, since it was demonstrated that MAM minimises the residual for the IOT 2004 deposits (the difference between CAM and MAM shows no systematic increase with increasing age of the sample and therefore seems to reflect the unbleached residual), MAM based ages of 554 ± 68 years (KPT 20/1) and 1044 ± 122 years (KPT 20/2) should give the best age estimates.

Although no independent age control is available to cross-check the luminescence results, their reliability is supported by stratigraphical data and the chronological context. (i) For both

locations, all ages are in agreement with their stratigraphical position (from above to below): IOT 2004 (S1) – 70-130 years (S2) – 2425-3000 years (M) in swale A, and IOT 2004 (S1) – 554 ± 68 years (S2) – 1044 ± 122 years (S3) – 3030 ± 350 years (M) in swale B (fig. 5.2). (ii) Additionally, the palaeotsunami layers can be compared with existing chronological data, which postulate 3-4 palaeotsunamis within the last 2800 years for Ko Phra Thong, the youngest of them having taken place 550-700 years ago (Jankaew et al., 2008). Both tsunamites in swale B match this age range (550-2800 years); the 554 ± 68 year old layer (KPT 20/1) is even congruent with the 550-700 year event. Furthermore, the deposition of both palaeotsunami layers coincides with strong ruptures of the Sunda Arc (Meltzner et al., 2010) and tsunami impact on other coasts of the Indian Ocean (e.g. Monecke et al., 2008). In contrast, for the last 200 years no tsunami strong enough to inundate the coastal plain of Phra Thong has been reported by historical records. Although a minor rupture of the Sunda Arc occurred in 1881 (Bilham et al., 2005), which would match the OSL age of the third palaeotsunami layer (KPT 2k/1-2), dated to 100 ± 30 years, it is not likely that the associated tsunami was capable of generating the observed sand layer (Okal and Synolakis, 2008). Thus, the interpretation of layer S2 in swale A still remains to be defined appropriately.

5.6 Conclusions

To establish a luminescence-based event chronology for Phra Thong Island, the combined dating of tsunamigenic sand sheets and surrounding littoral deposits is considered to be a promising strategy. Generally, both types of sediment revealed good luminescence properties and good signal intensities. Furthermore, OSL results are in good agreement with independent age control for littoral as well as tsunamigenic reference deposits. Thus, its application to sediments of unknown age, which cannot be cross-checked, should provide reliable chronological data as well.

OSL dating of IOT 2004 deposits reveals small residuals of less than 40 years when analysed with MAM, and thereby demonstrates the general suitability of the method for the dating of the Phra Thong tsunamites. Since the palaeotsunami deposits showed similar D_e distributions, their MAM based ages should also give reliable estimates for the time of deposition. Tsunamites with ages of several hundred years demonstrate that the small residuals observed in the IOT 2004 deposit rapidly become insignificant with increasing age. Nevertheless, the ages should be carefully discussed in their stratigraphical context. The application of OSL to littoral deposits revealed rather well bleached signals. Ages of a beach ridge and intertidal sand based on CAM match the independent radiocarbon chronology precisely, thus providing information for littoral deposits of unknown age.

Chapter 6

6 Local inundation distances and regional tsunami recurrence in the Indian Ocean inferred from luminescence dating of sandy deposits in Thailand[3]

Abstract: The Holocene beach-ridge plain of Phra Thong Island (Ko Phra Thong, SW Thailand) provides sedimentary evidence of several palaeotsunamis, in addition to the deposit of the 2004 Indian Ocean tsunami. Due to poor preservation conditions, these palaeoevent layers are restricted to swales. Correlation across beach ridges, which is important e.g. to reconstruct inundation distances, remains a major challenge. A primary tool for establishing a precisely confined correlation of the sand sheets is the use of chronological data. Since the application of radiocarbon dating is limited by the scarcity of appropriate material, this study utilised optically stimulated luminescence (OSL) dating of tsunamigenic quartz grains. Generally, the sediments showed favourable luminescence properties regarding signal intensity, dose recovery and thermal stability. Disturbances of the OSL signal due to partial bleaching were corrected using the minimum age model. At least three palaeoevents – being 490–550, 925–1035 and 1740–2000 yr old – were distinguished by dating the discontinuous sand sheets at four different sites. Besides this chronological framework, the OSL data provide the opportunity to correlate the discontinuous sand sheets between spatially separated sites within the same swale as well as across ridges. This allows for first estimates of inundation distances for the palaeotsunamis documented on Phra Thong Island. Furthermore, the two younger events overlap in age with contemporaneous tsunami and earthquake evidence from other coasts bordering the Indian Ocean.

6.1 Introduction

Geological evidence has been used successfully to identify prehistoric tsunami events and to reconstruct their recurrence probability in many risk areas of the world for more than twenty years (e.g. Atwater, 1987; Dawson et al., 1988; Nanayama et al., 2003; Pinegina et al., 2003; Cisternas et al., 2005; Dawson and Stewart, 2007; Engel et al., 2010; papers in Mastronuzzi et al., 2010). This is particularly important in regions that lack written sources, like many countries around the Indian Ocean, where historical records, if available, are restricted to the last 400 or so years (Murty and Rafiq, 1991; Kumar and Achyuthan, 2006; Dominey-Howes et al.,

---

2007). In contrast, changes in the coastal geomorphology by erosion, deposition, uplift and subsidence, caused by the 2004 Indian Ocean Tsunami (IOT) and its triggering earthquake, demonstrate that tsunami impact may leave its signature in the geological record (e.g. Szczuciński et al., 2006; Choowong et al., 2007; Kelletat et al., 2007; Kayanne et al., 2007; Sibuet et al., 2007; Srinivasalu et al., 2007; Fagherazzi and Du, 2008; Morton et al., 2008; Paris et al., 2009; Switzer et al., 2012). While co-seismic movement at near-field sites along the rupture area is used to detect palaeoearthquakes that might have generated past tsunamis (e.g. Rajendran et al., 2008; Sieh et al., 2008), the research on coasts distant from the seismic zones, such as SW Thailand, concentrates on sedimentary evidence of tsunami impacts (e.g. Monecke et al., 2008; Dahanayake and Kulasena, 2008; Jankaew et al., 2008, Brill et al., 2011). However, due to the scarcity of archives along the west coast of Thailand, an accurate chronology remains to be defined. The most promising results so far originate from Phra Thong Island (Ko Phra Thong), where up to four sand sheets, inferred to be tsunamigenic, and older than 2004, are preserved in the swales of a wide beach-ridge plain (Jankaew et al., 2008).

Although crucial for establishing recurrence rates of prehistoric tsunami events, the dating of tsunamigenic sand sheets on Phra Thong remains a major challenge (Jankaew et al., 2011). The importance of well-constrained chronological data is further stressed by the fact that dating of tsunamites seems to be the only possibility to correlate layers between different sites on the island, especially across ridges. This information is necessary, e.g. to reconstruct inundation distances that may function as a valuable indicator for the magnitude of the events. Due to intensive tropical weathering, bioturbation, root penetration and anthropogenic impacts, the preservation potential on Phra Thong is low, and the disturbed and discontinuous sand sheets persisted only in the lowest parts of the undulating topography. In addition, the use of radiocarbon dating is restricted by the scarcity of datable macro-remains in the peaty soils confining the tsunami deposits, and by the uncertainty of ages obtained from plant fragments inside the sand sheets, since it is often reworked material of an older age (Jankaew et al., 2008; Fujino et al., 2009). Thus, optically stimulated luminescence (OSL) dating may provide a useful tool to establish a reliable chronological framework for the tsunami history of the island.

In general, OSL dating has the advantage to measure the time elapsed since sedimentation and, therefore, provides direct information about the time of deposition, while sandwich dating with the radiocarbon technique results in limiting ages. Various studies conducted in the last few years demonstrate that luminescence dating is principally suited to determine burial ages of tsunamigenic sandy sediments (e.g. Huntley and Clague, 1996; Banerjee et al., 2001; Murari et al., 2007; Cunha et al., 2010), although it is associated with several uncertainties; especially partial bleaching of the luminescence signal due to short and highly turbulent transport conditions in tsunami waves (Bishop et al., 2005; Murari et al., 2007) or inhomoge-

neous dose rates may be a problem locally. Nonetheless, OSL dating of IOT deposits and pal-aeotsunami sediments of known age, conducted in two recent studies, proved the general ap-plicability of the method for tsunamigenic sand sheets on Phra Thong (Brill et al., 2012a; Prendergast et al., 2012). The presented work aims to use OSL ages of tsunamigenic quartz grains to (1) improve the chronology of tsunami events on Phra Thong, and (2) enable the correlation of distinct layers, preserved in different swales of the island. To achieve this, dis-continuous sand sheets inferred to be tsunamigenic were dated at several sites of the same swale. Based on these ages, a correlation of layers within the swale and, by considering exist-ing chronological data of previous studies, across ridges was conducted.

6.2 Physical setting

The island of Phra Thong is located off the Andaman Sea coast of southern Thailand, 125 kilometres north of Phuket (fig. 6.1a), where it forms part of a system of barrier islands (Sin-sakul, 1992). Separated from the mainland by tidal channels less than 4 km wide and 10 m deep, it extends up to 15 km from north to south and 8 km in an east-west direction. The to-pography of the island is dominated by several sequences of shore-parallel swales and beach ridges (fig. 6.1b), which reach heights of 2-5m above mean sea level (a.s.l.). While these structures are predominantly covered by mangroves and dense vegetation in the eastern part of Phra Thong, grassy ridges and wet, tree-lined swales build up a 3 km wide, open beach-ridge plain with favourable properties for the accumulation of tsunami deposits in the west of the island.

Although SW Thailand is part of the tectonically stable Malay-Thai Peninsula with negligible seismic activity during the Holocene (Tjia, 1996), the active subduction zone of the Sunda Arc is located directly west of the study area. Due to the convergence of the Indo-Australian Plate and the Sunda and Burma Microplates, the area is a major source of tsunami-generating earthquakes, which are capable of producing waves strong enough to reach the Thai coast, as observed in December 2004 (Lay et al., 2005; Subarya et al., 2006). Although no historical tsunami prior to 2004 has been reported to have affected SW Thailand significantly (Bilham et al., 2005; fig. 6.1a), convergence rates at the Sunda Arc (Løvholt et al., 2006) and evidence of co-seismic uplift (Rajendran et al., 2008; Meltzner et al., 2010) point to previous mega-thrust ruptures similar in magnitude to 2004, which probably resulted in severe tsunamis dur-ing prehistoric times.

Climatically, the study area is located in the sub-humid tropics with heavy rainfall during the summer monsoon and a dry period from December to February. Although the zone north of 5° N is generally characterised by the occurrence of tropical storms during the inter-monsoon periods (Pielke and Pielke, 1997), cyclone tracks in the Bay of Bengal are predominantly di-rected to the coasts of India, Bangladesh and Myanmar (Singh et al., 2000). For the eastern

coast of the Andaman Sea, historical records show no landfall of a cyclone within the last 150 yr (Murty and Flather, 2004). The tropical storm recorded closest to the study area was Cyclone Nargis in 2008, which hit the coastline of southern Myanmar 800 km to the north (Fritz et al., 2009a).
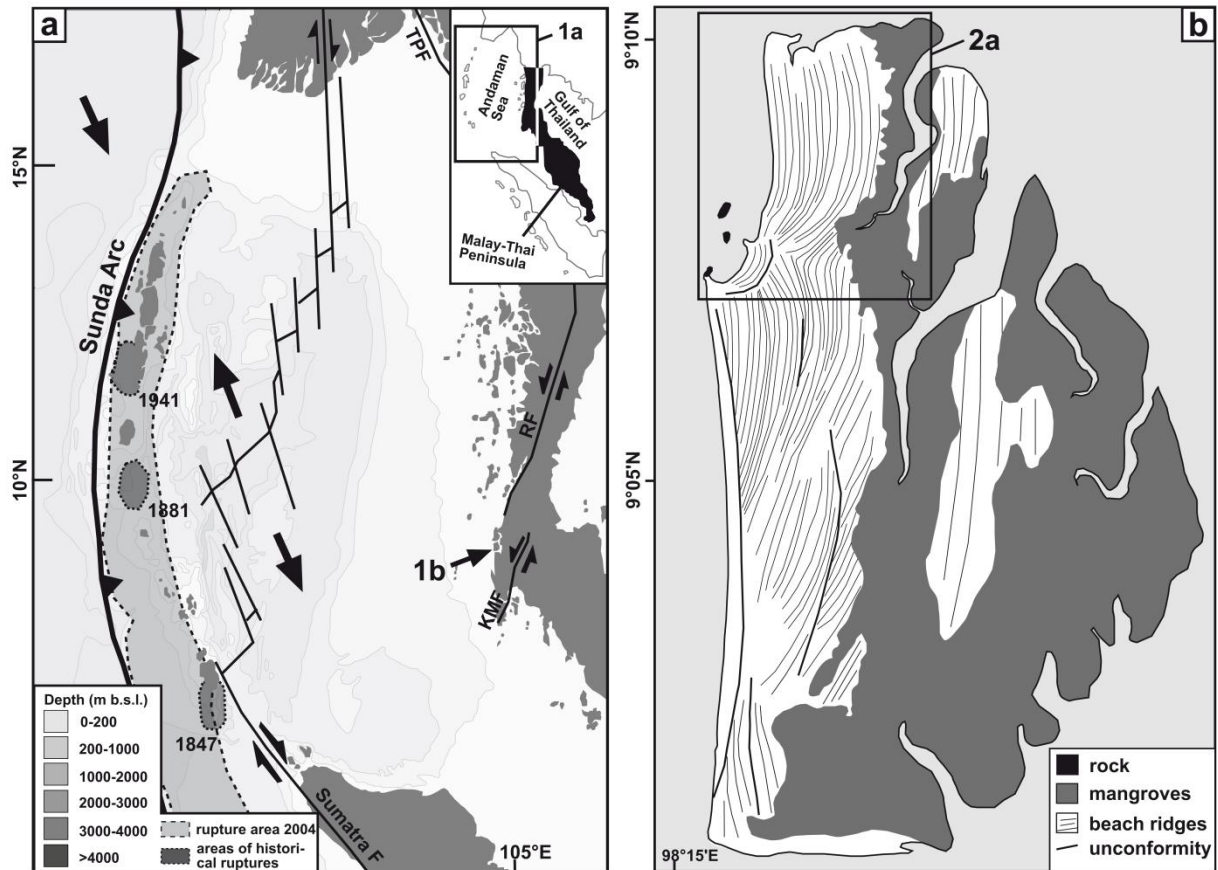
Figure 6.1: *Geographical and tectonic setting of the study area. (a) Tectonic structures of the Andaman Sea region (after Watkinson et al., 2008; KMF = Klong Marui Fault, RF = Ranong Fault, TPF = Three Pagodas Fault) with rupture areas of the 2004 megathrust (Subarya et al., 2006) and historical earthquakes (Bilham et al., 2005; Ortiz and Bilham, 2003) along the Andaman-Nicobar segment of the Sunda Arc. (b) Overview of Ko Phra Thong.*

6.3 Previous studies on Phra Thong Island

6.3.1 Evidence of palaeotsunamis

First palaeotsunamis on Phra Thong were identified by Jankaew et al. (2008) and Fujino et al. (2009). The former analysed two successive swales c. 400m east of the shoreline (swales X and Y, fig. 6.2a). Above sandy intertidal deposits, a succession of peaty soils and sharply bounded sand sheets was observed. While swale Y contained three sand sheets below that of the IOT 2004, only two pre-2004 layers were detected in swale X. All sand sheets resembled the deposits of the IOT 2004 in their sedimentary characteristics, revealing thicknesses of 5-10 cm, a composition of chaotic or normal graded medium to very fine sand and sharp con-

tacts to the peaty soils below, but lacked macro- and microfossils (Sawai et al., 2009). The sand sheets were assigned to prehistoric tsunami events, since landfalls of strong storms have not been reported; river runoff as well as aeolian dynamics can be excluded on Phra Thong, and sheet B chronologically correlates with tsunami evidence from Sumatra (Monecke et al., 2008). However, since the tsunamites were missing on the ridges, correlation between the layers of swale X and swale Y was not possible by other criteria than dating (Jankaew et al., 2008).
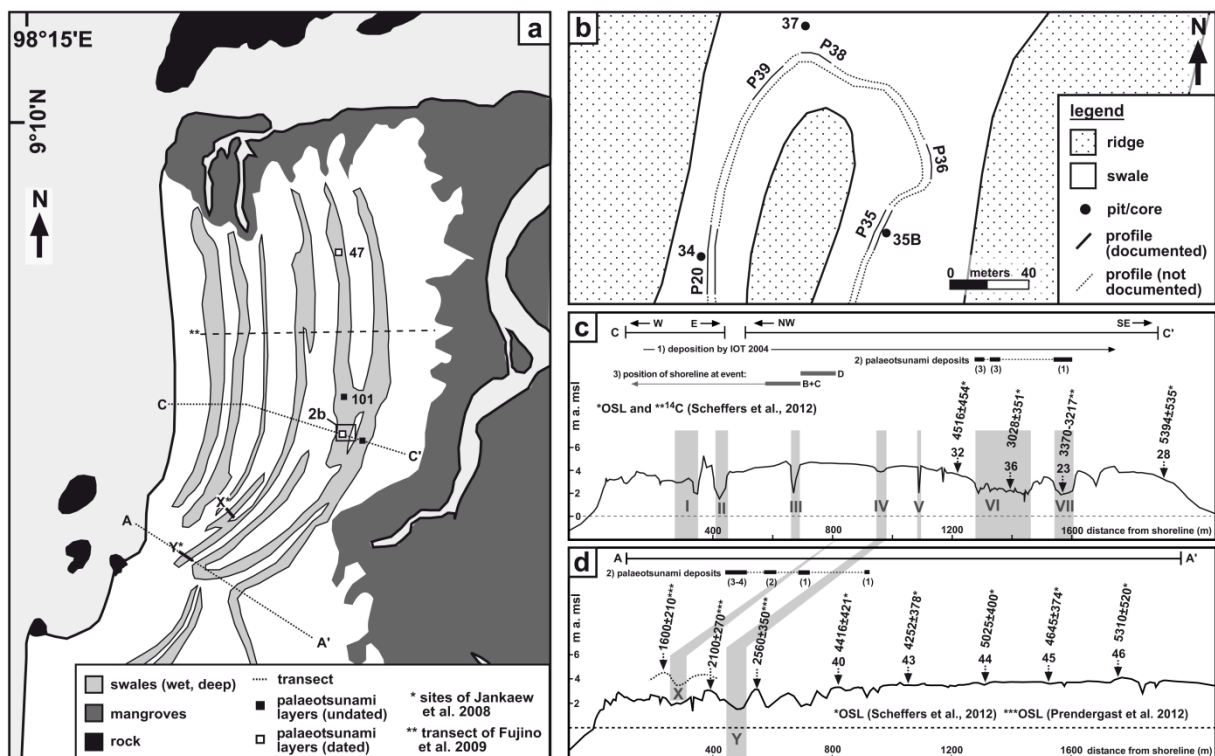
Figure 6.2: *Study area with sampling sites. (a) The north-western part of Phra Thong Island with the positions of deep and wet swales. Sampling sites of this and of previous studies are indicated. (b) Schematic overview of the southern section of swale VI (see fig. 6.2a for exact location). (c) Topographical cross section in a west-east direction along transect C (C-C' in fig. 6.2a) with position of swale VI and chronological data of the neighbouring beach ridges (Scheffers et al., 2012a). (d) Topographical cross section along transect A with beach-ridge ages from Prendergast et al. (2012) and Scheffers et al. (2012a).*

To determine ages for their tsunami deposits, Jankaew et al. (2008) used AMS-^{14}C dating of macro-remains. While leaves taken from within the tsunami layers produced conflicting results, data of plant fragments from the confining peat limited the age of the younger layer to 550-700 cal BP, and that of the older one to younger than 2200-2400 cal BP. In swale Y the age of all three pre-2004 sand sheets could only be limited to younger than 2500-2800 cal BP (Jankaew et al., 2008). More detailed age information for these deposits is presented by Prendergast et al. (2012) in the form of luminescence data. While the OSL ages confirm the correlation of layer B between both swales (350±50 and 380±50 yr), a correlation of the older layers in swale Y (2100±260 and 990±130 yr) and swale X (1410±190 yr) failed. Furthermore, the OSL ages of layer B are younger than expected from radiocarbon dating.

Fujino et al. (2009) analysed nine sediment cores from the northern part of the island (fig. 6.2a), showing a similar stratigraphy with intertidal sand overlain by peaty soils and up to two discontinuous sand sheets older than 2004. These could not be correlated laterally, not even by means of radiocarbon dating, since, different from Jankaew et al. (2008), bulk samples of peaty soil were used. Due to penetration of the sand layers and the soils by young roots, these ages (at least 1300 AD and older 1900 AD) are likely to underestimate the real ages significantly.

Considering the low precision of the ages presented by Fujino et al. (2009), as well as the uncertainty of the luminescence ages of Prendergast et al. (2012), the only well confined ages for tsunami deposits on Phra Thong so far are slightly younger than 550-700 yr for the youngest palaeotsunami and younger than 2500-2800 yr for two or three older events (Jankaew et al., 2008). A correlation of layers across ridges based on these ages remains fragmentary.

6.3.2 Holocene palaeogeography and sea levels

Both sea level and palaeogeography at the time of impact are important for the interpretation of prehistoric tsunamis. Regarding Holocene sea-level changes on the west coast of Thailand, model predictions of Horton et al. (2005) as well as field evidence of Scheffers et al. (2012a) point to a high stand of +2-3 m at 5-6 ka BP that was followed by a gradual regression to its present level, remaining below +1 m during the last 3000 years. In contrast, there is little information about the Holocene coastal evolution of Phra Thong Island. Although chronological data for the formation of the beach-ridge plain in the form of OSL ages from Prendergast et al. (2012) for transect A (fig. 6.2d) and Scheffers et al. (2012a) for transects A and C (fig. 6.2c and d) exist, it has not been used to discuss the shift in Holocene shorelines. Ridge ages of transect A, although with a poor resolution, cover the time from 5300 to 1600 yr ago, and those of transect C reach from 5400 to 3000 yr ago. Since each ridge and swale marks the position of a former shoreline, the correlation of these continuous structures between transects A and C allows for the approximate allocation of shorelines within the last 5500 yr (fig. 6.2c and d).

6.4 Methods

6.4.1 Stratigraphical methods

The stratigraphical data presented in this paper were obtained from trenches and pits with maximum depths of 1.2 m below surface (b.s.). Since digging was limited by the high groundwater table, the trench and pit data were supported by closed sediment cores to document the sediments down to 1.75 m b.s. The profiles were photographed, described and sam-

pled directly in the field. To establish an on-site facies stratigraphy, the sediment was characterised in terms of colour (Munsell Soil Color Charts), sedimentary structures and macrofossil remains. Grain size, sorting and carbonate content were estimated following Ad-hoc-Arbeitsgruppe Boden (2005). The topography of the study area was measured by means of a differential GPS (Leica SR 530) with less than 3 cm error.

Subsequently, selected reference profiles were sampled for laboratory measurements. Grain-size analyses were performed on dried fine-sediment samples (<2 mm) after treatment with H_2O_2 to remove organic matter using a laser particle sizer (Beckmann Coulter LS 13320). For the calculation of grain-size statistics (Method of Moments), the GRADISTAT software (Blott and Pye, 2001) was applied. Geochemical data include loss on ignition (LOI), determined by oven-drying at 105 °C for 12 h and ignition at 550 °C for 4 h (Beck et al., 1995). $CaCO_3$ was measured by the Scheibler method. To establish a chronological framework for the stratigraphical setting and to cross-check the luminescence ages, macrofossil and plant remains from soil below and above the tsunami layers were AMS-^{14}C-dated. Measurements were carried out at the radiocarbon laboratory of the University of Georgia at Athens (USA). Calendar ages were calculated from conventional radiocarbon years by means of the OxCal 4.01 software using the IntCal09 calibration curves of Reimer et al. (2009). All radiocarbon ages in the text are presented in 2σ sidereal years.

6.4.2 Luminescence dating

The optically stimulated luminescence technique (OSL) is based on the accumulation of a latent luminescence signal in certain mineral grains (typically quartz and potassium feldspar) due to the impact of ionising radiation in natural environments (decay of radioactive elements in the sediment and cosmic radiation) and the bleaching of this signal at exposure to sunlight (e.g. during sediment transport by wind or water). Thus, if luminescence signals are zeroed during transport, the accumulated signal at the time of sample extraction can be used to determine the time elapsed since the last transport cycle. The luminescence age is calculated by the formula: age = palaeodose/dose rate, where the palaeodose is the amount of radiation in Gy needed to build up the luminescence signal accumulated during burial (by comparing the intensity of the OSL signal with the response to known laboratory doses), and the dose rate defines the amount of absorbed radiation in Gy per unit of time (see e.g. Aitken, 1998; Duller, 2004 or Preusser et al., 2008 for a detailed description of the method). In this study we applied OSL on quartz grains from tsunamigenic sand sheets to determine ages for prehistoric tsunami events.

The tsunami layers were sampled for palaeodose determination using opaque plastic tubes and were processed in subdued red light. Dried samples were sieved into separate grain-size fractions between 100 and 250 μm and treated with HCl, H_2O_2 and sodium oxalate to remove

carbonate, organic material and clay. To obtain pure quartz, the sediment was separated with heavy liquid (2.62 and 2.68 g cm^{-3}) and finally etched with concentrated HF (40 %) for 45 min. All measurements were performed on a Risø TL/OSL DA 20 with a ^{90}Sr/^{90}Y beta source, delivering 0.0955 Gy s^{-1} to quartz grains at the sample position. Luminescence signals were detected through a Hoya U340 filter (7.5 mm) after blue LED stimulation, carried out at a temperature of 125 °C for 50 s. Small aliquots of 1mm diameter – after Duller (2008) approximately 20-50 grains – were fixed on steel discs using silicon oil. Determination of equivalent doses (D_e) followed the SAR protocol of Murray and Wintle (2000, 2003) with three regenerative doses, zero measurement (recuperation), repetition of the first regenerative dose (recycling ratio) and test doses of ~25% of the natural signal. The use of time integrals for the luminescence signal and the background subtraction followed the approach of Ballarini et al. (2007), with the background integral directly following the signal integral. Since this early background technique was designed to increase the percentage of the easily bleachable fast component, it provides general advantages for incompletely bleached samples. A ratio of 1:2.5 between signal length (0-0.4 s) and background length (0.4-1.4 s) was adopted from Cunningham and Wallinga (2010).

Table 6.1: *Dosimetry data of all samples. Depth = depth below surface, K = potassium content, Th = thorium content, U = uranium content, W = water content, LOI = loss on ignition, D = dose rate.*

sample	depth (cm)	K (%)	Th (ppm)	U (ppm)	grain size (µm)	W (%)	LOI (%)	D (Gy/kyr)
peat a. KPT 20/1	30	0.65±0.07	75.8±3.0	13.3±0.56		45.4	11.6	
KPT 20/1	41	0.50±0.07	86.8±3.5	13.5±0.56	125-200	17.2	0.9	8.19
peat a. KPT 20/2	45	0.63±0.07	83.3±3.3	12.1±0.51		21.1	5.5	
KPT 20/2	50	0.71±0.17	155.7±6.2	19.7±0.84	125-200	18.5	0.8	12.02
peat b. KPT 20/2	60	0.80±0.05	26.9±1.1	5.1±0.22		31.2	4.8	
peat a. KPT 35/1	20	0.83±0.11	114.0±4.6	18.5±0.77		27.7	11.3	
KPT 35/1	30	0.67±0.09	101.4±4.1	15.5±0.64	125-200	16.0	1.1	10.12
peat a. KPT 35/2	36	0.94±0.09	104.3±4.2	15.7±0.65		17.3	4.2	
KPT 35/2	43	1.03±0.12	122.0±4.9	17.3±0.72	125-200	18.3	0.8	11.52
KPT 35/3	52	0.59±0.04	13.7±0.5	3.0±0.13	125-200	11.9	0.7	3.35
peat b. KPT 35/3	60	0.62±0.05	16.8±0.7	6.5±0.27		18.1	4.5	
KPT 37/1	24	0.71±0.09	69.5±2.8	11.3±0.47	125-200	20.6	1.6	6.8
peat a. KPT 37/2	27	0.85±0.11	84.0±3.3	13.1±0.55		51.6	25.0	
KPT 37/2	30	0.91±0.16	138.2±5.5	19.9±0.83	125-200	23.8	1.5	10.83
peat b. KPT 37/2	40	0.78±0.12	96.0±3.8	14.9±0.62		29.8	18.6	
peat a. KPT 47/1	12	0.65±0.05	51.5±2.7	9.2±0.41		42.0	12.1	
KPT 47/1	20	0.61±0.09	75.2±1.2	11.7±0.32	125-200	20.0	0.9	7.33
peat a. KPT 47/2	25	0.93±0.10	74.0±3.0	12.4±0.52		22.0	5.2	
KPT 47/2	32	0.59±0.18	64.8±2.6	10.1±0.42	125-200	17.7	0.8	6.21
peat a. KPT 47/3	38	0.22±0.04	12.8±0.5	3.5±0.15		19.5	4.3	
KPT 47/3	50	0.19±0.02	10.8±0.6	2.9±0.14	180-200	17.0	1.2	1.61
peat b. KPT 47/3	60	0.22±0.02	15.5±0.7	3.8±0.21		19.0	5.8	

The effects of thermal pre-treatment were analysed by applying preheat plateau and thermal transfer tests. For this, the corrected OSL signal was measured in dependence of increasing preheat temperatures between 160 °C and 280 °C (after room temperature bleaching of the natural signal using blue LEDs in the case of the thermal transfer test). To guarantee the applicability of the samples for OSL dating, the recuperation and recycling ratios were analysed (Wintle and Murray, 2006). Additionally, we performed dose recovery tests with the laboratory radiation in the range of the natural doses. For the calculation of mean equivalent doses, the central age model (CAM), in case of well-bleached deposits, and the minimum age model (MAM), in case of incomplete bleaching, of Galbraith et al. (1999) were applied, whereas over-dispersion and the shape of D_e distributions were consulted to define the state of bleaching. The expected scatter, σ_b, used for calculations with MAM, was taken from the average over-dispersion of well-bleached samples of the setting.

Dosimetry samples were taken from tsunamigenic sand sheets as well as the confining soil. The dose rate was calculated separately for the layers and the surrounding material from K, Th and U concentrations, measured via Neutron Activation Analyses at Becquerel Laboratories (Canada), and from in-situ water and organic carbon contents of the samples (after Madsen et al., 2005), using the layer model of the ADELE software (Kulig, 2005). The results are presented in table 6.1.

6.5   Results and discussion

6.5.1   Lithostratigraphy of swale VI

Samples were taken from a deep and wet swale in the northern part of Phra Thong, approximately 1.3 km east of the present shoreline (swale VI, fig. 6.2). The stratigraphy was documented along a 1.2 km long, south-north directed section of the swale. It is based on seven profiles, generated from trenches (KPT 20, 35, 36, 39 and 47) and pits (KPT 37 and 101), with core data being used to extend the stratigraphies of KPT 20 (core KPT 34), KPT 35 (core KPT 35B) and KPT 37 (core KPT 37B) even below groundwater level (fig. 6.2a, b). Generally, all analysed profiles showed a similar succession of sediments (fig. 6.3). Representative profiles of the typical stratigraphy (KPT 20/34) and the stratigraphy of the wettest sections (KPT 37) are presented in Chapter 6.5.1.1.

6.5.1.1 Reference profiles KPT 20/34 and KPT 37

Figure 6.4 shows the combined data of trench KPT 20 and core KPT 34. The base, from 1.20 to 0.71 m b.s., was composed of medium sand (mean = 260-570 μm) of light grey colour (2.5Y 6/1) at the bottom and light greyish brown (2.5Y 5/2) towards the top. The sand contained wood fragments, but lacked fossils (in the same depositional unit of KPT 35, marine

molluscs and coral fragments occurred where the deposits were situated below sea level; b.s.l.). The content of organic matter was low (0.2-0.5 %) and carbonate was absent. At 0.71 m b.s., a sharp contact separated the greyish sand from a succession of peaty soils and sand sheets (S1-S4). The former were characterised by dark brown colour (10YR 3/3), muddy sand (mean = 150-210 μm) with high amounts of organic carbon (5-12 %) and absence of $CaCO_3$ or fossils. All peaty strata comprised densely packed modern and subrecent roots, but lacked macroscopic plant fragments (except for the uppermost peat at 0.33-0.11 m b.s.).
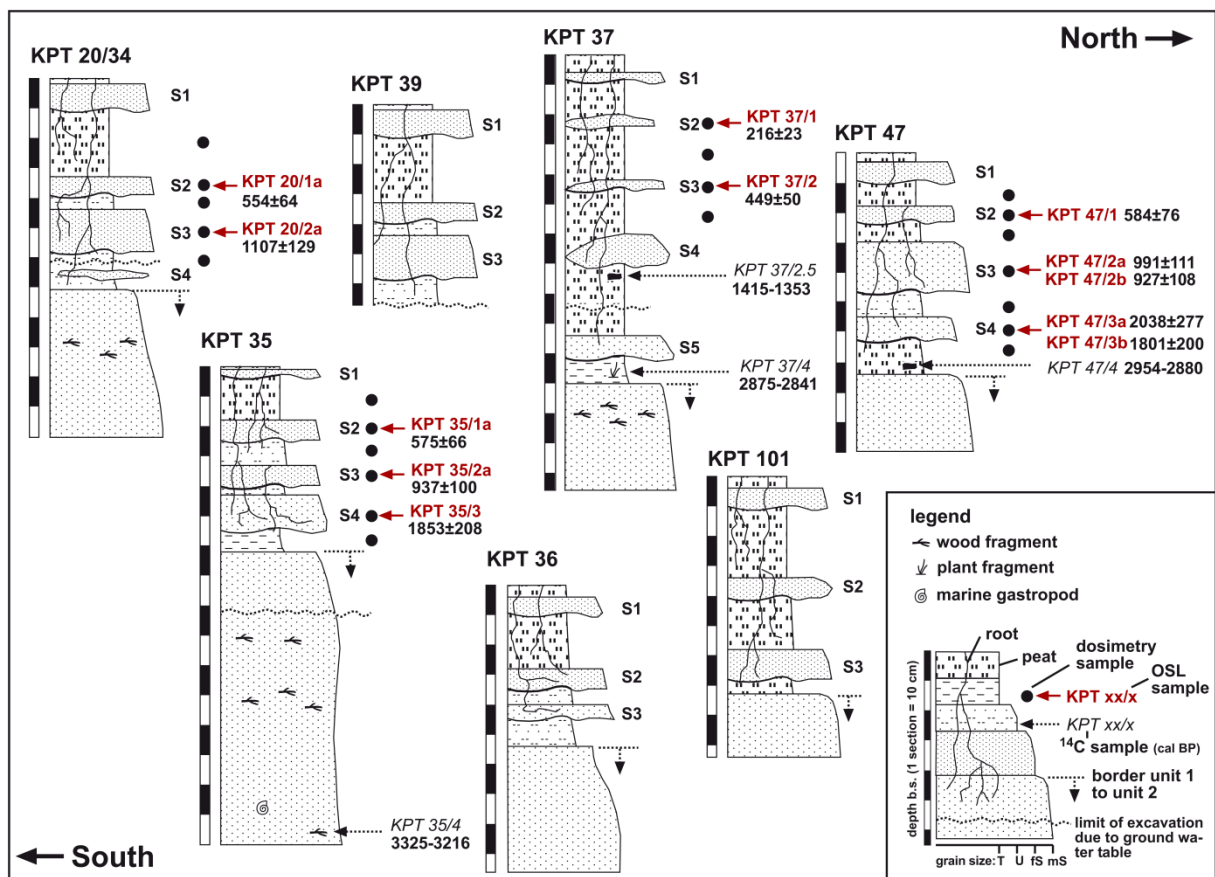
Figure 6.3: *Stratigraphy and chronology of all documented profiles.*

Common for the sand sheets were sharp contacts to the peaty soil below, moderate sorting and one or more graded subunits. S1 was light grey (10YR 6/1) and revealed a bimodal grain size composition, with peaks in the fine sand (88-96 μm) and medium sand (269-517 μm) fractions. Overall, it showed a fining-upward trend (mean = 190 μm at the base to 100 μm at the top), and was laterally continuous with a variable thickness of up to 10 cm. Besides elevated concentrations of $CaCO_3$ (8-15 %) and decreased organics (1.5-2.5 %) compared to the confining soil, it contained small fragments of indefinable marine shells and muddy rip-up clasts. All other layers (S2-S4) revealed a light greyish brown colour (10YR 6/2) and lacked carbonate as well as fossils. Their discontinuous lateral extends and the varying thicknesses were particularly prominent in trench KPT 20 (figs. 6.4a and b). All three layers showed a bimodal composition of medium sand (269-324 and 517-567 μm) and fine sand (96.5-106 μm). While

two fining-upward sequences were documented in S2, layers S3 and S4 revealed a massive structure. Similar to the soil strata, all sand sheets were penetrated by modern roots.

Compared to KPT 20/34, a slightly different stratigraphy was revealed in KPT 37 and KPT 101, located in the deepest parts of swale VI. The particularly wet conditions resulted in thicker and slightly better preserved peat strata; possibly due to bioturbation, the embedded sand sheets were extremely thin and discontinuous. The stratigraphical characteristics of KPT 37 are presented in figure 6.5: the base was composed of greyish brown (10YR 6/2), fine to medium sand void of carbonate and fossils. Macro-remains were restricted to occasional wood fragments. Above a sharp boundary at 1.10 m b.s., the sandy deposits were covered by a succession of peaty soils and sand sheets. Compared to those of KPT 20/34, the very dark brown (10YR 2/2) peaty soils contained more organic matter (10-25 %) and were apparently thicker (14-34 cm). Embedded in the peaty soils, a total of five sand sheets, S1-S5, were distinguished: S1-S4 were exposed at the pit walls and characterised by discontinuous extents even over short distances (fig. 6.5b). S5 was not reached by digging, but could be identified in the core (fig. 6.5f). Laminated leaves at the top of S2 and S3 document the improved preservation conditions at this place (fig. 6.5e). While S1 and S2 (fig. 6.5d) contained carbonate (7-16 %) and small fossil fragments, S3-S5 lacked $CaCO_3$.
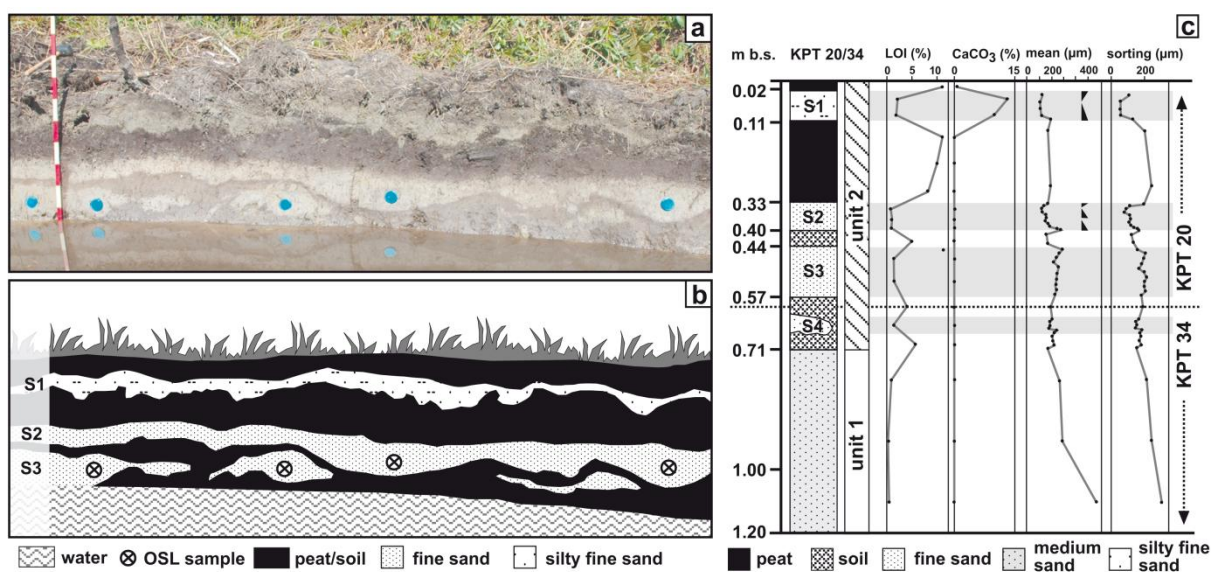
Figure 6.4: Combined stratigraphy of trench KPT 20 and core KPT 34 (see fig. 6.2b for location). (a) Photograph of KPT 20. Each section of the scale represents 10 cm. (b) Schematic profile of KPT 20 (sketch of the profile in fig. 6.4a) with explanations of the sedimentary units. (c) Succession of sediments in profile KPT 20/34 with selected analytical parameters. The succession is representative for all other sites sampled in swale VI. S1–S4 = tsunami deposits.

6.5.1.2 General stratigraphy and depositional environments

The succession of deposits in swale VI resembles the one described by Jankaew et al. (2008) and Fujino et al. (2009). It can be divided into two sediment units: the basal part of all pro-

files, i.e. the greyish sand below the sharp transitions at 0.71 and 1.10 m b.s. in KPT 20/34 and 37, respectively, was defined as unit 1. All deposits above the contact, i.e. the sequence of alternating peaty soil and sand sheets, were summarised in unit 2. This succession was the same at all seven sites investigated in swale VI. However, the number of sand sheets in unit 2 as well as their thickness, sedimentary structure and granulometry were variable (fig. 6.3). A maximum of five sand layers was observed in KPT 37 (S1-5). All other profiles contained either four (KPT 20/34, 35 and 47) or three sand sheets (KPT 36, 39 and 101).
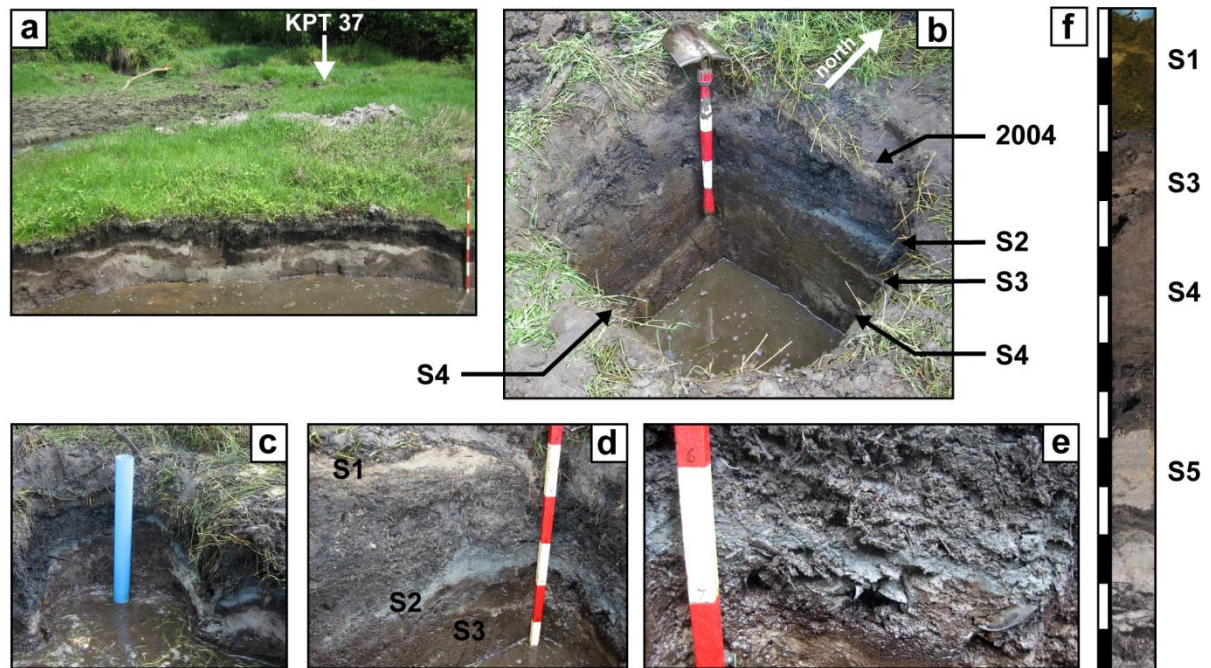
Figure 6.5: The stratigraphy of KPT 37. (a) View from trench KPT 39 to the north with the location of pit KPT 37. (b) Northern and western wall of pit KPT 37 with three discontinuous sand sheets below the IOT 2004 deposit (S2-4). (c) Core KPT 37B directly next to the pit. (d) Detail photograph of sand layers S1 and S2 (greenish grey); they appeared to be two separate layers. (e) Laminated leaves at the top of S2. (f) Sediment core KPT 37 extends the stratigraphy down to the intertidal sand of unit 1 (each segment of the scale represents 10 cm). While layer S2 is missing in the core, an additional layer S5 is present.

While the greyish sand of unit 1 reflects deposition in an intertidal environment, the peat and soil strata of unit 2 were accumulated under swampy conditions inside the swales after those had been separated from the sea by beach-ridge formation. The sand sheets reflect short interruptions of this environment by flooding events. The uppermost sand sheet (S1) was formed by the IOT in December 2004. All older layers (S2-5) revealed similar sedimentary characteristics as the IOT deposit; differences in geochemistry (zero instead of 8-15% $CaCO_3$), fossil content (no fossils in the older layers) and geometry (discontinuous extent) can be addressed to post-depositional changes (Szczuciński, 2012). Since the prehistoric sand sheets are interpreted to have the same origin as those described by Jankaew et al. (2008) and Fujino et al. (2009), they are referred to as tsunamites of unknown age (see Chapter 6.3, as well as Jankaew et al. (2008) for discussion). Some uncommon features of palaeotsunami deposits in

swale VI were detected in S2 of KPT 37, which contained carbonate and fossils, a characteristic that can be observed for the 2004 deposit, but is missing in all palaeotsunami layers. Although the IOT deposit and S2 in KPT 37 were clearly developed as two separate layers (fig. 6.5d), it might indicate that S2 is only a subunit of the 2004 deposit, which is separated by reworked plant debris. While the IOT deposit was present in all profiles throughout the swale, the extent of the palaeotsunami layers was laterally discontinuous and a correlation between distinct profiles based on the analysed sediment signatures was not possible.

6.5.2 Dating tsunami deposits in swale VI

6.5.2.1 Radiocarbon dating

Some limiting ages for the whole succession of tsunamigenic sand sheets are given by radiocarbon dating (tab. 6.2): a wood fragment taken from the marine sand of unit 1 in KPT 35 gave an age of 3165-3345 cal BP (UGAMS-8050); charcoal from the basal peat in KPT 47 and plant fragments from the basal clay of KPT 37 provided ages of 2859-2991 cal BP (UGAMS-8053) and 2785-2923 cal BP (UGAMS-8051); additionally, another charcoal fragment from the top section of the peat between S4 and S5 in KPT 37 dated to 1345-1516 cal BP (UGAMS-8052).

*Table 6.2: Radiocarbon data from swale VI. All samples were measured in the Center for Applied Isotope Studies, University of Georgia, Athens (USA). * Calibrated ages calculated with IntCal09 (Reimer et al., 2009).*

Lab code	sample	depth (cm b.s.)	material	$\delta^{13}C$ (‰)	^{14}C (BP)	sidereal yrs (cal BP, 2σ)*	sidereal yrs (cal AD/BC, 2σ)*	sidereal yrs (cal BP, 1σ)*	sidereal yrs (cal AD/BC, 1σ)*
UGAMS-8050	KPT 35/4	175	Wood fragment	-28.9	3040±25	3345-3165	1396-1216 BC	3325-3216	1376-1267 BC
UGAMS-8051	KPT 37/4	110	plant fragment	-29.8	2760±20	2923-2785	974-836 BC	2875-2841	926-846 BC
UGAMS-8052	KPT 37/2.5	60	plant fragment	-31.7	1520±25	1516-1345	435-605 AD	1415-1353	535-597 AD
UGAMS-8053	KPT 47/4	100	charcoal	-26.7	2820±25	2991-2859	1042-910 BC	2954-2880	1005-931 BC

6.5.2.2 Luminescence dating

Ten samples from sand sheets of four different profiles were taken for luminescence dating of the palaeotsunamis (fig. 6.3): one sample each from the upper two palaeolayers of KPT 20 (KPT 20/1a and 20/2a) and KPT 37 (KPT 37/1 and 37/2), as well as from all three prehistoric sand sheets in KPT 35 (KPT 35/1a, 35/2a and 35/3). In case of KPT 47, the youngest palaeotsunami was sampled once, and sheets S3 and S4 twice (KPT 47/1; 47/2a, b and 47/3a, b). The shine-down and dose response curves (fig. 6.6), as well as the results of laboratory experiments (fig. 6.7) proved favourable luminescence properties for all samples: the dose recovery tests generated values with less than 5% difference between measured and given dose; the acceptance criteria regarding recycling ratio (0.90-1.10) and recuperation (less than 50 mGy)

were missed by only 14% and 16.8 %, respectively (fig. 6.7). Based on preheat plateau and thermal transfer tests, a preheat temperature of 220 °C was selected for all samples.
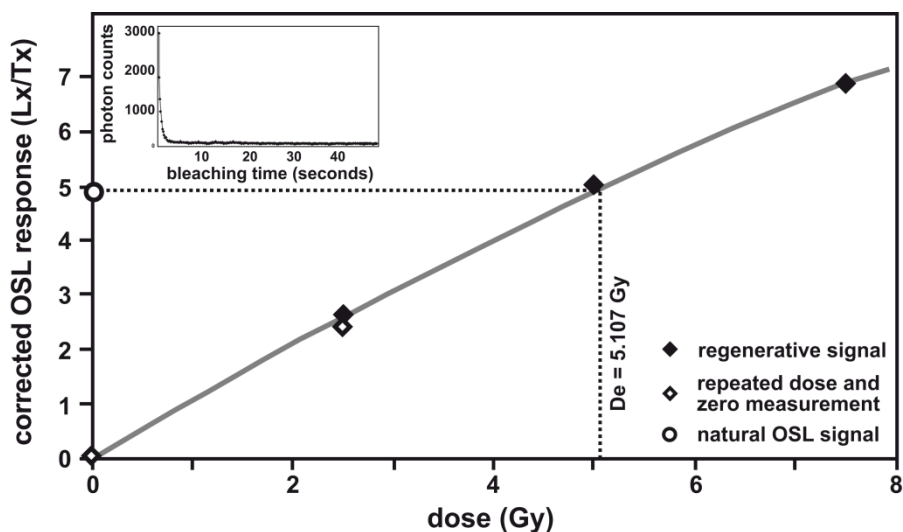
Figure 6.6: Typical luminescence signal of the tsunamites of the study area (KPT 20/1a). Shine-down curve (upper left corner) and SAR growth curve.

Statistical analyses of the accepted aliquots (20-57 aliquots per sample) revealed three different types of D_e distributions (fig. 6.8): (i) in case of KPT 20/1a, 20/2a, 35/1a, 35/3, 37/2, 47/2a, 47/2b, 47/3a and 47/3b, the aliquots revealed unimodal, slightly over-dispersed (6.3-15.6 %) and positively skewed (0.5-2.1) D_e distributions (fig. 6.8, type 1), indicating well-bleached material; (ii) KPT 35/2a and 47/1 were slightly over-dispersed (12.1-12.7 %), stronger positively skewed (2.2-2.8) and consisted of two D_e populations, of which the younger one accounted for the biggest part of the aliquots (fig. 6.8, type 2). Although the over-dispersion is small, skewness and some higher D_e values (forming the second mode) point to a minor influence of partial bleaching; (iii) KPT 37/1 showed significantly higher over-dispersion (28.2 %) and was characterised by several D_e populations (fig. 6.8, type 3), indicating poor bleaching or sediment mixing. Taking the average over-dispersion of the well-bleached deposits, i.e. those with type 1 D_e distributions, a σ_b value of 11% (the average of 6.3-15.6 %) was defined for age calculation with MAM.

To determine mean D_e values for the incompletely bleached deposits (type 2 and 3 D_e distributions), the minimum age model was applied. Since KPT 35/2a and KPT 47/1 (type 2) show characteristics more or less equal to deposits of the IOT 2004, which revealed minimised residuals of 28-40 yr using MAM compared to 53-83 yr using CAM (Brill et al., 2012a), MAM should provide reliable ages. For KPT 37/1 (type 3), where multimodality and over-dispersion point to additional influence of sediment mixing during transport or after deposition, the results should be handled with care. In case of type 1 D_e distributions, different from the modern analogue, the palaeotsunami deposits seem to be completely bleached. This discrepancy can be explained by the much older ages of the prehistoric tsunamites, since similar residuals

like those observed for the IOT 2004 are small compared to the dating error of 500-2000 year old deposits. Thus, although it was demonstrated that MAM minimises the offset between expected age and OSL age for the IOT 2004 deposits (Brill et al., 2012a), mean D_e values for the well bleached samples (type 1) were calculated by CAM. Anyway, the differences between CAM and MAM-based ages are not significant (tab. 6.3).
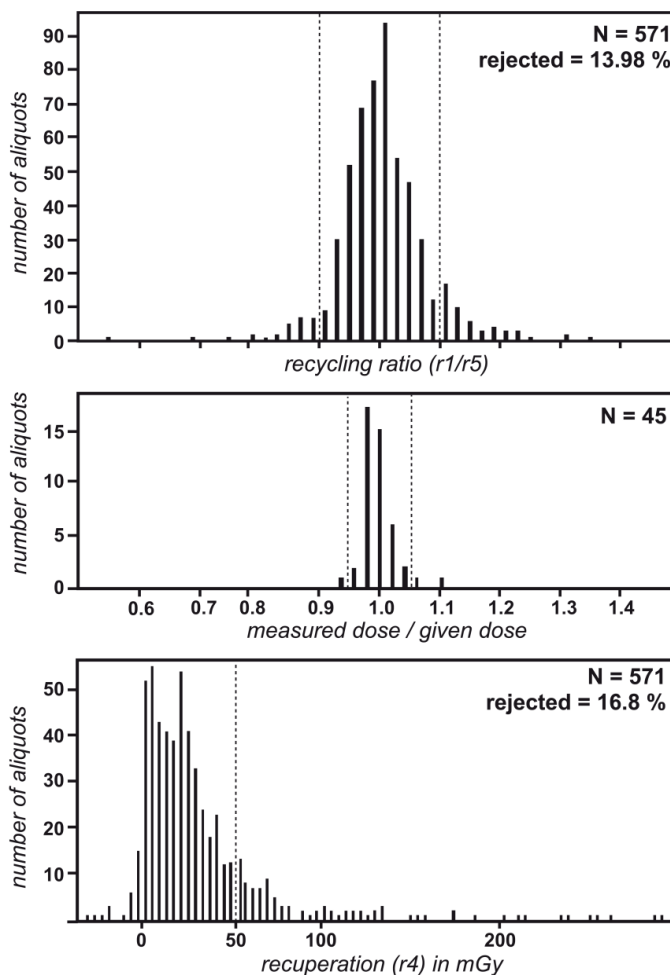
Figure 6.7: *Summary of recycling ratio, dose recovery and recuperation data of all samples. The dotted lines mark the limits of the acceptance criteria (recycling ratio: 0.9-1.1, dose recovery: 0.95-1.05, recuperation: <50 mGy). Only 14% of all measured aliquots (N) were rejected because of their recycling ratio and 16.8% due to their recuperation. Mean dose recovery values (computed from 4–5 aliquots per sample) all matched the acceptance criteria.*
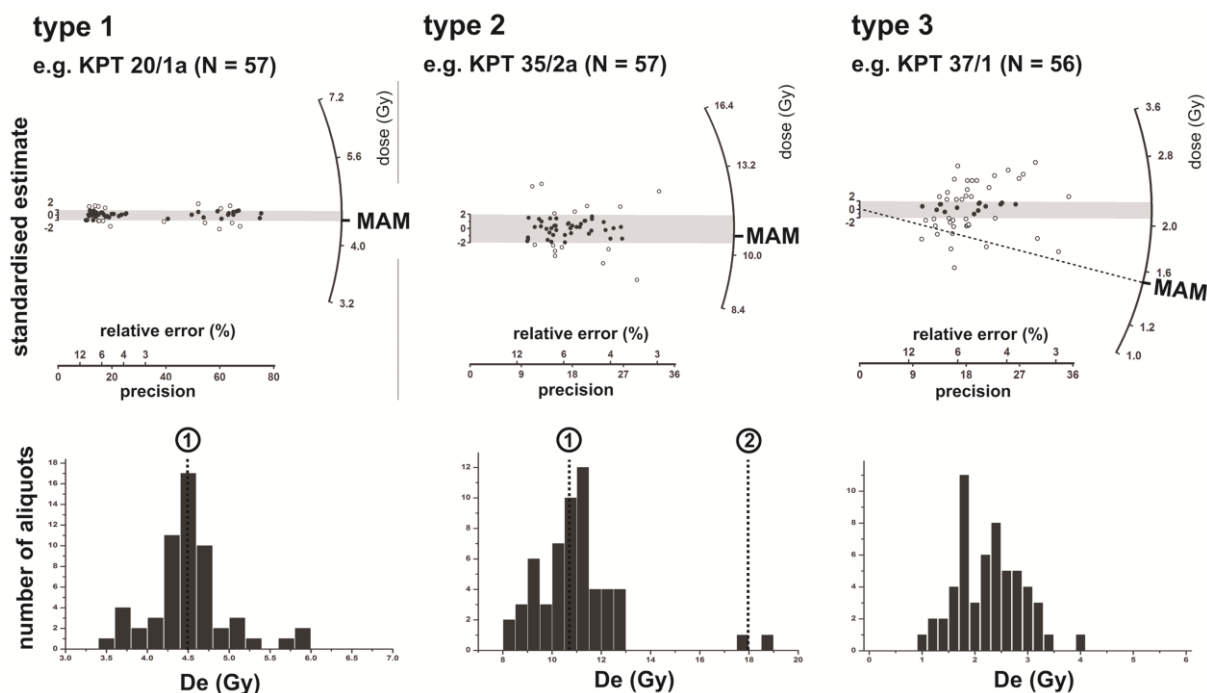
Figure 6.8: The different types of D_e distributions. Grey shaded areas mark mean D_e values calculated with CAM. Encircled numbers indicate D_e populations.

Table 6.3: Summarised characteristics of the D_e distributions, mean equivalent doses, age models and ages for all samples (results of selected model in bold type). σ_b = expected scatter, skew. = skewness, ovd. = over-dispersion, D_e pop. = number of signal populations, CAM = central age model, MAM = minimum age model.

Sample	N	σ_b	skew.	ovd.	D_e pop.	D_e CAM (Gy)	age CAM (years)	D_e MAM (Gy)	age MAM (years)
KPT 20/1a	57	11	0.7	6.3	1	**4.48±0.18**	**554±64**	4.45±0.19	552±68
KPT 20/2a	40	11	0.7	11.1	1	**14.12±0.29**	**1107±129**	12.52±0.37	1044±122
KPT 35/1a	55	11	1.1	10.9	1	**5.72±0.08**	**575±66**	5.67±0.28	571±65
KPT 35/2a	57	11	2.2	12.1	2	10.85±0.17	941±102	**10.66±0.22**	**937±100**
KPT 35/3	39	11	1.8	10.1	1	**6.16±0.12**	**1853±208**	6.08±0.11	1837±201
KPT 37/1	56	11	0.3	28.2		2.17±0.09	319±36	**1.47±0.09**	**216±23**
KPT 37/2	38	11	1.4	15.6	1	**4.85±0.11**	**449±50**	4.58±0.21	440±47
KPT 47/1	40	11	2.8	12.7	2	4.14±0.14	594±75	**4.07±0.09**	**584±76**
KPT 47/2a	42	11	2.1	11.4	1	**6.16±0.12**	**991±111**	6.08±0.11	988±110
KPT 47/2b	22	11	1.1	13.2	1	**5.76±0.17**	**927±108**	5.62±0.28	916±103
KPT 47/3a	33	11	0.8	12.8	1	**3.33±0.08**	**2038±277**	3.18±0.21	2028±273
KPT 47/3b	20	11	0.5	13.4	1	**3.08±0.11**	**1801±200**	2.81±0.29	1794±198

6.5.2.3 The chronology of tsunami events

The chronological framework of the deposits in swale VI is given by radiocarbon ages of the basal peat or clay in KPT 47 and KPT 37 (KPT 47/4 and 37/4) as well as from unit 1 in KPT 35 (KPT 35/4). While the latter dates the deposition of marine sand under intertidal conditions before swale VI was separated from the sea to 3165-3345 cal BP, KPT 47/4 and KPT 37/4 provide ages of 2859-2991 cal BP and 2785-2923 cal BP for the period directly after the initiation of the swale by accumulation of the seaward beach ridge (fig. 6.3). Simultaneously, they provide maximum limiting ages for the lowest palaeotsunami layer of each profile. All three

ages are in good agreement and limit the deposition of all tsunamigenic sand sheets in swale VI to younger than 2800-3000 cal BP.

Direct ages for the palaeotsunami layers are provided by luminescence dating. These data are all younger than 2800-3000 yr and, thus, agree with the limiting radiocarbon data. Furthermore, within the OSL ages of the same profiles, no inversions occur. The comparison of all data sets reveals three distinct time intervals with a clustering of layer ages (all ages of a cluster match within their errors; fig. 6.9). The first cluster comprises the youngest palaeoevents in KPT 20, KPT 35 and KPT 47 as well as the second palaeolayer in KPT 37. The second palaeolayers in KPT 20, KPT 35 and KPT 47 fall into the second cluster. Cluster three aggregates the oldest event deposits in KPT 35 and KPT 47.
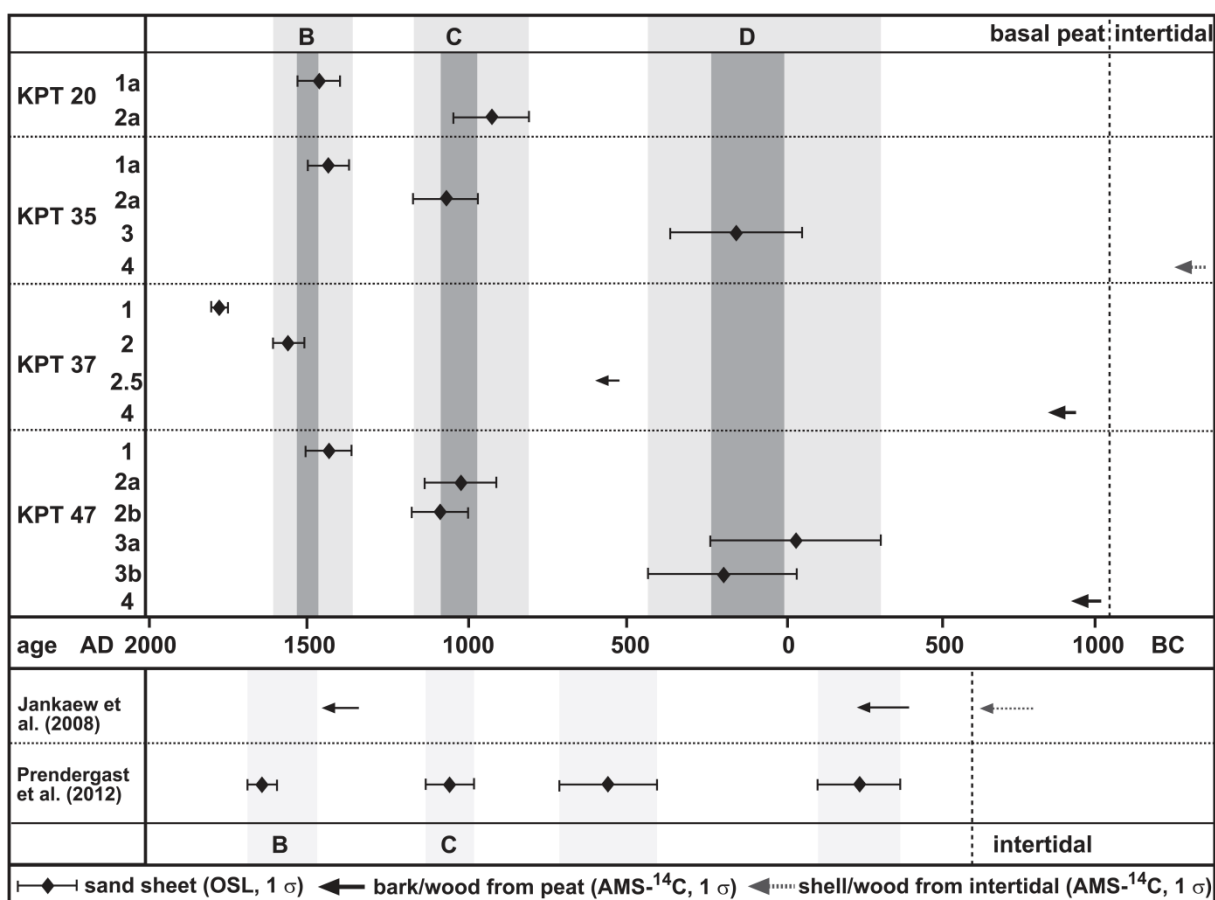
Figure 6.9: *Age plot of all dated profiles in swale VI (upper part) in relation to the results of other studies (lower part). The comparison of the four different profiles of swale VI shows that the layer ages cluster within intervals 400–660 (B), 820–1230 (C) and 1600–2300 (D) years (light grey areas). The dark grey areas indicate the weighted mean of all ages inside a cluster. Each cluster is related to one palaeotsunami event (B, C and D).*

Additionally to the IOT 2004, which is defined as event A, we found deposits of at least three older tsunamis, namely events B, C and D, with ages of 400-660 yr (1610-1350 AD), 820-1230 yr (1190-780 AD) and 1600-2300 yr (410 AD to 290 BC), respectively (light shaded areas in fig. 6.9). Their impacts can be timed more precisely by using the weighted mean of all ages inside a cluster (dark shaded areas in fig. 6.9); this way, events B, C and D are dated

to 492-554 yr (1518-1456 AD), 925-1035 yr (1085-975 AD) and 1743-1999 yr (267-11 AD). A potential fourth event X is present solely in KPT 37, where it is located between the deposits of the IOT 2004 and event B. Although it was dated to an age of 193-239 yr (1817-1771 AD) and luminescence dating of the modern 2004 tsunami deposits on Phra Thong showed much smaller offsets of less than 50 yr (Brill et al., 2012a), we cannot rule out the possibility that it is part of the 2004 deposit (as stated in Chapter 6.5.1.2 it might be a sublayer of the IOT deposit), particularly, since a similar layer is missing at all other sites in swale VI (as well as in other swales on Phra Thong). The only possible counterpart mentioned in historical records is the 1762 AD earthquake off Myanmar (Dominey-Howes et al., 2007), which is considered unlikely to have generated a tsunami strong enough to inundate Phra Thong Island (Okal and Synolakis, 2008).
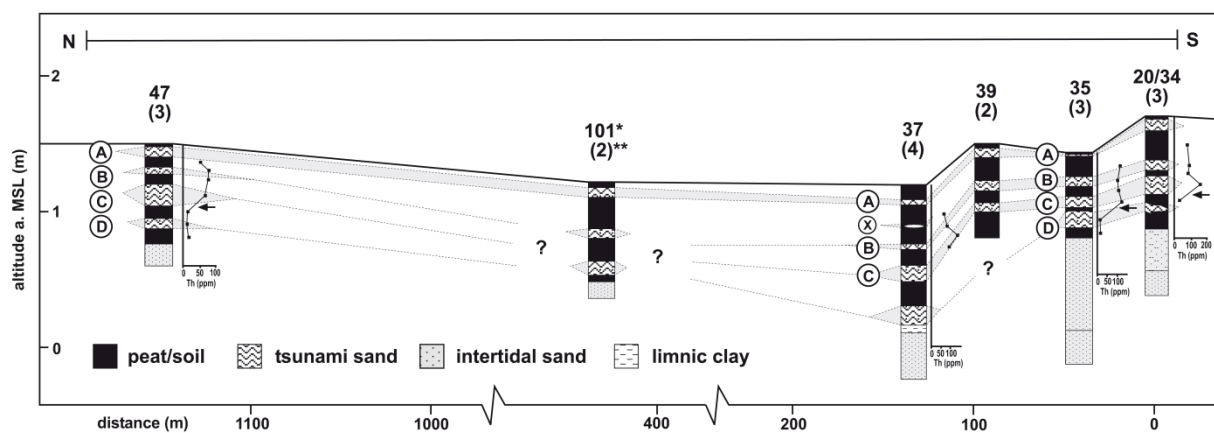
Figure 6.10: *Spatial correlation of palaeotsunami deposits A, B, C, D and X between the different sites in swale VI based on chronological data. * ID of the profile, e.g. KPT 101; ** number of palaeotsunami layers.*

6.5.3 Correlation of palaeotsunami deposits

6.5.3.1 Intra-swale correlation

Based on luminescence ages and radiocarbon data, we correlated the distinct sand sheets in the profiles of swale VI with events B, C and D. This way, it was possible to trace the deposits of all three events from KPT 20 in the south to KPT 47 in the north (fig. 6.10). While this is confirmed by OSL ages for KPT 20, KPT 35, KPT 37, and KPT 47, in case of the undated profiles KPT 39 and KPT 36, the correlation is based on visual extrapolation from layers of neighbouring profiles. Additionally, for the third palaeolayer in KPT 37, the correlation with event C is supported by the radiocarbon date of 1345-1516 cal BP from the peat below, which is too old for event B and too young for event D. Only in KPT 101, which is undated and spatially isolated from the nearest profiles, none of the two sand sheets can be related with certainty. Besides chronological data, the concentrations of ^{232}Th and ^{238}U (which were measured for dose rate determination; tab. 6.1) may function as another indicator to correlate the sand

sheets. The thorium concentrations show a sharp decline directly below event layer C in all measured profiles (KPT 20, 35 and 47; fig. 6.10); thus, the border between events C and D forms a significant marker, which can be identified by radionuclide analysis.

6.5.3.2 Inter-swale correlation

Considering the overall successful correlation of sand layers in swale VI, we related events B, C and D with precisely dated counterparts in other swales on the island as well; the youngest palaeotsunami of Jankaew et al. (2008) with an age slightly younger than 1450-1300 AD, correlates with the 492-554 yr old (1518-1456 AD) layer B of swale VI. Two or three older events are definitely younger than 500-800 BC and could therefore be counterparts of layer C (1085-975 AD) and layer D (267-11 AD) in swale VI. The OSL data of Prendergast et al. (2012) for these layers suggest ages of 990±130 yr (1140-980AD), 1410±190 yr (780-400 AD) and 2100±260 yr (160 AD-360 BC). While the youngest date matches precisely the age of event C, a correlation of event D with one of the other layers is not possible.

Taking the boundary conditions at the time of impact in the form of water level and palaeogeography into account, additional, information about minimum inundation distances can be obtained. While the tide level at the time of prehistoric tsunami impacts is not determinable, the sea level was < 1 m above present for all three events, an insignificant value compared to the tidal range of 2.5m (Scheffers et al., 2012a). Similarly, the palaeotopography has changed only little during the last two millennia, since palaeosol formation and the effects of the IOT 2004 document rather stable ridge heights (Scheffers et al., 2012a). Solely the position of the shoreline has changed significantly during the last 2000 yr. By correlating the undated ridges and swales of transect C with dated counterparts in transect A (swale X that marks the 2500 BP shoreline is identical with swale IV in transect C, and swale Y, which indicates the coastline at 2000 BP is located between swales III and IV of transect C), approximate shoreline positions in transect C can be estimated for events B, C and D (fig. 6.2c): 1800 yr ago, when event D hit the island, the shoreline was directly east of swale III (~500m west of swale VI), and during events B and C it was somewhere west of swale III (at least 600m west of swale VI). This implies minimum inundation distances of 500m for event D, and at least 600m (probably much more) for events B and C.

6.5.3.3 Basin wide correlation

In a wider geographical context – i.e. by considering the coasts of all countries affected by the IOT 2004 – counterparts for events B, C and D exist as well. The youngest palaeotsunami of 1518-1456AD is supported by sedimentary evidence from Ban Bang Sak (1450-1250 AD; Brill et al., 2011) and Krabi (1425-1410 AD; Harper, 2005) in western Thailand, Sumatra (younger than 1400-1290 AD; Monecke et al., 2008) and the Andaman Islands (younger than

1300-1200 AD; Malik et al., 2010). Contemporaneous evidence for the 1085-975 AD tsunami (event C) is postulated from Sumatra (younger than 990-780 AD; Monecke et al., 2008), Sri Lanka (ca. 1000 AD; Ranasinghage et al., 2010) and eastern India (c. 1000 AD; Rajendran et al., 2006). Additionally, for both periods (when events B and C took place, respectively), uplifted corals on the Andaman Islands and in Northern Sumatra (uplift comparable or bigger than 2004) prove strong ruptures of the Sunda Fault (c. 1450 AD and 1000 AD; Rajendran et al., 2008; Meltzner et al., 2010). The oldest palaeotsunami of Phra Thong, event D, is less well supported by evidence from other locations. The only comparatively contemporaneous evidence is provided by possible tsunami deposits from Thailand (Brill et al., 2011) and eastern India (Rajendran et al., 2006).

6.6 Conclusions

The study shows that in absence of appropriate material for radiocarbon dating, the optically stimulated luminescence technique can be successfully applied to improve the knowledge about palaeotsunami frequencies. On Phra Thong Island, the luminescence data revealed three prehistoric tsunami events prior to the IOT 2004 (event A): event B took place 490-550 yr ago, event C 925-1035 yr ago and event D occurred between 1740 and 2000 yr ago. A possible fourth palaeotsunamite, dated to 190-240 yr, is most probably only a poorly bleached sublayer of the 2004 tsunami deposit. Besides their contribution to a better event chronology of the region, the luminescence ages also enable the correlation of various distinct tsunami deposits on the island; although discontinuous, events B, C and D could be traced at spatially separated sites within a single swale, as well as across beach ridges. For at least two palaeotsunamis (events B and C), dated counterparts in swales 500 m apart exist and, thus, give information about minimum inundation distances. Furthermore, the OSL ages enable correlation with contemporaneous tsunami evidence from other coasts around the Indian Ocean for all three palaeoevents, which can be used as another indicator for the magnitude of the tsunamis.

Chapter 7

7 Holocene sea levels along the Andaman Sea coast of Thailand[4]

Abstract: *For the Malay-Thai Peninsula several sea-level curves for the younger Holocene, based on field evidence as well as on hydro-isostatic modelling of a far-field site, have been published. The general assumption is a rapid rise to a mid-Holocene maximum up to +5 m above present sea level, followed by a constant or oscillating regression. However, from the Andaman Sea coast of Thailand, which was affected by the 2004 tsunami, only isolated observations are available regarding Holocene sea levels. Thus, the timing and magnitude of the Holocene highstand as well as the course of the regression remain to be defined. As several palaeotsunamis could be detected in the meantime it is important to know the related sea levels as exactly as possible to judge the energy, inundation width and potential wave height of these events. Therefore, fixed biological indicators from the rocky coasts of the Phang-nga Bay and Phuket, as well as morphological indicators from beach-ridge and swale sequences along the exposed west coast (Ko Phra Thong) were studied, to gain information about the Holocene sea-level development in this region. While oyster and coral data from the Phang-nga Bay and Phuket document a Holocene maximum of +2.6 m at 5700 cal. BP, the ridge crests and swale bases in the northwest of the study area point to maximum heights of +1.5-2.0 m above the present level around 5300 years ago. During the last 3000 years, to when the largest part of the Holocene palaeotsunami deposits from Thailand was dated, relative sea levels (RSL) in both areas did not exceed +1.5 m.*

Keywords: *Beach ridges; Biological indicators; Holocene; Mid-Holocene highstand; Relative sea level; Thailand*

7.1 Introduction

In the aftermath of the Indian Ocean tsunami (IOT) of December 2004, numerous studies on the Holocene tsunami history of the affected areas have been undertaken (e.g. Brill et al., 2011; Dahanayake and Kulasena, 2008; Jankaew et al., 2008; Monecke et al., 2008; Rajendran et al., 2006). Along the west coast of southern Thailand sedimentary evidence of potential predecessors of the IOT 2004 in form of sandy deposits and boulders has been reported from beach-ridge sequences on Ko Phra Thong (Fujino et al., 2009; Jankaew et al., 2008), coastal plains at Ban Bang Sak (Brill et al., 2011), Pakarang (Neubauer et al., 2011) and Thap

---

Lamu (Rhodes et al., 2011; Yawsangratt et al., 2009) and caves in the Phang-nga Bay (Harper, 2005). While the oldest of these events were dated to more than 5000 years at Pakarang Cape (Neubauer et al., 2011), most evidence in Thailand documents palaeotsunamis (at least four different events) that occurred during the last 3000 years.

To distinguish deposits (sand sheets and/or boulders) of tsunamis from those of other extreme wave events, such as storms, that leave similar sedimentary evidence (e.g. Morton et al., 2007; Switzer and Jones, 2008; Tuttle et al., 2004) and to estimate the magnitudes of the associated events, it is important to know the water level at the time of impact. While in microtidal areas tsunami inundation depends nearly exclusively on the energy of the event, the topography and the relative sea level (RSL), in meso- to macrotidal areas the tide level during a tsunami is important too. Since RSL and the tidal range may have differed significantly from modern values during the last millennia, both RSL and tidal situation may make a difference of many metres in the level of wave or flow impact. While there is no possibility to calculate the tide level at the time of impact and potential variations of the tidal range, the positions of former sea levels can be reconstructed from morphological, biological and archaeological indicators, in the best case with a precision of ±5 cm and ±20 years (Milne et al., 2009; Yu et al., 2009). The resulting sea-level curves should give both the error margins regarding the altitudinal variability of an index point, as well as the error of the respective dating method. For the microtidal coast of southwest Thailand, a sea-level curve may help to identify the potential energy of palaeotsunamis by providing information about the maximum altitude above RSL reached by their deposits.

Sea-level curves constructed on the basis of field indicators reflect the local development of RSL, which is controlled by a variety of interacting processes (e.g. Gehrels, 1999; Pirazzoli, 1991). Generally, for continental coastlines in the lower latitudes (far-field sites of Clark et al., 1978), Holocene sea-level changes are mainly determined by ocean refill due to melting ice sheets, hydro-isostatic lowering of the shelf margins and geoidal eustasy (ocean siphoning) (Mitrovica and Milne, 2002; Mitrovica and Peltier, 1991; Peltier, 1999, 2002; Woodroffe and Horton, 2005). However, locally the RSL trend may significantly be influenced or even dominated by phenomena such as tectonic movements, subsidence or auto-compaction of sediments (e.g. in Bangladesh: Islam and Tooley, 1999). Since SW Thailand is inferred to be more or less tectonically stable and other local factors are negligible at our study sites, the interplay between glacial eustasy, hydro isostasy and geoidal eustasy controlled the RSL development during the Holocene (Horton et al., 2005). In the course of postglacial ice melting a rapid rise of RSL took place (Hanebuth et al., 2000), resulting in a high stand several metres above present RSL (glacial eustasy). This maximum was followed by a more or less continuous fall (isostatic rebound and ocean siphoning), whereas spatial variability of these factors was capable of causing regional differences in magnitude and timing of the highstand. However, important for the interpretation of palaeotsunami deposits is solely the height of RSL at

the time of impact. Thus, the main aim is to reconstruct the time and magnitude of the Holocene maximum, as well as the course of sea-level fall afterwards, while the determination of controlling processes is not an essential part of this study.

7.2 Holocene sea levels along the Malay-Thai Peninsula

Precise sea-level measurements for Thailand in the form of GPS-corrected tide gauge data and satellite altimetry are restricted to the last decades (Trisirisatayawong et al., 2011). For the time prior to measurements, sea levels have to be reconstructed either by field evidence or model approaches (glacial isostatic adjustment models (GIA), e.g. Mitrovica and Vermeersen, 2002). While no evidence of higher RSL than today has been found in the western Indian Ocean (Camoin et al., 1997, 2004), in most parts of the Indo-Pacific region (including the Malay-Thai Peninsula), in agreement with the typical sea-level pattern of far-field locations (Bradley et al., 2008; Mitrovica and Milne, 2002), sea level rose quickly to a mid-Holocene maximum, which was followed by a steady regression to the modern level (Woodroffe, 2009; Woodroffe and Horton, 2005). However, as a function of meltwater input, hydro isostasy and geoidal eustasy, the timing and magnitude of this high stand is spatially variable (Horton et al., 2005; Woodroffe, 2005; Zong, 2004).

For the Malay-Thai Peninsula the existence of a mid-Holocene sea-level maximum has already been postulated on the basis of geological field evidence from the Strait of Malacca (Geyh et al., 1979; Hesp et al., 1998), Malaysia (Tjia, 1996) and Thailand (Sinsakul et al., 1985, 1992). However, timing, magnitude and number of Holocene highstands varied significantly. For the coast of southern Thailand (Gulf of Thailand and Andaman Sea coast), a sea-level maximum of +4 m at 6000 BP, and two relative maxima at 4000 BP (+2.5 m) and 2600 BP (+2 m) were postulated by Tjia (1996) and Sinsakul (1992). However, considering the great altitudinal range of sea-level indicators used in those studies, the data are considered to be inadequate for constructing precise sea-level curves (Horton et al., 2005; Woodroffe and Horton, 2005). Recent sea-level reconstructions based on both reliable field evidence (Choowong et al., 2004; Horton et al., 2005; Scoffin and Le Tissier, 1998) and model results (Horton et al., 2005) predict a single Holocene high stand of +1-5 m, followed by a gradual fall to present RSL for the Malay-Thai Peninsula. Since hydro-isostatic effects resulted in significant spatial differences, each RSL curve is valid only for a small geographical area. So far, a detailed sea-level reconstruction for the study area (SW Thailand) is mainly based on GIA models which point to a high stand of +2-3 m at around 6000 years ago (Horton et al., 2005). The only reliable field evidence available for SW Thailand is intertidal reef-flat corals from southeast Phuket that indicate a gradual falling sea level from at least +1 m to the present level during the last 6000 years (Scoffin and Le Tissier, 1998). However, since their 11

index points provide only minimum indictors they are not capable of validating the modelled height and timing of the Holocene maximum.
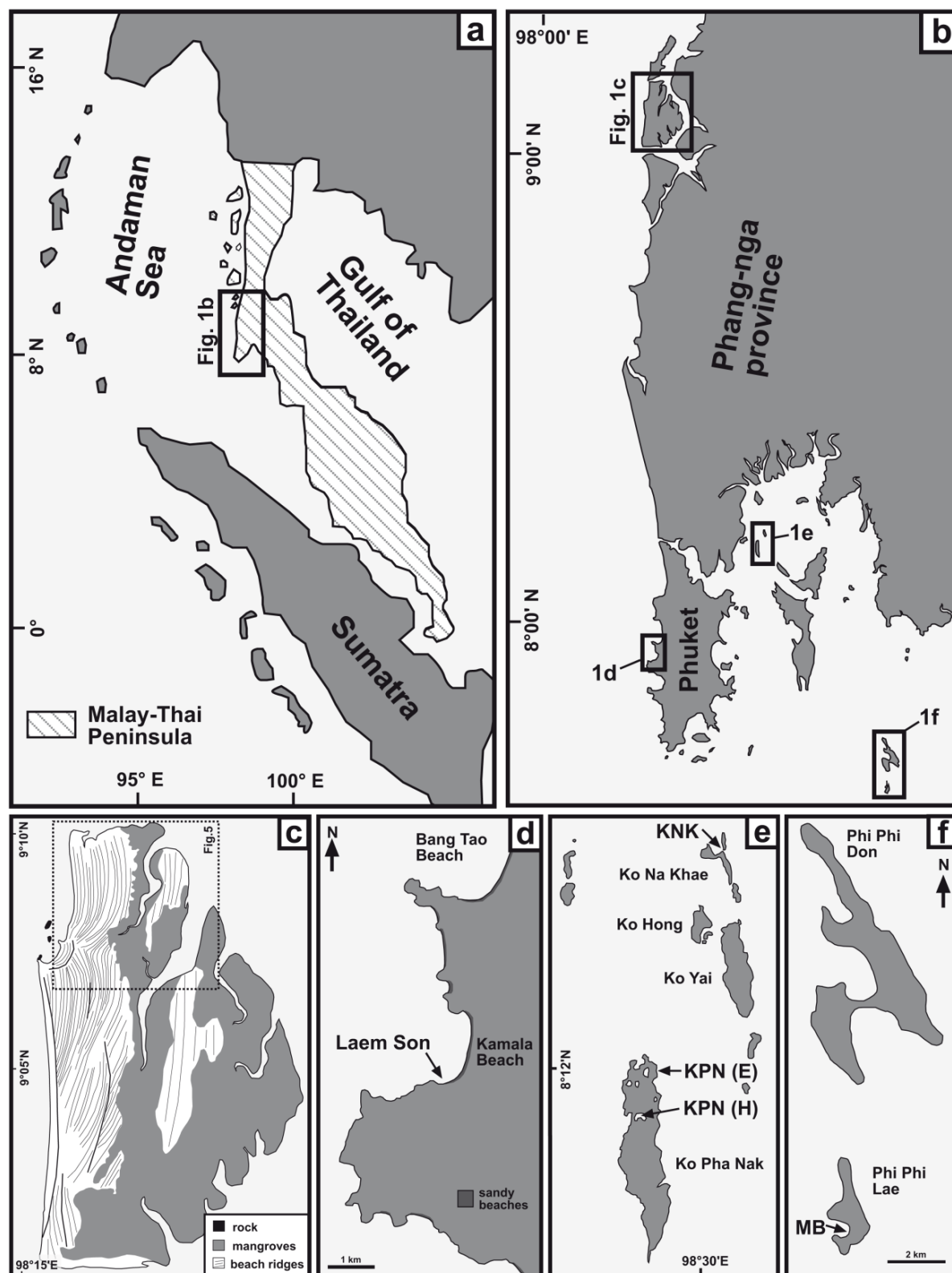
Figure 7.1: *Geographical position of the study area. (a) Map of the Malay-Thai-Peninsula. (b) Overview of southwest Thailand with the locations of the study sites: (c) Ko Phra Thong, (d) Kamala Beach (western Phuket), (e) Ko Pha Nak and Ko Na Khae (Phang-nga Bay) and (f) Phi Phi Islands.*

7.3 Regional setting

The Andaman Sea coast of southern Thailand (between 9° and 7°30′N) is part of the Malay-Thai Peninsula (figure 7.1a), a drowned and eroded, N-S orientated mountain belt. Tectonically, this area is located on the relatively stable Sunda Plate (Tjia, 1996) with little tectonic activity during the Holocene compared with the seismically active zones to the west (Dheeradilok, 1995), where the Sunda Arc subduction zone is a major source of earthquakes and tsunamis. Since southwest Thailand is located in the sub-humid tropics with heavy rainfall (2500 to 3000 mm/yr) mainly during the summer monsoon and a dry period from December to February, dense vegetation and intensively developed soils (laterites on bedrock, podsols on beach ridges) are characteristic elements of the landscape.

Normal coastal dynamics are controlled by micro- to mesotidal conditions with dominant semi-diurnal character (Admiralty Tide Tables, 2003). For the tide gauge station at the Phuket Royal Marina a maximum spring tide range of 2.82 m, a minimum neap tide range of 0.40 m and a mean tide range of 1.55 m were calculated from the data of 2010; mean sea level (MSL) is defined at +2.02 m above the lowest astronomical tide (LLW). Annual and seasonal differences in the order of <0.3 m are typical for the region and do not influence significantly the accuracy of sea-level reconstructions. The waves are generally moderate with heights <2 m (Choowong et al., 2008). Especially in the calm areas of the Phang-nga Bay this allows the formation of nearly horizontal bio-constructive benches. More energetic conditions, which have significant influence on coastal forming, are common during the summer monsoon. However, tropical cyclones are not reported from the west coast of southern Thailand within the last 150 years (Murty and Flather, 2004).

The northern part of the study area, from Ko Phra Thong to the northern spit of Phuket, is a sedimentary coast, characterised by sandy beaches, tidal flats and barrier islands (Sinsakul, 1992). Although exposed to the leeward side of the trade winds and distant from the cyclone tracks (Murty and Flather, 2004; Singh et al., 2000), beach-ridge systems are a characteristic element of this area. Especially Phra Thong Island, located 125 km north of Phuket and separated from the mainland by tidal channels, is dominated by coast-parallel beach ridges and swales (figure 7.1b).

In contrast, the southern part of the study area is dominated by rocky coastlines. While the coast of Phuket is formed by sandy beaches alternating with granite headlands, the islands of the Phang-nga Bay in the east of Phuket consist of Permian limestone (Watkinson et al., 2008).The spatial pattern of the islands as well as the form of single islands follow the structurally predetermined N-S direction (Tjia, 1996; Watkinson et al., 2008). Long-lasting tropical karstification has transformed the limestone into karst towers with steep slopes to the surrounding sea. These islands exhibit well developed karst features such as karren, sinkholes, speleothems and caves. In some cases caves connect deep, nearly vertical sinkholes in the

interior of the islands with the sea, which are locally called 'hong'. There, in contrast to the exposed cliffs outside the hongs, wave impact is reduced to a minimum. Because of the input of river sediments from the north, the inner parts of the Phang-nga Bay are characterised by forms of coastal progradation such as deltas and tidal flats, mostly covered by *Rhizophora*-dominated mangrove forests. Nautical charts show relatively shallow water (5–10 m water depth) in this part of the Phang-nga Bay with greater water depths only along former river channels, whereas at its southern end, around the Phi Phi Islands, deep water conditions (20–30 m water depth) occur immediately at the shoreline. In consequence, the wave impact from the Andaman Sea is stronger, which results in more extended beaches (e.g. the tombolo of Phi Phi Don). Since contemporaneously the input of fresh water and suspension diminishes, coral reefs are a frequent feature in the south of the Phang-nga Bay.

7.4   Sea-level indicators

In this study, two different groups of indicators were investigated for evidence of former sea and tide levels: (1) fixed biological indicators, attached to rocky shorelines in exposed and sheltered positions, and (2) morphological indicators of a beach-ridge plain. Other kinds of evidence often used for sea-level reconstruction, such as microfossils and pollen (Engelhart et al., 2007; Gehrels, 1999; Horton et al., 2003, 2005, 2007; Scott and Medioli, 2005; Van de Plassche, 1986), paralic peat (Brückner et al., 2010; Gehrels, 1999) or archaeological indicators (e.g. Devillers et al., 2007; Morhange et al., 2001), are missing in the coastal archives of SW Thailand.

7.4.1   Fixed biological indicators

As Tomanek and Helmuth (2002) stated, the rocky intertidal zone is among the most physically harsh environments on earth. Marine invertebrates and algae living in this habitat are alternatively pounded by waves and exposed to thermal extremes during low tide periods; additionally, they must deal with strong selective pressures due to predation and competition for space. As a result, the steep physical gradient and spatially condensed community has made the rocky intertidal zone an ideal 'natural laboratory' to study the distribution of organisms in relation to tidal levels (Baker and Haworth, 2000; Baker et al., 2001; Coates, 2008; Kelletat, 1997; Laborel and Laborel-Deguen, 1994, 1996, 2005; Pirazzoli, 2005; Stephenson and Stephenson, 1949; Tomanek and Helmuth, 2002). Generally, the greater the slope of the shore and the lesser the variation of the rock surface the more clearly delineated the distribution pattern will be. Along the limestone and granite coasts of the Phang-nga Bay and Phuket bio-erosive notches, benches of rock oysters, belts of boring bivalves and boring sea-urchins, as well as coral colonies exist. Since they occur in form of recent as well as dead or inactive

formations, they were used to precisely determine past sea levels for southwest Thailand (fig. 7.2).
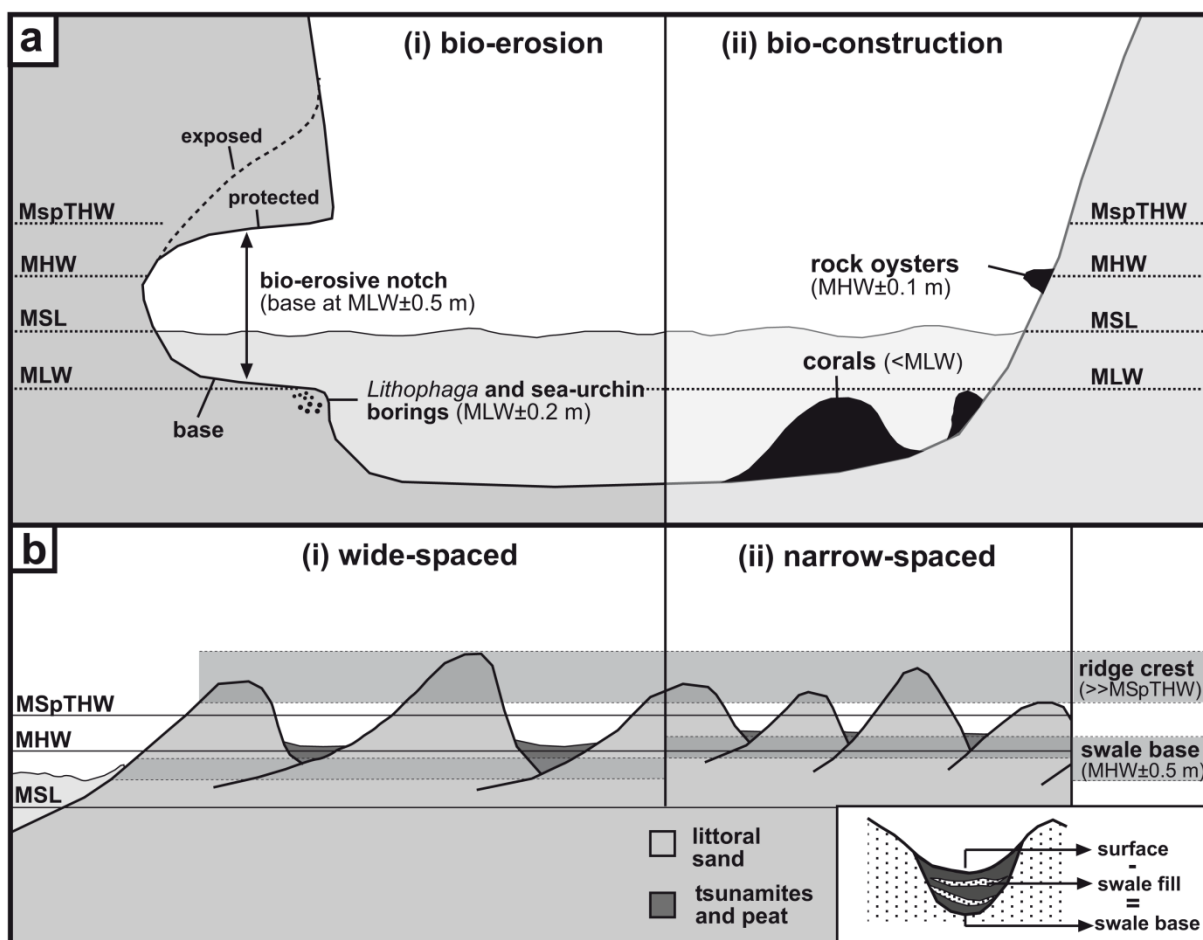
Figure 7.2: *Sea-level indicators used in this study. (a) Biological indicators of rocky coasts. (b) Geomorphological indicators of the beach-ridge plain on Ko Phra Thong.*

There seems to be no general agreement about the relationship between indicators and tide levels. However, reliable altitudes can be obtained by comparison with recent counterparts at the same location (Pirazzoli, 2005). In most cases bio-erosive notches, formed by organisms living in the wave zone, give a good idea of the maximum tidal range (Kelletat, 2005). The recent notches in the study area are not totally exposed during mean low water (MLW), but drowned for almost 1 m; their base is treated as an indicator for MLW (±50 cm). While Laborel and Laborel-Deguen (2005) put boring bivalves (*Lithophaga* sp.) and sea urchins in the sublittoral below LLW, in the Phang-nga Bay living sea urchins and boring bivalves were found directly below MLW (±20 cm). Less disputable is the indicative range of oysters and corals. The upper limit of the closed belt of rock oysters (*Saccostrea cucullata*) marks mean high water (MHW) with an indicative range of ±10 cm; coral colonies grow at most to MLW and thus represent minimum indicators of past sea levels (fig. 7.2a).

7.4.2 Morphological indicators

Sedimentary coastlines offer an independent archive for former RSL. The interpretation of the beach ridges and swales on Ko Phra Thong, regarding their indicative meaning in respect to RSL (fig. 7.2b), was based on the following arguments:

(1) Beach ridges, as can be seen by their internal structure, are built by waves which reached at least the height of their crest, normally have been even higher (Otvos, 2000; Taylor and Stone, 1996). Single ridges are formed by the swash of waves higher than normal (the berm is the initial stage) and ridge crests may be formed decimetres to metres above spring tide high water (SpTHW) (Otvos, 2000; Scheffers et al., 2012b). The base of the ridge generally starts above the intertidal zone around MHW but, depending on the spacing between neighbouring ridges, can be slightly above or below.

(2) If sediment supply is sufficient, ridges will more or less continuously be added at the seaward site, forming a succession of ridges and swales (depression between two successive ridges), whereas the cyclicity of ridge formation may be explained by small-scale sea-level variations, occasional storm impact or sediment supply. For densely spaced beach ridges the intervening swales are rather narrow. In this case, the altitude of the swale bases should be at MHW or slightly above. The base of wider ridges may form as deep as at MLW (Taylor and Stone, 1996).

(3) It is likely that the ridge crests in the last centuries and millennia have lost some of their initial height (e.g. by strong rain, storm overwash or tsunami inundation), whereas the swales have been filled up with the deposits moved by these processes plus the organic material of peaty soils. On Phra Thong Island the erosion of the ridge crests is documented by the lack of an A_h-horizon in the site specific podsols, while the swale bases are mainly covered by several decimetres of peaty soil and tsunamigenic sand sheets.

The indicative height of the ridge crests was considered to be too imprecise to mark a specific sea level, therefore, they were only interpreted in their position relative to the recent berm. Instead, the bases of the rather narrow swales were used as an indicator for MHW ±0.5 m, the accuracy of ±0.5 m being a rather conservative empirical value (fig. 7.2b).

7.5 Methods

To establish a sea-level curve for southwest Thailand, all index points were related to the astronomical tides. For this, principally two different approaches can be used: one possibility is to relate the indicators to the exact tide level during measurements, by taking the astronomical tide level from tide gauge data and correcting them for the exact position (if not identical with the tide gauge station) and the actual air pressure. In the absence of disturbances by waves,

accuracy within the variation of tidal markers (e.g. MHW), which may differ from year to year and season to season in the amount of 1-2 decimetres, can be achieved. The second approach is based on relating the indicators to significant markers in the field which precisely correlate with specific tide levels. Since along the rocky coasts of the study area such a marker was always present in the form of the uppermost closed belt of rock oysters (*Saccostrea cucullata*), which in sheltered positions represents MHW ±10 cm, it was used to determine the height of the biological sea-level indicators. The levelling was carried out with a levelling staff over short, nearly vertical distances, which allowed measurements with an insignificant error margin. At the sedimentary coast of Phra Thong, where a constant sea-level marker was missing, the levelling followed the first approach (the tide level during measurements was calculated from the gauge data of Kuraburi) using a differential GPS (Leica SR 530). To get the height of the swale bases, the thickness of the terrestrial infill (peaty soil and tsunamigenic sand sheets) was measured for most swales (in some cases it could only be estimated) and subtracted from the surface height.

To establish a chronology for the levelled index points, three different dating methods were applied: (1) a speleothem from a bio-erosive notch was dated by means of the U/Th technique at the University of Heidelberg (Germany). (2) The ages of corals, molluscs and organic macro remains were determined by radiocarbon dating at the laboratories of Beta Analytic (Florida) and the University of Georgia (Athens), using radiometric dating and AMS. A marine reservoir effect of $\Delta R = -2$ was adopted from Southon et al. (2002). All data were calibrated to 2σ-sidereal years using the IntCal09 and Marine09 data sets of Reimer et al. (2009). (3) To date littoral sand from beach ridges and swales, the optically stimulated luminescence (OSL) technique was applied, which generally proved to be applicable for the dating of beach ridge plains (e.g. Nielsen et al., 2006; Roberts and Plater, 2006); the preparation and measurement of OSL samples followed the procedure described in Brill et al. (2012a) for littoral deposits at the same location (Ko Phra Thong).

The sample processing was carried out in subdued red light. Dried samples were sieved and treated with HCl, H_2O_2 and sodium oxalate to remove carbonate, organic material and clay. To obtain pure quartz, the sediment was separated with heavy liquid and finally etched with concentrated HF. Measurements were performed on a Risø TL/OSL DA 20 with a $^{90}Sr/^{90}Y$ beta source. Luminescence signals were detected through a Hoya U340 filter (7.5 mm) after blue LED stimulation, carried out at a temperature of 125 °C for 50 s. The determination of equivalent doses followed the SAR protocol of Murray and Wintle (2000, 2003). The effects of thermal pre-treatment and the luminescence characteristics were analysed by performing preheat-plateau, thermal-transfer and dose recovery tests. Mean equivalent doses were calculated by means of the central age model (Galbraith et al., 1999). Dose rates were calculated from K, Th and U concentrations (determined by means of NAA at Becquerel Laboratories, Canada) and in situ water contents of the samples, using the ADELE software (Kulig, 2005).

7.6 Results

Figure 7.1 shows the areas where the sea-level index points of this study were taken from. These are the beach-ridge sequences of Phra Thong Island as well as the granite headland Laem Son at the southern end of Kamala Beach (Phuket), the island group around Ko Pha Nak and Ko Hong in the inner part of the Phang-nga Bay and the Phi Phi Islands, southeast of Phuket.

Table 7.1: Radiocarbon (a) and U/Th (b) dating results for the index points from the Phang-nga Bay and Phuket. Radiocarbon ages were measured at Beta Analytic (Florida), U/Th ages were measured at the Institut für Umweltphysik, Heidelberg (Prof. Dr A Mangini); calibrated ages are based on the Marine09 data set of Reimer et al. (2009); a marine reservoir effect of $\Delta R = -2$ was adopted from Southon et al. (2002). KPN (E): Ko Pha Nak East; KPN (H): Ko Pha Nak Hong; KNK: Ko Na Khae; KPP MB: Ko Phi Phi Maya Beach.

(a) Radiocarbon data

Sample	Location	Altitude (m a MHW)	Ind. Height (m a. RSL)	Lab code	Material	δ^{13}C (‰)	Conv. Age (yr BP)	Cal. age (2σ) (yr cal. BP)	Cal. Age (AD/BC, 2σ)
Thai 11-14	Laem Son	−1.36	≥0.24	Beta-298446	coral	−2.3	6280±50	6877–6618	4928–4669 BC
Thai 11-15	Laem Son	−1.18	≥0.42	Beta-298447	coral	−1.5	1280±40	914–726	AD 1036–1224
Thai 11-16	Laem Son	−1.18	≥0.42	Beta-298448	coral	−1.8	1220±40	873–675	AD 1078–1276
Thai 11-17	Laem Son	−1.03	≥0.57	Beta-298449	coral	−2.4	1120±40	765–610	AD 1186–134
Thai 11-18	Laem Son	−1.00	≥0.6	Beta-298450	coral	−2.2	5760±50	6282–6026	4333–4077 BC
Thai 11-19	Laem Son	−0.97	≥0.63	Beta-298451	coral	−1.6	830±50	534–333	AD 1417–1618
Thai 11-20	Laem Son	−0.89	≥0.71	Beta-298452	coral	−0.9	5960±60	6518–6259	4569–4310 BC
Thai 11-8	KPN (H)	0.70	0.7±0.1	Beta-298444	oyster	−0.1	1610±30	1256–1083	AD 695–868
Thai 11-9	KPN (H)	0.85	0.85±0.1	Beta-298426	oyster	−0.6	2730±30	2575–2328	626–379 BC
Thai 11-3	KPN (E)	1.00	1±0.1	Beta-298441	oyster	−0.1	2490±30	2281–2052	332–103 BC
Thai 11-7	KNK	1.50	1.5±0.1	Beta-298443	oyster	−0.1	3790±30	3830–3631	1881–1682 BC
Thai 11-21	Laem Son	0.08	≥1.68	Beta-298453	coral	−2.9	830±40	530–373	AD 1421–1578
Thai 11-11	KPN (H)	1.70	1.7±0.1	Beta-298445	oyster	−0.8	2740±30	2599–2336	650–387 BC
Thai 11-12	KPN (H)	1.90	1.9±0.1	Beta-298427	oyster	−1	3560±30	3544–3364	1595–1415 BC
Thai 11-22	Laem Son	0.60	≥2.2	Beta-298454	coral	−1	4380±50	4711–4390	2762–2441 BC
Thai 11-13	KPN (H)	2.60	2.6±0.1	Beta-298428	oyster	0.4	5350±40	5845–5605	3896–3656 BC
Thai 11-23	KPP MB	1.50	≥3.1	Beta-298429	coral	−8.1	23,190±130	28,000–26,910	26,051–24,961 BC
Thai 11-2	KPN (E)	1.50	dislocated	Beta-298440	oyster	−3.3	> 43,500	49,026–44,848	47,077–42,899 BC
Thai 11-4	KPN (E)	2.40	dislocated	Beta-298442	Marine gastropod	−0.7	30,1240±640	36,759–34,500	34,810–32,551 BC

b) U/Th data

Sample	Location	Altitude (m a. MHW)	Lab code	Material	Uncorrected age (yr)	Corrected age (yr BP, 2σ)	Corrected age (AD/BC, 2σ)
Thai 11-5	KPN (E)	3.60	HD-5353	stalagmite	21400	19000±1300	17,000±1300 BC
	δU (‰)	^{238}U (µg/g)	^{232}Th (ng/g)	^{230}Th (pg/g)			
	209.6±7.3	0.0557±0.0001	5.43±0.024	0.1963±0.0053			

7.6.1 Holocene sea-level evidence at rocky coasts

Laem Son (Kamala Beach). The west coast of Phuket is characterised by granitic headlands and bays with narrow, sandy beaches. Laem Son is the headland south of Kamala Beach (fig. 7.1d). At its northern spit (the southern end of Kamala Beach) the solid granite rocks are covered by large corestones, resting on a rough, seaward dipping slope. Between the granite corestones, coral boulders as well as small, dead corals in living position (mostly *Porites lu-*

tea) are hidden. Today these in situ corals are located well above the highest level of living corals (i.e. MLW). The thin crusts are attached to the surrounding boulders and mostly covered by green algae and bored by worms and tiny crabs (fig. 7.3c and d). A total of nine samples of dead in situ corals, the lowest at -1.36 m below MHW and the highest at 0.6 m above MHW, were taken (fig. 7.3a and b) and dated to ages between 530-373 and 6877-6618 cal. BP (Thai 11-14-22, tab. 7.1). Considering a tidal range of 1.60 m, the index points are located between 0.24 and 2.20 m above their maximum living level (MLW) and thus indicate higher sea levels during the last 6800 years with a maximum of at least +2.20 m at 4700-4400 cal. BP.
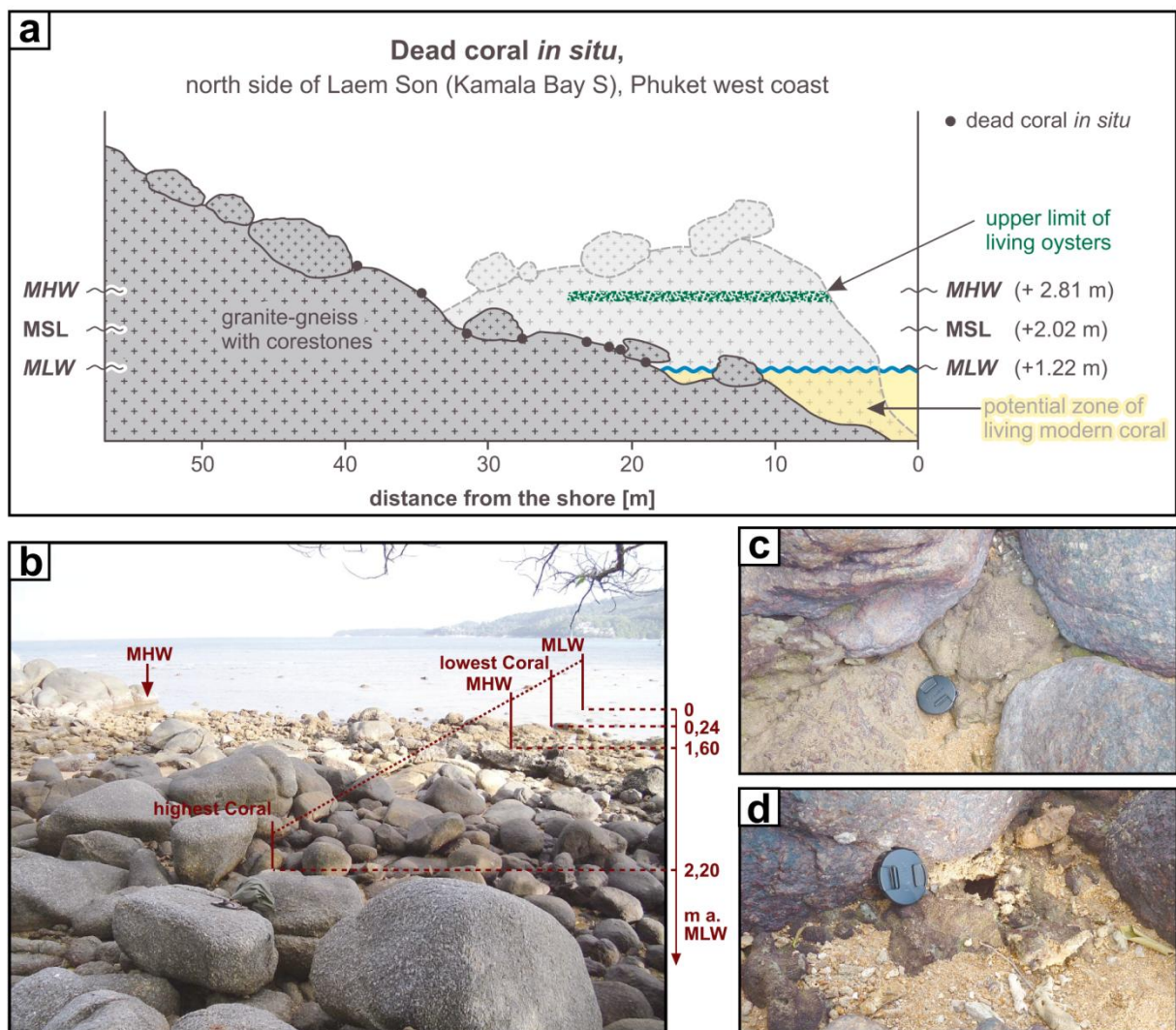
Figure 7.3: Sea-level indicators at Laem Son (Kamala Beach). (a) Schematic overview of the sampling site; dead in situ corals are located between granitic core stones well above the zone of modern coral growth. (b) Photograph of the corestone-covered beach; the zone with dead in situ corals reaches from MLW to 60 cm above MHW. (c) Dead in situ coral in the gap between the granitic corestones; (d) the corals form thin, c. 3 cm thick crusts, which are attached to the corestones.

Phang-nga Bay

The area of the Phang-nga Bay is characterised by limestone islands. Their steep coasts show features of bio-construction (oysters) as well as bio-erosion (borings and notches). The most impressive forms are horizontal notches that are the result of bio-erosion (bio-corrosion and bio-abrasion) by littorinids, limpets, chitons and other gastropods (plus micro-organisms) grazing on endolithic cyanophyceae and chlorophyceae. Today only the lowermost notch is actively formed. The highest notch, generally much more incised than the active one, often shows a remarkably flat roof, cave openings and a thick cover of flowstone on its floor, as well as curtains of speleothems with diameters of up to 3 m. As the speleothems are formed in an open notch situation and always above the reach of waves (not dissolved if drowned in sea water, but bored by micro-organisms and bivalves), the sharp lower limits of hanging stalactites may also be used as a sea-level indicator.

(1) On the east coast of Ko Pha Nak (KPN (E) in fig. 7.1e) up to three different notch levels are developed. The upper one is incised more than 10 m deep at a height of 2.50-4.50 m above MHW. Its floor is covered with a thick flowstone and well developed speleothems partly hide the notch from outside. Borings of bivalves cover its walls and the roof up to 4.50 m above MHW. The middle notch (at 2 m above MHW) is much less incised than both the upper notch and the active one (fig. 7.4). A stalagmite from the inner part of the highest notch was U/Th dated to 19,000±1300 years (Thai 11-5, tab. 7.1). Dislocated molluscs, incorporated in lithified sediments that cover the basal flowstone in the upper notch (at 2.50 m above MHW) and a vertical crack in the limestone cliff (at 1.50 m above MHW, figs. 7.4d and f), yielded radiocarbon ages of 36,759-34,500 and 49,026-44,848 cal. BP (Thai 11-2 and -4, tab. 7.1). An in situ oyster found in another crack at +1 m above MHW was dated to 2281–2052 cal. BP (Thai 11-3, tab. 7.1). With a tidal range of 1.60 m, higher sea levels of up to +4.10±0.5 m (upper notch, height of the base above MLW), +6.10±0.2 m (bivalve borings) and +1.0±0.10 m (oysters) are indicated.

(2) Inside a hong of Ko Pha Nak (KPN (H) in fig. 7.1e) notch levels above the active one are missing. However, in a sheltered position of the hong, dead in situ oysters (*Saccostrea cucullata*) reached altitudes of up to +3 m above the belt of living organisms (fig. 7.4g). A total of five samples between 0.85 and 2.6 m above MHW yielded ages between 1256-1083 and 5845-5605 cal. BP (Thai 11-8, -9 and -11, -12, -13, tab. 7.1), indicating a maximum sea-level height of +2.60±0.10 m at 5850-5600 cal. BP.

(3) Along the northern coast of Ko Na Khae (KNK in fig. 7.1e) a narrow beach is developed in front of the limestone cliff. Here the upper notch reaches from 3.50 to 4.90 m above MHW. While sea-urchin borings cover the cliff up to 1.30 m above MHW, the highest bivalve borings were found at the roof of the upper notch (4.90 m above MHW). An in situ oyster (*Saccostrea cucullata*) at 1.5 m above MHW, which was hidden in a vertical

crack, gave an age of 3830-3631 cal. BP (Thai 11-7, tab. 7.1). Considering a tidal range of 1.60 m, notches indicate higher sea levels of up to +5.10±0.5 m (height of the base above MLW), bivalve borings of +6.50±0.2 m, sea-urchin borings of +2.90±0.20 m and oysters of +1.50±0.1 m.

(4) While elevated notch levels on the Phi Phi Islands were found along several sections of the coast, bio-constructive forms others than of recent organisms were missing. Only at Maya Beach (MB in fig. 7.1f) a single coral at 1.50 m above MHW (3.10 m above MLW), recovered from a crack in the limestone cliff, could be dated to 28,000-26,910 cal. BP (Thai 11-5, tab. 7.1). Another kind of young sea-level indicator is given by a nearly horizontal rock platform (about 6-7 m wide) developed in sandstone at the west coast of Phi Phi Don. The platform is situated close to MHW; less than 1 m above it, honeycomb weathering and small tafoni were found.
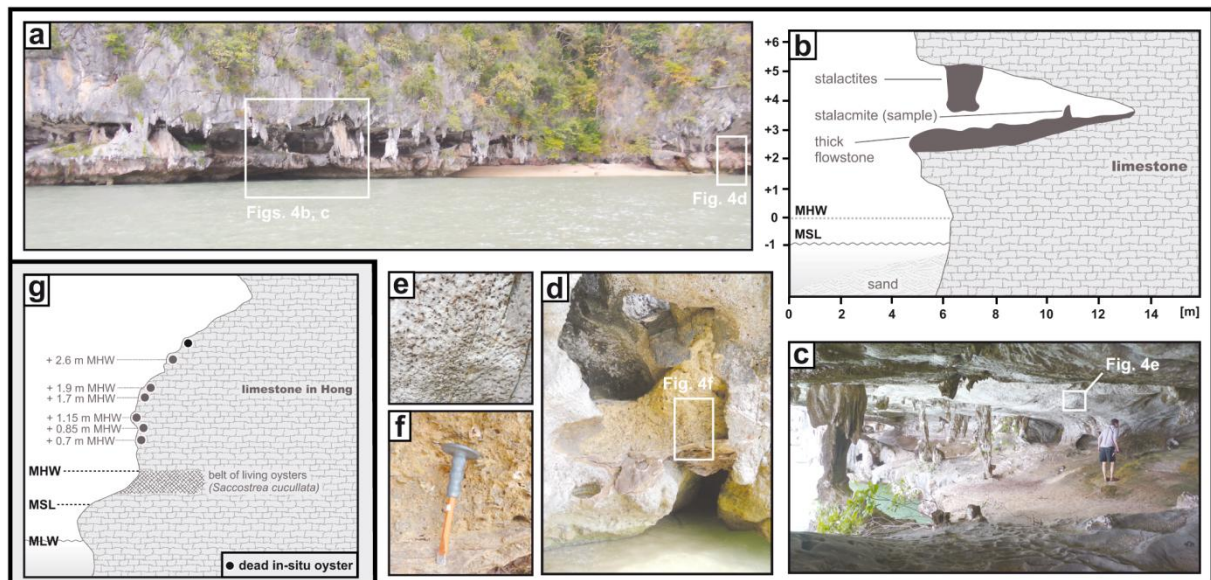
Figure 7.4: *Sea-level indicators on Ko Pha Nak (Phang-nga Bay). (a-f) Ko Pha Nak East: along the steep limestone coast to the left of the narrow beach a deep bio-erosive notch is developed several metres above the recent notch (a-c); the walls and the floor are covered with flowstones and stalagmites (b, c); Lithophaga borings can be found at its roof (e). To the right of the beach a flowstone-covered crack in the limestone cliff contains a lithified shell deposit with dislocated oysters (d, f). (g) Ko Pha Nak Hong: dead in situ oysters were sampled up to 2.60 m above the living zone of modern oysters.*

7.6.2 Holocene sea-level evidence at the sedimentary coast of Ko Phra Thong

Phra Thong Island is dominated by sequences of more or less shore parallel beach ridges and swales, occasionally cut by discordances that document erosion events (e.g. Scheffers et al., 2012b). While in the eastern part these structures are predominantly covered by mangroves and dense vegetation, grassy ridges and wet, tree lined swales build up a 2.5-3 km wide open beach-ridge plain in the west of the island (figs 7.1c and 7.5). In the northern part of this

beach-ridge plain four shore-perpendicular transects were levelled (transects A-D in fig. 7.5). The chronology was based on a total of 13 OSL samples, taken from ridges (KPT 12, 24-26, 28, 32, 40 and 43-46; tab. 7.2 and fig. 7.5) and intertidal sand at the swale bases (KPT 2 and 36; tab. 7.2). Additionally, three organic samples from peaty soils at the swale base were dated by means of radiocarbon (tab. 7.2b). Further chronological information was obtained from OSL results of Prendergast et al. (2012). Figure 7.5 documents the results of transect A: from the east to the west the ages decline from 5300±500 to 1600±200 years, revealing no age inversions. In the same direction the heights of the ridge crests (from 3.30 to 1.50 m above MHW) and the swale bases (from 2.30 to 1.15 m above MHW) show a decreasing trend. Transects B and C reveal similar tendencies (oldest ages in the east and youngest ages in the west as well as decreasing topography towards the present shoreline), with only a single age inversion in transect C (KPT 32). Because of the high dating uncertainties of the ages for KPT 24, 25 and 26 (all ages overlap within their error margins), no clear trend could be observed in transect D.

Table 7.2: Luminescence (a) and radiocarbon (b) dating results for the index points from Ko Phra Thong. OSL data were carried out by DB and NK in the Marburg Luminescence Lab (*ages for R1-3 and S1 are taken from Prendergast et al., 2012). Radiocarbon samples were measured at the University of Georgia (Athens); calibrated ages are based on the IntCal09 data set of Reimer et al. (2009).

(a) OSL data

Sample	Location	Distance (m)	Altitude (m a. MHW)	Lab code	U (ppm)	Th (ppm)	K (%)	Water (%)	De (Gy)	Age (years)
R1	ridge	180	1.92							1600±200*
R2	ridge	300	2.25							2100±270*
S1	swale	370	−0.45							2500±250*
R3	ridge	450	2.40							2560±350*
KPT 2j	swale	740	0.68	MR-0787	4.1±0.13	17.7±0.40	0.15±0.01	23.10	4.43±0.060	2480±240
KPT 12	ridge	770	3.12	MR-0791	0.8±0.05	2.7±0.18	0.03±0.01	11.90	2.73±0.08	2324±197
KPT 40	ridge	954	2.54	MR-1522	5.9±0.61	26.7±1.34	0.2±0.01	1.17	7.66±0.43	4416±421
KPT 43	ridge	1050	2.75	MR-1524	2.7±0.07	6.1±0.27	0.05±0.01	1.20	2.94±0.07	4252±378
KPT 32	ridge	1170	3.32	MR-1514	3.7±0.16	17.8±0.91	0.4±0.01	6.05	5.75±0.17	4516±454
KPT 36	swale	1300	0.70	MR-1519	2.3±0.10 6.5±0.56	9.1±0.48 16.8±0.84	0.5±0.01 0.6±0.02	16.70	5.00±0,06	3028±351
KPT 44	ridge	1310	2.99	MR-1526	1.9±0.06	7.6±0.27	0.2±0.01	2.85	3.66±0.07	5025±400
KPT 45	ridge	1500	3.03	MR-1528	1.2±0.06 4.7±0.14	4.2±0.23 10.8±0.73	0.2±0.01 0.05±0.01	1.65	4.10±0.1	4645±347
KPT 46	ridge	1730	3.36	MR-1531	4.5±0.19 1.2±0.08	12.4±0.64 3.22±0.15	0.2±0.01 0.07±0.01	2.16	4.81±0.19	5310±520
KPT 28	ridge	1800	3.53	MR-1512	2.8±0.13	12.9±0.67	0.3±0.01	1.63	5.55±0.06	5394±535
KPT 25	ridge	4500	3.25	MR-1509	3.4±0.14	18.7±0.96	0.17±0.01	0.23	151.5±7.70	126,301±14,398
KPT 24	ridge	4600	3.47	MR-1506	1.2±0.06 4.2±0.12	3.8±0.21 20.7±0.75	0.14±0.01 0.01±0.01	2.42	123.6±8.45	104,587±10,565
KPT 26	ridge	4900	3.90	MR-1511	1.5±0.07	6.0±0.32	0.26±0.01	2.43	121.0±4.76	106,950±8318

(b) Radiocarbon data

Sample	Location	Distance (m)	Altitude (m a. MHW)	Lab code	Material	δ^{13}C (‰)	Conv. Age (yr BP)	Cal. Age (yr cal. BP, 2σ)	Cal. Age (cal. AD/BC, 2σ)
KPT 35B/1	swale	1300.00	0.70	UGAMS-8050	wood	−28.90	3040±25	3345–3165	1396–1216 BC
KPT 37/2	swale	1300.00	−0.69	UGAMS-8051	plant fragment	−29.80	2760±20	2923–2785	974–836 BC
KPT 23/7	swale	1550.00	−0.20	UGAMS-8045	wood	−29.30	3080±30	3370–3217	1421–1268 BC
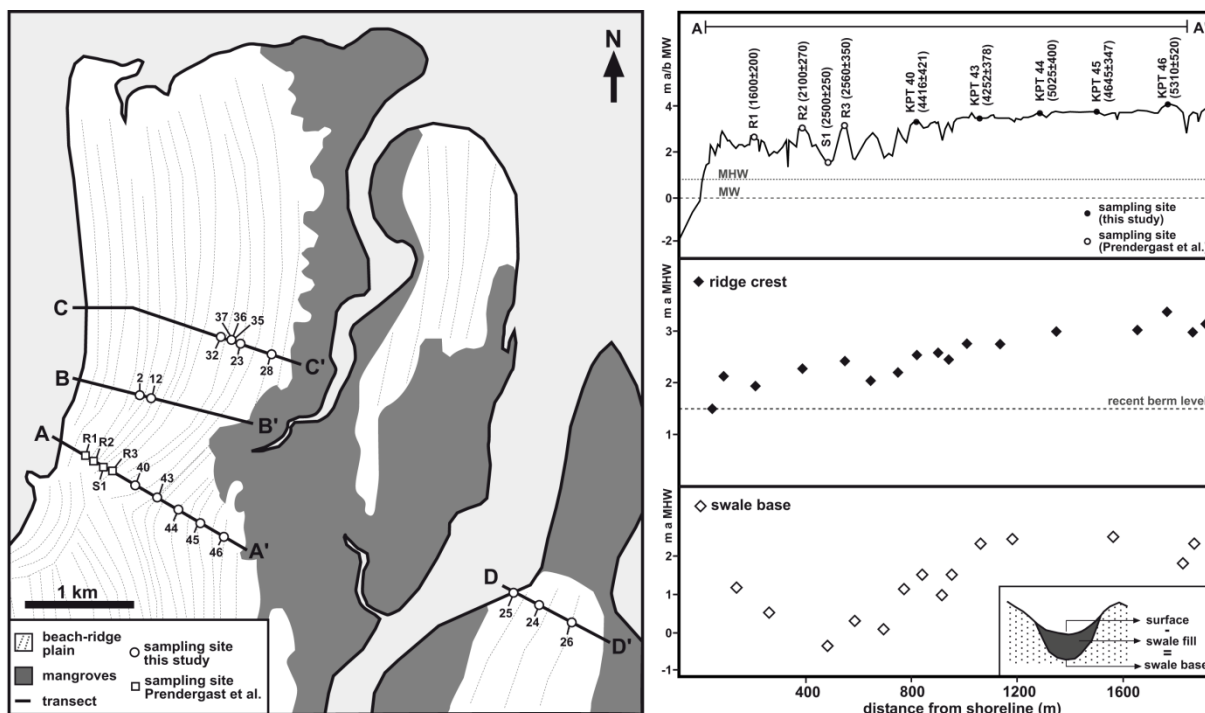
Figure 7.5: *The beach-ridge plain on Ko Phra Thong. (a) In the northern part of the island four transects were levelled and sampled for dating. (b) Topographic cross-section along transect A: the heights of the ridge crests and swale bases are plotted against the distance from the present shoreline. Since the island developed from the east to the west, the ages become relatively older towards the east. In the same direction the heights of ridge crests and swale bases show a slightly increasing trend.*

7.7   Discussion

7.7.1   The chronology of sea-level index points

Galleries of sea-urchin and *Lithophaga* borings, often found around 4.5-5.5 m above MSL as well as directly above the living oyster belt (from MHW to nearly +0.90 m above MHW), certainly belong to higher sea levels than today. Similarly, bio-erosive notches indicate sea levels up to 3.50-5.50 m above the present one. However, as pure destructive forms they could not be dated directly. Mainly, even relative ages can only be estimated: from the thick flowstones and the very well developed speleothem inside, some of them about 3 m in diameter, pre-Holocene ages are suspected for the upper notch; a long-lasting sea-level highstand of pre-Holocene age is also supported by the deep incision of the upper notch (up to 10 m (figs. 7.4c and d), deeper caves leading into the islands).The intermediate notch, which is only preserved as remnants at isolated places, seems to be eroded by both the recent and the upper notch and thus is certainly the oldest of the three. Therefore, it must result from a sea-level highstand of at least last-interglacial age (probably even older). Borings of bivalves and sea-urchins located at the roof of the upper notch must be younger than this, but still are estimated to be of pre-Holocene age. In some cases minimum ages could be achieved by dating constructive forms (not necessarily connected to sea level), inside the notches: according to a

speleothem age of 20 ka, the upper notch at the eastern side of KPN definitely pre-dates the Holocene.

Bio-constructive indicators (oysters and corals) as well as sedimentary sea-level markers (ridges and swales) could be dated with isotopic methods (radiocarbon) and luminescence dating. In the case of in situ organisms and morphological structures, the dating results reflect the age of the sea level indicated by this index point. If organisms have been dislocated (gastropod in the upper notch and oyster in the crack fill at KPN), they only provide maximum ages for the corresponding sea levels. Considering this, bio-erosive indicators cannot be used to reconstruct a sea-level curve. However, they prove the existence of up to 6 m higher sea levels during the younger Pleistocene. On the basis of ridge-crest data from the eastern part of Phra Thong (KPT 24, 25, 26), the last pre-Holocene highstand can be related to the last interglacial around 125 ka BP, a period of widespread 4-6 m higher eustatic sea levels (e.g. Church et al., 2008; Rohling et al., 2008). Although the corresponding OSL data are too imprecise to define an exact time (covering an age range of 94-140 ka within their error ranges) and the recent altitude of the ridges is a sea-level indicator too poor to give an exact altitude (compare section 'Sea level indicators'), they must be related to the Eem, since sea level was many metres below its present position during the intervening glacial periods. In contrast, it was possible to combine all data of in situ oysters and corals, as well as ridges and swales to a Holocene sea-level curve (section 'Holocene sea-level curves').

7.7.2 Holocene sea-level curves

Our tentative sea-level curves cover only the ages we have found in our samples. Nevertheless, those from the Laem Son coral profile, as well as those from oysters in the Phang-nga Bay show the same trend and maximum altitude lower than +3 m compared with modern RSL (fig. 7.6a); the maximum of +2.5-3.0 m was timed to c. 5700 cal. BP. Both time and magnitude of the highstand match the GIA model predictions (Horton et al., 2005) quite precisely. From the reconstruction of former sea levels back to about 5300 BP out of the sedimentary archive of the ridge and swale sequences of Phra Thong Island we tentatively deduce a highstand around 5300 BP in the order of +1.5-2.5 m above RSL (fig. 7.6b). The limited height of the uppermost beach ridges just below +5 m above MSL and their difference in altitude of about 1 m to the original swale bottoms point to a slightly lower highstand in the northwest of the study area. At least three possible explanations can be mentioned for this difference:

Figure 7.6: Sea-level curves for the study area. (a) Sea-level curve based on bio-constructive index points from Kamala Beach and the Phang-nga Bay; the reconstructed sea-level trend is nearly identical with that predicted by GIA models. (b) Sea-level curve for Ko Phra Thong based on ridge crest and swale base data; compared with the area around Phuket and the Phang-nga Bay (a), the Holocene maximum is slightly smaller.
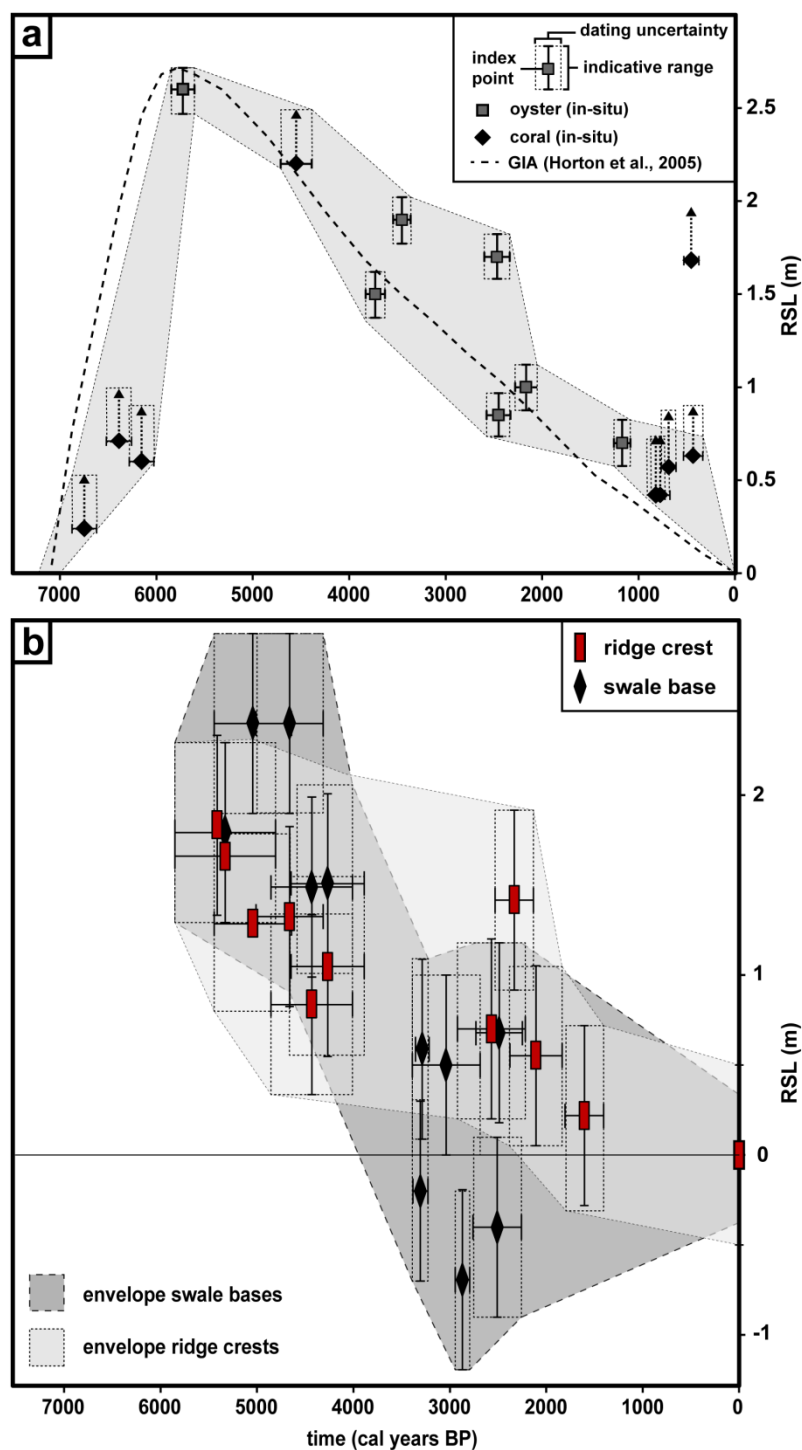
(1) There is the possibility of local effects in the form of neo-tectonic movements in the order of 1 m during the younger Holocene. Although the assumption of complete neotectonic quiescence during the Holocene (Tjia, 1996) might be too simplistic (Fenton and Sutiwanich, 2005), the vague data of historical earthquakes and seismic activity in prehistoric times (Department of Mineral Resources, http://www.dmr.go.th/main.php?filename=ActiveFault_Eng) do not provide any quantitative information about amount, timing and spatial distribution of Holocene tectonic movements. Recent GPS measurements support

97

the assumption of tectonic activity during the Holocene, pointing to cycles of long-term slow uplift and shorter periods (several decades) of accelerated subsidence induced by strong earthquakes at the Sunda Fault subduction zone (Meltzner et al., 2006; Trisirisatay-awong et al., 2011). However, because of the repeated switchover between uplift and subsidence, which predominantly compensate each other, it is very difficult to quantify the absolute effect on the Holocene sea-level curve. Moreover, there is no hint for significant spatial variations which could explain the differences in the sea-level curves of Phuket and Phra Thong.

(2) The second possible reason is compaction of the ridge-and-swale-sediment sequence. But as it consists of fine to medium well sorted sand, this is a vague argument, not supported by similar observations elsewhere.

(3) The third, probably most reasonable explanation relates the difference to spatially variable hydro-isostatic effects (Horton et al., 2005).

Based on our index points (limited in number, but taken from exposed and sheltered sites and from very different indicators) we conclude that slightly higher sea and tide levels in the order of present spring tide range (about 2.5 m) existed for the Holocene.

7.7.3 Implications for the interpretation of palaeotsunami deposits

In case of palaeotsunamis that are only preserved in the form of sedimentary evidence, maximum inland extent, indicating inundation, and maximum height above RSL, indicating run-up or wave height, of the deposits can be used to estimate event magnitudes. Considering the sea-level fluctuations described in the section 'Holocene sea-level curves', the reference level for these indicators, i.e. RSL, was at the most 2.5 m above present level for palaeotsunami evidence from western Thailand, which covers only the last 5000 years (Brill et al., 2011; Jankaew et al., 2008; Rhodes et al., 2011). This may mean that sea levels during low water had been at the levels of modern high water (considering constant spring tide ranges of ~2.5 m), all in all a nearly comparable situation for palaeotsunami landfalls during the last millennia. For example, the well constrained palaeotsunami deposits from Ko Phra Thong (Jankaew et al., 2008) and Ban Bang Sak (Brill et al., 2011) comprise one event at 500-700 cal. BP and 2-3 additional tsunamis younger than 2500 cal. BP. Taking today's sea level as a basis, the waves of these events had to override ridges up to 5 m (above low water) and inundation reached up to 1300 m inland. Considering the corresponding RSL of +1-1.5 m at 500-2500 years ago, the minimum waves that had the potential to cross the barrier (reduced to 3.5-4 m at low water) could have been slightly lower than at present RSL. However, this difference of at the most 1.5 m is completely compensated by the potential differences in tide levels (diurnal variation between high water and low water) of 1.5-2.0 m.

Much lower RSL compared with the present level (and therefore with more influence on the spread of tsunami deposits) are characteristic for the early Holocene prior to 7000 cal. BP, a period that lacks contemporaneous tsunami evidence in Thailand. During the last 7000 years, instead, coastline progradation (e.g. of the Phra Thong beach-ridge plain) had much more influence on the distribution of tsunamites than sea-level movements. However, only the combined data of palaeotsunami deposits, palaeogeography and RSL at a given time allow a well-grounded interpretation of event magnitudes.

7.8   Conclusions

For the west coast of southern Thailand, glacial isostatic adjustment models predict a mid-Holocene sea-level highstand with regionally variable altitude. Field evidence in the form of fixed biological indicators from rocky coasts as well as beach ridges and swales from a sedimentary coast, was used to quantify the exact timing and altitude of this sea level maximum: (1) Sea level had reached its maximum of +2.5-3 m 5700 years ago. Following this highstand, sea level gradually dropped to its present level; oscillations have not been observed. (2) Regional differences between Phra Thong Island in the north and Phang-nga Bay in the south, probably as a result of hydro-isostasy, are in the order of at the most 1 m at the time of the Holocene maximum.

These sea level variations effect the interpretation of palaeotsunami deposits regarding the magnitude of associated events. However, RSL during the ages so far elaborated for Thailand´s palaeotsunamis, i.e. the last 5000 years, was in the order of +2.5 m and thereby comparable with the difference between high water and low water. Thus, its influence on deposition by tsunamis is too low to be distinguished from diurnal variations of tide levels.

Chapter 8

8 Coastal evolution of southwest Thailand during the Holocene – implications for the site-specific occurrence of palaeotsunami deposits

Abstract: The reconstruction of tsunami recurrence in southwest Thailand, where the historical record is short, is predominantly based on sedimentary evidence of prehistoric events from coastal geoarchives. Since geological palaeotsunami records are dependent on the deposition and preservation of tsunami deposits, the existence of near-shore archives suitable for preservation has considerable influence on the length and completeness of local archives. This study reconstructs Holocene changes in palaeogeography for three short sections of the west coast of Thailand based on sediment drill cores to evaluate the influence of coastal evolution on local tsunami records. The patterns of palaeotsunamis archived on Phra Thong Island, i.e. four events within the last 3000 years, and at Ban Bang Sak, up to three events within the period 1200-2000 cal BP and another event at 500-700 cal BP, can be explained by the time windows provided by the evolution of favourable environments. At Pakarang Cape, instead, only one prehistoric tsunami at 1000-1200 cal BP is archived, although a back-reef lagoon, which proved to be a suitable environment for preservation, was persistent for several millennia.

8.1 Introduction

The reconstruction of tsunami recurrence prior to historical documentation depends on geological evidence of tsunami impact. In far-field settings without significant co-seismic uplift or subsidence due to triggering earthquakes, tsunami-laid sediment – either terrestrial material in offshore environments (e.g. Feldens et al., 2009; Smedile et al., 2011) or marine material deposited onshore (e.g. Dawson et al., 1988; Atwater and Moore, 1992; Hindson and Andrade 1999; Mastronuzzi and Sanso, 2000; Minoura et al., 2001; Nanayama et al., 2003; Pinegina et al., 2003; Cisternas et al., 2005; Switzer et al., 2005; Jankaew et al., 2008; Monecke et al., 2008; Scheffers et al., 2008; Vött et al., 2009; Engel et al., 2010; May et al., 2012) – is the most common indicator of past tsunami impact. However, the presence of onshore tsunami deposits in near-shore archives relies on (i) the deposition of entrained material during tsunami inundation of coastal areas, (ii) the preservation of these deposits over longer time periods, and (iii) the capability to discriminate tsunami-laid deposits from background sedimentation.

While deposition is significantly influenced by the propagation and the magnitude of tsunami waves, the preservation and discrimination potential is mainly controlled by long-term weathering conditions, bioturbation and morphodynamics in the environments tsunamites have been deposited in (Peters and Jaffe, 2010; Szczuciński, 2012).

Due to the short historical record of the region (Kumar and Achyuthan, 2006; Dominey-Howes et al., 2007; Alam et al., 2012), geological evidence of previous tsunamis is of particular importance for the coastlines around the Indian Ocean. By flooding large sections of low lying areas and leaving behind a centimetres to decimetres thick sheet of sand, the 2004 Indian Ocean tsunami (IOT) demonstrated the general conservation potential of tsunami deposits along the west coast of Thailand (e.g. Szczuciński et al., 2006; Hawkes et al., 2007; Hori et al., 2007; Goto et al., 2007; Kelletat et al., 2007; Choowong et al., 2007, 2008; Srisutam and Wagner, 2010; Fujino et al., 2010; Naruse et al., 2010). However, most near-shore environments proved to be unsuitable archives for long-term preservation of tsunami deposits. After less than 10 years most of the IOT 2004 deposits in mangrove areas had been reworked by bioturbation and in many coastal plains tsunami evidence was disturbed by soil formation, erosion and human activity (Szczuciński, 2012). In archives with sandy background sedimentation, such as beaches and sandy ridge plains, discrimination of tsunami deposits was hardly possible after only a few years. On the other hand, favourable archives – i.e. low energy environments with fine-grained background sedimentation and insignificant post-depositional disturbance – turned out to be wet swales of beach-ridge plains, coastal lakes and lagoons (Jankaew et al., 2008; Fujino et al., 2009; Sawai et al., 2009; Brill et al., 2012b). However, due to the general predominance of sediment erosion over sediment accumulation, these environments are scarce along the coastline of southwest Thailand (Szczuciński, 2012), where all coastal lakes and lagoons are invariably the result of tin mining activities, thus, providing a potential tsunami archive for the last two centuries only (Chansang, 1988). This demonstrates the importance of long-term palaeogeographical evolution as a factor in palaeotsunami research, since it explains the existence and lifetime of geoarchives suitable to preserve tsunami evidence.

In this study we present palaeogeographical reconstructions – based on existing stratigraphical data as well as new sedimentary evidence – for three sections of the west coast of Thailand for which evidence of IOT 2004 predecessors had been identified: (a) The beach-ridge sequences on Phra Thong Island (Jankaew et al., 2008; Brill et al., 2012a, b; Prendergast et al., 2012), (b) the coastal plain of Ban Bang Sak (Brill et al., 2011), and (c) the coastal plain of Pakarang Cape (Neubauer et al., 2011). By doing this, the role of coastal evolution in providing and defining local time windows for the preservation of onshore tsunami deposits was analysed.

8.2 The study area

8.2.1 Coastal geomorphology and stratigraphy

Southern Thailand is part of the Malay-Thai Peninsula, surrounded by the Gulf of Thailand to the east and the Andaman Sea to the west (figs. 8.1a, b). In contrast to the wide and flat coast along the Gulf of Thailand, at the west coast of the peninsula mountain chains reach close to the Andaman Sea, resulting in the characteristic alternations between steep, rocky headlands and mangrove covered areas or sandy beach-ridge plains (Dheeradilok, 1995; Liew et al., 2010). The three study sites – Ko Phra Thong, Pakarang and Ban Bang Sak – are located in the northern part of southwest Thailand, where offshore barrier islands accompany intertidal flats, sandy beaches and coral reefs at the mainland (fig. 8.1c). Generally, the evolution of coastal areas and changes in the positions of shorelines are controlled by (i) the type of rocks and the availability of sediment sources, (ii) the dynamics of dominant transport processes and weathering, (iii) the position of sea level, and (iv) tectonic activity (Vött and Brückner, 2006; Bird, 2008). In the study area, these factors are well documented for the last decades, but little is known about potential variations during the Holocene:

(i) Bedrock and sediment sources. The west coast of Thailand is characterised by granite outcrops forming headlands, and Quaternary deposits that constitute beaches and narrow sedimentary plains (Sinsakul, 1992; Liew et al., 2010). Recent coastal landforms mainly derive their material from the sediment load of small local rivers, and from marine sources mainly consisting of organogenic components such as corals, molluscs and foraminifera (Di Geronimo et al., 2009).

(ii) Transport processes and weathering. Coastal dynamics as the north-directed littoral drift (Di Geronimo et al., 2009), moderate waves <2 m (Choowong et al., 2008), and mesotidal conditions with a spring tide range of 2.5-4.0 m (Admirality Tide Tables, 2003) are the dominant parameters to form western Thailand's shorelines by causing erosion and deposition, locally. Exceptionally strong wave conditions as they occur during the passage of tropical cyclones have not been recorded within the last 150 years (Murty and Flather, 2004). Where streams and rivers cross the coastal plain, fluvial dynamics may shape the coastline at least on a local scale, whereas eolian transport is not significant. Due to the hot and humid conditions of Thailand's tropical climate, weathering processes are intensive and fast, producing material that may be washed from slopes during strong rainfall events.

(iii) Sea level. All coastal processes are reliant on the position of the relative sea level. Due to the rapid glacio-eustatic sea-level rise after the last glacial maximum (LGM), Holocene coasts did not evolve prior to c. 7000 years BP, globally (Woodroffe and Horton, 2005; Milne et al., 2009; Brückner et al., 2010). When the meltwater contribution of

the postglacial transgression decreased, regionally diverging factors started to control the courses of relative sea levels (Fleming et al., 1998; Gehrels et al., 1999). As a tropical far-field site, SW Thailand experienced a Holocene sea-level maximum around 5500 years BP, followed by a continuous drop in sea-level to its present position (Horton et al., 2005; Scheffers et al., 2012a). Due to differences in hydro-isostasy the height of the Holocene maximum varied regionally, with at least +2.6 m in the southern part (Phuket and Phang-nga Bay) and +1.5-2.0 m on Phra Thong Island (Scheffers et al., 2012a).
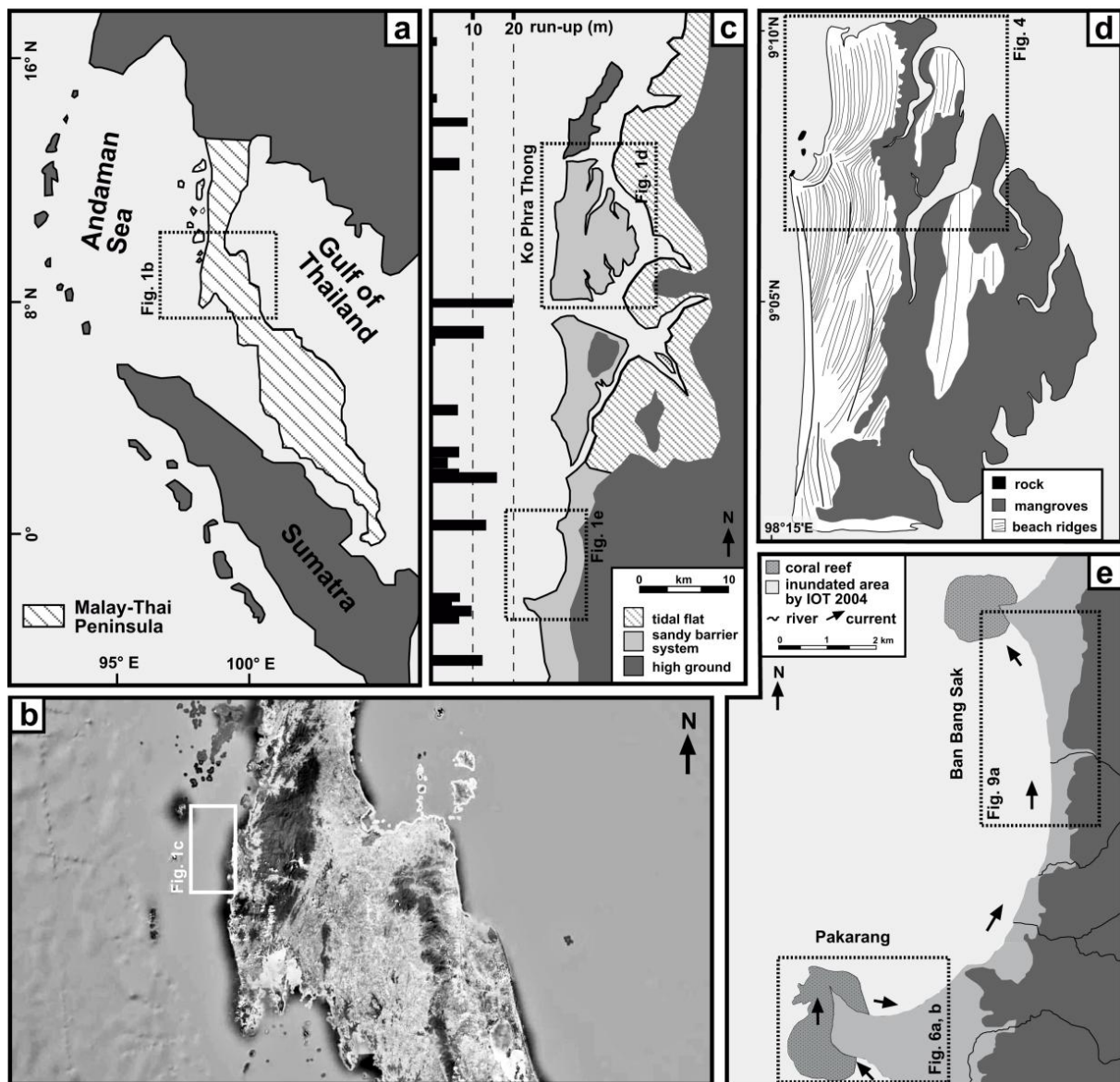
Figure 8.1: *Geographical overview of southwest Thailand. (a) Location of the Malay-Thai Peninsula. (b) Satellite image of southwest Thailand (Google Earth, 2012). (c) The west coast of Phang-nga province with sedimentary environments after Sinsakul (1992) and run-up heights of the IOT 2004 according to Tsuji et al. (2006). (d) Schematic geomorphological map of Phra Thong Island. (e) Location of Ban Bang Sak and Pakarang Cape with the inundation area of the IOT 2004 (Fujino et al., 2009).*

(iv) Tectonics. Although there is no evidence of strong tectonic activity in SW Thailand during the Holocene (Fenton and Sutiwanich, 2005), recent GPS data point to cycles of

slow uplift lasting for centuries and shorter periods (several decades) of accelerated subsidence as a reaction to strain accumulation and release by strong earthquakes at the Sumatra subduction zone (Meltzner et al., 2006; Trisirisatayawong et al., 2011). However, due to the repeated switchover between the counteracting processes, the vertical displacements are unlikely to result in overall uplift or subsidence of the coast.

Generally, there is little information about the way these factors have influenced the coastal evolution of Thailand during the Holocene. While for the Gulf of Thailand at least a Holocene stratigraphy of coastal deposits and general trends of shoreline variations have been established (Sinsakul, 2000; Tanabe et al., 2004), only scarce palaeogeographical data is available for the west coast. Sinsakul (1992) and Dheeradilok (1995) describe the general succession of coastal sediments, starting with alluvial deposits of Pleistocene age or weathered Tertiary bedrock that are followed by a 5-20 m thick Holocene sequence younger than 9000 years and consisting of basal mangrove peat, littoral deposits of the Holocene transgression, open marine and intertidal sediments, as well as mangrove peat or littoral deposits on top. Locally, more detailed Holocene stratigraphies have been established, e.g. in the coastal plain of Ban Bang Sak (Brill et al., 2011) and the mangrove area of Thap Lamu (Rhodes et al. 2011). But time-resolved information about the palaeogeographical evolution of the coastal zone, including shoreline variations, shifts of depositional milieus and changes in coastal geomorphology, are lacking so far.

8.2.2 Tsunami risk in southwest Thailand

The primary source of tsunamis at the coast of SW Thailand is the Sunda Arc subduction zone. To trigger tsunamis strong enough to affect the study area, the associated earthquakes have to be of magnitude M_w8 or bigger and generated in a segment of the Sunda Arc that directly faces the Andaman Sea (Løvholt et al., 2006; Okal and Synolakis, 2008). Only these events have sufficient energy to generate waves that may cross the Andaman Sea without losing too much speed on the broad and gently dipping continental shelf off SW Thailand (Di Geronimo et al., 2009). Regional and local differences along the coast of the study area are caused by the refraction of the tsunami waves at the Andaman and Nicobar Islands, as well as by the relief of the near-shore bathymetry.

Hitherto, only one tsunami with significant impact on the Thai coast, the IOT 2004, has been recorded by modern measurement techniques and historical documentation. Other historical ruptures in the relevant segments of the Sunda Arc occurred in AD 1847, 1881 and 1941, but due to magnitudes $< M_w8$, the associated tsunamis were recorded by tide gauges only and had no effect on the Thai coast (Bilham et al., 2005). However, further information about tsunami recurrence intervals is provided by (i) sedimentary evidence of at least 3-4 prehistoric tsuna-

mis in the coastal geoarchives of the study area within the last 3000 years (Jankaew et al., 2008; Fujino et al., 2009; Brill et al., 2011, 2012a, b; Prendergast et al., 2012), and (ii) evidence for prehistoric earthquakes in form of uplifted and subsided corals or marine terraces along the Sunda Arc with ages of c. 500 and 1000 years BP (Rajendran et al., 2008; Meltzner et al., 2010). The associated recurrence intervals are supported by estimates of stress accumulation caused by plate convergence that propagate return periods of c. 270 years for $M_w8.5$ ruptures in the Andaman and Nicobar segments, and 400-600 years for mega-ruptures $> M_w9$ similar to 2004 (Løvholt et al., 2006; Subarya et al., 2006).

8.3 Methods

The reconstruction of geographical, geomorphological and ecological coastal changes is based on sedimentary data, as it has successfully been established for coastal areas worldwide in geoarchaeological contexts (e.g. Kraft et al., 2003; Brückner et al., 2006; Vött et al., 2006, 2007; Engel et al., 2009; Kelterbaum et al., 2012). The new stratigraphical information presented in this paper was obtained from open and closed vibracores, drilled with an Atlas Copco mk 1 corer, reaching maximum depths of 9 m below ground surface (b.s.). The position and elevation of each coring site was measured with a differential GPS system (Topcon HiPer Pro) providing high-precision records with an error of ±3 cm. Open sediment cores were photographed and a tentative on-site stratigraphy was established following Ad-hoc-Arbeitsgruppe Boden (2005) including characterisation of the strata in terms of colour, sedimentary structure, grain size, carbonate content and macroscopic fossils.

Subsequently, each stratum was sampled for quantitative laboratory analyses in order to characterise the adjacent depositional environments more specifically. Grain-size analyses have been performed on the air-dried fine fraction (<2 mm), after treatment with H_2O_2 to remove organic matter, using a laser particle sizer (Beckmann Coulter LS13320 Mikro) to assess the hydrodynamic conditions during sedimentation. For the calculation of grain-size statistics after Folk and Ward (1957), the GRADISTAT software was applied (Blott and Pye, 2001). The coarse fraction (>2 mm) was classified in terms of material (coral/mollusc fragment, concretion, pebble/gravel) under the binocular; the taxonomy and ecology of molluscs were determined after Abbott (1991) and Tantanasiriwong (1978). Geochemical analyses, as an indicator for weathering intensity, hydrological milieu and sediment source, included loss on ignition (LOI), $CaCO_3$ content (Scheibler method), and concentrations of the elements calcium (Ca), magnesium (Mg), iron (Fe), sodium (Na) and potassium (K) determined by flame atomic absorption spectroscopy (Perkin Elmer A-Analyst 300).

A chronological framework with AMS-^{14}C dates (University of Georgia at Athens, USA) from macrofossils and macroscopic plant remains was established for the stratigraphical settings. Calendar ages (2 sigma) were calculated from conventional radiocarbon years by means

of the OxCal 4.01 software using the IntCal09 calibration curves of Reimer et al. (2009) and a marine reservoir effect of ΔR = -2 as recommended by Southon et al. (2002).

Table 8.1: Radiocarbon data from Pakarang Cape and Phra Thong Island. All ages have been measured at the University of Georgia (Athens, USA) and calibrated using the IntCal09 calibration curves of Reimer et al. (2009) with a marine reservoir effect of ΔR = -2 (Southon et al., 2002).

lab code	site	sample	material	δ¹³C (‰)	¹⁴C (BP)	sidereal yrs (cal BP, 2σ)	sidereal yrs (cal AD/BC, 2σ)
UGAMS-4968		PAK 4/6	coral fragment	-1.0	4440±30	4371-4110	2422-2161 BC
UGAMS-4969		PAK 4/7	coral fragment	-2.4	4930±30	4990-4725	3041-2776 BC
UGAMS-4970		PAK 5/10	coral fragment	-1.4	4100±30	3875-3641	1926-1692 BC
UGAMS-4971		PAK 5/11	piece of bark	-27.5	1060±25	1053-927	898-1023 AD
UGAMS-8054	Pakarang Cape	PAK 22/11	piece of bark	-28.4	1190±25	1179-1013	771-937 AD
UGAMS-11124		PAK 22/19	shell valve	-1.2	2280±25	1970-1814	21 BC-136 AD
UGAMS-11125		PAK 23/13	massive coral	-3.8	4570±30	4856-4676	2907-2727 BC
UGAMS-11126		PAK 31/11	shell valve	-1.9	5700±30	6200-5995	4251-4046 BC
UGAMS-11127		PAK 32/5	wood fragment	-29.7	modern	modern	modern
UGAMS-11128		PAK 32/14	plant fragment	-29.8	5030±30	5895-5663	3946-3714 BC
UGAMS-11129		PAK 33/5	plant fragment	-28.7	150±25	284-0	1667-1950 AD
UGAMS-8044		KPT 11T	plant fragment	-26.0	4310±30	4963-4835	3014-2886 BC
UGAMS-8045		KPT 23/7	wood	-29.3	3080±30	3370-3217	1421-1268 BC
UGAMS-8046	Ko Phra Thong	KPT 23/15	plant fragment	-27.9	4650±25	5466-5312	3517-3363 BC
UGAMS-8047		KPT 27/11	plant fragment	-28.1	35090±170	40913-39474	38964-37525 BC
UGAMS-8048		KPT 29/22	plant fragment	-27.2	6080±30	7148-6805	5199-4856 BC
UGAMS-8049		KPT 34E	charcoal	-26.6	2190±25	2311-2131	362-182 BC

8.4 Previous work and new stratigraphical data

Stratigraphical information of coastal geo-archives exists from previous research focusing on the identification, dating and correlation of tsunami deposits (Brill et al., 2011, 2012b; Neubauer et al., 2011). However, this study supplements the existing coastal stratigraphies with 15 additional sediment cores that extended vertical to greater core depths on Phra Thong Island, lateral in shore perpendicular direction along Pakarang Cape, and parallel to the shoreline at the site of Ban Bang Sak. Existing and new stratigraphical data were evaluated in terms of (i) the potential of different depositional environments as archives for tsunami deposits, (ii) the time-dependent evolution of these environments during the Holocene, and (iii) the relationship between coastal evolution and the preservation of tsunami deposits.

8.4.1 Classification of coastal sediments into depositional units

A classification of coastal sediments according to sedimentary units has already been established for the location Ban Bang Sak by Brill et al. (2011). Since the stratigraphical data of Pakarang and Ko Phra Thong revealed similar successions of deposits, the description of sed-

iment cores from all three sites was based on a modified version of this classification which is documented in figure 8.2.

stratigraphy	unit	characteristics	int.	stratigraphy	su	Ban Bang Sak	Pakarang	Ko Phra Thong	interpretation
	IV	decalcified, no fossils	terrestrial		IVc	clayey sand to sandy clay, reddish brown or brown, with palaeosols and stone fragments		X	alluvial/fluvial/artificial
					IVb	clayey silt, olive brown, soft, homogeneous		X	lake
					IVa	black to dark brown peat with abundant plant remains			back-barrier swamp
	III	greyish brown to yellowish white, medium to coarse sand	marine		III	shell fragments, partially cemented	coral and shell fragments partially cemented	decalcified no fossils	littoral to supralittoral
	II	grey colour, rich in carbonate and fossils, high Na, Ca and Mg contents			II.2	well sorted fine to medium sand, marine shell walves and fragments			shallow subtidal
					II.1c	X	massive coral	X	coral reef
					II.1b	X	homogeneous silt with angular coral fragments	X	lagoon
					II.1a	X	homogeneous silt	X	
	I	yellowish to reddish brown, decalcified, no fossils, high iron values and low contents of soluble salts (Na, Mg, Ca)	terrestrial		Ib	laminated clay or sand with pebbles	X	clayey sand with rounded pebbles	alluvial/fluvial
					Ia	sandy clay and weathered stone fragments	X		weathered bedrock

marine shell   coral fragment   cemented sand   plant fragment   pebbles   angular stone

Figure 8.2: *Classification of sedimentary units for Phra Thong, Pakarang and Ban Bang Sak.*

The general succession of sediments starts with yellowish-brown, oxidised clay and sand without carbonate and fossils at the base (unit I), followed by well sorted, grey sand rich in $CaCO_3$ (unit II), and either yellowish white, partly cemented medium to coarse sand (unit III) or poorly sorted, decalcified peat, clayey silt or loam (unit IV) on top. Occasionally this background sedimentation is interrupted by sharply bordered sand sheets composed of material completely different from the confining in-situ deposits (allochthonous layers A, B and C). Where relevant, local sedimentary features, additional subunits for Pakarang (units II.1a-c, shaded in fig. 8.2), and site-specific features for existing subunits extended the classification.

The complete succession of these new subunits is documented in core PAK 23 (fig. 8.3), where homogeneous, poorly sorted, grey silt without macroscopic fossils (unit II.1a) is followed by 80 cm of massive *Porites* corals between 6.90 and 5.70 m b.s. (unit II.1c) and grey, fine-sandy silt with high percentages (>50 %) of coral rubble (*Porites* sp. and *Acropora* sp.) and fragments of *Turritella* sp., *Strombus urceus*, *Cypraea* sp., and Veneridae until 3.70 m b.s. (unit II.1b). Up to the top follow well-sorted, grey fine sand with occasional valves of the shallow marine species *Tellina perna*, *Duplicaria duplicata*, *Littorina scabra*, *Fragum unedo* and thin-shelled species of Veneridae until 2.47 m b.s. (unit II.2), moderately sorted, brownish sand (unit III), and unsorted, decalcified, reddish-brown loam above 0.95 m b.s. (unit IVc), interrupted by a sharply bordered sheet of fine sand at 0.26-0.42 m b.s. (layer A).
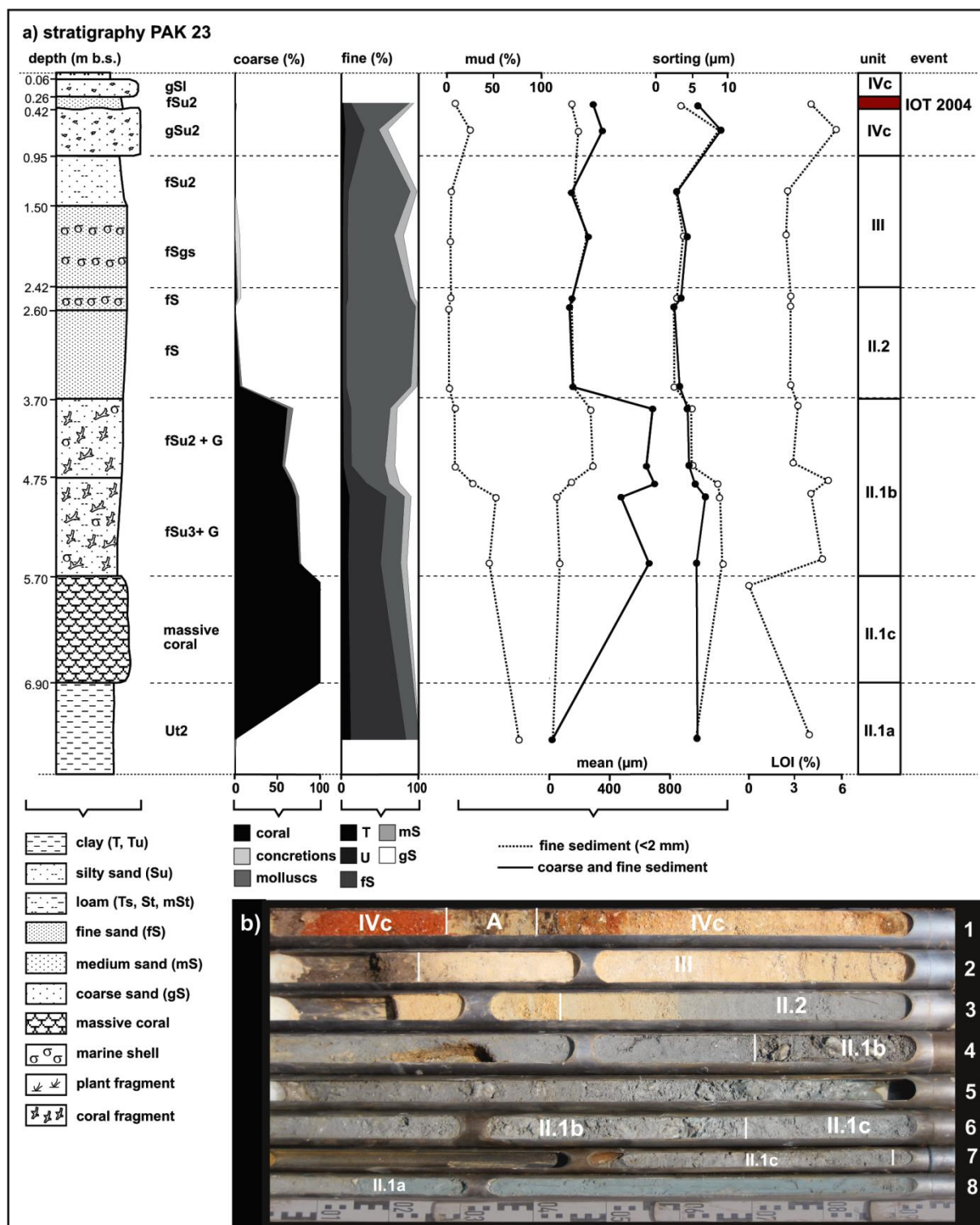
Figure 8.3: *Stratigraphy of sediment core PAK 23.*

8.4.2 Phra Thong Island

Previous work

Apart from some small rocky outcrops at the western coast, Phra Thong Island is formed by sequences of almost shore-parallel beach ridges that reach altitudes of 3-5 m above mean sea level, while the intervening swales are on average about 1 m lower (fig. 8.4). Along the sheltered, eastern coast, these structures are predominantly covered by mangroves and dense vegetation (fig. 8.1d). In the western part grassy ridges and swales – some of them shallow, dry and grass-covered, some of them deep, wet and swampy – build up an open beach-ridge plain that developed within the last 5500 years subsequent to the mid-Holocene sea-level maximum, while the eastern part formed already in the last interglacial period (Scheffers et al., 2012a; fig. 8.4). In December 2004, the western section of Phra Thong was inundated by more than 10 m high tsunami waves that reached inland distances of up to 2 km from the shoreline. The tsunami left behind a 5-20 cm thick sheet of sand. Today, this evidence cannot be distinguished from pre-existing sediments on the ridges, but in contrast is well preserved in the wet swales (Jankaew et al., 2008). The stratigraphy of the swale fill down to 2 m b.s. reveals at least four sand sheets of previous tsunamis younger than 3000 years that were embedded in peat deposits of a back-barrier environment (Jankaew et al., 2008; Fujino et al., 2009). The events yield luminescence ages of c. 550, 1000, 1450 and 2000 years (Jankaew et al., 2008; Brill et al., 2012a, b; Prendergast et al., 2012).
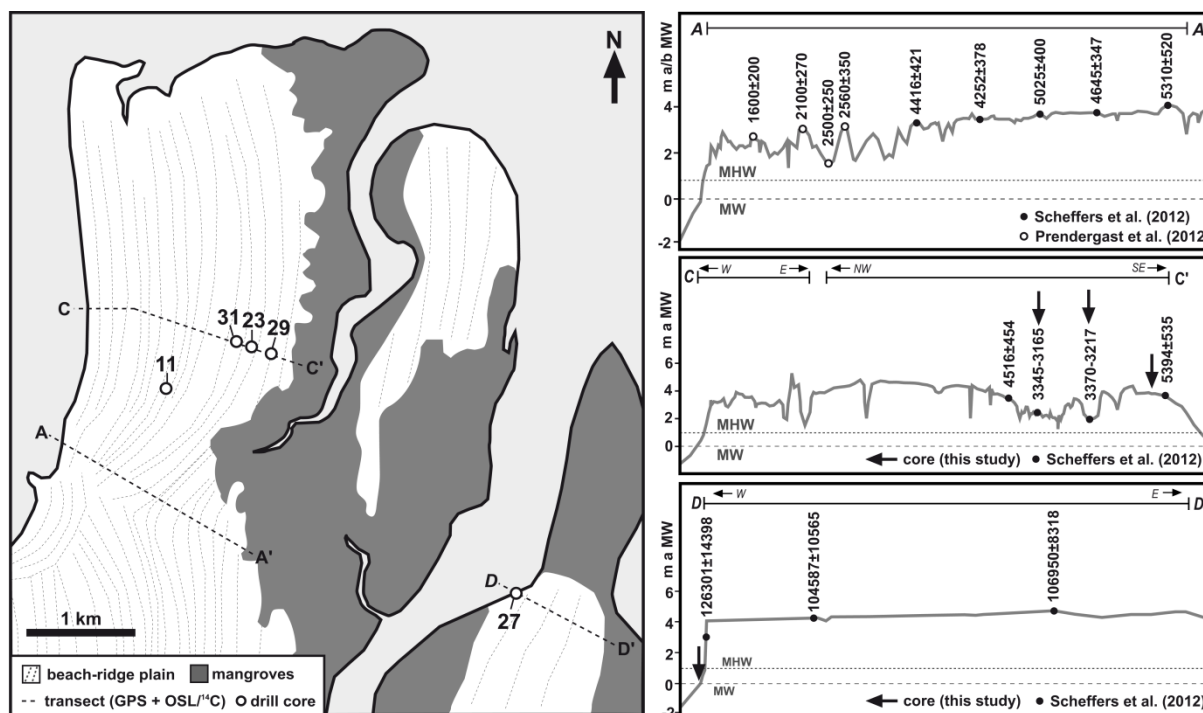
Figure 8.4: *Northern part of Phra Thong Island (see fig. 8.1 for location) with sediment cores, as well as topographic and chronological information along three shore-normal transects.*

New stratigraphical data

To understand the coastal evolution of Phra Thong Island beyond the progradation of the beach-ridge plain, the stratigraphy was extended to depths of up to 9 m b.s. with a total of five sediment cores located at different distances from the shoreline (fig. 8.4). KPT 27 at the beach of the Eemian part of the island, KPT 29 on the easternmost beach ridge of the Holocene part, and KPT 23, 31 and 11 in three successive swales to the west (figs. 8.4 and 8.5). The succession of units along this east-west transect is presented in figure 8.5:
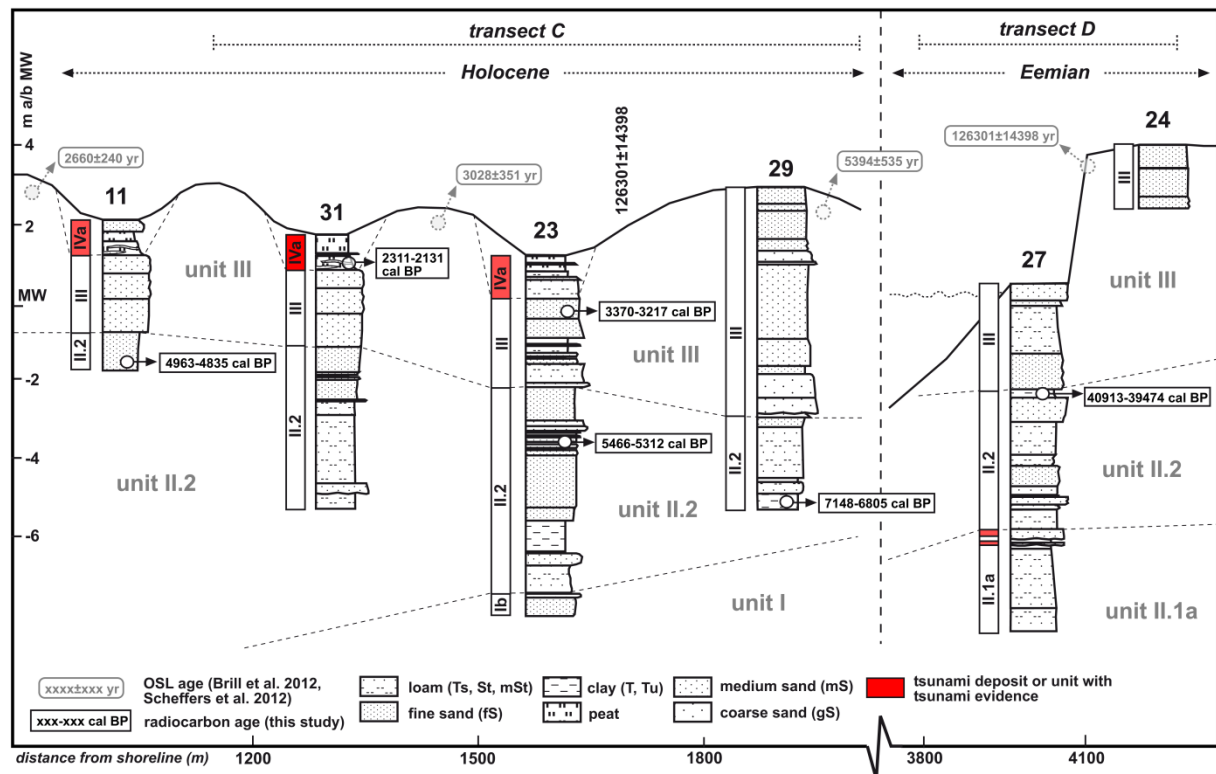
Figure 8.5: *Stratigraphical cross section of Phra Thong Island in shore-perpendicular direction based on sediment cores KPT 27, 29, 23 31 and 11.*

Core **KPT 27** reaches a depth of 9 m b.s. From the base to 6.37 m b.s., the grey clayey silt of unit II.1a is documented. Between 6.86 and 6.37 m b.s., the muddy substrate is interrupted by two sharply bounded, 6 and 24 cm thick, allochthonous layers of medium sand. The following 2.80 m are composed of grey fine to medium sand with the occasional occurrence of plant remains and organic laminae (unit II.2). In the uppermost 3.56 m, the succession is completed by yellowish grey, partially stratified sand (unit III). Different from the typical properties given in the unit classification, the sediment column of KPT 27 is completely decalcified. Further west, the basal section of core **KPT 29**, between 8.00 and 5.74 m b.s., starts with well sorted, silty fine sand with abundant marine shell valves (unit II.2). The following 5.70 m up to ground surface are composed of yellowish white, decalcified sand (unit III).

Core **KPT 23** is composed of reddish and decalcified sand with gravel which is characteristic for unit Ib at the base. Above a sharp contact at 8.65 m b.s., well sorted, grey sands with shell

valves and coral fragments (unit II.2) are documented, covered by yellowish white medium to coarse sand (unit III) at 3.35-1.10 m b.s. On top, dark brown peat (unit IVa) alternates with sharply bound, allochthonous sand layers at 0.62-0.53 and 0.21-0.15 m b.s.

Cores **KPT 31** and **KPT 11** reveal similar successions of units. While KPT 31 reaches a depth of 7 m and consists of grey, shell-rich fine to medium sand (unit II.2) until 2.80 m b.s., in KPT 11 unit II.2, in the form of grey fine sand with marine molluscs, is only documented from 4.00 to 2.90 m b.s. Above, both cores show sequences of brownish coarse sand assigned to unit III and, in the uppermost 70-90 cm, strata of brown peat (unit IVa) intercalated with allochthonous sand sheets.

Generally, the coastal complex documented in the five sediment cores is separated into two sections (fig. 8.5): Section 1 comprises only KPT 27 which is situated more than 2 km east of the other cores. The vertical succession from unit II.1a at the base over unit II.2 to unit III on top is chronologically assessed by a radiocarbon date of 40,913-39,474 cal BP (tab. 8.1) from unit II.2. The stratigraphy of the second section (KPT 29, 23, 31 and 11) is characterised by unit Ib beneath 7 m below mean sea level (b.s.l., only in KPT 23), followed by unit II.2 between 7 m b.s.l. and mean water. Three organic samples from unit II.2 were ^{14}C-dated to 7148-6805 cal BP at 5 m b.s.l. in KPT 29, 5466-5312 cal BP at 3.50 m b.s.l. in KPT 23, and 4963-4835 cal BP at 1.70 m b.s.l. in KPT 11 (tab. 8.1). Above mean water, most sediment is related to unit III that was dated to 3370-3217 cal BP in KPT 23 (tab. 8.1). In the swales, unit IVa, intercalated with allochthonous sand sheets, forms the uppermost 100 to 50 centimetres.

8.4.3 Pakarang Cape

Previous work

Pakarang Cape is the headland south of Ban Bang Sak (fig. 8.1). The sedimentary promontory developed behind a Holocene coral reef that, although already dead, forms a 600 m wide intertidal platform in front of the western shoreline (figs. 8.6b, c). The adjacent coastal plain between the reef platform in the west and the high ground in the east is gently undulating without significant morphology (fig. 8.6e) except of artificial tin mining lakes (figs. 8.6b, g). While the western coast of the cape was strongly eroded during the IOT 2004 with a shoreline retreat of at least 30 m (Neubauer et al., 2011), recovery of the former beach proceeded rapidly after the event, resulting in a more than 3 m high post-2004 beach ridge by 2009 (Fig. 8.6d). In contrast, the northern shoreline is subject to ongoing coastal erosion that has led to uprooted trees and the exposure of beachrock (Fig. 8.6f). The stratigraphy of coastal deposits that form Pakarang Cape as described by Neubauer et al. (2011) indicates open marine influence and the existence of a back-reef lagoon below the sediments of the recent coastal plain. Additionally to the IOT 2004 that caused deposition of tsunami-laid sand onshore

(Szczuciński et al., 2006) and movement of coral boulders on the intertidal reef platform (Goto et al., 2007, 2009, 2010), these lagoonal deposits comprise evidence of a prehistoric tsunami 1000-1200 years ago (Neubauer et al. 2011).
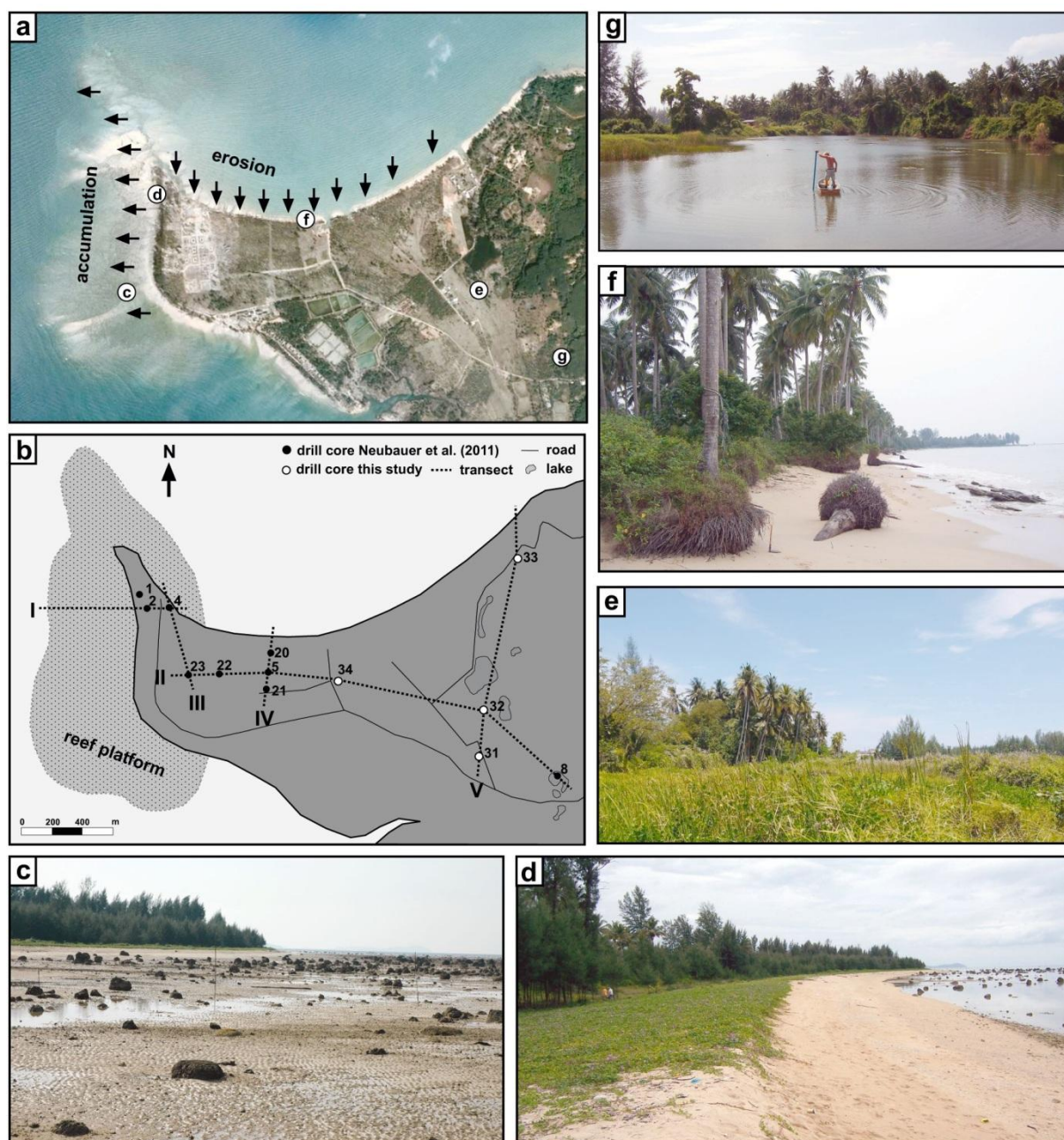
Figure 8.6: *Geo-archives at Pakarang Cape: (a) Satellite image with position of photographs c-g and trends of littoral sediment dynamics; (b) Schematic map with position of cores and transects; (c) Reef platform with boulders; (d) Present beach ridge; (e) Coastal plain; (f) Recent coastal erosion at the northern shoreline; (g) Artificial tin mining lake.*

New stratigraphical data

In addition to the sediment cores that have previously been described in terms of depositional milieus and tsunami evidence by Neubauer et al. (2011), supplementary stratigraphical data was collected further inland at the core sites of PAK 31, 32, 33 and 34 (Fig. 8.6b). At its base

core **PAK 31** is composed of yellowish brown, decalcified, stiff clay with pebbles (unit Ib). Above a sharp, erosive contact at 7.51 m b.s., grey silty fine sands with occasional plant fragments and shallow marine fauna are documented (unit II.2), whereas the basal section is particularly coarse and poorly sorted. From 4.74 to 0.48 m b.s. follows yellowish-white coarse sand with more than 50% of coarse fraction (> 2 mm) in the form of gravel and concretions of cemented sand. The uppermost 50 cm of this stratum, dedicated to unit III, are affected by soil formation, which is truncated at 0.48 m b.s. by an allochthonous layer of 25 cm thick, brownish fine sand (layer A).

A similar succession of deposits is revealed by core **PAK 32**. The decalcified yellowish-brown clay with weathered rock fragments (unit Ia) at its base is covered by grey silty fine sand with shell valves of shallow marine species (unit II.2) above a sharp contact at 6.17 m b.s. The yellowish-white medium to coarse sand with abundant shell fragments and gravel (>20%) between 3.31 and 1.27 m b.s., dedicated to unit III, is interrupted by a sharply bounded sheet of fine sand (layer B) at 1.80-1.52 m b.s. The stratigraphy is terminated by soft, decalcified mud (unit IVb) between 1.27 and 0.51 m b.s., and brown, decalcified loam (unit IVc) until ground surface, interrupted only at 0.28-0.03 m b.s. by an allochthonous fine sand layer with a sharp base (layer A).

In core **PAK 33** the stiff, brown clay of unit Ia is reached at a depth of 5.28 m. The grey fine sands above had a sharp lower contact and consist of particularly coarse (gravel) and poorly sorted material (unit II.2). From 2.00 to 0.63 m b.s. brownish fine to medium sands with plant remains and soil formation on top comprise unit III. Superimposed on unit III, a 30 cm thick sheet of allochthonous, carbonate-rich fine sand (layer A) is documented, followed by brownish, decalcified loam (unit IVc).

The 7 m deep core **PAK 34** starts with grey silty fine sand with shallow marine shells and plant fragments (unit II.2), covered by yellowish-white, partially cemented coarse sand with mollusc fragments and gravel at 2.45-0.19 m b.s. (unit III). The uppermost decimetres of unit III are decalcified and affected by soil development; between 1.60 and 1.53 m b.s. the coarse sand is interrupted by a sharply bounded sheet of fine sand (layer B). On top, between 0.19 and 0.08 m b.s., another carbonate-rich fine sand layer with sharp lower contact (layer A) is documented and covered only by organic detritus.

The stratigraphical data of all cores were correlated in order to reconstruct the general succession of units and their spatial trends from west to east (transects I and II in fig. 8.7 and appendix 2) and from north to south (transects III, IV and V in appendix 2), and chronologically evaluated on the basis of radiocarbon data (tab. 8.1). Within these units spatial trends of coarse material (>2 mm) were revealed, documenting diminishing trends in the abundance of coral fragments from west (reef) to east (high ground), and of silicious gravel from east to west (fig. 8.8).
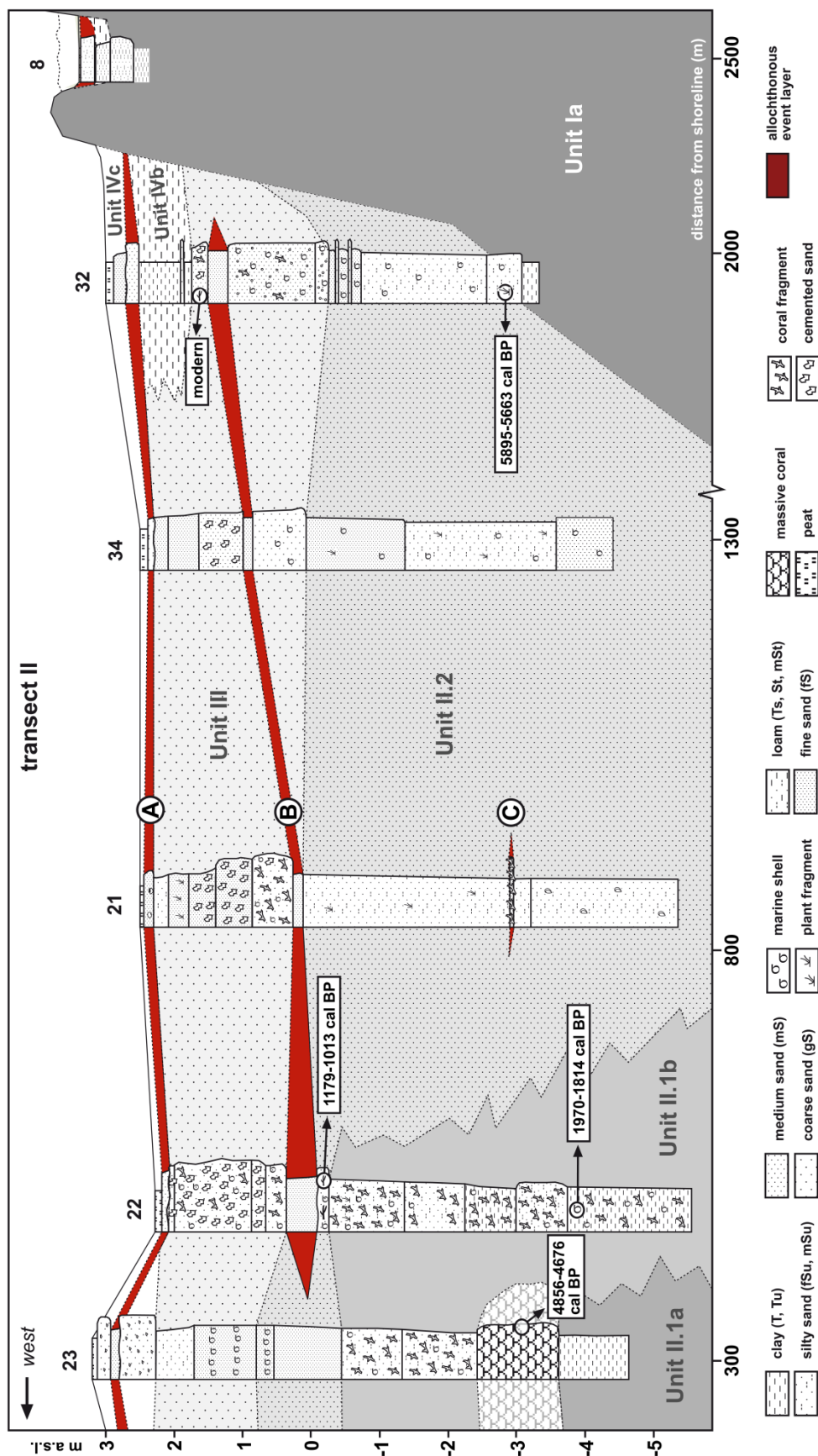
Figure 8.7: *Stratigraphical cross section of Pakarang coastal plain along transect II (see fig. 8.6b for location).*
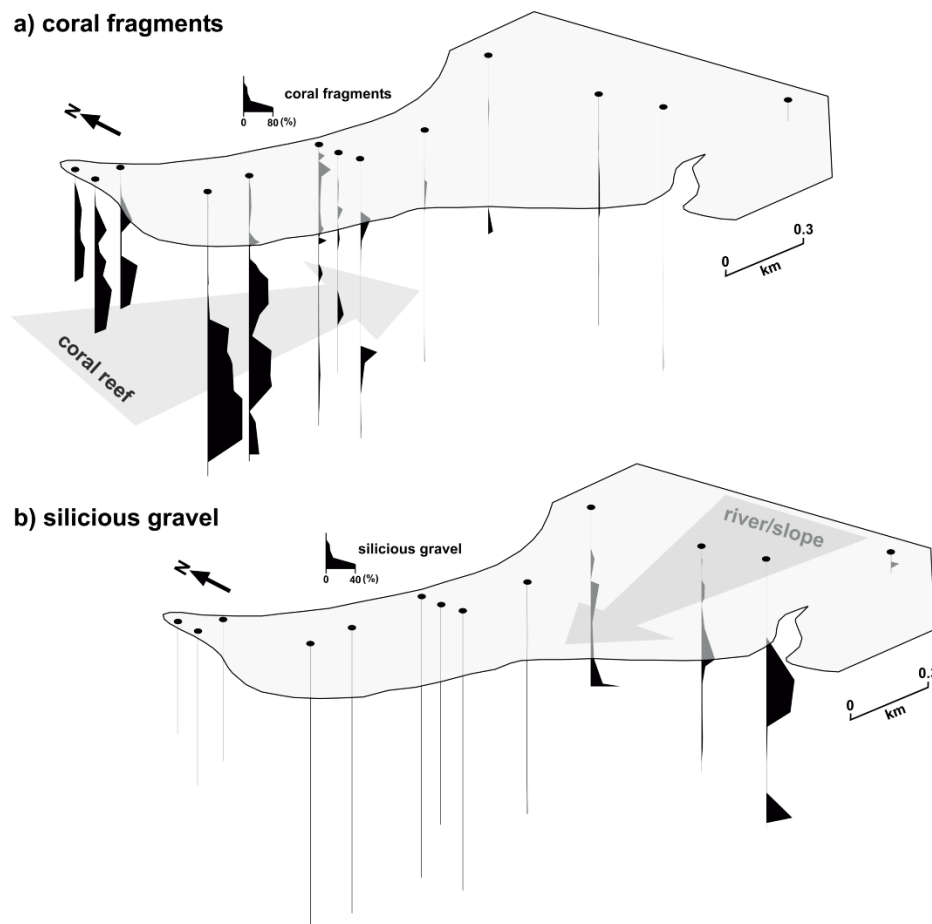
Figure 8.8: *Trends of coarse material (>2 mm) in sediment cores from Pakarang. With increasing distance from the respective source areas, the abundance of coral fragments decreases inland, i.e. from west to east (a), that of silicious gravel seawards, from east to west (b).*

Unit I is outcropping at the eastern end of the coastal plain in PAK 8 and steeply dipping to 3-4 m b.s.l. in PAK 31, 32 and 33. In all other cores further seaward unit I could not be reached by this drilling (fig. 8.7). On top, separated by an erosive contact, unit II is present in all cores (except PAK 8). In the eastern part of the plain, from PAK 32 to PAK 21, **unit II.2** forms the whole stratigraphy up to mean water level (fig. 8.7). Its basal contact with unit I below is chronologically constrained by radiocarbon ages of 5895-5663 cal BP in PAK 32 and 6200-5995 cal BP in PAK 31, while the top section yields ages of 1053-927 cal BP in PAK 5 and 1179-1013 cal BP in PAK 22. Towards the reef, from PAK 2 in the west to PAK 22 in the east, unit II.1 comprises most of the sediments (fig. 8.7), whereas **unit II.1a** and **unit II.1c** appear only below 3 m b.s.l. in PAK 23 and yield an in-situ coral age of 4856-4676 cal BP. **Unit II.1b** extends to shallower and more reef-distal parts of the stratigraphy and was dated to 1970-1814 cal BP on the basis of a shell in PAK 22, while coral fragments in PAK 4 yield ages of 4990-4725 cal BP and 4371-4410 cal BP.

Above mean water level the coastal plain is mainly formed by the sediments of **unit III** (fig. 8.7), resulting in a more or less planar ground surface with significant morphology present

only along the western shoreline (beach ridge at PAK 1 and 2). Plant fragments within unit III yield ages of 0-280 cal BP in PAK 33 and "modern" in PAK 32, coral fragments in PAK 5 were dated to 3875-3641 cal BP. **Unit IV** appears only locally on top of unit III, e.g. in PAK 8 and 32 (unit IVb) or PAK 23 (unit IVc), where it forms rather thin strata. Equally, the allochthonous sand sheets can be correlated between all cores, resulting in three separate layers: (i) **Layer A** is present in all cores except for PAK 1 and 2; it covers the whole coastal plain in the form of a decimetres thick sand sheet. (ii) Embedded in deposits of unit II in the west (PAK 2, 4, 22) and unit III (PAK 21, 34, 32) in the east, **layer B** is gently inclined towards the sea (fig. 8.7). (iii) **Layer C** is only present in transect IV (PAK 5, 20, 21), where it is enclosed in deposits of unit II.2.

8.4.4 Ban Bang Sak

Previous work

The coastal area of Ban Bang Sak is dominated by a 300 m wide coastal plain along its southern section that broadens to more than 1 km in northern direction (fig. 8.9a). Only where small rivers reach the Andaman Sea and form gently dipping alluvial plains, the Holocene sediment sequence extends further eastwards (e.g., along transect B in fig. 8.9a). The morphology of the coastal plain is characterised by more or less prominent successions of beach ridges and swales (figs. 8.9c, d). Coastal sediment successions have already been described by Brill et al. (2011; chapter 10) for two transects in the southern part of the area (transects A and B in figs. 8.9a, d). Generally, an alluvial complex at the base is followed by sediment of the marine transgression and beach-ridge progradation, and finally topped by alluvial sedimentation and deposits of back-barrier swamps inside the swales. Within this succession evidence of a palaeotsunami at 500-700 cal BP (event B), and several events between 1180 and 2000 cal BP (events C) was identified (Brill et al., 2011).

New stratigraphical data

With the aim to expand the information about coastal sediments spatially along the coastline, additional data from cores further north and south of transects A and B were included (fig. 8.10). Proceeding from south to north, the transect starts with core BBS 2, drilled to a depth of 1.20 m b.s. in an artificial lake. Decalcified, stiff brown clay (unit Ia) at the base is covered by soft, decalcified, olive brown silt (unit IVb) above a sharp contact at 0.90 m b.s. On top, a 68 cm thick, graded allochthonous sand layer with abundant shell fragments (layer A) terminates the succession. Some 400 m further north, cores BBS 38 and BBS 39, at distances of 300 and 200 m from the shoreline, respectively, show a very similar stratigraphy. Stiff, yellowish clay with weathered rock fragments which is characteristic for unit Ia is already reached at a depth of 2.35-2.47 m b.s., followed by reddish-brown, decalcified sand with

gravel (unit Ib) in both cores. Above a sharp contact at 0.23 m b.s., a sheet of carbonate-rich fine sand (layer A) terminates the succession in BBS 38, while BBS 39 is characterised by decalcified sandy clay between 0.75 and 0.21 m b.s. (unit IVc) before the sediment column is topped by a sharply bounded, calcareous fine sand layer (layer A).
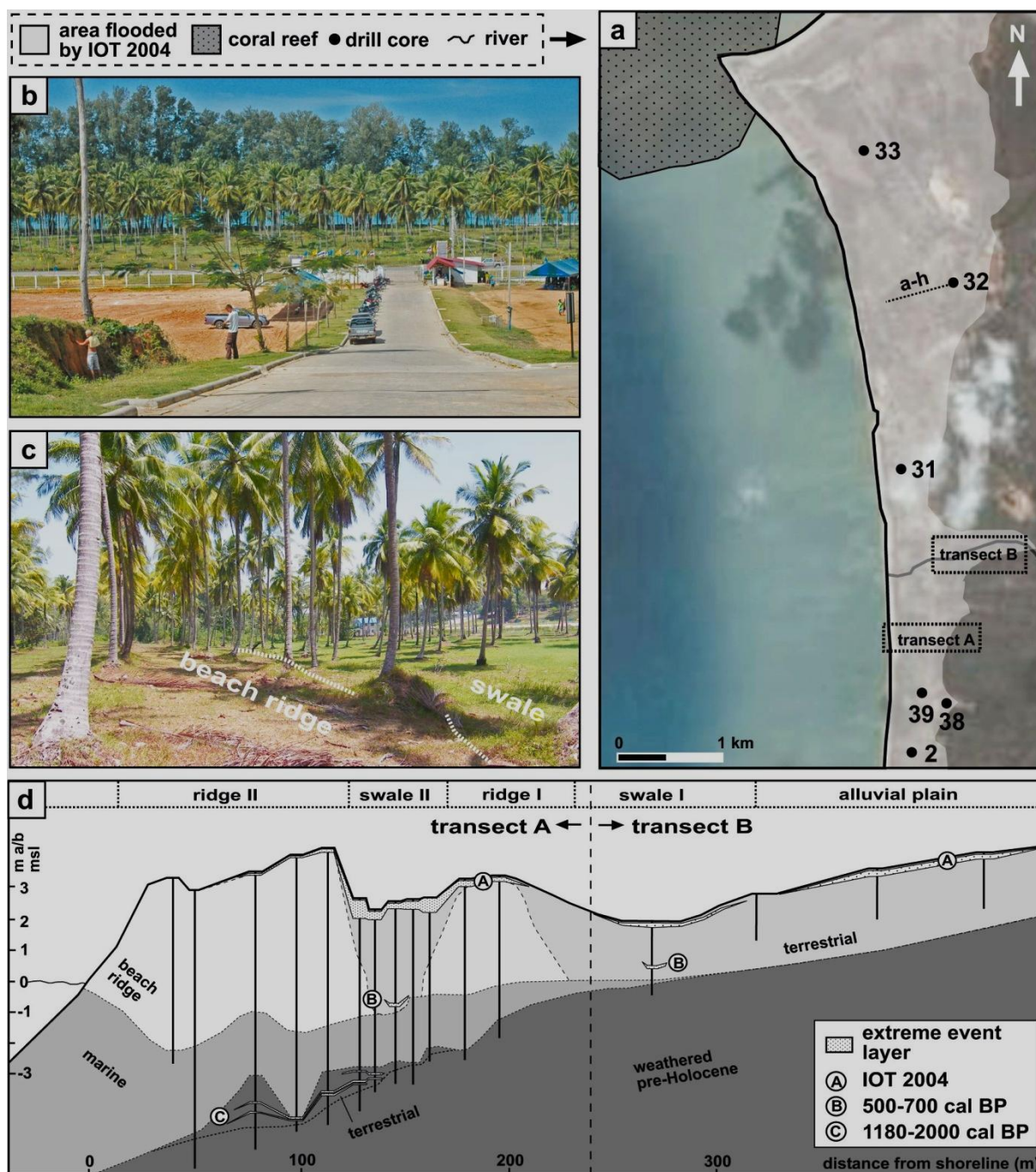
Figure 8.9: Ban Bang Sak – setting and previous work. (a) Schematic map with positions of cores and transects. (b) View to the west on the coastal plain along transect A. (c) Boundary between beach ridge and swale in transect A. (d) Stratigraphical cross section of the coastal sediments along transects A and B after Brill et al. (2011) and Chapter 10.
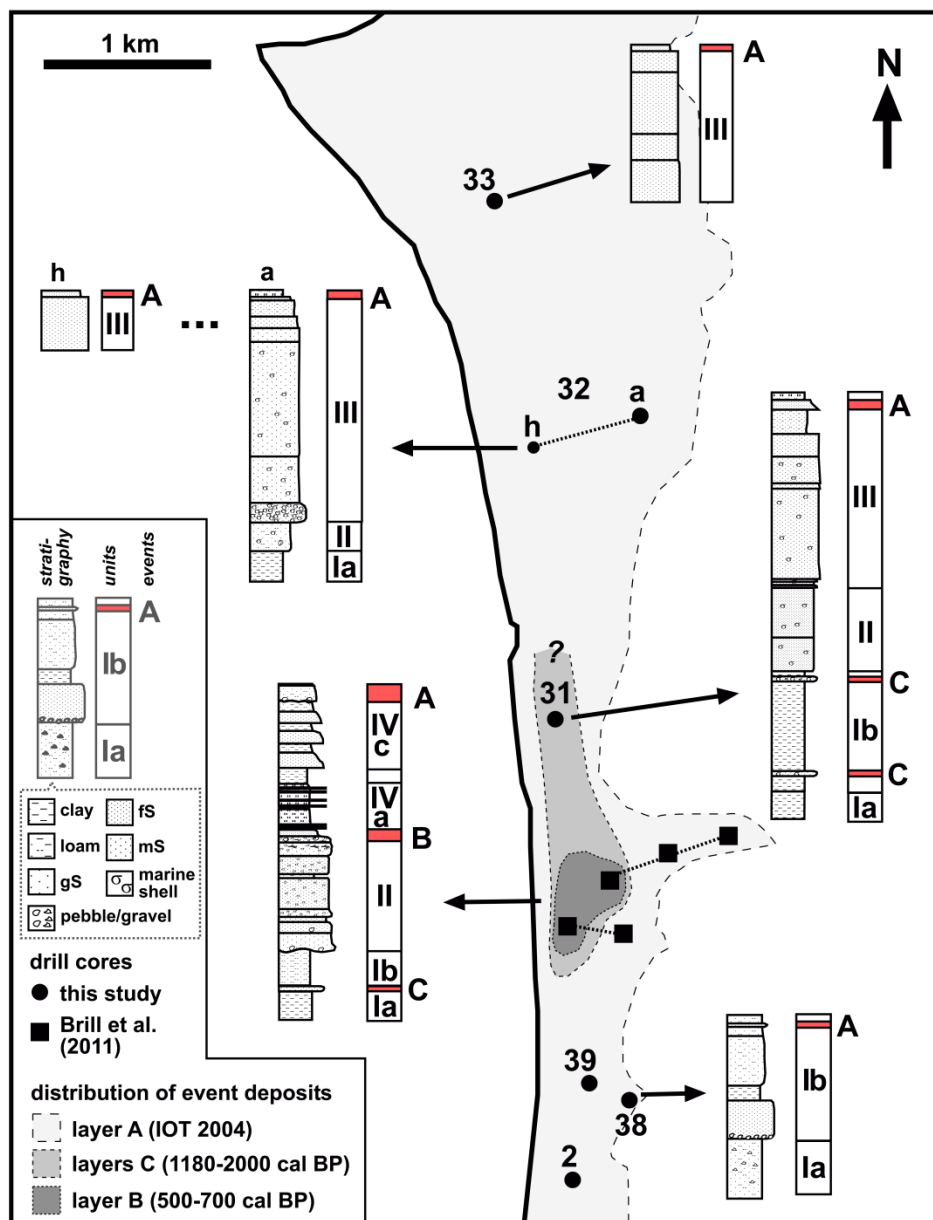
Figure 8.10: Variation of the coastal stratigraphy at Ban Bang Sak in shore-parallel direction. Evidence of events B and C is restricted to the area between transect A and BBS 31.

Core **BBS 31** was taken directly behind the most seaward beach ridge, at a distance of 150 m from the shoreline 700 m north of transects A and B. Reaching down to a depth of 8.00 m b.s., the lowermost 50 cm are composed of stiff, decalcified mud (*unit Ia*). Between 7.50 and 5.30 m b.s. follows grey, decalcified and homogeneous mud (*unit Ib*) that is interrupted at 7.35-7.26 and 5.56-5.48 m b.s. by thin sand layers with shell fragments and sharp contacts (*layers C*). Above an erosive border at 5.34 m b.s., grey calcareous fine sand with marine shell fragments (*unit II.2*) continues until 3.70 m b.s., where it is covered by yellowish-white, partially cemented medium sand with shell fragments and soil formation on top (*unit III*). The succession is terminated by a graded fine sand layer rich in carbonate (*layer A*). Another 1200 m further north, core **BBS 32a** was taken at a distance of 450 m from the shoreline. Here the

decalcified, stiff clay of *unit Ia* is reached at 5.40 m b.s., and sharply overlain by calcareous, grey sand with marine shell valves (*unit II.2*). Between 4.48 and 0.20 m b.s., the stratigraphy is composed of yellowish-white medium to coarse sand with shell fragments and soil formation in the uppermost section (*unit III*). The last 20 cm are allochthonous fine sand with shell fragments (*layer A*). A series of seven short cores (BBS 32b-h), reaching a depth of 1 m b.s. each, demonstrates the absence of unit IV for the whole distance between BBS 32a and the recent beach ridge, as well. Core **BBS 33** originates from the coastal plain another 1000 m north of BBS 32 and 350 m east of the shoreline. From 3.00 to 0.15 m b.s., the core is composed of yellowish-white medium to coarse sand with mollusc fragments and soil formation in the top section (*unit III*). It is terminated by a 15 cm thick sheet of calcareous fine sand (*layer A*).

8.5   Discussion

8.5.1   Interpretation of depositional environments

The interpretation of stratigraphical units in terms of associated depositional environments was mainly adopted from Brill et al. (2011), who assigned unit Ia to weathered bedrock, unit Ib to alluvial deposits, unit II.2 to shallow subtidal conditions, unit III to littoral and beach-ridge sediments, unit IVa to back-barrier swamp, unit IVb to coastal lake, and unit IVc to terrestrial sediments of alluvial or artificial origin (fig. 8.2). The new subunits introduced at Pakarang are related to sedimentation in back-reef environments as described by Rasser and Riegl (2002) and Montaggioni (2005), whereas unit II.1a is assigned to deposition in a back-reef lagoon without input of allochthonous material from the reef (distal to the reef), unit II.1b to back-reef lagoon conditions with significant input of reef material (proximal to the reef), and unit II.1c to the bio-constructive reef body itself. Significant discrepancies in the properties of coring KPT 27 which is completely decalcified, although all other criteria point to deposition under marine conditions, are probably due to the last interglacial age of the deposits. The sea level of up to 120 m below its present position during the LGM (Bard et al., 1990; Lambeck and Chappell, 2001) exposed marine sediments of the last sea-level maximum, such as the eastern part of Phra Thong Island, to intensive terrestrial weathering conditions that were accompanied by solution and leaching of carbonates (fig. 8.11).

The allochthonous sand layers detected at all three study sites are interpreted as evidence of extreme wave events. In the coastal plain of Ban Bang Sak layer A which can unequivocally be related to the IOT 2004 is present on top of all cores, covering the low lying area from BBS 2 in the south to BBS 33 in the north (fig. 8.10). While evidence of the 500-700 year old palaeotsunami identified in transects A and B (Brill et al., 2011; Chapter 10) is absent in all new sediment cores, the sand sheets embedded in unit Ib of BBS 31 (layers C) can be related

to wave events that impacted the coast between 1180 and 2000 years ago (Brill et al., 2011). On Phra Thong Island, the allochthonous sand sheets enclosed in unit IVa of KPT 23, 31 and 11 are congruent with the description of tsunami-laid sand from the IOT 2004 and several late-Holocene predecessors described by Jankaew et al. (2008), Brill et al. (2012a, b), and Prendergast et al. (2012). The two allochthonous sand layers incorporated in unit II.1a of KPT 27 reveal similar characteristics as the IOT 2004 deposits and the Holocene palaeotsunamites in unit IVa; thus, they may provide evidence of last interglacial tsunamis. At Pakarang, layer A covers the whole coastal plain and unambiguously can be related to the IOT 2004. While sand sheet B is in congruence with a prehistoric tsunami dated to 1000-1200 cal BP (Neubauer et al., 2011), the sheet of coral fragments in unit II.2 of PAK 5, 20 and 21 (layer C) is rather interpreted as a storm deposit since its composition and appearance is in stark contrast to the modern analogue of the IOT 2004.

8.5.2 Holocene coastal evolution of western Thailand

8.5.2.1 Ko Phra Thong

The stratigraphy of Ko Phra Thong is clearly separated into (i) an eastern part which formed during the last interglacial sea-level maximum and (ii) a western part of Holocene age (fig. 8.5). (i) The stratigraphy of KPT 27, dated to the last interglacial on the basis of luminescence ages (Scheffers et al., 2012a), reveals a regressive sediment sequence starting with a sheltered subtidal environment that is replaced by shallow subtidal-intertidal conditions and ending with beach-ridge formation (fig. 8.5). The sequence must have been deposited in the course of shoreline progradation during the sea-level maximum between 120 and 130 ka ago (fig. 8.11a). (ii) The Holocene framework of the island is composed of a transgressive sediment sequence that erosively overlies the basal alluvium, and a regressive sequence on top. The marine transgression started prior to 7150-6800 cal BP (minimum age KPT 29/22) and lead to shallow marine conditions between the rocky outcrops near the present shoreline in the west and the Pleistocene part of the island in the east (fig. 8.11a). The regression subsequent to the Holocene sea-level maximum 5500 years ago was accompanied by shoreline progradation from east to west forming a coastal plain with alternating beach ridges and swales. The impulse for the periodical formation of ridges and swales may be attributed to small-scale sea-level variations in the range of few decimetres over several decades or centuries (e.g. Tanner, 1995), since crustal movement due to strain accumulation and release at the Sunda Arc (Meltzner et al., 2006) is capable to cause relative sea-level changes in this dimension (Trisirisatayawong et al., 2011). Sediment supply might be an important factor as well. Formation of the first Holocene beach ridges started 5500 years ago and continued until the last century, interrupted by episodic phases of ridge erosion indicated by erosive discordances within the ridge plain, locally (Scheffers et al., 2012a), and probably terminated due to human-induced mod-

ern sea-level rise. While from 5500 to 3500 years BP only dry and shallow swales formed, deeper swales with swampy environmental conditions do not occur before 3300 cal BP.
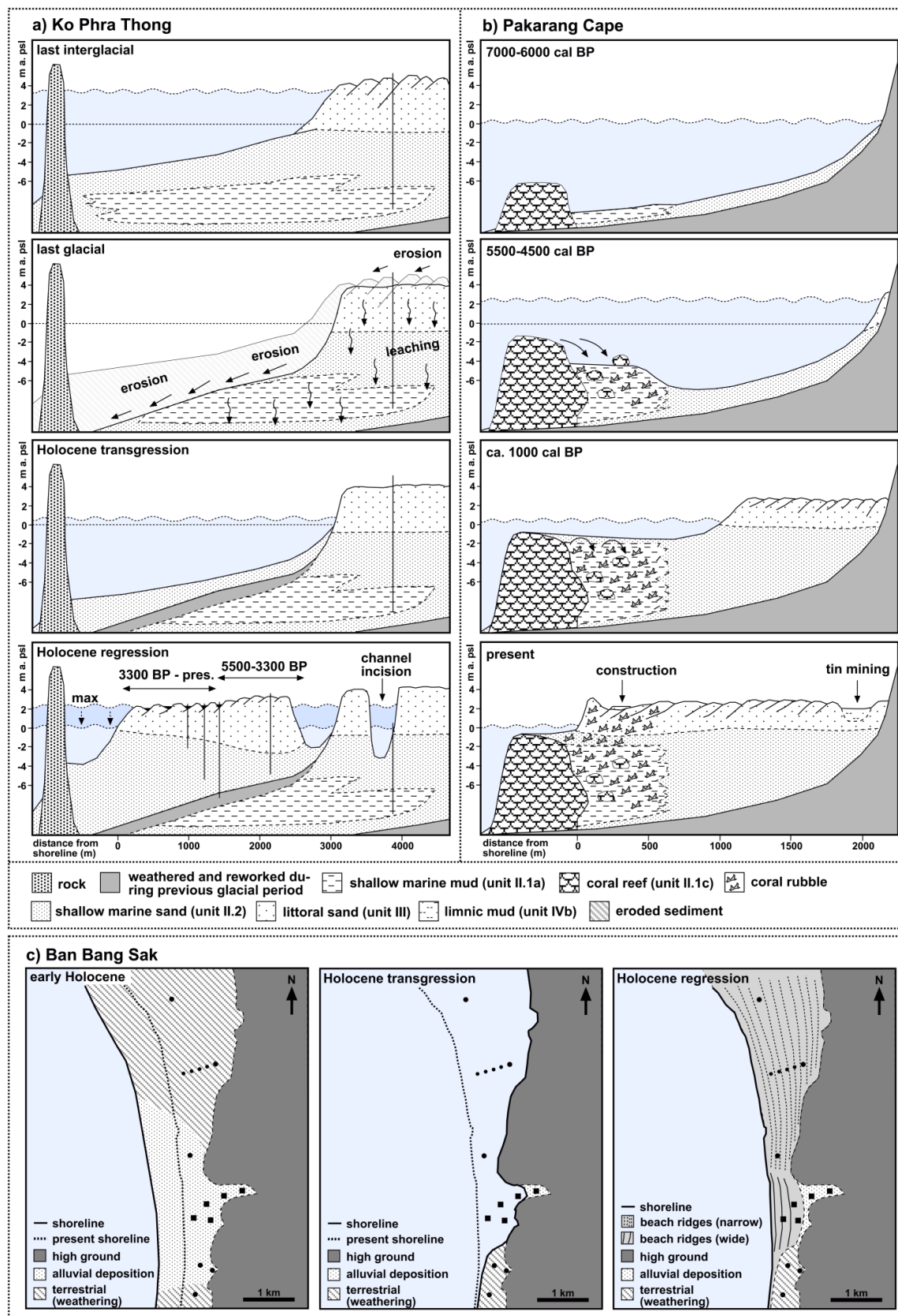
Figure 8.11: *Palaeogeographical evolution scenarios. (a) Phra Thong Island, (b) Pakarang, (c) Ban Bang Sak.*

8.5.2.2 Pakarang

The Holocene transgression reached the modern coastline of Pakarang around 6000-6200 years ago (fig. 8.11b). Similar to other coasts of the Indian Ocean (e.g. Camoin et al., 1997) the marine transgression was accompanied by initiation of coral growth in the form of a fringing reef several hundred meters offshore which successively aggraded to the low water level of the Holocene sea-level maximum at 5500 years BP. Leeward of the reef the formation of a back-barrier lagoon allowed for sedimentation in a very calm milieu, while more distal, between lagoon and mainland, shallow marine conditions persisted. Based on the abundance of coarse material, sediment input from two directions – the reef and the mainland – seems to have controlled deposition during the following regression (fig. 8.8). Although the growth of the reef complex at Pakarang Cape mainly terminated between 5500 and 4500 cal BP, probably as result of falling sea level after the Holocene maximum (age of coral fragments and boulders on reef platform; Neubauer et al., 2011), sediment input from the reef (coral rubble) and small rivers successively continued to fill the lagoon and caused shoreline progradation at the mainland (fig. 8.11b). Finally, the shallow marine section between reef and mainland was completely silted up by 1000 cal BP, and the prograding coastal plain reached the eastern edge of the reef platform. During the last two centuries tin mining activity resulted in the formation of artificial lakes that cover large parts of the modern coastal plain.

8.5.2.3 Ban Bang Sak

The chronology of coastal evolution at Ban Bang Sak is based on stratigraphical data of transect A (Brill et al., 2011) as presented in figure 8.9d: the pre-transgressive alluvial environment (unit I) was replaced by shallow marine conditions in the course of the marine transgression 1200 years ago (unit II). Subsequent coastline progradation led to beach-ridge formation (unit III) and separation of deep swales with back-barrier swamp conditions behind the ridges. Due to siltation and decreasing sea-water influence in the course of shoreline progradation these back-barrier swamps turned into ponds of standing water and depressions with alluvial influence within the last 200-300 years (unit IV). Finally, artificial sediment input locally led to a nearly complete masking of the former topography. However, spatially significant differences in coastal evolution can be recognised (fig. 8.10). Further to the south (BBS 2, 38 and 39) the pre-Holocene bedrock reaches higher elevations relative to sea level and hindered an ingression by the sea (fig. 8.11c). Thus, the area south of transects A and B remained a terrestrial environment throughout the Holocene with only minor alluvial deposition and intensive tropical weathering. North of transects A and B, the complete transgression-regression cycle took place, but in contrast to the area around transects A and B the ridges are narrower and the associated swales too shallow to accommodate the establishment of back-barrier swamps and coastal lakes (fig. 8.11c).

8.5.3 Relation between tsunami evidence and palaeogeography

The existence of sedimentary evidence of prehistoric tsunamis is not only a result of tsunami occurrence and wave impact on the coast, but is as well reliant on the preservation of tsunami-laid deposits over periods of centuries or millennia. Since the preservation potential is dependent on the existence of adequate geo-archives, the development of coastal ecosystems and coastal morphology has significant influence on local tsunami records (e.g. Nichol et al., 2010; Dura et al., 2011; Grand Pre et al., 2012). On Phra Thong Island tsunami evidence is present for the last 3000 years in the form of sand sheets accumulated in back-swamp peat (Jankaew et al. 2008, Prendergast et al. 2012, Brill et al. 2012a, b). Thus, the oldest recorded palaeotsunami is approximately contemporary with the onset of wet swale formation ca. 3300 years ago, whereas the narrow swales that were formed prior to 3300 BP did not provide adequate archives to preserve tsunami deposits (fig. 8.12).
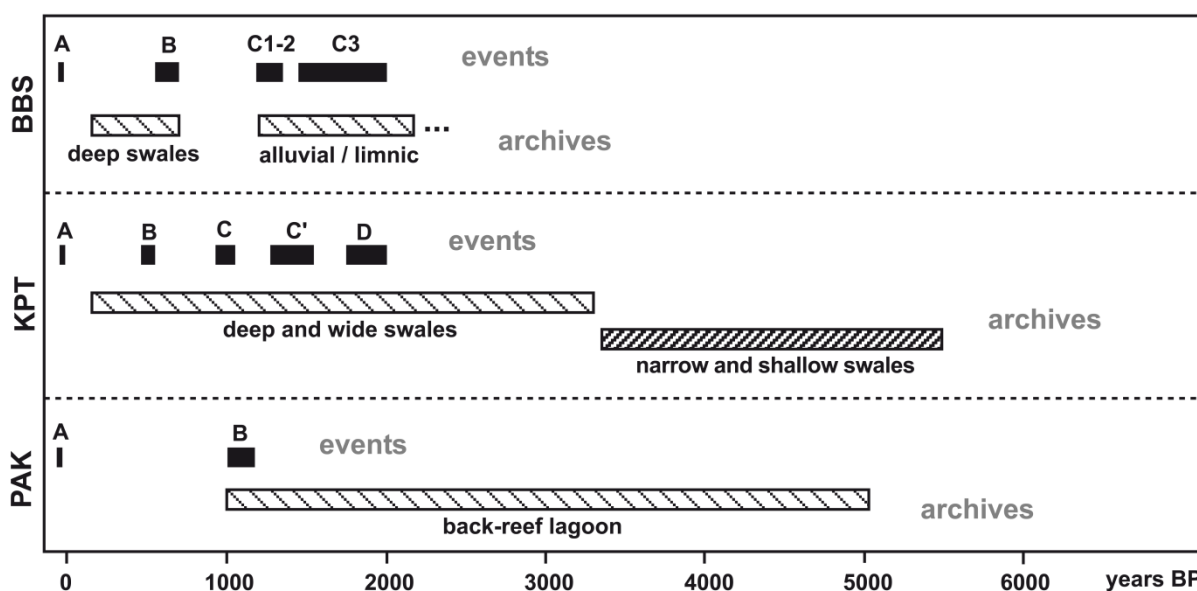
Figure 8.12: Relationship between the existence of tsunami evidence and coastal environments at Ban Bang Sak (BBS), on Phra Thong Island (KPT), and at Pakarang Cape (PAK).

In the case of Pakarang the IOT 2004 deposits demonstrate the favourable preservation conditions in lakes (PAK 8). However, since all lakes are younger than 200 years, the only preserved palaeotsunami deposit (event B at 1000-1200 cal BP) was recorded in the facies of the former back-reef lagoon. After the siltation of this lagoon c. 1000 years ago further evidence of tsunamis, such as the well-constrained 500 cal BP event (Jankaew et al., 2008; Brill et al., 2012b), is absent. However, no older tsunami event prior to 1200 cal BP is recorded, although the lagoon existed since at least 5000 years BP (fig. 8.12).

At Ban Bang Sak tsunamites have been recorded for the period 1180-2000 cal BP (events C) and for 500-700 cal BP (event B). The former are contemporary with the fine grained terrestrial deposition which ended 1200 years ago, and event B took place just after the initiation of

back-barrier swamp conditions in deep swales, whereas between 1200 and 700 cal BP, a period without tsunami evidence, shallow marine conditions without preservation potential dominated (fig. 8.12). Only where back-barrier swamps or calm alluvial environments were formed in the course of palaeogeographical evolution, tsunamites could be preserved for hundreds of years, resulting in spatial restriction of event B and C deposits to the area between transect A and BBS 31 (fig. 8.10).

8.6   Conclusions

Since the preservation of palaeotsunami deposits is dependent on the existence of suitable near-shore archives, palaeogeographic evolution of the coast has significant influence on local tsunami records. Due to the spatially and temporally varying palaeogeography and ecology during the Holocene the coastal sites Pakarang, Ban Bang Sak and Phra Thong Island show very different tsunami records, although located less than 50 km apart from each other: evidence exists for the last 3000 years on Phra Thong Islands, the period between 1200 and 2000 cal BP and the last 700 years at Ban Bang Sak, and a single event from 1000-1200 cal BP at Pakarang. The occurrence of evidence of specific tsunamis at one place and their absence at nearby locations can at least partially be explained by local differences in palaeogeographical evolution. However, other factors should be considered as well, since the occurrence of tsunami evidence is not always contemporaneous with the time windows provided by favourable environments as demonstrated (i) by the discrepancy between tsunami evidence and existence of a back-reef lagoon at Pakarang (fig. 8.12), and (ii) for the mangrove area of Thap Lamu, where Rhodes et al. (2011) describe only a single 2700-4300 year old tsunami deposit, although the mangrove environment that provided the adjacent archive was persistent during the last 7000 years.

Chapter 9

9 Short- and long-term effects of tsunami impact on coastal landforms and ecosystems of SW Thailand

9.1 Introduction

Tsunami inundation of coastal areas is not only associated with economic damage to artificial infrastructure and loss of life, but may as well go along with significant impact on natural environments. Besides extensive onshore deposition of sand- to boulder-sized sediment of marine origin, tsunami flow may shape the coastal geomorphology and affect near-shore ecosystems in many different ways (Dawson, 1994; MacInnes et al., 2009; May et al., 2012).

- Striking features of tsunamigenic erosion on land are so called *trimlines*, sharp boundaries that may mark the limit of tsunami inundation (Scheffers et al., 2012c). Trimlines are the result of soil erosion and removal of vegetation during tsunami run-up (Dawson, 1994; Borrero, 2005).

- The most common morphological effects of tsunami impact are *beach erosion, shoreline retreat* and *erosive lowering of coastal surfaces* (Dawson, 1994; Borrero, 2005; Kench et al., 2008; Paris et al., 2009). Beach erosion by dislocation of sediments from the littoral zone onshore and offshore goes along with the steepening of beach profiles and near-shore bathymetry (Goto et al., 2010b). Due to the concentration of backwash in morphological depressions, the erosive power of return flows often leads to widening of river mouths and tidal channels (Paris et al., 2009; Fagherazzi and Du, 2008).

- Tsunami run-up may be associated with the *formation of barriers* in the form of ridges and ramparts perpendicular to the flow direction (Dawson, 1994; Scheffers et al., 2009), as well as with the *breaching of existing barriers*, often accompanied by the deposition of washover fans (May et al., in press).

- At near-field sites tsunamis are often accompanied by co-seismic subsidence and uplift. These land level changes can provoke a drop or rise of the local water level, which in return may trigger ecological changes in coastal environments, e.g. from a marsh to shallow marine conditions or from an intertidal flat to a terrestrial environment (e.g. Nichol et al., 2007). Similar *ecological impact on coastal environments* may be triggered by barrier breaching, as described for the 1755 tsunami in Portugal (Andrade, 1992) and from Lefkada, Greece (May et al., 2012), or barrier formation. Engel et al. (2009) suggest that tsunami induced barrier formation on Bonaire (Netherland Antilles) transformed a sheltered marine embayment into a hyper-saline water body; erosion of protective dunes by the IOT 2004

caused hydrological changes in lagoons and estuaries of India (Pari et al., 2008; Paris et al., 2009). Furthermore, tsunami inundation may result in partial or even irreversible damage of coral reefs (Brown, 2005) and mangrove forests (Giri et al., 2008).

9.2 Insights from a modern analogue – Monitoring impacts of the IOT 2004

9.2.1 Short-term effects in Thailand

Intensive and contemporary post-tsunami field surveys provide a detailed picture of the impact of the IOT 2004 on coastal zones of southwest Thailand. This includes damage to man-made infrastructure and buildings, coastal geomorphology, as well as coastal ecosystems.

Impact on man-made structures

The destruction of buildings and infrastructure along the coastlines of SW Thailand with its tourist industry provoked public attention globally. The damaging effect was mainly caused by high flow velocities and floating objects within the tsunami onshore flow. Dependent on coastal bathymetry, e.g. severe damages in pocket beaches with flow-concentrating shoreline configuration, and the type of construction, the extent of destruction varied locally (e.g. Rosetto et al., 2007; Sczcucínski et al., 2006).

Impact on morphology

Along the most severely affected coastlines of Thailand strong erosion of beaches associated with significant shoreline retreat was observed after the IOT 2004. Choowong et al. (2008a) report a shoreline retreat of more than 20 m, and reduction of the beach area to two thirds of the pre-event surface in the Khao Lak area. More than 30 m of landward retreat were observed at Pakarang Cape (Neubauer et al., 2011). Typical features of the eroded beaches directly after the impact were steeper, non-equilibrium beach profiles and erosive scarps with uprooted trees well above beach-berm level at the landward limit of erosion (Sczcucínski et al., 2006; Kelletat et al., 2007; Fagherazzi and Du, 2008). In contrast, the coastal plains of SW Thailand were dominated by deposition (Sczcuciński et al., 2006; Umitsu et al., 2007). Sharp trimlines similar to those observed after the IOT 2004 in Indonesia (Paris et al., 2009) and after many historical events, e.g. the 1755 Lisbon tsunami in Portugal (Scheffers and Kelletat, 2005) or the Lituya Bay tsunami in 1958 (Fritz et al., 2009b), were missing in Thailand (Kelletat et al., 2007). Destruction of smaller plants by high flow velocities, saltwater inundation and sediment cover created sparsely vegetated areas in the run-up zone (Sczcuciński et al., 2006). But since no soil erosion occurred and most robust Casuarina and palm trees survived inundation, no clear trimlines were formed (Scheffers et al., 2012c).

River mouths and tidal channels were particularly affected by erosive processes. Due to the concentration of backwash currents, many river mouths in the Nam Khem area were widened to wedge-shaped channels; sandy barriers in front of river mouths accumulated by alongshore drift were eroded by tsunami run-up (Umitsu et al., 2007; Kelletat et al., 2007). On coastal plains, fan-shaped return channels formed every 50-200 m due to the accentuation of linear morphological depressions by tsunami backwash. At the shores of tidal channels, 100-400 m long and 10-100 m wide flood scours were generated by tsunami run-up (Sczuciński et al., 2006; Fagherazzi and Du, 2008).

Impact on Ecosystems

The IOT 2004 had significant impact on exposed sections of the coral reefs of SW Thailand, e.g. offshore Ko Rach Yai, the Phi Phi Islands, or the Similan Islands (Kelletat et al., 2007). The damage was caused mainly by sedimentation of tsunami deposits on reef organisms as well as the turbidity of the water after the tsunami and not by dislocation of coral colonies and physical damage by floating objects. The result was a significant retreat of coral growth rates during the first few years after the tsunami (Scheffers et al., 2010). However, most Thai reefs were only slightly damaged; severely affected (> 50% of the reef area) were only 13% of the reefs (Department of Marine and Coastal Resources, 2005; Brown, 2005). Other affected eco-systems were mangrove forests that were locally destroyed within 20 m distance from the shoreline, although the largest part of the Thai mangrove areas did not suffer damage at all (Sczuciński et al., 2006). Furthermore, sea water flooding yielded contamination of soils and groundwater in the inundation zones (Sczuciński et al., 2005; Bozke et al., 2006).

9.2.2   Five years after – Recovery of tsunami-affected systems

Most damages to natural ecosystems and landforms as well as artificial infrastructure and housing caused by the IOT 2004 along the coast of SW Thailand had vanished only five years after the event; others were close to their complete recovery (Brückner and Brill, 2009). Espe-cially the majority of houses, hotels and tourism infrastructure that was destroyed or damaged by the tsunami waves had been rebuild within only two years (Brückner and Brill, 2009). Dif-ferent from trimlines of other tsunamis, e.g. that of the Lisbon 1755 tsunami which is still visible after more than 250 years (Scheffers et al., 2012c), areas that were without vegetation directly after the IOT 2004 recovered very fast: due to favourable growth conditions in the humid climate of SW Thailand, most affected areas were already covered by dense vegetation within only two month. After five years up to 10 m high Casuarina trees had grown and new soils had formed on tsunami deposits (Sczuciński, 2012).

a) Impact of the Indian Ocean tsunami 2004
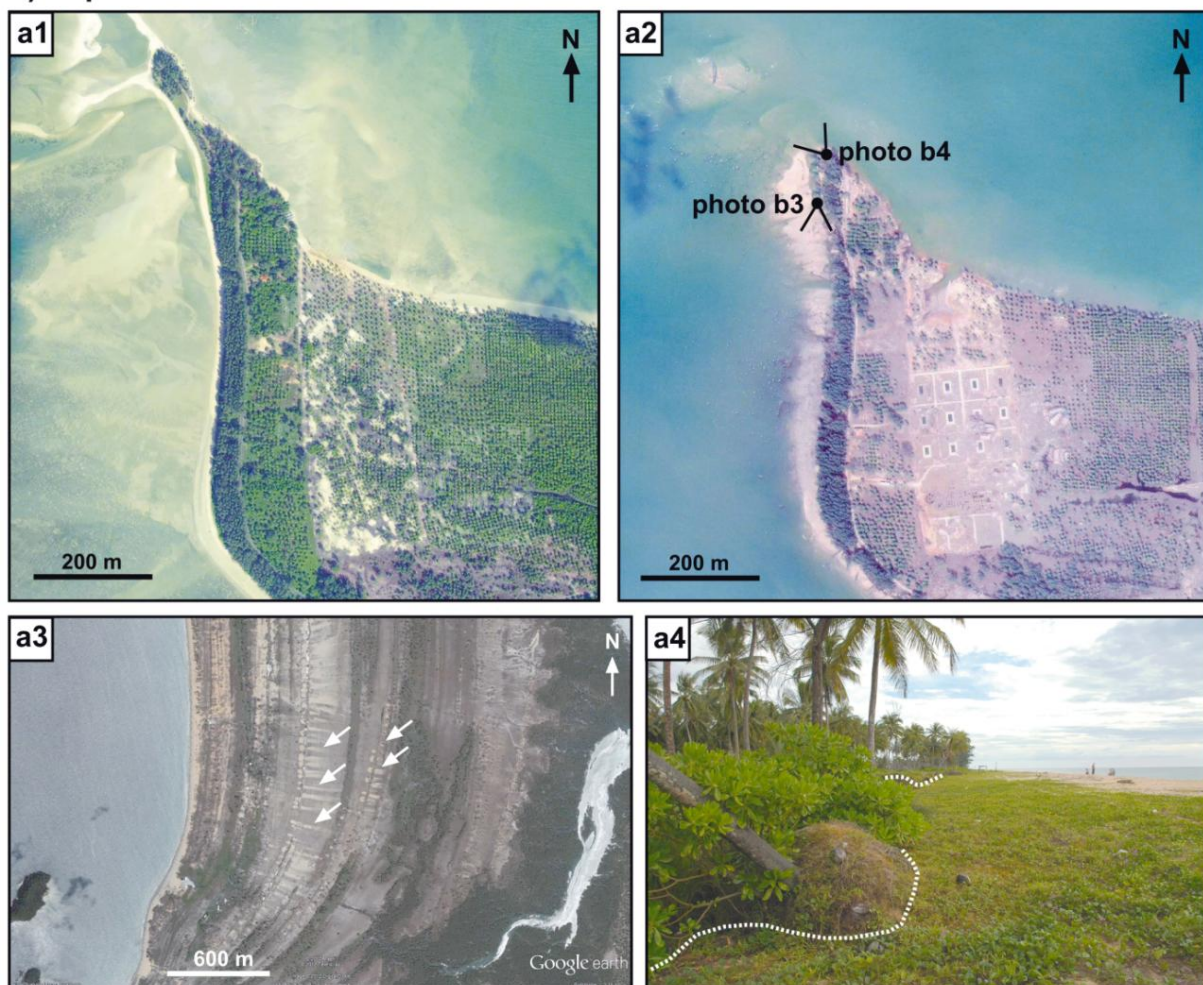
b) Recovery between 2005 and 2012
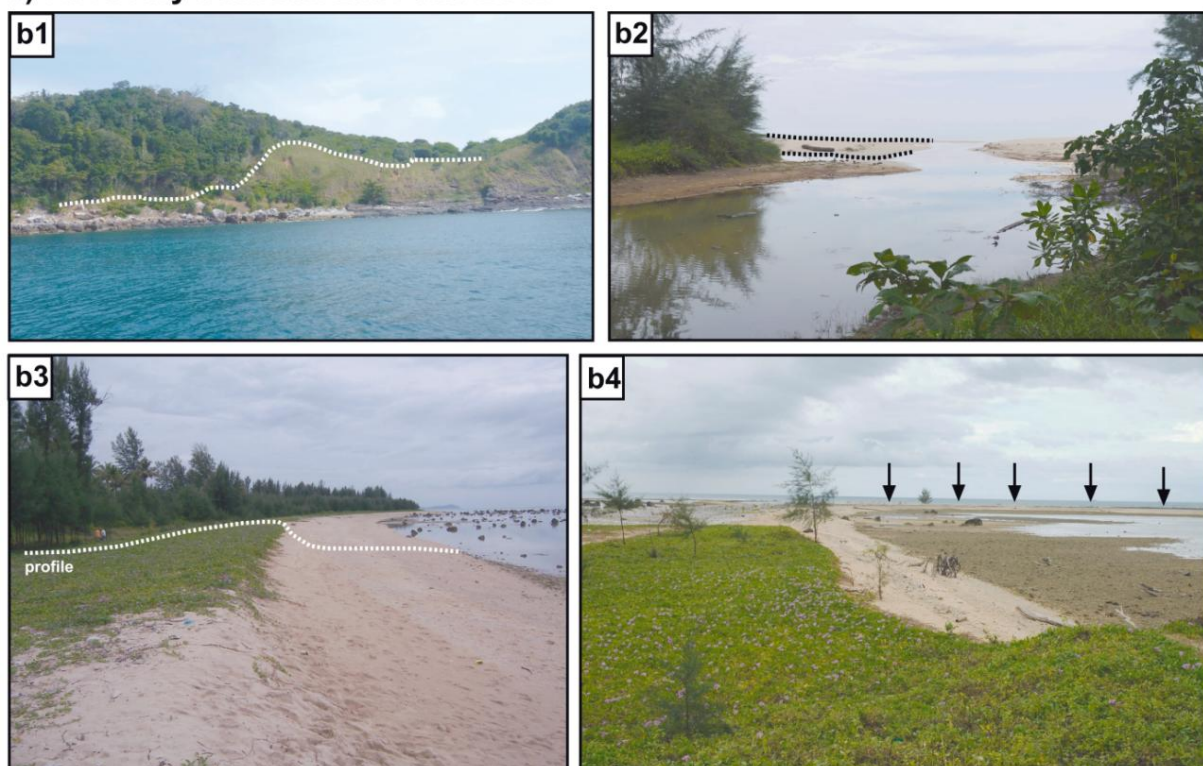
Figure 9.1: Examples for tsunami impact on coastal geomorphology (a) and recovery within the last seven years (b). a1 – Pakarang Cape prior to the IOT 2004 (Ikonos Satellite Image: CRISP, 2003), a2 – Pakarang Cape directly after the IOT 2004 (Ikonos Satellite Image: CRISP, 2004), a3 – tsunamigenic sand blows on Phra Thong Island (Google Earth image of February 2006), a4 – erosive scarp in the coastal plain of Pakarang, b1 – the trimline of the IOT 2004 on Phi Phi Don is almost invisible due to re-establishment of vegetation (photo: D. Kelletat in January 2011), b2 – re-established sand barrier in front of a river mouth at Ban Bang Sak, b3 – beach ridge at the western coast of Pakarang that was formed after the IOT 2004, b4 – reformation of a sand spit at the northern end of Pakarang Cape.

Similarly, eroded beaches re-established their pre-tsunami shoreline positions and equilibrium profiles within a few years: The total recovery of 20 m shoreline retreat and beach-profile steepening in Khao Lak took only two years (Choowong et al., 2008a). At Pakarang Cape the formation of a 3 m high post-tsunami ridge proceeded rapidly (Neubauer et al., 2011), and in 2012 first trees were already visible on a newly established sand spit. The beach fauna of disturbed coastlines recovered even faster, within only a few months after the tsunami (Kotwicki and Szczucińsci, 2006; Kendall et al., 2006). Even most coral reefs reached nearly pre-event conditions within only five years after the tsunami (Brückner and Brill, 2009), and total recovery of the most severely affected reefs will probably be reached within the next 5-10 years (Sczuciński et al., 2006).

In conclusion, the IOT 2004 had no significant effects on geomorphology or coastal ecosystems. Its impact was masked by normal processes within only a few years (Wong, 2009; Liew et al., 2010). Kelletat et al. (2007) explain the rather weak impact of the tsunami compared to its extraordinary magnitude by the relatively low flow velocities of less than 8 m/s that were estimated for onshore flow at the Thai coast. The impacts recorded at the study locations shortly after December 2004 – beach erosion, shoreline retreat, channel erosion and generation of erosive scarps with uprooted trees – were nearly completely balanced by our last visit in April 2012.

9.3   Tsunami impact in the geological record

9.3.1 Summary of tsunamis in the geological records of Phra Thong, Ban Bang Sak and Pakarang

The evaluation of long-term effects of tsunami impact on coastal ecosystems and landforms is based on the sedimentary contexts of palaeotsunami deposits at Ban Bang Sak (described in Chapter 4), on Ko Phra Thong (described in Chapters 5, 6 and 8), and at Pakarang Cape (described in Chapter 8):

(i) On *Ko Phra Thong* the deposits of the IOT 2004 form a continuous sand sheet that covers ridges and swales up to 2 km inland. In addition, a maximum of four palaeotsunami layers is preserved in the deeper swales of the island. Each of the sand sheets, the modern one as well as the prehistoric deposits, is confined by peat strata; only below the oldest

layer the material is clayey. While the lower contact is sharp and erosive, the upper one is usually gradual (fig. 9.2).

(ii) At *Pakarang Cape*, the IOT 2004 deposit sharply overlies a sandy pre-tsunami soil in the coastal plain and clay in artificial lakes. The sand sheet is already covered by recent soil and lake deposits, respectively. A sandy palaeotsunami layer (1000-1200 cal BP) was identified in a depth of 2-3 m below surface, where it is confined by grey, sandy or silty sediment with abundant coral rubble and shell fragments (fig. 9.3).

(iii) At *Ban Bang Sak,* the IOT 2004 sand sheet overlies the pre-tsunami soil in the beach-ridge plain and brownish loam in the alluvial plain. It is covered by a thin initial soil (fig. 9.4). Evidence of prehistoric tsunamis is given by event layer B (500-700 cal BP) which is preserved solely in the swales. It is comprised by grey sand and peat close to the shoreline and by brownish loam in landward direction. Several event layers C (1180-2000 cal BP) are preserved in a depth of 5-6 m below surface and surrounded by yellowish, decalcified clay (fig. 9.4).
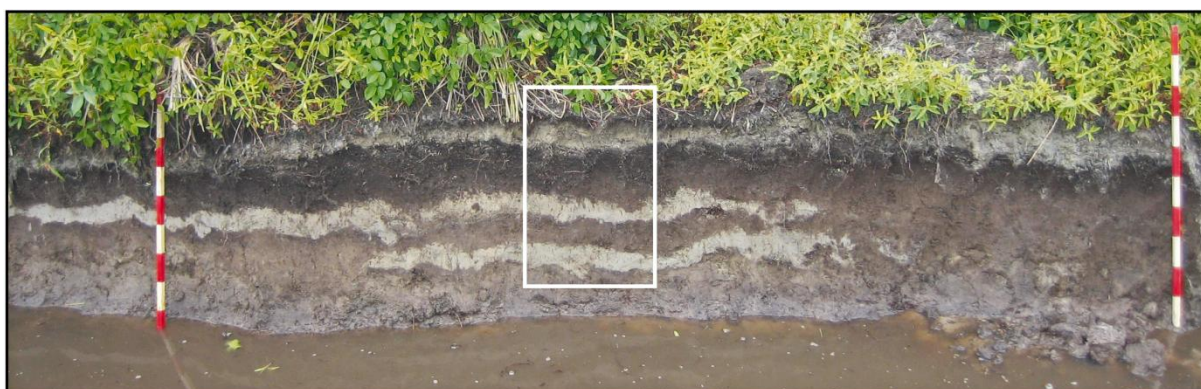
substrate	environment
peat	back-barrier swamp
tsunami sand	IOT 2004
peat	back-barrier swamp
tsunami sand	palaeotsunami (1450-1520 AD)
peat	back-barrier swamp
tsunami sand	palaeotsunami (970-1080 AD)
peat	back-barrier swamp

Figure 9.2: Tsunami impact on Phra Thong Island. The sand sheet of the IOT 2004, as well as all palaeotsunami deposits are confined by peat accumulated in a back-barrier-swamp environment. A change in background sedimentation after tsunami events did not occur.
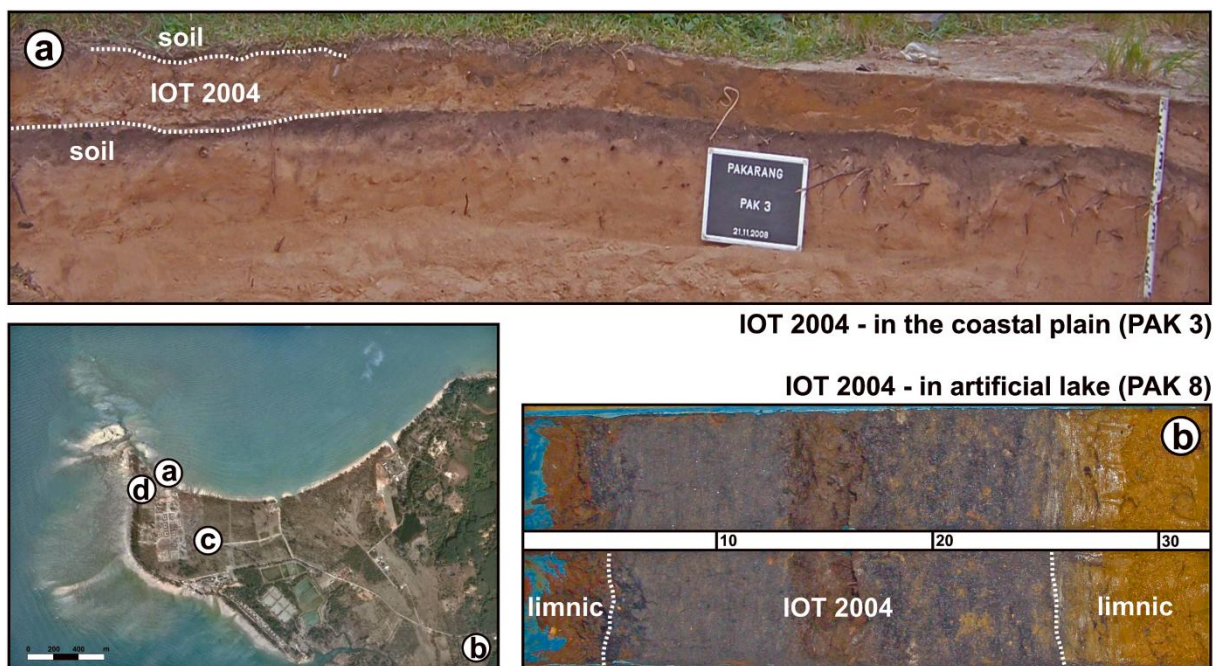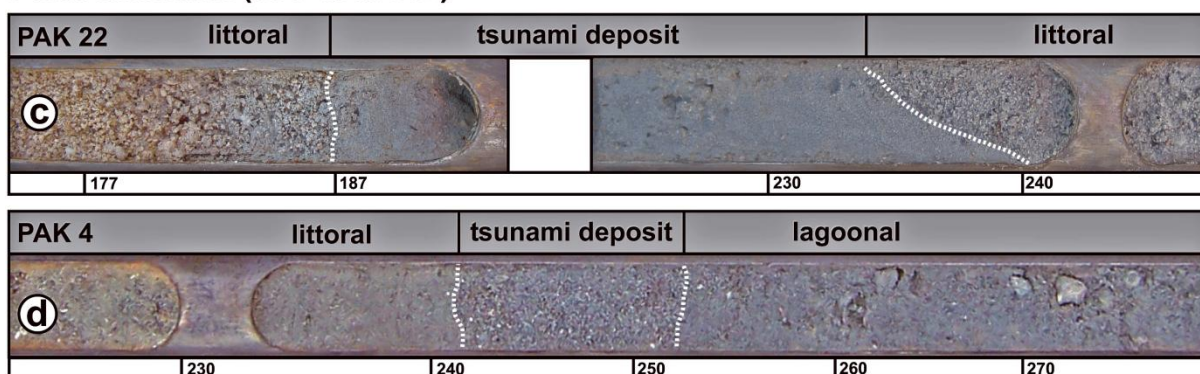
Figure 9.3: Tsunami impact at Pakarang Cape. The pre-2004 environments re-established short time after the IOT 2004 in the coastal plain (a), as well as in artificial lakes (b). The palaeotsunami of 800-1000 AD caused no change of background sedimentation in PAK 22 (c); in PAK 4 instead the lagoonal pre-event milieu was displaced by a littoral environment (d).

9.3.2 Tsunami impact on near-shore environments deduced from the sedimentary record

To investigate the impact of tsunamis on the archives their sediments were deposited in, the background sedimentation before and after the event, i.e. the deposits directly below and above the tsunami layers, have to be compared regarding their ecological indication. In agreement with monitoring of tsunami-affected ecosystems during the last 7 years, the geological record demonstrates the immediate re-establishment of pre-impact conditions after the IOT 2004 at all study sites: On Phra Thong Island, back-barrier swamps cover the swales before and after the event (fig. 9.2); at Ban Bang Sak, terrestrial soil formation and an alluvial

milieu remain stable after the tsunami (fig. 9.4); at Pakarang, limnic sedimentation prevailed in lakes and soil formation continued in the coastal plain (fig. 9.3). For prehistoric tsunami events, the impact on depositional environments was more diverse:

(i) Phra Thong Island. Similar to the IOT 2004, all prehistoric events caused no changes in the ecology of pre- and post-tsunami sedimentation. Before and after the events the same back-barrier swamp (indicated by peat above and below the tsunamites) was dominating the swales of the island (fig. 9.2). Since, in addition, no significant capping of beach ridges took place, the long-term effect of tsunamis on the ecological and morphological evolution of Phra Thong seems to be negligible.

(ii) Pakarang. The Palaeotsunami that took place c. 1000 years ago was preserved only in the deposits of a former back-reef lagoon. While the tsunami had no apparent impact on the background sedimentation at the rim of the lagoon (littoral sands before the event were followed by littoral deposits after the tsunami; fig. 9.3c), it caused a shift from lagoonal mud to littoral sediments in its centre (fig. 9.3d). Thus, by filling the back-reef lagoon with tsunami deposits, the event might have accelerated its transformation into a littoral zone. An impact on the destruction of the coral reef by potential earlier tsunamis some 4000-5000 years ago, as suggested by Neubauer et al. (2011), is rather speculative and not proved by geological evidence. The death of all corals found at Pakarang (the coral boulders on the intertidal platform as well as the coral fragments in the lagoon and coastal plain sediments) between 4000 and 5000 years ago might as well be the result of the dropping sea level after the Holocene high stand 5500 years ago (see Chapter 7) and not the effect of destructive tsunami impact, especially since the IOT 2004 was not associated with significant destruction of coral reefs.

(iii) Ban Bang Sak. The 1300-1450 AD tsunami caused a shift from a sheltered intertidal environment before the event (marine sand below event layer B) to back-barrier swamp conditions after the event in swale II (BBS 1 in fig. 9.4b). Further inland, in swale I, the same event had no effect on the environment and was followed by re-establishment of the pre-event alluvial sedimentation (BBS 34 in fig. 9.4b). The shift from intertidal conditions to a swampy environment is the result of ongoing barrier formation. Even though swale II was already separated from the sea by a beach ridge, the tsunami might have influenced its complete isolation by locking remaining inlets in the sandy barrier and, thus, changing its hydrology and sedimentation. In contrast, events C have not been associated with environmental changes at all (fig. 9.4c). After the events, the same alluvial environment as before was re-established (above and below, the same alluvial mud was deposited).
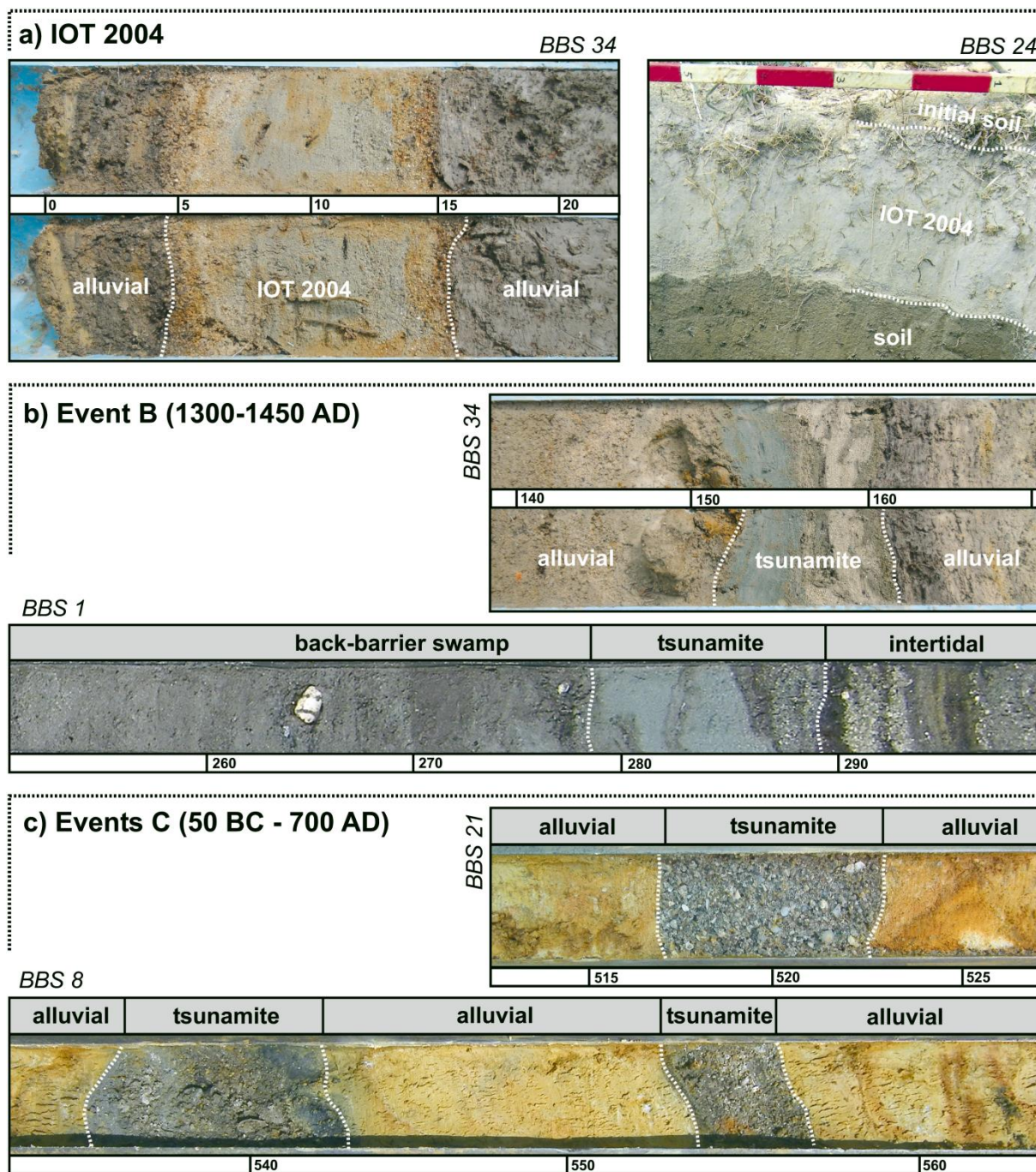
Figure 9.4: Tsunami impact in the geological record of Ban Bang Sak. (a) IOT 2004 deposits in the alluvial plain (BBS 34) and the ridge system (BBS 24). (b) Event B in the inland swale I (BBS 1) and the seaward swale II (BBS 8). (c) Events C in cores BBS 8 and BBS 21.

Chapter 10

10 Sediment transport and hydrodynamic parameters of tsunami waves recorded in onshore geoarchives – a case study from Thailand

Abstract: *In regions with a short historical record the assessment of long-term tsunami risk strongly depends on geological evidence of prehistoric tsunami events. While dating tsunami deposits is already well established, magnitude assessment based on sedimentary remains is still a major challenge. In this study two different approaches were applied to deduce transport processes and hydrodynamic parameters of tsunami events from onshore deposits found in the coastal plain of Ban Bang Sak, southwest Thailand. (1) The maximum offshore sediment source was determined using granulometry, geochemistry, mineralogy and foraminifera of the tsunamites and reference samples from various marine and terrestrial environments. (2) By means of sedimentation modelling, onshore flow velocities and flow depths of associated tsunami waves were estimated. In case of the 2004 Indian Ocean tsunami (IOT), modelled flow velocities of 3.7-4.9 m/s, modelled onshore flow depths of up to 5.5 m, and a sediment source shallower than 45 m water depth – including littoral sediments transported as bedload and suspended load from the shallow subtidal zone – are in agreement with quotations based on survivor videos and post-tsunami surveys. For a 500-700 year old predecessor, comparable flow velocities and flow depths of 4.1-5.9 m/s and 7.0 m, respectively, were modelled, indicating a similar magnitude as the IOT 2004. Also comparable values of maximum transport distance and depth of wave erosion were found. In case of three older tsunami candidates, dated to 1280-2000 cal BP, the deposits partly indicate similar source areas with water depths of less than 45 m, and partly even shallower source areas restricted solely to the beach. While the former are interpreted as tsunami events similar to 2004, the latter are more likely storms or tsunamis of a lower magnitude.*

Keywords: *Tsunami; Tsunami deposit; Foraminifera; Hydrodynamics; Sediment transport; Thailand*

10.1 Introduction

Due to the continuous recording of tide gauges and satellites, observations and videos of eye witnesses, as well as contemporary post-tsunami field surveys, modern tsunamis are excellently documented in terms of their triggering events, their chronological sequence, wave parameters and impact on coastal communities and infrastructure (e.g. Liu et al., 2005: Indian

Ocean tsunami (IOT) of 2004). Remarkably less information is available for historical tsunamis, where at least the time of impact (year and/or day) is known and rough information about wave heights and impacts exist (e.g. Dawson et al., 1995: 1755 Lisbon tsunami). In case of prehistoric tsunami events, in contrast, all information has to be drawn from the geological record.

Thus, the three main goals in studying prehistoric tsunami deposits are (1) the confirmation of the tsunami origin, (2) dating and correlation of tsunami events, and (3) the quantification of tsunami magnitudes (Sugawara et al., 2008). Although identification, especially the discrimination from tempestites (e.g. Morton et al., 2007; Switzer and Jones, 2008; Peters and Jaffe, 2010), and dating of tsunami deposits are still problematic in many cases (e.g. Jankaew et al., 2008; Yawsangratt et al., 2009), the determination of event magnitudes is the topic least understood. Even for modern tsunamis that have been intensively studied, like the IOT 2004, no clear picture of the complex transport processes and onshore hydrodynamics does exist (e.g. Paris et al., 2009).

Using any quantitative parameter of tsunami size, even relative ones that are influenced by site-specific factors and, therefore, are valid only at a single location (e.g. inundation height, flow velocity, inundation distance, run-up height, etc.) as measures for the tsunami magnitude, and not only universal ones such as the offshore wave height (Papadopoulos and Imamura, 2001), several strategies have been applied to deduce magnitudes from tsunami deposits: (1) For boulder-sized deposits, wave height and flow velocity have been estimated from transport formula that are mainly based on weight, size, as well as lateral and vertical displacement of the boulders (e.g. Nott, 2003; Imamura et al., 2008; Goto et al., 2010; Engel and May, 2012). In case of sandy tsunamites, (2) the maximum inland extent, as an indicator for tsunami run-up and inundation, has been used to estimate minimum wave heights (e.g. Pinegina and Bourgeois, 2001, Peterson et al., 2011) or the geometry of ruptures that triggered the event (Nanayama et al., 2003). Other studies employed (3) the source of tsunami sediments deduced from microfossils (e.g. Davies et al., 2003; Nagendra et al., 2005; Costa et al., 2012) or mineralogical aspects (Switzer et al., 2005), to assess amplitudes, periods, or transport distances of prehistoric events (Uchida et al., 2010). Lately, (4) inverse sedimentation models have been used to estimate hydrodynamic parameters including flow speed, flow depth and run-up height on the basis of onshore deposits (Jaffe and Gelfenbaum, 2007; Moore et al., 2007; Smith et al., 2007; Soulsby et al., 2007). Inverse models can be accomplished by forward approaches that model the deposit characteristics for different inundation scenarios (Apotsos et al., 2009, 2012; Prichard and Dickinson, 2008).

This study combines the application of the inverse model TsuSedMod (Jaffe and Gelfenbaum, 2007) and the sedimentology and microfauna-based reconstruction of offshore sediment sources to deposits of the IOT 2004 and potential predecessors from the coastal plain of Ban

Bang Sak, Thailand (Brill et al., 2011). By evaluating the approach for the modern analogue of 2004, for which specifications regarding onshore flow depth, flow speed and sediment source exist, the magnitude of palaeoevents is estimated. While the boundary conditions at the time of impact, such as tide level, sea level and topography, are well known for modern events, these parameters may have differed significantly from present conditions for prehistoric tsunamis. This and the potential effect of post-depositional changes have to be considered for ancient tsunamites.

10.2 The study area

10.2.1 Physical setting of Ban Bang Sak

The coastal plain of Ban Bang Sak is located at the west coast of southern Thailand, which is part of the Malay-Thai Peninsula (fig. 10.1a). Although located in the sub-humid tropics north of 5 °N, southwest Thailand has not been affected by the landfall of tropical cyclones within the last 150 years (Murty and Flather, 2004), but was only exposed to normal coastal dynamics controlled by moderate waves <2 m and tides of 1.5-3.5 m (Choowong et al., 2008a). Tectonically, southwest Thailand is part of the relatively stable Sunda Plate with only minor tectonic activity during the Holocene (Fenton and Sutiwanich, 2005), and the occurrence of strong earthquakes is restricted to the Sunda Arc (fig. 10.1a), where the convergence of the Australian-Indian Plate with the Sunda and Burma Microplates is a major source of ruptures (Lay et al., 2005), which are capable to produce tsunami waves strong enough to reach the Thai coast (Okal and Synolakis, 2008).

The coastal geomorphology of the study area is characterised by steep, rocky headlands that vary with intertidal flats and sandy beach-ridge plains (Sinsakul, 1992; Dheeradilok, 1995). The offshore topography to the west is gently sloping and shows no near-shore irregularities off Ban Bang Sak (Di Geronimo et al., 2009; figs. 10.1a, b). Generally, Holocene coastal deposits are less than 20 m thick and overly alluvial Pleistocene sediments or deeply weathered Tertiary bedrock (Dheeradilok, 1995). In case of Ban Bang Sak they form a 300-500 m wide coastal plain that is geomorphologically characterised by a succession of coast-parallel beach ridges and swales (figs. 10.1c, d and 10.2). Its stratigraphy was described by Brill et al. (2011) as shown in figure 10.1d: The surface of the pre-Holocene terrestrial deposits (unit 1) forms a gently dipping slope that is burrowed by transgressive intertidal sand (unit 2). In the course of coastal progradation the tidal flat was topped by two generations of beach ridges (unit 3) and terrestrial deposits (peat, alluvial deposits, artificial material) that accumulated in the depressions of the intervening swales (unit 4). The swales proved to be an appropriate geo-archive for deposits of tsunami events. Besides the sand sheet of the IOT 2004 (event A), a second layer was found in the swale nearest to the coast reflecting an older tsunami dated to 500-700

cal BP (event B). Additional evidence of up to three extreme wave events, either tsunami or storm and dated to 1180-2000 cal BP (events C), occurs in the upper section of the terrestrial deposits at the base (Brill et al., 2011).
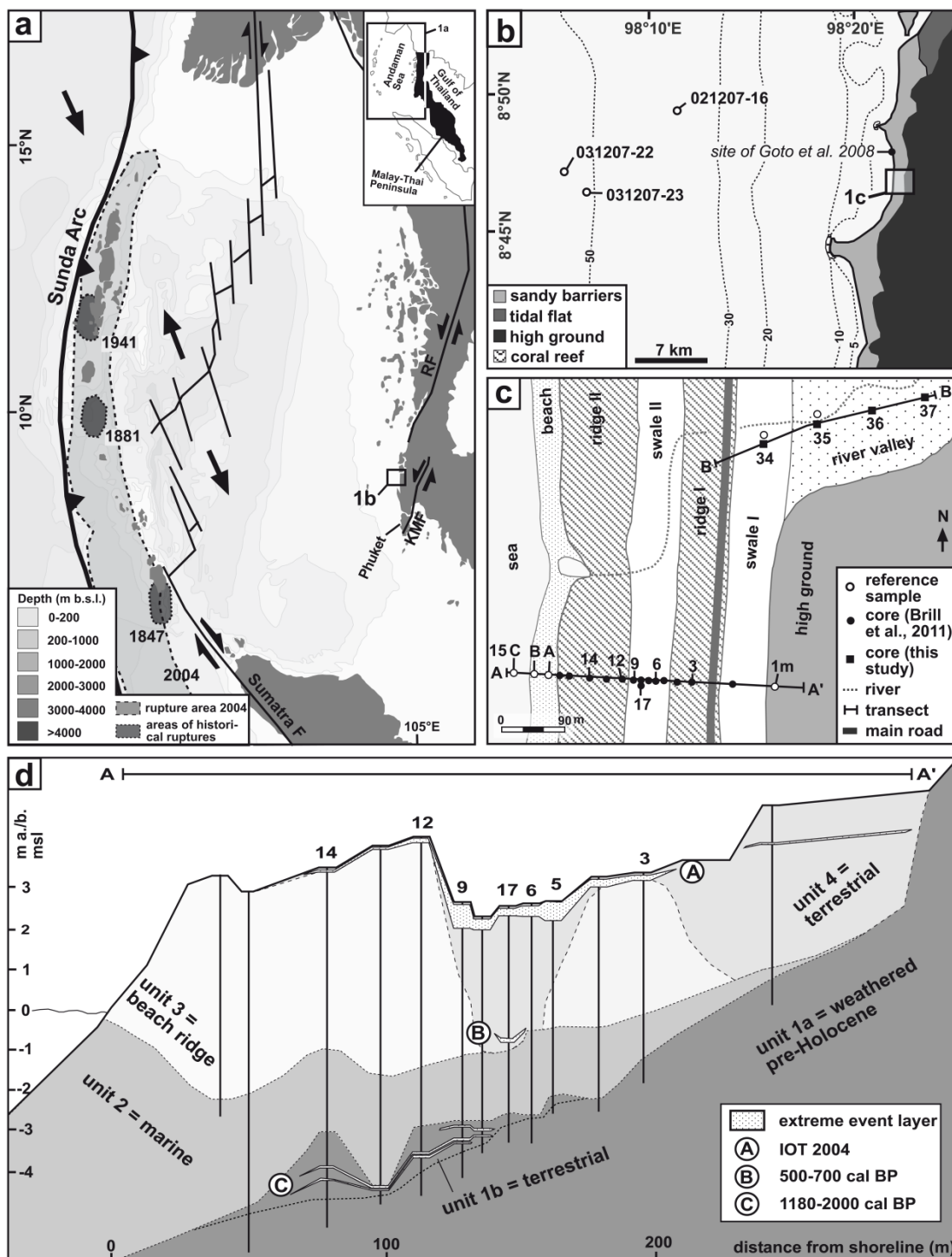
Figure 10.1: Overview of the study area. (a) Map of the Andaman Sea with rupture areas of historical earthquakes along the Andaman-Nicobar Segment of the Sunda Arc (according to Bilham et al., 2005), and main tectonic structures of the area after Watkinson et al. (2008). KMF = Klong Marui Fault, RF = Ranong Fault. (b) The shelf offshore Ban Bang Sak with locations of offshore reference samples. (c) Morphological division of Ban Bang Sak coastal plain with positions of transects A and B. (d) Cross section through the sediments of the coastal plain along transect A (after Brill et al., 2011).
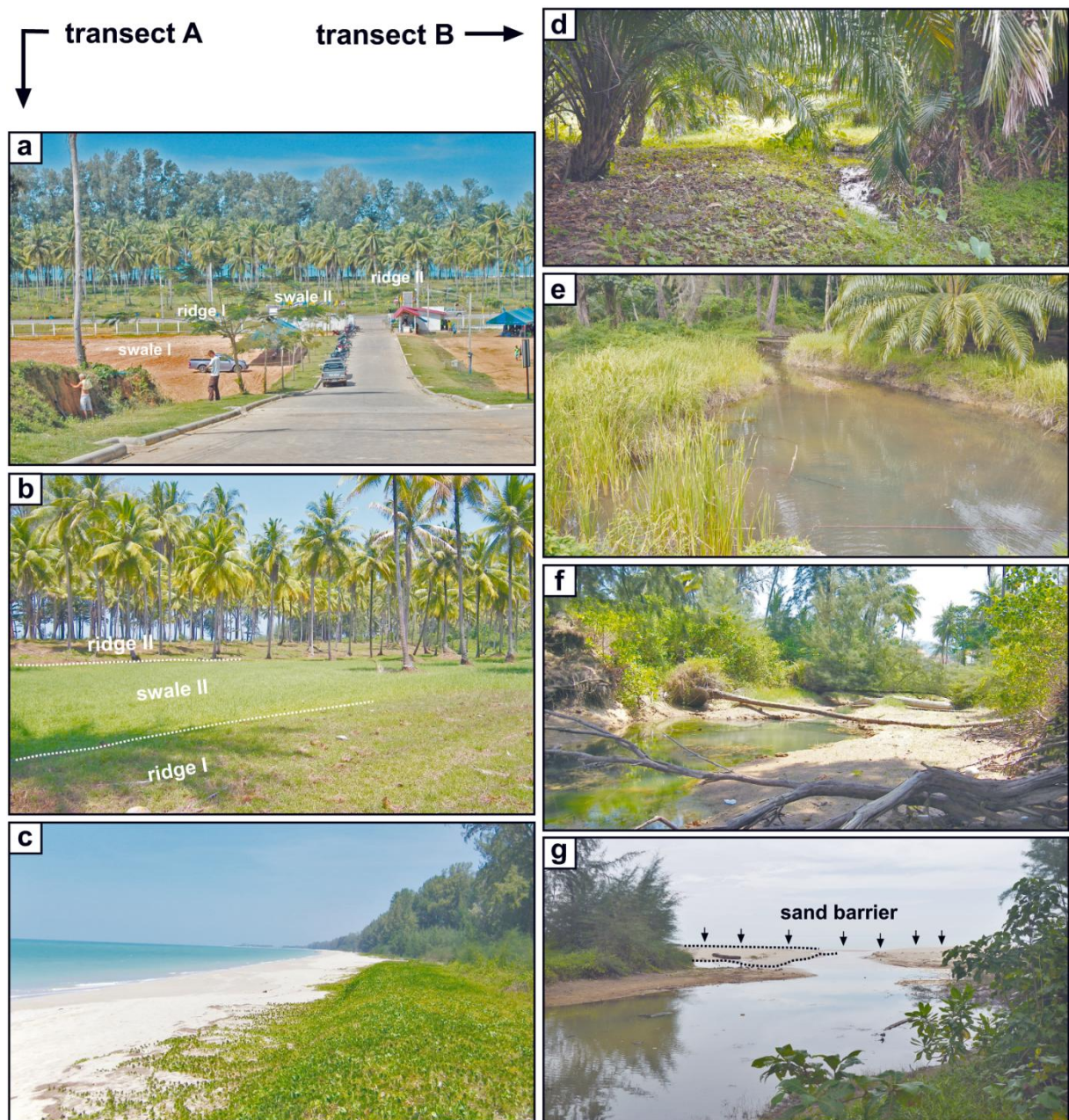
Figure 10.2: Recent environments along transects A (a-c) and B (d-g). (a) View from the hills at the eastern end of transect A (compound of the Rajaprajanugroh #35 School) in western direction. (b) View from ridge I in western direction. (c) The beach in transect A. (d) River channel in the gently dipping alluvial plain. (e) Backwater of the river in swale II. (f) Incised river channel in the cemented sediments of ridge II. (g) The river mouth with shore-parallel sand barrier at its seaward end.

10.2.2 Holocene tsunami events

On December 26, 2004, at 7.59 a.m. local time, a M_w9.1-9.3 earthquake struck the area 100 km west of Sumatra and resulted in a 1300 km long rupture of the Sunda Arc subduction zone with maximum vertical slip of 20 m (Lay et al., 2005; Subarya et al., 2006). The seafloor displacement generated a tsunami that reached the Thai coast during high tide in form of a

trough leading wave (Tsuji et al., 2006). While at Phuket the initial withdrawal of sea water arrived at 9.30 a.m. local time and the first wave crest followed at 10 a.m. (Szcuciński et al., 2006), at the coastline of Khao Lak the initial trough was recorded at 10 a.m. and the first wave crest arrived 30 minutes later (Bell et al., 2005; Hawkes et al., 2007). Prior to the final withdrawal of the sea, three major waves flooded the coastal plains of Phuket and Phang-nga, with the first or second wave showing the largest amplitude, but the third wave, riding on the previous ones, being the highest (Hori et al., 2007; Choowong et al., 2008b). For the area of Khao Lak, based on post-tsunami field surveys, eyewitness accounts and survivor videos, the magnitude of the tsunami was partly documented: maximum inundation exceeded 1000 m, run-up reached 11-14 m above mean sea level (a.s.l.), and the wave height was 6-13 m above tide level (a.t.l.) (Matsutomi et al., 2005; Tsuji et al., 2006). The most reliable estimates of onshore flow velocities, inferred from survivor videos, are 6-8 m/s (Rosetto et al., 2007). Although the impact on coastal communities and infrastructure was disastrous, the long-term effect on coastal geomorphology was remarkably low (Kelletat et al., 2007).

Although several historical earthquakes along the Sunda Arc prior to 2004 have triggered tsunamis in the Andaman Sea (Bilham et al., 2005; fig. 10.1a), none of them was strong enough to leave a noticeable imprint at the coast of Thailand (Okal and Synolakis, 2008). In contrast, for prehistoric times, convergence rates at the Sunda Arc (Løvholt et al., 2006; Subarya et al., 2006) and evidence of co-seismic uplift and subsidence along the rupture zone (Rajendran et al., 2008; Meltzner et al., 2010; Grand Pre et al., 2012) point to possible previous megathrust ruptures similar in magnitude to 2004, which probably resulted in severe tsunamis. Additionally, sedimentary evidence of prehistoric tsunamis was found at several locations in southwest Thailand (e.g. Jankaew et al., 2008; Brill et al., 2011, 2012a, b; Prendergast et al., 2012) and other countries around the Indian Ocean (e.g. Monecke et al., 2008; Rajendran et al., 2006; Malik et al., 2011). While this evidence documents the occurrence of palaeotsunamis between 500 and 4000 years BP, there is scarce information about the magnitudes of these events.

10.3 Methods

The new stratigraphical data presented in this paper were obtained from closed vibracores, drilled with an Atlas Copco mk 1 corer, and from short plastic pipes hammered into the sediment. To measure the position and elevation of each coring site a differential GPS system (Topcon HiPer Pro) was used. In the laboratory, a tentative stratigraphy was established following Ad-hoc-Arbeitsgruppe Boden (2005). Subsequently, each sedimentary stratum was sampled for laboratory analyses with a sampling interval of 1-2 cm applied to potential tsunami layers.

Grain-size analyses were performed on the air-dried fine fraction (<2 mm) after treatment with H_2O_2 to remove organic matter using a laser particle sizer (Beckmann Coulter LS13320

Mikro). For the calculation of grain-size statistics after Folk and Ward (1957), the GRADI-STAT software was applied (Blott and Pye, 2001). The separation of different grain-size components followed the approach of Moore et al. (2007) using peak fitting software (Seasolve PeakFit v. 4.12). Geochemical analyses included loss on ignition (LOI), $CaCO_3$ content (Scheibler method), and X-ray fluorescence on powder samples measured with a handheld XRF spectrometer (Niton Xl3t 900 GOLDD); the mineralogical composition was determined by X-ray diffractometry performed on a Siemens D5000 (40 kV; 40 mA; Cu $K_{\alpha 1}$[Å]: 1.54060, $K_{\alpha 2}$[Å]: 1.54443; 2Θ range: 2-80°; continuous scan; 0.02° steps for 1 s). Qualitative and semi-quantitative mineral composition was determined from measured XRD spectra via search and match software (EVA V13, Bruker AXS) using the ICDD database. Samples for foraminifera analyses were wet sieved to separate the fraction > 100 μm. The taxonomy was determined under the light microscope mainly on the basis of Loeblich and Tappan (1987, 1994) and the database WoRMS (2012). To guarantee statistical significance, at least 300 individuals per sample were studied. Statistical processing of foraminifera, XRF and XRD data was performed via cluster analyses and Principal Component Analyses (PCA) using the PAST 2.14 software (Hammer et al., 2001) after exclusion of highly correlating parameters using Spearman's rank correlation coefficient and after omitting rare taxa.

To estimate hydrodynamic parameters of tsunami inundation, the inverse model of Jaffe and Gelfenbaum (2007), TsuSedMod, was applied, which has already been tested on deposits of the 1998 Papua New Guinea tsunami (Jaffe and Gelfenbaum, 2007), the IOT 2004 (Spiske et al., 2010) and the 2009 Samoa tsunami (Jaffe et al., 2011). The model works with the simplifying assumptions that (1) onshore tsunami flow is steady and uniform, (2) transport and deposition of sediment is dominated by suspension load (>90%), and (3) no erosion is caused by following waves or backwash. Only where these assumptions apply – ideally, in fairly shallow and gently sloping coastal plains that are flooded by long tsunami waves (Apotsos et al., 2012) – the model is considered to provide reliable values for onshore flow speed by computing the shear velocities necessary to produce the observed deposits (Jaffe and Gelfenbaum, 2007). Required input data are the averaged grain-size distribution and the thickness of those sections of the tsunamites which are considered to have been deposited from suspension during a single inflow (according to Jaffe et al. (2011) these "suspension graded" sections are characterised by normally graded, unimodal grain-size distributions that successively become finer, better sorted and more positively skewed towards the top), as well as the flow depth. Since the flow depth was (mainly) unknown for the IOT 2004 and the palaeotsunamis at the study site, minimum values were estimated via the Froude number, which should be 0.7-1.0 in the subcritical onshore flow of tsunamis (Nanayama and Shigeno, 2006; Spiske et al., 2010). Other model parameters were kept constant for all samples: resuspension coefficient, eddy viscosity and settling velocity were adopted from Jaffe and Gelfenbaum (2007), and a Manning's n of 0.03 for bottom roughness from Jaffe et al. (2011); sediment density (2.68 g/cm³),

salinity (33‰) and water temperature – in the Andaman Sea the uppermost 60 m show a constant temperature of 25 °C (Osborne and Burch, 1980) – were adapted to the local conditions.

10.4 Results

The coastal stratigraphy of Ban Bang Sak, including evidence of the IOT 2004 and potential predecessors, was previously documented along a shore normal cross section (transect A, fig. 10.1c) by Brill et al. (2011). Due to anthropogenic impact at the eastern end of transect A the sediments inside of swale I were strongly disturbed and the occurrence of tsunami layers was restricted to the area west of it (fig. 10.1d). To laterally extend the evidence of tsunami layers, a second transect perpendicular to the shoreline and consisting of four sediment cores (BBS 34, 35, 36, and 37), was established 400 m to the north (transect B, fig. 10.1c). Transect B starts 250 m east of the shoreline on ridge I, crosses swale I, and runs eastward on the gently dipping alluvial plain of a small river to its maximum inland position 430 m east of the shoreline and 4 m a.s.l. (figs. 10.2 and 10.3).

10.4.1 The general stratigraphy of coastal sediments at Ban Bang Sak

Core BBS 34 is located 360 m east of the shoreline in the densely vegetated depression of swale I (fig. 10.3). Reaching a depth of 3 m below surface (b.s.), the bottom section is composed of stiff, yellowish clay void of carbonate and macro remains. Above an erosional contact at 1.90 m b.s., grey coarse sand with a carbonate content of 10% follows. Subsequently, a 5 cm thick peat layer at 1.74-1.69 m b.s. is covered by decalcified, greyish brown loam with alternating clayey and sandy sections. At 1.02 m b.s. the uppermost clayey section is overlain by a grey, multiple graded fine sand layer, 14 cm thick, with a sharp contact, marine shells and rip-up clasts at the base, and a high $CaCO_3$ content (40-50%). From 0.88 to 0.24 m b.s., alternating strata of decalcified, greyish brown clay and sandy loam follow. Again, a sharply bordered fine sand layer occurs between 0.24 and 0.13 m b.s. It is characterised by a grey colour, basal shell fragments, and high carbonate content (40-50%). The uppermost 13 cm are composed of brown clay without carbonate.

Cores BBS 35, 36 and 37, drilled on the alluvial terrace at distances of 390, 400 and 430 m east of the shoreline, reach depths of 1.40-1.60 m b.s. (fig. 10.3). All three are composed of greyish brown, decalcified strata of clay and loamy sand. The coarser sections contain rounded quartz pebbles, whereas in the finer sections plant fragments and wood are observed. While BBS 35 is entirely composed of these deposits, in BBS 36 and 37 the clayey top section is interrupted by sharply bordered layers of grey fine sand with shell fragments at the base and high carbonate contents (40-50%).
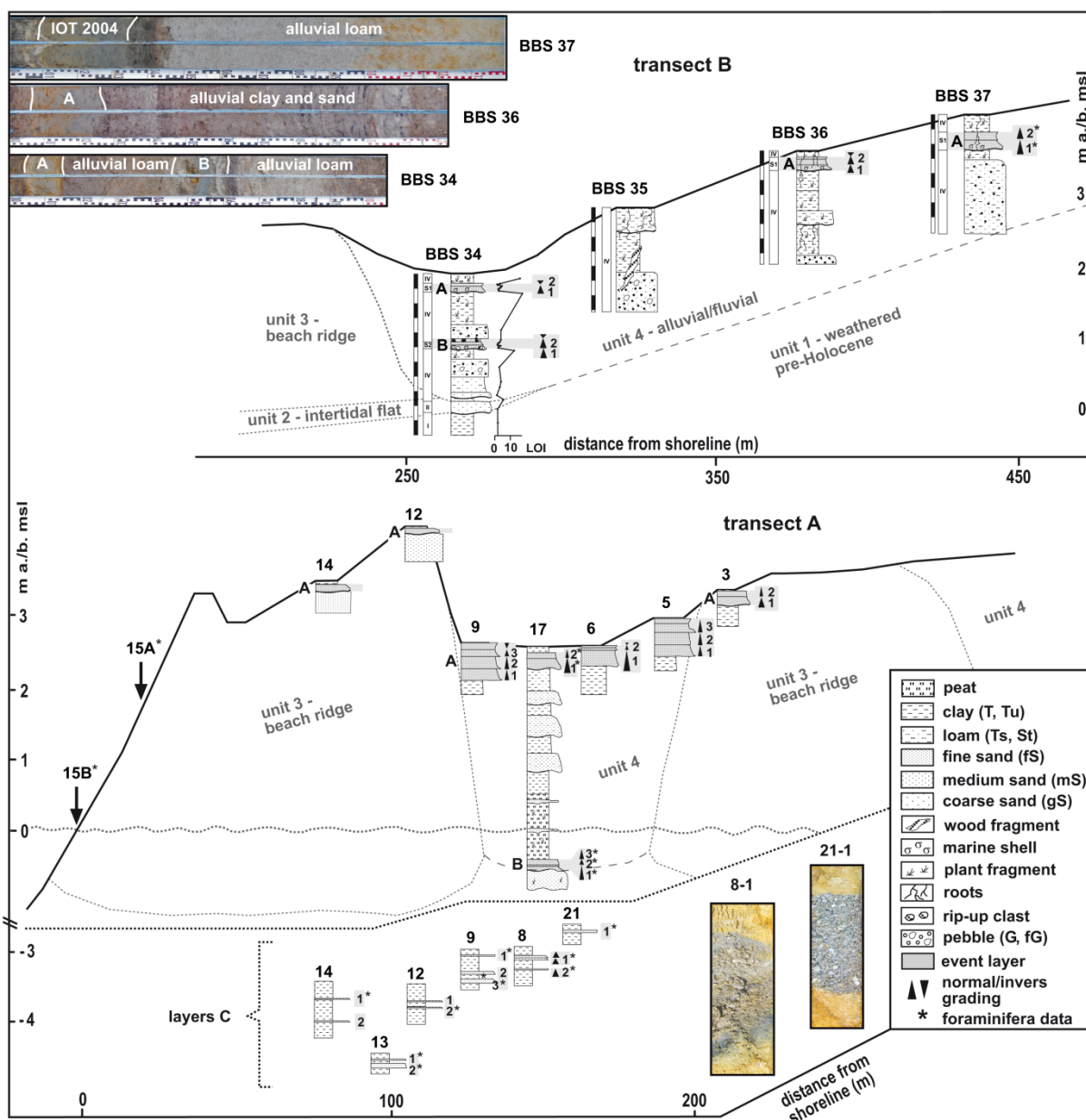
Figure 10.3: *Schematic cross sections of the coastal plain along transects A and B. For transect B the complete stratigraphy of cores BBS 34-37 is presented. For transect A only the geometry and sedimentary structure of event layers A, B and C is documented, while the division into units is adopted from Brill et al. (2011).*

All deposits described in cores BBS 34-37 clearly correspond to the stratigraphical record of transect A described by Brill et al. (2011; fig. 10.1d): The yellowish clay at the base of BBS 34 is consistent with the weathered pre-Holocene of unit 1. The grey coarse sand that followed in the same core can be related to the intertidal sand of unit 2. Although both units are restricted to core BBS 34, at least the pre-Holocene bedrock must be present at locations BBS 35-37 as well, but was not reached by drilling. The decalcified loam and clay strata which compose most of cores 35-37 and dominate the upper 1.70 m in BBS 34 are equal to sediments of unit 4 that were interpreted as alluvial deposits. Unit 4 forms the fill of swale I and extends as a sheet of unknown thickness towards the east. The CaCO$_3$ rich fine sand layers at

the top of BBS 34, 36 and 37 represent the IOT 2004 deposit. It is continuously present throughout transect B; its absence in core 35, which is directly next to the river, is probably due to fluvial erosion. The fine sand layer at 1.02-0.88 m b.s. in BBS 34 corresponds to event layer B and, within transect B, is spatially restricted to swale I (fig. 10.3).

10.4.2 Sediment characteristics of tsunami layers and reference samples

As a data base for the estimation of event magnitudes, detailed multi-proxy analyses of the IOT 2004 sand sheet and the palaeo-event layers were conducted. To study lateral trends at the transect scale, the IOT deposit was analysed continuously, involving the new data of transect B (BBS 34, 36, 37) and selected cores from transect A (BBS 14, 12, 9, 6, 17, 5, 3) (fig. 10.3). Since the extent of deposits was not continuous in case of event B, only layers in cores BBS 34 (swale I) and BBS 17 (swale II) were examined. For layers C, lateral correlation was hardly possible (Brill et al., 2011) but all cores with evidence (located 70-160 m from the shoreline) were analysed. Vertical trends in grain size at the core scale were studied in 1-2 cm intervals for deposits of the IOT 2004 and event B, while only one sample was taken from each layer of events C. Foraminifera spectra were analysed exemplarily for coarse and fine sections of layers A and B, as well as layers C (fig. 10.3). Geochemistry and mineralogy analyses, due to scarcity of material from layers C, were restricted to layers A and B.

Additionally, surface sediment samples from different depositional environments of the setting were analysed as references for potential source areas of the tsunami transported material (tab. 10.1). Besides reference samples from the near-shore zone (subtidal at -2 m, beach and berm; fig. 10.1c) and terrestrial environments (limnic, alluvial, fluvial and weathered bedrock), three shelf samples from water depths of -62, -57 and -45 m (fig. 10.1b) that were not disturbed by tsunami backwash were provided by Klaus Schwarzer (Kiel University).

Table 10.1: Granulometry, mineralogy, and geochemistry of deposits from reference environments. C1-C6 = modes of grain size components determined by peak fitting (dominant components highlighted with bold letters); XRF = X-ray fluorescence; XRD = x-ray diffractometry; elements: Zr = zircon, Sr = strontium, Fe = iron, Ti = titanium, Ca = calcium, K = potassium; minerals: Q = quartz, KF = potassium feldspar, Gib = gibbsite, Ka = kaolinite; Ca = calcite; Ar = aragonite, Ca-Mg = magnesium calcite, Ha = halite.

sample	environment		mean (μm)	sorting (μm)	components (grain size)					XRF (%)						XRD (%)							
					C1 (μm)	C2 (μm)	C3 (μm)	C4 (μm)	C5 (μm)	Zr	Sr	Fe	Ti	Ca	K	Q	KF	Gib	Ka	Ca	Ar	Ca-Mg	Ha
021207-16	at -45 m	offshore	156.0	4.6	7.0	46.0	**235.0**	551.0		0.04	0.09	0.96	0.08	18.99	0.45	55				19	16	10	
031207-23	at -57 m	offshore	143.0	4.2	15.3	49.7	**194.0**	571.0	1091.0	0.05	0.07	0.84	0.10	14.74	0.46	63	5			12	13	5	1
031207-22	at -62 m	offshore	136.2	4.6	6.4	40.5	78.3	**223.0**	571.0	0.05	0.07	0.87	0.07	16.01	0.39	53	7			19	15	7	
BBS 15A	berm	near-shore	699.3	1.8	**903.0**					0.03	0.22	0.42	0.02	22.32	0.23	60	5			3	29	4	
BBS 15B	beach	near-shore	375.7	1.8	229.0	470.0				0.06	0.26	0.50	0.10	23.73	0.22	51	11			3	31	4	
BBS 15C	At -2 m	near-shore	169.1	1.6	**152.0**	489.0	1350.0			0.05	0.23	0.49	0.05	22.05	0.60	56	9			3	25	6	1
BBS 35/4	fluvial	onshore	756.1	1.8	**885.0**					0.13	0.00	0.32	0.08	0.00	0.73	83	10	7					
BBS 34A/1	alluvial	onshore	32.4	8.2	4.9	19.0	81.0	217.0	539.0	0.08	0.02	2.71	0.42	1.78	2.14	45	24	7	11	4	9		
BBS 1m	bedrock	onshore	83.3	14.1	**0.9**	**4.4**	38.0	269.0	**684.0**	0.04	0.00	3.18	0.59	0.32	1.32	82	9	9	9				

10.4.2.1 Granulometry

Vertical variations of grain size parameters revealed subdivisions into several subunits for layers A and B. Separation of subunits was based on mean grain size, by discriminating successions of normally and inversely graded sections (e.g. Fujiwara and Kamataki, 2008; Naruse et al., 2010), and sorting, using the reversal point within the vertical trend where sorting is the poorest as a border between subsequent subunits (Srisutam and Wagner, 2010). Figure 10.3 summarises the number of subunits for all studied event layers (detailed visualisations of vertical grain size trends are given in figure 10.4 for representative deposits of the IOT 2004 (BBS 37) and event B (BBS 34), more data is presented in appendix 3): Layer A consisted of 1-3 normally graded and not more than one inversely graded subunit which always formed the top of the layers. In case of layer B, 2-3 subunits with normal grading and up to one inversely graded subunit on top were distinguished. For layers C, discrimination of subunits was solely based on visual criteria, revealing 1-2 normally graded subunits in layers BBS 8-1 and BBS 8-2, and a massive structure in case of BBS 21-1 and BBS 9-3. Due to the coring technique the bedding in all other layers C was disturbed and prohibited the discrimination of subunits.
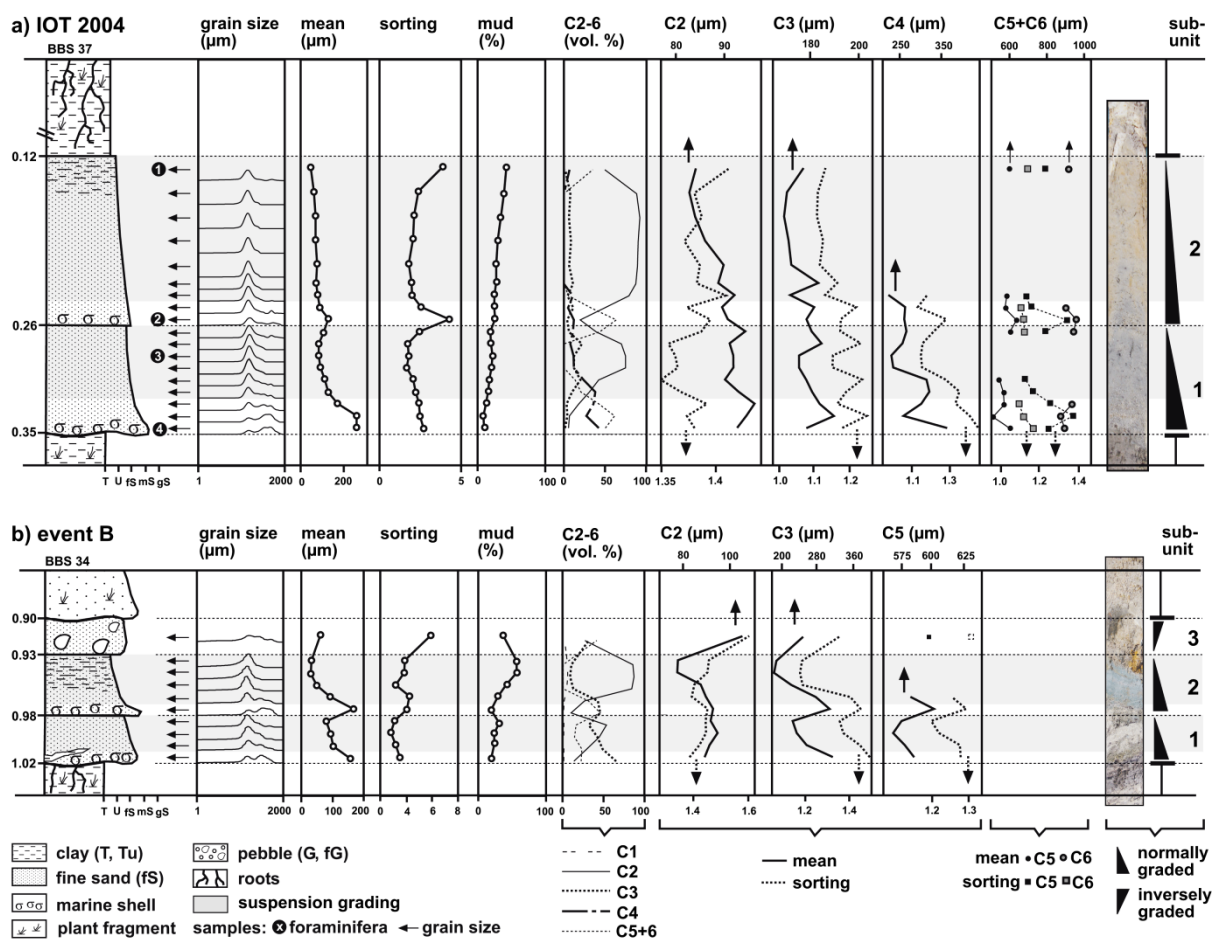
Figure 10.4: Exemplary documentation of vertical trends in grain size and grain-size components of the IOT 2004 sand sheet in BBS 37 (a), and the deposit of event B in BBS 34 (b).

By peak fitting, up to six grain-size components C1-6 were differentiated in the deposits of layer A (fig. 10.5), with peaks at <25 µm (C1, mud), 70-82 µm (C2, very fine sand), 150-260 µm (C3, fine to medium sand), 330-450 µm (C4, medium sand), 480-650 µm (C5, medium to coarse sand), and 850-1500 µm (C6, coarse sand). The same components, except for C4, were identified in layer B and some layers C (fig. 10.5). Vertically, the components varied in their relative ratios (see fig. 10.4 for BBS 37 and 34, and appendix 3 for all other cores). The basal centimetres of normally graded subunits showed a mixture of components C2-6, while the top consisted only of C1-3, clearly dominated by C2. In inversely graded sections a mixture of C2-6 was observed throughout the whole subunit. Vertical variations of mean grain size of C3, C4 and C5 mainly reflected the general fining and coarsening trends of the subunits or accentuated them. C2 only in some cores showed a weak trend in concordance with the general grading of the subunits; in most cores no clear fining or coarsening trend was observable. C1 and C6 showed no vertical trends in all cores.
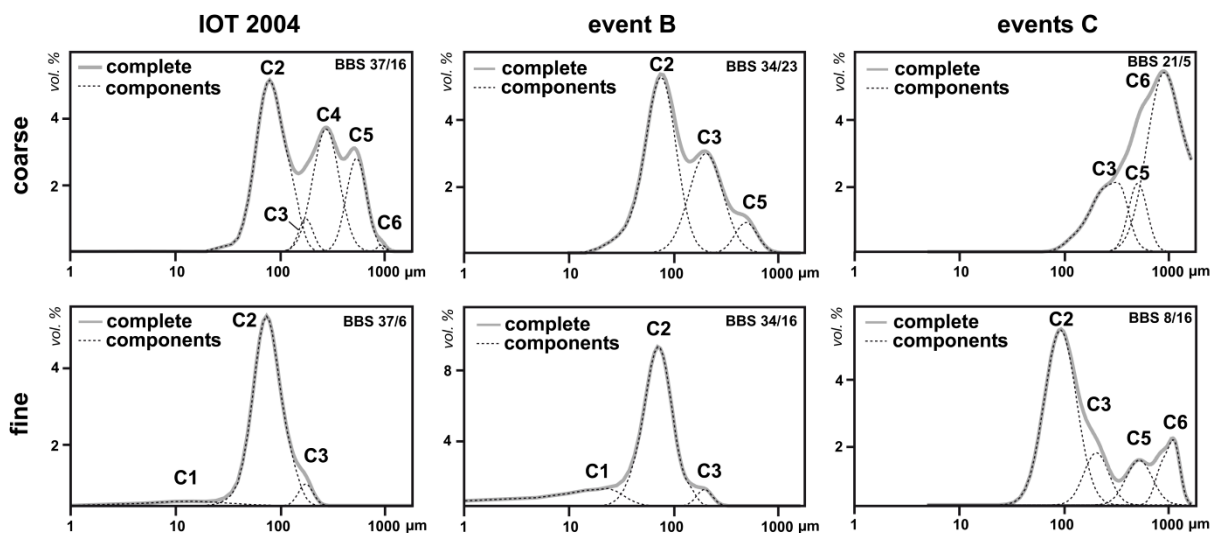
Figure 10.5: *Grain-size components in coarse and fine-grained sections of the IOT 2004, events B and C.*

Lateral trends in layer A revealed only a weak general thinning- and fining-inland trend that was obscured by topography controlled variations. Within the lowermost subunit of layer A (subunit 1), which can be correlated in all cores, no clear lateral trend was observed either. On the component scale, C2-5 showed similar landward trends like the bulk samples with, if at all, only weak thinning and fining in transect A, and slight coarsening and thickening in transect B.

10.4.2.2 Geochemistry and mineralogy

Mineralogical compositions determined by XRD analyses, and geochemical patterns analysed by means of XRF are exemplarily presented for layers A and B in figure 10.6. The composition of reference environments is given in table 10.1. Included were only the elements calci-

um (Ca), iron (Fe), potassium (K), titanium (Ti), strontium (Sr), and zircon (Zr), which had percentages of at least 0.1% in all samples.
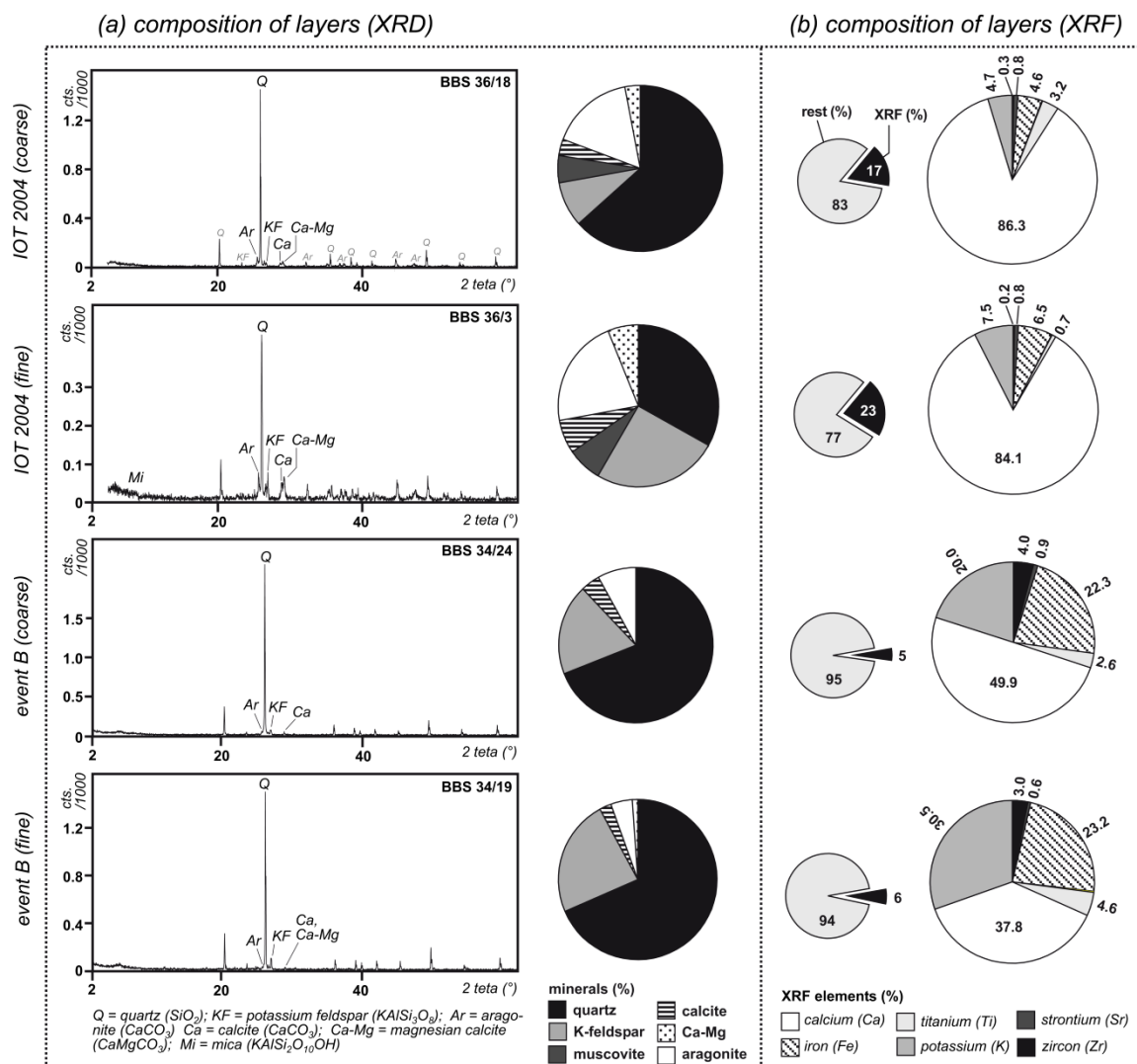
Figure 10.6: Mineralogical and geochemical compositions of tsunami deposits. XRD spectra (a) and XRF patterns (b) of coarse- and fine-grained sections of the IOT 2004 and event B.

By PCA the XRF dataset was reduced to three principal components (PCs) that describe 89% of the total variability: PC1 (63.7%) is characterised by low values of marine (Ca, Sr) and high percentages of terrestrial elements (Zr, Fe, Mn, Ti, K); PC2 (15.9%) has highly positive factor scores for Sr, Ca, Mn and K, and negative ones for Zr; PC3 is negatively correlated with Fe, Mn and Ti, and shows positive associations with Ca, K, Zr and Sr. Plotting of PC1 versus PC2 reveals distinct groups for reference samples from the shelf, the littoral zone, alluvial and fluvial environments. The IOT 2004 and event B deposits form separate groups but match none of the reference patterns (fig. 10.7a).

In case of the XRD results, PCA generated three PCs that account for 75% of the total scatter. PC1 (40.6%) shows positive factor scores for the minerals calcite, aragonite, magnesium calcite and halite, and negative ones for quartz, potassium feldspar, gibbsite and kaolinite. PC2

(21.7%) is characterised by negative values for potassium feldspar and muscovite, but positive factor scores for quartz, gibbsite, kaolinite, calcite and halite. PC3 (12.8%) is highly negatively associated with quartz and halite, and positively with kaolinite and gibbsite. Similar to the XRF results, a sample group for each reference environment (shelf, littoral and terrestrial) could be separated, while the IOT 2004 and event B deposits form distinct groups that match none of the reference patterns (fig. 10.7b).
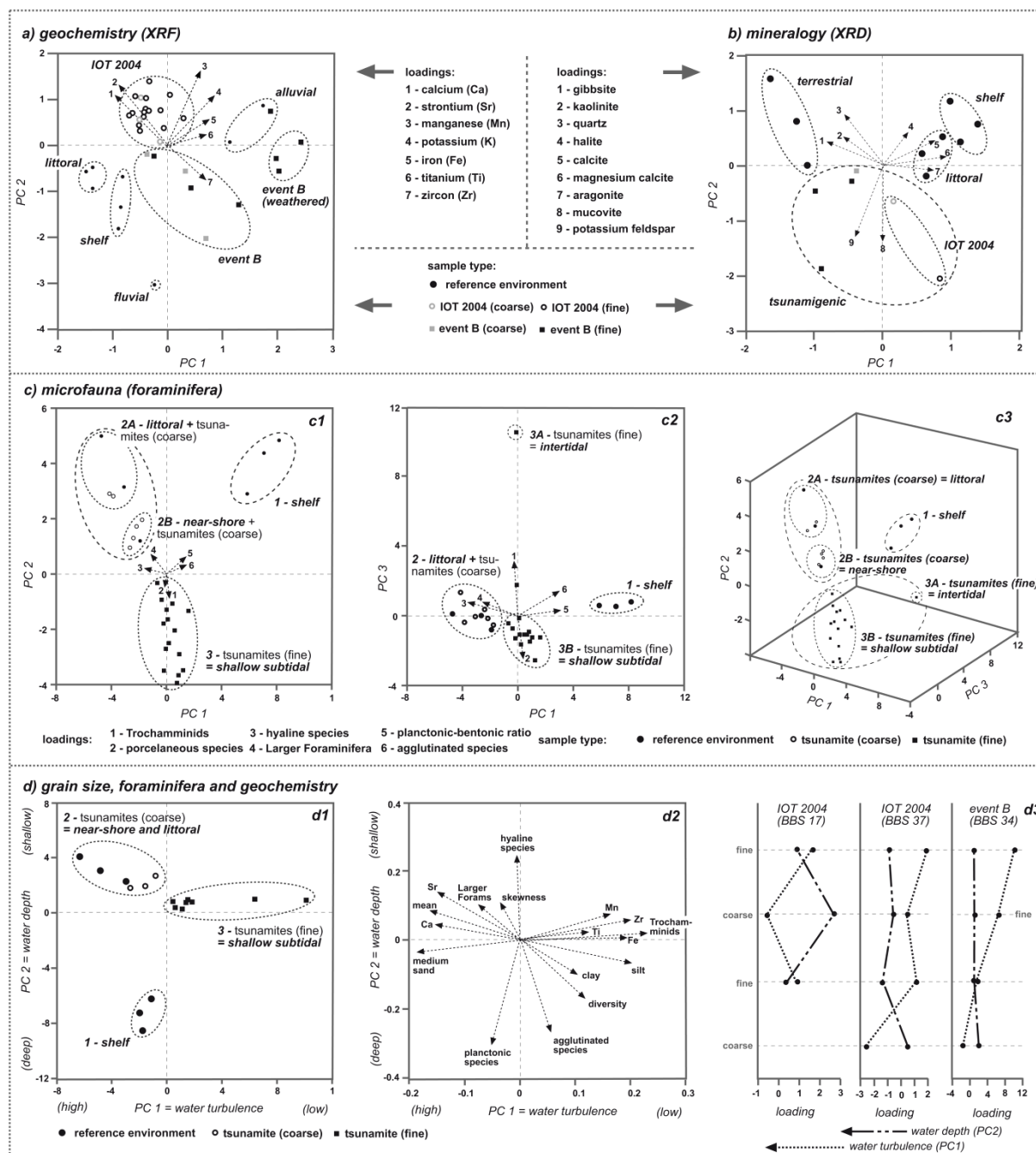
Figure 10.7: *Principal component analyses for laboratory parameters of tsunamites and reference samples: (a) PC1 versus PC2 of XRF data. (b) PC1 versus PC2 of mineral composition. (c) Plots of PC1, PC2 and PC3 on the basis of foraminifera associations. (d) Synthesis of grain-size, foraminifera and XRF data: (d1) sample loadings of PC1 and PC2; (d2) parameter loadings of PC1 and PC2; (d3) vertical variations of PC1 and PC2 in the IOT 2004 and event B deposits.*

10.4.2.3 Foraminifera

Foraminifera associations have been exploited statistically by cluster analyses and PCA. Additionally to highly correlating species, samples with <100 individuals (preclusion of BBS 14-C2 and all terrestrial reference samples) as well as foraminifera species that were present in less than three samples and did not reach 5% dominance in at least one sample (preclusion of 80 species) were excluded, while the percentages of important foraminifera groups – agglutinated species, hyaline species, porcelaneous species, trochamminids, larger foraminifera – and indices – Fisher alpha and planktonic-benthonic ratio – were incorporated in cluster analyses and PCA.
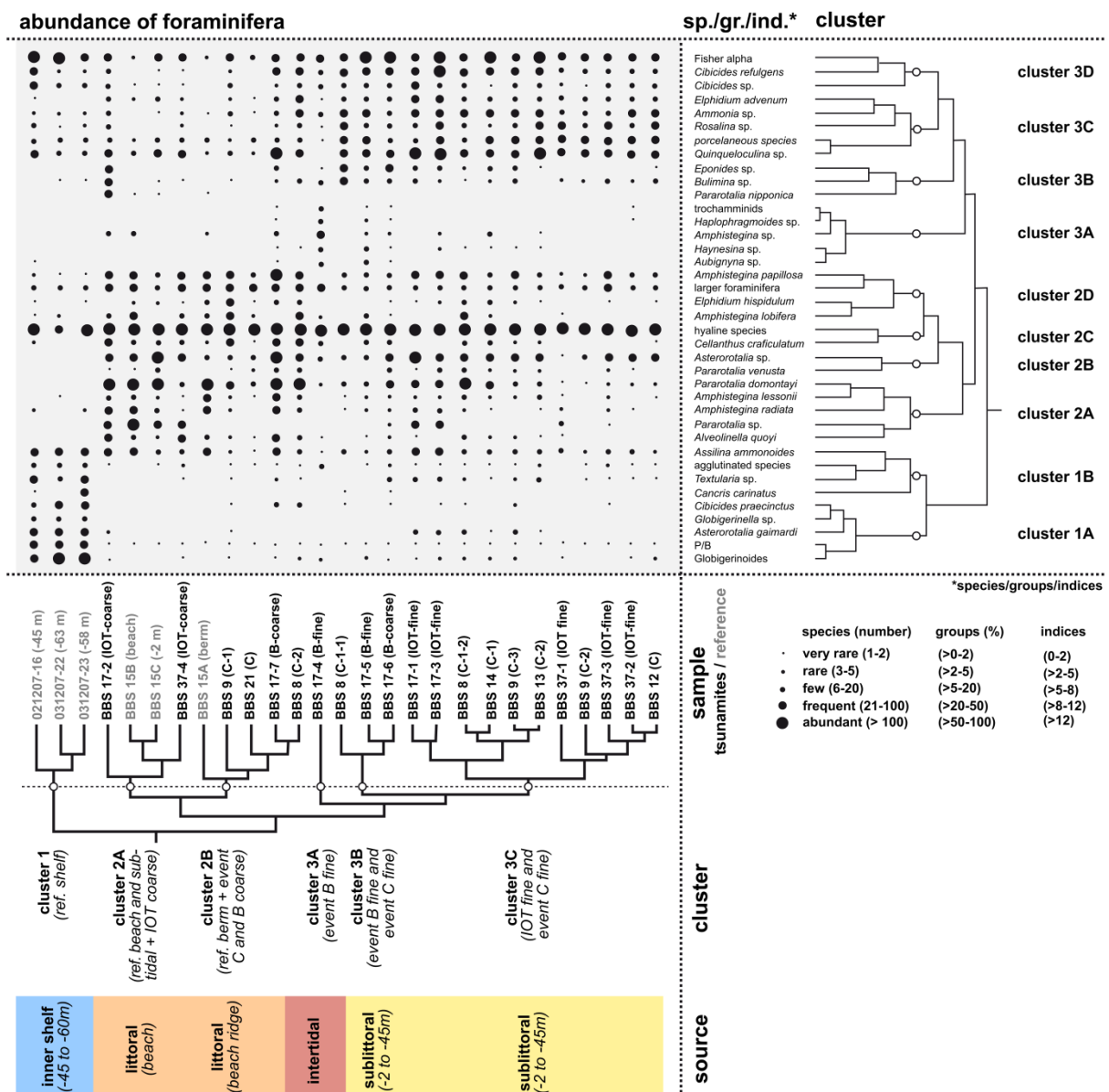
Figure 10.8: *Cluster analyses for tsunami-laid sand and reference samples based on foraminifera associations.*

Cluster analyses revealed three principal groups of samples (fig. 10.8): Cluster 1 comprises the shelf reference samples characterised by high abundances of *Globigerinella* sp., *Asteroro-*

talia gaimardi, *Cibicides praecinctus*, *Cancris carinatus*, and *Textularia* sp. Cluster 2 contains the beach and near-shore reference samples, as well as the coarse sections of the IOT 2004 and events B and C. It can be divided into cluster 2A (IOT 2004, as well as beach and shallow subtidal reference samples) and cluster 2B (events B and C, as well as beach-ridge reference sample), and is dominated by *Pararotalia* sp., *Amphistegina* spp., *Asterorotalia* spp., and *Alveolinella quoii*. Cluster 3 is formed by the fine sections of the IOT 2004, and events B and C. While cluster 3A, i.e. the finest section of event B (BBS 17-4), contains intertidal species such as *Haynesina* sp. and *Haplophragmoides* sp., clusters 3B and 3C comprise all other fine grained sections of the tsunami layers and are characterised by high numbers of *Cibicides* spp., *Elphidium advenum*, *Ammonia* spp., *Rosalina* spp., *Eponides* sp., *Bulimina* spp., and *Quinqueloculina* spp.

By PCA the foraminifera data were reduced to three principal components that account for 62% of the total variability: PC1 (25%) has high positive factor scores for planktonic and agglutinated species and negative ones for hyaline species and larger foraminifera. PC2 (20.6%) is positively related to planktonic species and larger foraminifera and negatively to porcelaneous species, and PC3 (16.5%) has high positive factor scores for trochamminids and negative scores for porcelaneous species (fig. 10.7b). Plotting of the three PCs reveals the same groups of samples like the cluster analyses: group 1 contains the shelf reference samples and is equal to cluster 1, group 2 (with subgroups 2A and 2B) summarises the littoral reference samples and coarse-grained sections of all tsunamites (equal to cluster 2), and group 3 includes the fine-grained sections of tsunami deposits just like cluster 3. Group 3 is further separated into the subgroups 3B and 3A (BBS 17-4), whereas the latter is identical with cluster 3A (fig. 10.7b).

10.4.2.4 Synthesis of measured parameters

For all samples with information about grain size, geochemistry and microfauna, PCA was performed on the complete data set (fig. 10.7d). PC1 (28.1%) is positively correlated with the mud fraction (silt and clay), terrestrial elements (Ti, Fe, Mn, Zr), agglutinated foraminifera and trochamminids, and shows negative factor scores for the sand fraction, marine elements (Sr and Ca), larger foraminifera and planktonic species. PC2 (24.8%) has highly positive loadings for hyaline foraminifera, larger foraminifera and skewness, and negative ones for planktonic and agglutinated foraminifera (fig. 10.7d2). Plotting of PC1 against PC2 reveals the same sample groups as the foraminifera data, separating the shelf reference samples (group 1), littoral deposits and coarse-grained tsunamites (group 2), as well as fine-grained tsunami deposits (group 3).

10.4.3 Modelling of hydrodynamic parameters

Inverse modelling of flow speed and flow depth was conducted for all event deposits with suspension graded sections. Since grain-size bimodality may indicate the influence of bedload transport (Sugawara et al., 2008), only unimodal sections of normally graded subunits were regarded as suspension graded. Appropriate sections were found in all normally graded subunits of layers A and B except for BBS 6-2 and BBS 5-3 (fig. 10.3 and appendix 3). Due to the wide sampling interval no suspension grading was detected in layers C. TsuSedMod used the bulk grain size and the thickness of suspension graded sections to calculate flow velocities (tab. 10.2). Since flow depth was unknown, it was determined iteratively by using a Froude number of 1. For the IOT 2004 deposits, onshore flow depths between 3.0 and 5.5 m and flow velocities of 3.0-4.9 m/s were derived. Layer B revealed slightly higher values of flow depth (4.0-7.5 m) and flow velocity (4.0-5.9 m/s).

Table 10.2: *Input and output parameters of the sedimentation model TsuSedMod (Jaffe and Gelfenbaum, 2007) for the IOT 2004 and event B. * input values are derived from suspension graded sections of the subunits only.*

	sample	subunit	distance to shore (m)	thickness* (cm)	mean* (µm)	density* (g/cm³)	min. flow depth a.s. (m)	min. flow depth a.t.l. (m)	flow velocity (m/s)
IOT 2004	BBS 9	3	129	8	78.4	2.68	2.5	3.5	3.3
		2		16	81.9		5.0	6.0	4.6
		1		13	84.7		5.5	6.5	4.9
	BBS 17	2	146	12	84.6	2.68	4.0	4.9	4.2
		1		12	85.6		3.5	4.4	3.9
	BBS 6	1	154	18	81.9	2.68	4.5	5.4	4.4
	BBS 5	2	162	18	80.6	2.68	4.0	5.1	4.1
		1		16	81.3		4.0	5.1	4.3
	BBS 3	2	194	8	76.4	2.68	2.5	4.2	3.3
		1		10	80.1		3.5	5.2	3.8
	BBS 34	1	260	3	72.8	2.68	4.0	5.0	4.2
	BBS 36	2		6	70.4	2.68	2.2	3.5	3.0
		1		4	94.3		3.5	4.8	3.9
	BBS 37	2		12	75.4	2.68	3.5	6.0	3.9
		1		5	94.5		3.0	5.5	3.7
event B	BBS 17	3	146	3	61.3	2.68	6.0	3.9 /5.5 /7.1*	5.2
		2		3	77.7		7.5	5.4 /7.0 /8.6*	5.9
		1		4	88.5		7.5	5.4 /7.0 /8.6*	5.9
	BBS 34	2	260	4	44.5	2.68	4.0	3.9 /5.5 /7.1*	3.9
		1		3	93.2		4.0	3.9 /5.5 /7.1*	4.1

10.5 Discussion

10.5.1 Sources of tsunami deposits

Granulometry

Using the modes of grain-size components C1-6 (fig. 10.5) and relating them to different reference samples, source areas of the tsunami deposits were determined: Component 1 seems to have its origin in the muddy pre-tsunami soils, C2 was most probably derived from the subtidal zone below two meters water depth (-2 to -45 m), C3 and C4 are probably related to the beach, C5 to the beach ridges, and C6 represents shell fragments from various marine environments. Tsunami deposits of the IOT 2004 and event B are generally dominated by marine material from the subtidal zone between -2 and -45 m (C2) in the fine section, and by material from the beach and beach ridges (C3 and C5) in the coarse sections. In contrast, the granulometry of layers C points either to the littoral zone (beach and beach ridges) as the only sediment source (e.g. BBS 21-1), or to a mixed sediment source from the littoral and -2 to -45 m water depth. However, although most of the onshore tsunami deposits have their origin at the beach and the zone between -2 and -45 m, the presence of a minor contribution from the shallow shelf deeper 45 m water depth cannot be excluded by means of granulometry, since C2 is also a minor component of the shelf reference samples.

Geochemistry and mineralogy

Neither the IOT 2004 deposits nor that of event B can be related to one of the reference environments based on XRF and XRD analyses (figs. 10.7a, b). Both event deposits have their own geochemical and mineralogical signatures. However, the IOT 2004 deposits are most closely related to the marine environments of the shelf and the littoral zone in respect of both, mineralogy and geochemistry. The differences are probably the result of post-depositional weathering, which is known to affect easily leachable minerals and elements after only a few years (Szczuciński, 2012). The deposits of event B reveal less marine influence and a chemical and mineralogical signature tending slightly more towards terrestrial environments, especially in the upper part of the layer (figs. 10.6 and 10.7). These differences rather point to more intensive weathering of the event deposits due to their older age, than to differences between the source areas. Thus, although the chemical and mineralogical properties of the IOT 2004 and event B all in all point to marine source areas of the deposits, due to post-depositional changes the data are not adequate for a further differentiation of marine environments.

Foraminifera

Both, PCA and cluster analyses reveal three main groups or clusters of samples based on their foraminifera associations (figs. 10.7 and 10.8). Clusters 1 and 2 can be related to offshore

source areas on the basis of reference samples within the clusters: Cluster 1 represents material from the inner shelf (-45 to -60 m), and cluster 2 can be assigned to littoral and near-shore deposits. Thus, the coarse-grained sections of the tsunami deposits contained in cluster 2 were derived from the beach and the shallow shoreface. Cluster 3 originates from source areas not covered by reference samples. Since most species characteristic for the inner shelf at -45 to -60 m water depth are absent, the samples inside cluster 3, the fine-grained sections of tsunami deposits, are supposed to represent shallower water, i.e. the zone between -2 and -45 m. The incorporation of marsh fauna in cluster 3A, i.e. the top section of event B, is probably the result of post-depositional processes connected to the intertidal marsh that established after event B. In conclusion, foraminifera associations of the IOT 2004, event B and most layers of events C point to sediment sources in the littoral zone for coarse-grained sections, and in the subtidal zone shallower than 45 m water depth for fine-grained parts. Although cluster analyses point to further subdivision of sources between -2 and -45 m (clusters 3B and 3C), they cannot be quantified, since reference samples in these water depths are missing. Different from that, some layers of events C exclusively come from the littoral zone (BBS 21-1, BBS 9-C1).

Synthesis

The driving factors that predominantly determine the joint sedimentary characteristics of grain size, geochemical and mineralogical compositions, as well as foraminifera content (fig. 10.7d) are interpreted as the turbulence of the water during sedimentation (PC1) and the water depth at the source area (PC2). Together they define two main sediment source areas for onshore tsunami deposits of the IOT 2004 and its predecessors (fig. 10.9): Coarse-grained sections were eroded at the beach and the shallow subtidal down to 2 m water depth, while fine-grained material originates from water shallower than -45 m (a more precise localisation was hindered by missing reference samples between -2 and -45 m). Sediments from terrestrial environments and the inner shelf below 45 m water depth are not significant contributors. This result is consistent with previous estimates for IOT 2004 deposits in Thailand that postulate source areas shallower than 20 m water depth (Szczuciński et al., 2006; Hawkes et al., 2007; Srisutam and Wagner, 2010). However, tsunami deposits represent mixtures of sediment originating from different zones (e.g. Hawkes et al., 2007; Sawai et al., 2009; Horton et al., 2011), and the dominance of sediment derived from the beach and near-shore zone may mask evidence of more distal source areas that are simply underrepresented and, thus, statistically insignificant. Hence, the determined source areas indicate the zones where most material was eroded, but probably do not indicate the maximum water depth of tsunami wave erosion.
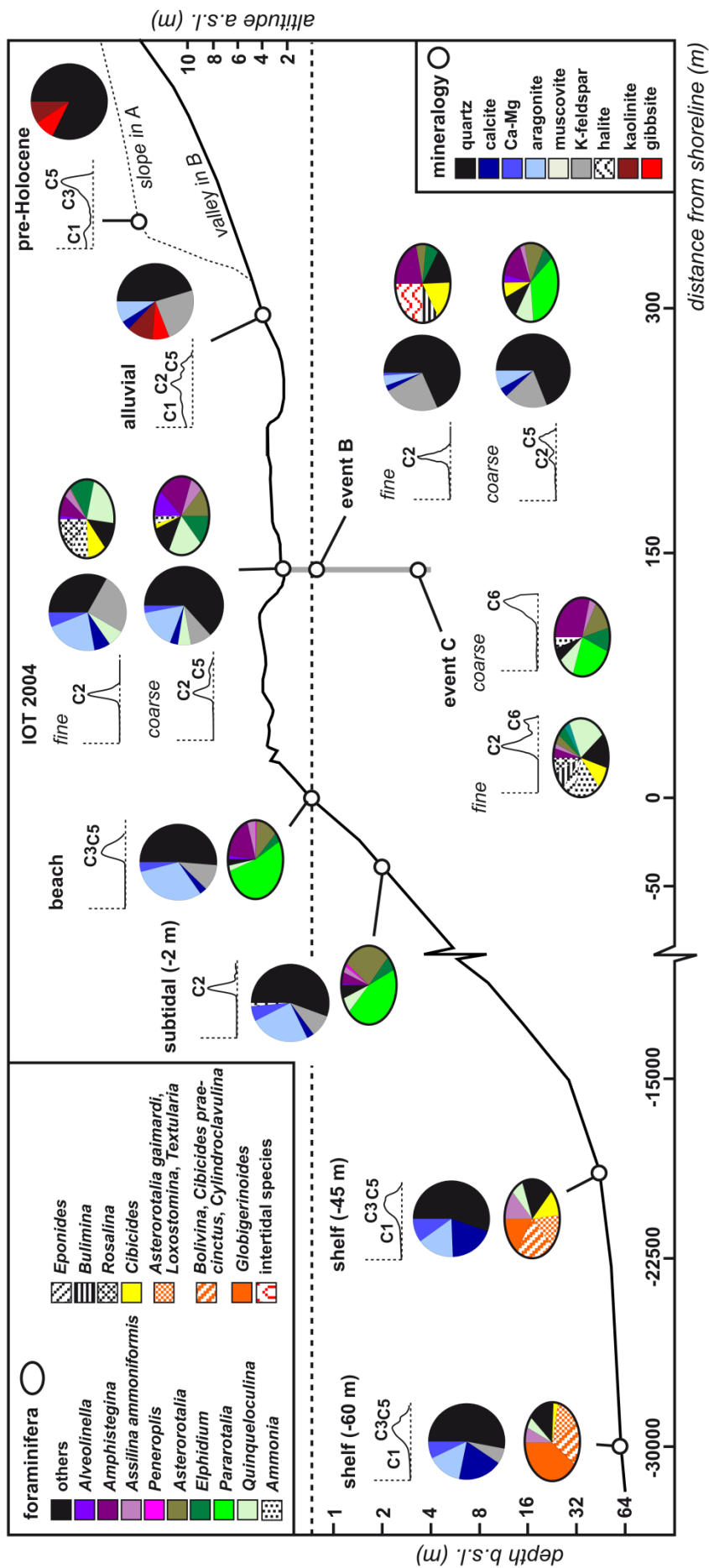
Figure 10.9: *Signatures (grain size [curve], mineralogical composition [circles], foraminifera association [ellipsoids]) of onshore tsunami deposits compared to reference samples from terrestrial and marine environments.*

10.5.2 Tsunami inundation and transport processes

Each subunit of the tsunami deposits (fig. 10.4) is supposed to be accumulated by a single inflow or backwash of the tsunami wave train. Considering the sedimentary structure of ideal onshore tsunami deposits (Fujiwara and Kamataki, 2008) and its proposed modification due to erosion by subsequent waves (Naruse et al., 2010), the observed succession of normally and inversely graded subunits in the IOT 2004 deposits reflects three tsunami inflows and the final withdrawal of the water (fig. 10.10). This number of inundating waves is in accordance with observations from the Thai coast (Bell et al., 2005; Szczuciński et al., 2006; Hori et al., 2007). While the run-up deposits of inflows 1 and 2 are continuous throughout both transects, a third inflow unit is preserved only at the margin of swale II (BBS 9), and backwash deposits are restricted to the deeper parts of the swales. This discontinuity is probably the result of interactions between the second and the third tsunami wave which led to a combined sedimentary unit locally, and re-erosion of inflow deposits by concentrated final backwash in topographic depressions (e.g. Fagherazzi and Du, 2008). The subunits of event B reflect three tsunami inflows and – in swale I – the final backwash.
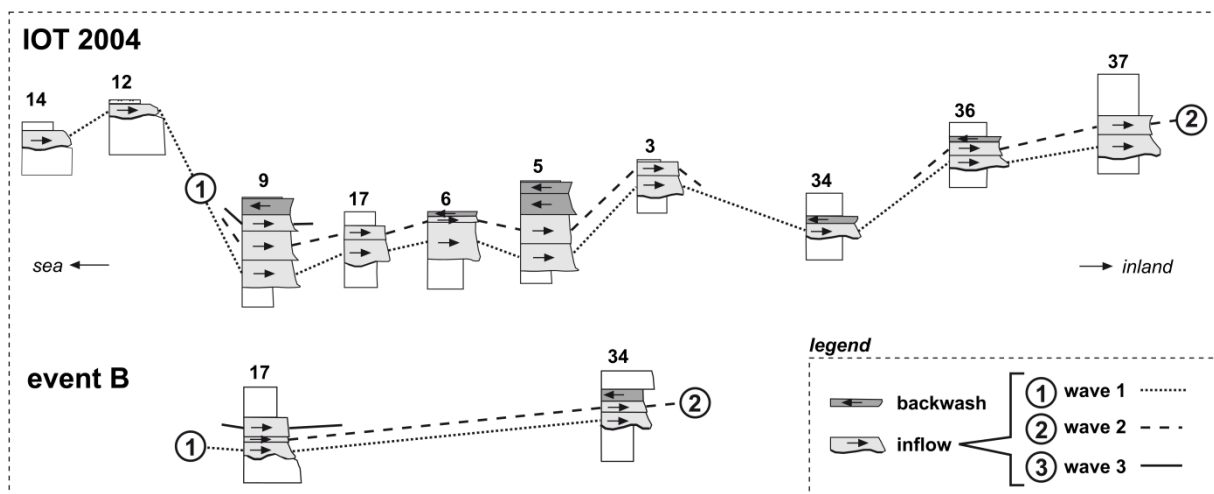
Figure 10.10: Lateral correlation of inflow and backwash units in the sand sheets of the IOT 2004 and event B.

Although tsunami inflow proceeded from the west to the east approximately perpendicular to the coast, the continuous inflow deposits of the first two IOT 2004 waves show only slight fining and thinning trends (see appendix 3), because deposition and erosion of the tsunamites is affected by changes in topography as well. While the absence of any shore-normal trend in the third inflow deposit and layer B is due to their discontinuous spread, the missing trend in the IOT 2004 backwash layer is explained by its deviating flow direction due to flow concentration in topographic depressions (Umitsu et al., 2007).

The vertically varying percentages of grain-size components C1-6 within inflow and backwash units reveal different transport processes (Nanayama and Shigeno, 2006; Fujiwara and Kamataki, 2008; Moore et al., 2011): the basal sections of inflow deposits as well as the

whole backwash units that are poorly sorted and dominated by littoral sediment sources (C3-6) seem to have been transported as bedload or traction carpet, while the top sections of inflow layers that are well sorted and mainly composed of sediment from submarine sources (C2) were deposited out of suspension. This assumption is supported by vertical variations of PC1 (water turbulence) and PC2 (water depth) in the deposits of the IOT 2004 and event B (fig. 10.7d3) that reveal repeated changes from sedimentation under highly turbulent conditions to settling from suspension. The vertical and lateral fining trends of grain-size components C3-5 indicate that material from the littoral zone is sorted during onshore tsunami flow, while material derived from distant sources (C2) that has been transported over kilometres in the tsunami waves is already well sorted at the coast and, thus, shows no significant lateral or vertical trends in onshore tsunami deposits. Since sediment from distant sources (-2 to -45 m) dominates the tsunami deposits at Ban Bang Sak, the trends within bulk samples are only vague and mainly the result of declining bedload and increasing suspension load percentages.

10.5.3 The magnitude of tsunami events

10.5.3.1 Hydrodynamic parameters of tsunami inundation inferred from inverse modelling

Based on the correlation of subunits with successive tsunami inflows, shore normal trends of flow velocity and flow depth were reconstructed for waves 1 and 2 of layers A and B, respectively, using the inverse model TsuSedMod (Jaffe and Gelfenbaum, 2007). Between 130 m and 430 m east of the shoreline the calculated flow depth slightly decreased from 5.5 m to 3.0 m in wave 1 of the IOT 2004. For the second inflow, a comparable reduction of water depth from 5.0 m to 3.5 m was calculated. The respective flow velocities decreased from 4.9 to 3.7 m/s during the first inflow and from 4.6 to 3.9 in wave 2 (fig. 10.11a). Thus, the relative strengths of the first two inflows are comparable. Measured tsunami wave heights for a flat coastal plain ~1 km north of the sampling site revealed values of 6-11 m a.t.l. (since the IOT 2004 arrived at high tide, the tide level was at +1.50 m a.s.l.) at a distance of 50-400 m from the shoreline (Goto et al., 2008). These values should be representative for the study location as well. Assuming this, flow depths calculated with TsuSedMod are slightly too low (fig. 10.11a). However, since the model depths are based on Froude numbers of 1.0 and therefore represent minimum estimates, the results seem to give quite realistic values of minimum flow depths. The most reliable reference for the evaluation of modelled flow velocities is 6-8 m/s inferred from survivor videos from the Khao Lak area (Rosetto et al., 2007). Since distance from the shoreline and topography at this site remains unclear, the values are expected to be maximum estimates. Thus, the velocities derived with TsuSedMod, although approximately one third lower, seem to be realistic.
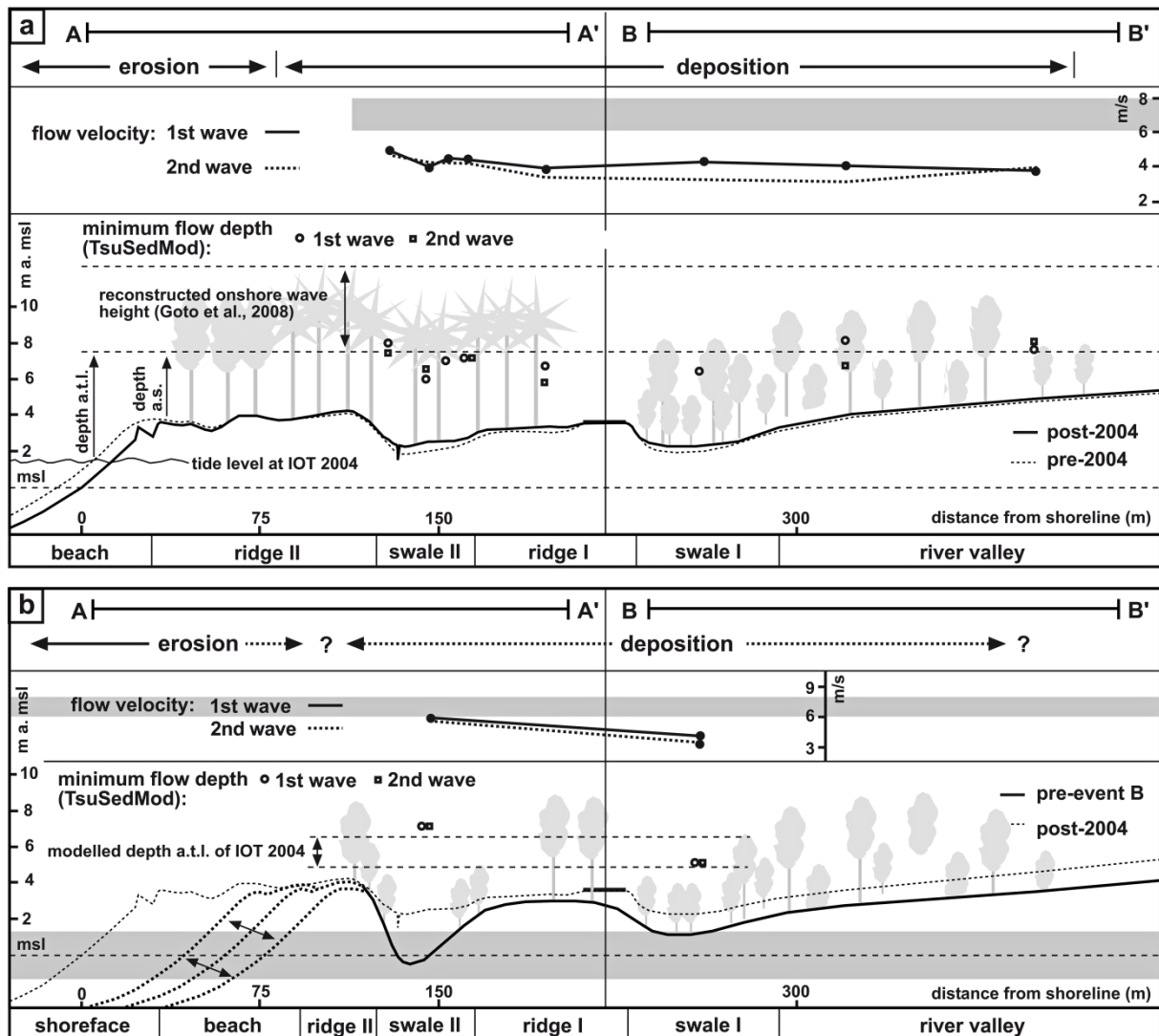
Figure 10.11: *Modelled flow depths and flow velocities for the IOT 2004 (a) and event B (b) perpendicular to the shoreline using the inverse model TsuSedMod (Jaffe and Gelfenbaum, 2007). (a) Modelling results for the three waves are compared to flow velocities reconstructed from survivor videos (Rosetto et al., 2007) and flow depth estimates from post-tsunami survey (Goto et al., 2008). (b) Modelled parameters are compared to IOT 2004 modelling results corrected for altitude changes in tide level and ground surface, as well as shifts in shoreline position. a.t.l. = above tide level; a.s. = above surface.*

In case of layer B, although based on only two cores, flow depth and flow velocity decreased with increasing distance from the shoreline; further inland the deposit of event B is not preserved (fig. 10.11b). During the first inflow the calculated water depth reduced from 7.5 m at 146 m east of the shoreline to 4.0 m at 360 m. Over the same distance, flow velocity diminished from 5.9 to 4.1 m/s. The second inflow reveals comparable model results with velocities of 5.9-4.0 m/s and depths of 7.5-4.0 m. All in all, the modelled flow velocity and depth of event B are slightly higher compared to the IOT 2004. However, for a reasonable interpretation of these values, the boundary conditions at the impact time of event B have to be considered (fig. 10.11b): (i) sea level 600 years ago, which is the inferred timing of event B (Brill et al., 2011), had already reached its present position, but tide level is not predictable and may

have been up to 2.5 m lower than that during the IOT 2004, if event B occurred during low tide (Scheffers et al., 2012a); (ii) the ground surface prior to inundation by event B was ~3 m lower than today at BBS 17 and 1 m lower at BBS 34, respectively (fig. 10.11b); (iii) although the exact position of the shoreline is unknown, it was definitely located east of its present position, somewhere within ridge II (coastal accretion; Brill et al., 2011).

Since tide level and level of ground surface are not constant, the onshore flow depth above ground surface as calculated by TsuSedMod is not adequate to compare values of the IOT 2004 and event B. Better comparability is ensured by using the flow depth above tide level, which accounts for differences in water level and surface elevation. Assuming a moderate tide level around mean water for event B, the flow depths calculated for event B are comparable to that modelled for the IOT 2004 (tab. 10.2 and fig. 10.11). The further east position of the shoreline reduces the inland distance of the sampling sites by up to 100 m. Since flow depth and velocity generally decrease with distance from the shoreline (e.g. Jaffe and Gelfenbaum, 2007; Richmond et al., 2011), elevated values compared to the IOT 2004 have to be expected at each sampling site for waves of the same size.

Potential post-sedimentary disturbances of event B deposits, which would affect modelling results, are reduction of deposit thickness by erosion or soil development and changes in grain size due to bioturbation (Szczuciński, 2012). While changes in thickness have only a minor effect on the results of TsuSedMod, the model is sensitive for grain size changes (Jaffe and Gelfenbaum, 2007). However, significant disturbances, if present, would have been detected in the suspension graded sections. The effect of variations in bed roughness, which was only estimated empirically, was discussed elsewhere (Jaffe and Gelfenbaum, 2007; Jaffe et al., 2011).

10.5.3.2 *Wave parameters estimated from sediment sources*

Uchida et al. (2010) used the maximum offshore sediment source (water depth and distance from the shoreline) of tsunami deposits determined on the basis of foraminifera associations, to estimate hydrodynamic parameters (period and amplitude) of the associated tsunami waves. The same is possible for sediment sources of tsunami deposits from Ban Bang Sak. However, the rather wide source area of 45 to 2 m water depth that was determined for the local tsunamites implies transport distances between 20 km (40 m water depth) and less than 8 km (10 m water depth). Although the corresponding wave parameters in the model of Uchida et al. (2010) are in agreement with those measured during the IOT 2004, i.e. wave periods of 10-30 minutes and maximum offshore amplitudes of 1-2 m (Choowong et al., 2007; Tsuji et al., 2006), they do not allow for a prediction of unknown wave parameters in case of prehistoric tsunami events. A smaller range of the source area which would be necessary to improve the model input parameters is limited by (i) missing reference samples from water depths between

2 and 45 m which hinders a further differentiation on the basis of comparison, and (ii) the shallowness of the source area that does not allow for a detailed discrimination of depth levels based on the ecological ranges of foraminifera as it was done in other regions, e.g. by Nanayama and Shigeno (2006), Uchida et al. (2010), or Horton et al. (2011).

10.6 Conclusions

The applicability of sedimentation modelling with TsuSedMod and the determination of sediment sources as approaches to assess the local tsunami magnitude were validated by using the intensively studied tsunami of 2004 as a modern analogue. (1) Modelled onshore flow velocities of 3.7-4.9 m/s and a maximum flow depth of 5.5 m are reasonable values compared to the 6-8 m/s fast and 7-11 m deep onshore tsunami flow that was reconstructed on the basis of survivor videos and post-tsunami surveys from the study area (Rosetto et al., 2007; Goto et al., 2008). (2) Multi-proxy analyses indicate that material from the littoral zone transported as bedload, and suspended sediment from water shallower than 45 m water depth were the main sources of the IOT 2004 onshore tsunami deposits. Although this sediment source area is in accordance with sedimentary studies from other locations in southwest Thailand, the determination is not precise enough to use it for the assessment of wave parameters.

Since both approaches provide realistic results for the IOT 2004, they were suggested to be applicable for prehistorical tsunami deposits at Ban Bang Sak as well. (i) For the youngest predecessor that was dated to 500-700 cal BP, flow velocities of 4.1-5.9 m/s and, taking changes in tide level and ground surface between the two events into account, flow depths of 7.0 m were modelled. Just as in the case of the IOT 2004, the maximum offshore sediment source of its deposits was mainly the area shallower than 45 m water depth. All in all, the predecessor is suggested to have had a similar magnitude as the IOT 2004. The rather low values compared to inflow speeds reported elsewhere (e.g. 10-15 m/s during the IOT 2004 along northern Sumatra: Borrero, 2005) are due to the shallow and wide shelf of SW Thailand and therefore typical of the study area, even for mega tsunamis like the IOT 2004. (ii) As for several prehistorical events dated to 1180-2000 cal BP, the sedimentary structure did not allow for the application of sediment modelling. However, the maximum offshore sediment source was mainly the area shallower than 45 m water depth, which points to similar transport distances of onshore deposits like 2004. Only one of these events that showed sediments solely derived from the littoral zone down to 2 m water depth is attributed to storms or small tsunamis rather than a mega-event such as the IOT 2004.

Chapter 11

11 Synthesis and conclusions

11.1 Introduction

To conclude what this study can contribute to a better understanding of tsunami risk in southwest Thailand and the whole Indian Ocean, *Chapter 11.2* provides a synthesis of the results from all study sites by commenting directly on the research hypotheses and research goals formulated in *Chapter 1.2*. Eventually, *Chapter 11.3* gives a perspective on the value of the presented results for the assessment and handling of future tsunami risk.

11.2 New insights into the tsunami histories of Thailand and the Indian Ocean

11.2.1 Sedimentary evidence of prehistoric tsunamis

Hypothesis 1 – The coastal sediment record of southwest Thailand is an appropriate archive to improve the database of prehistoric tsunamis in the Indian Ocean.

Ad goal I - Identification of new palaeotsunamis

Various types of coastal sedimentary archives in the study area were investigated in order to identify so far undetected evidence of prehistoric tsunamis. For this, extreme coastal flooding events, either storm or tsunami, had to be identified first, and distinguished into tsunami-laid sediments and storm-induced deposits, in a second step.

(i) Evidence of extreme wave events. The identification of extreme flooding events in the coastal sediment successions of the study area was based on sedimentary properties that reflect highly energetic flow conditions, such as sharp basal contacts, rip-up clasts, flow structures, and graded sublayers, as well as on the allochthonous marine origin of these layers, indicated by marine fauna and geochemistry, confined by terrestrial or brackish background sedimentation. Event deposits older than 2004 could be traced at least at three locations within the study area (fig. 11.1): In the deeper swales of the beach-ridge plain on Phra Thong Island (palaeoevents B, C, and D in *Chapter 6*), in swampy swales (palaeoevent B) and fine-grained alluvial deposits (palaeoevents C1-3) at Ban Bang Sak (*Chapter 4*), and in a back-reef milieu (palaeoevent B) and the sheltered subtidal (palaeoevent C) at Pakarang Cape (*Chapter 8*). The existence of event layers is dependent on the suitability of the site-specific geoarchives for the accumulation and preservation of evidence, and on the persistence of these archives during

the Holocene. Since coastal evolution varied locally, the number and timing of events record-ed on Phra Thong, at Ban Bang Sak, and at Pakarang Cape is different at each site (*Chapter 8*), whereas at all other locations visited during field work in Thailand – mangrove forest and lagoons on Phuket, dry and water-filled karst sinkholes of the tower karst islands Hong and Pha Nak, sandy coastal plains on Kho Khao Island and at Ban Bang Niang – due to different reasons – e.g. the age of the landforms, the exposure to tsunamis and storms, bioturbation, and weathering – no clear evidence of past extreme events could be identified at all (fig. 11.1).
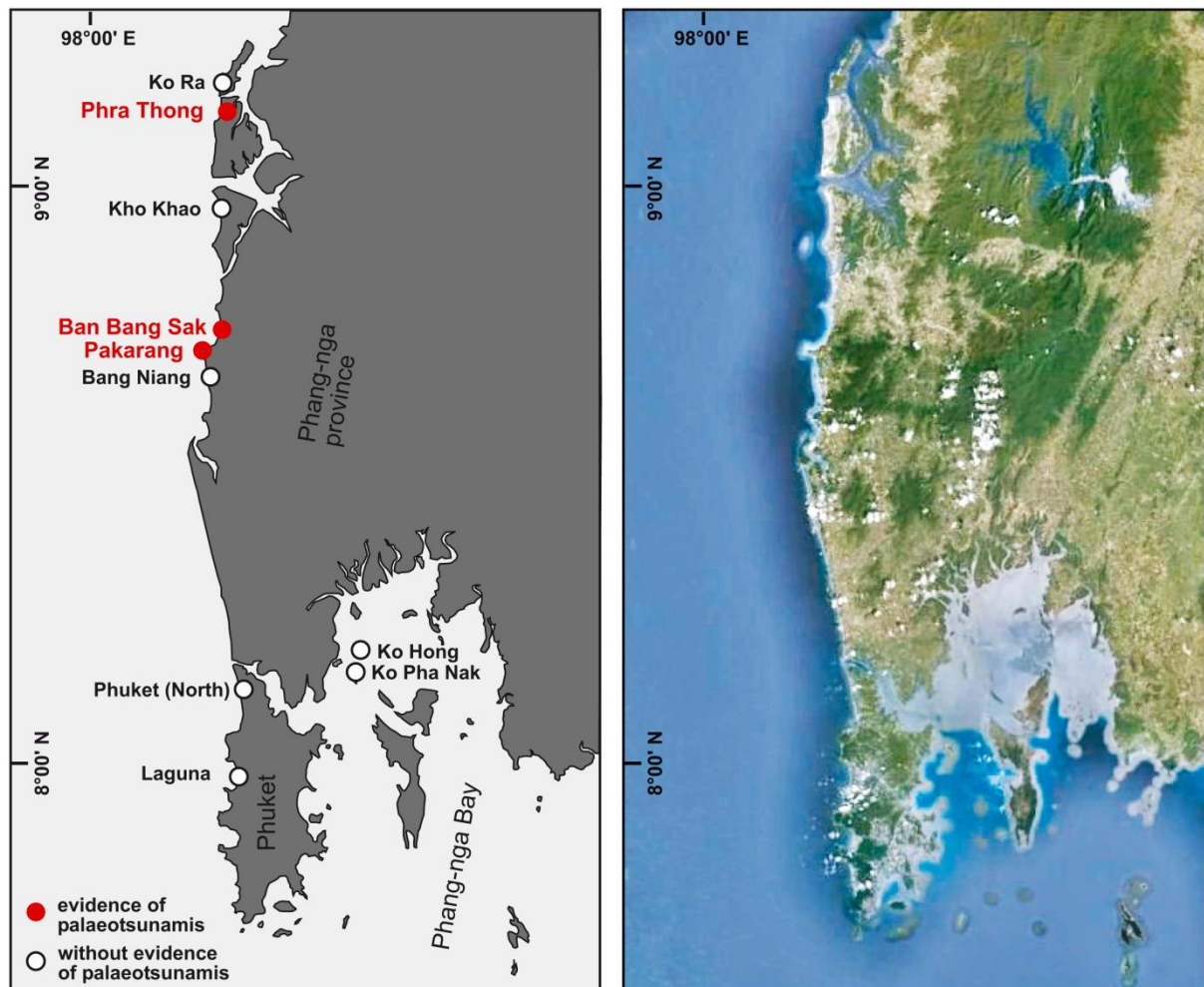
Figure 11.1: Schematic map and satellite image (Google Earth, 2012) of locations investigated during field work in southwest Thailand. Only Ko Phra Thong, Ban Bang Sak and Pakarang Cape yield definite evidence of prehistoric tsunamis, whereas all other sites are characterised by a lack of suitable geoarchives.

(ii) Discrimination between tsunamites and tempestites. Since sedimentary imprints of storm and tsunami due to very similar hydrodynamic transport and sedimentation processes as well as similar sediment source areas cannot be discriminated on the basis of universal sedimentary criteria alone, site-specific strategies to distinguish between both types of sediments were ap-plied. This included (a) comparison with local variations of the IOT 2004 deposit as a refer-ence for a modern tsunamite, (b) the evaluation of probabilities for the impact of bypassing storms and tsunamis, and (c) inferences from magnitude parameters, such as inundation

width, onshore flow depth, or impact radius. By these criteria, all palaeoevent layers on Ko Phra Thong, event layer B and two layers C from Ban Bang Sak, as well as layer B from Pakarang Cape were assigned to a tsunami origin, whereas palaeoevent C at Pakarang Cape and one of the events C from Ban Bang Sak could have been generated either by strong storms or tsunamis.

→ *Although the general preconditions in the study area do not favour the preservation of tsunami-laid deposits, evidence of palaeotsunamis could be identified locally and, thus, could be used to expand the record of prehistoric tsunamis in the Indian Ocean.*

11.2.2 The chronology of Holocene tsunami events

Hypothesis 2 – Sedimentary imprints of tsunamis can be used to establish recurrence intervals for local and regional events.

Ad goal II - Dating of palaeotsunamis

Local tsunami chronologies for the study area were established (i) by dating newly identified evidence at Ban Bang Sak and Pakarang Cape, and (ii) by improving the ages of poorly dated tsunami evidence on Phra Thong Island using appropriate dating techniques.

(i) Dating of the newly identified palaeotsunami deposits at Pakarang Cape and Ban Bang Sak was based on the radiocarbon technique (*Chapters 4 and 8*). If possible, terrestrial plant remains from in-situ strata above and below the tsunami deposits (sandwich dating) were used for dating, in order to avoid errors due to reservoir effects and contamination with fossil carbon, as well as age over-estimation due to relocated or reworked material. By this, ages of 1000-1200 cal BP for event B at Pakarang Cape, and 500-700 cal BP for event B at Ban Bang Sak were determined. Where only material from inside the tsunami deposits was available for dating, the determined ^{14}C-ages were interpreted as maximum values for the age of the tsunamites, so that all three palaeoevents C at Ban Bang Sak could only be dated to the period between 1180 and 2000 cal BP.

(ii) The tsunami deposits on Ko Phra Thong had already been identified by Jankaew et al. (2008), but could not be dated with sufficient precision and accuracy by radiocarbon. As an alternative approach, optically stimulated luminescence was applied to determine direct ages for the tsunami-laid sand sheets (*Chapters 5 and 6*). The applicability of the approach could successfully be evaluated by dating the modern reference deposit of the IOT 2004 with an age offset of less than 40 years. In case of prehistoric tsunamis, OSL yielded ages of 490-550 years for event B, 925-1035 years for event C, and 1740-2000 years for event D.

Ad goal III – correlation of spatially distinct tsunami evidence

In a second step, the ages of tsunami layers were used to correlate spatially distinct palaeotsunami evidence on different spatial scales. The combined dataset of various sites enabled to reconstruct better constrained recurrence intervals for the study area (fig. 11.2):
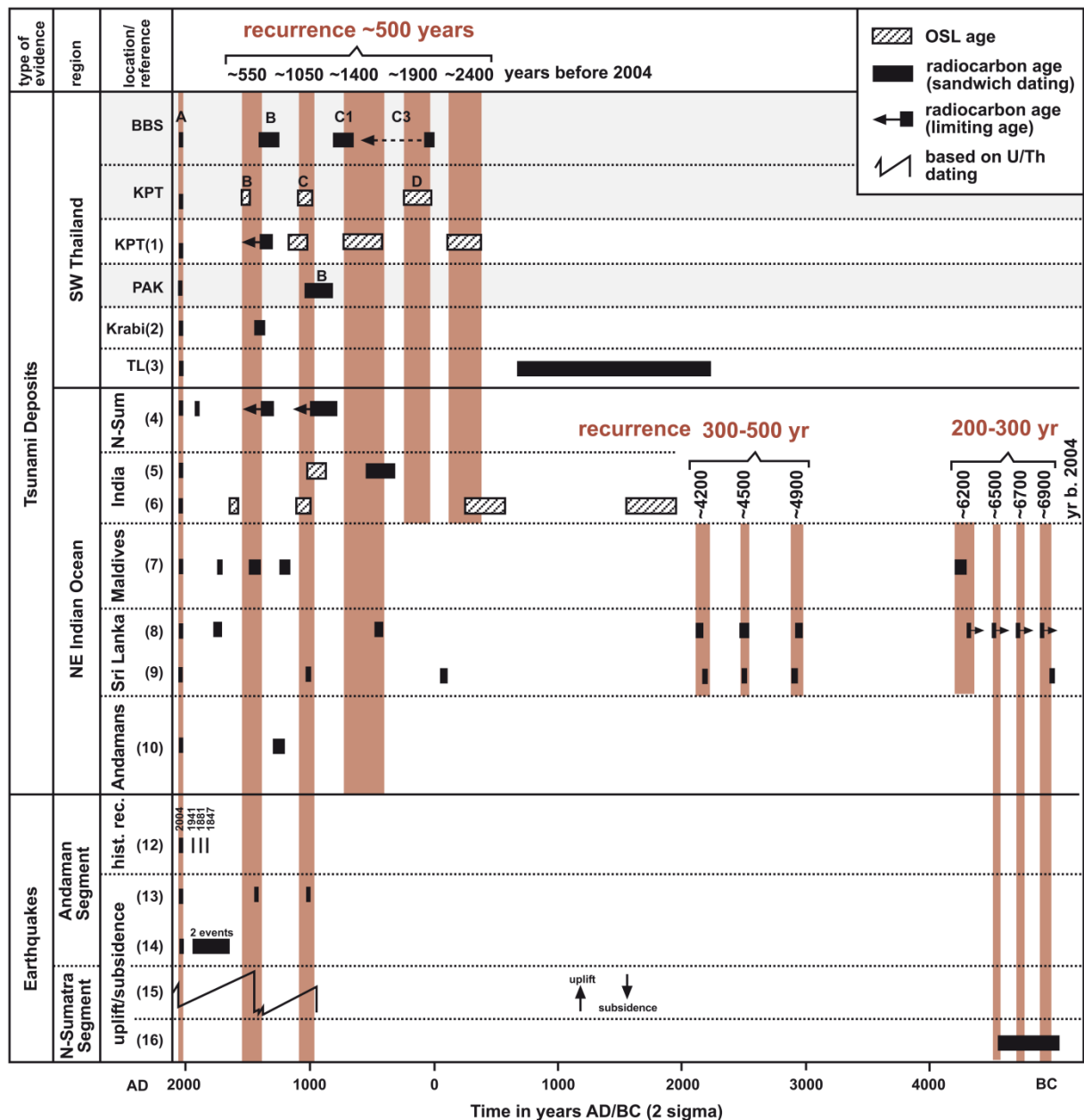
Figure 11.2*: Correlation of geological tsunami evidence from Thailand (shaded areas mark results of this study: BBS = Ban Bang Sak, KPT = Ko Phra Thong, PAK = Pakarang; 1 – Jankaew et al., 2008 and Prendergast et al., 2012; 2 – Harper, 2005; 3 – Rhodes et al., 2011) and other coastal areas around the Indian Ocean (4 - Monecke et al., 2008; 5 – Rajendran et al., 2006, 2011; 6 – Nair et al., 2011; 7 – Mörner, 2007; 8 – Jackson, 2008; 9 – Ranasinghage et al., 2010; 10 – Malik et al., 2010) with historical (12 – Bilham et al., 2005) and geological earthquake evidence (13 – Rajendran et al., 2008; 14 – Malik et al., 2011; 15 – Meltzner et al., 2010; 16 – Grand Pre et al., 2012) in the North-Sumatra-Andaman Zone.*

The local scale: Time-overlapping tsunami evidence in distinct swales of Ko Phra Thong that – since laterally discontinuous and highly variable in its sediment characteristics – could not be correlated by other criteria than dating was linked on the basis of OSL ages and chronological data of previous and parallel studies (Jankaew et al., 2008; Prendergast et al., 2012). By this, a local recurrence period of 500-600 years was estimated for tsunamis on Phra Thong Island. In case of Pakarang (one dated palaeotsunami) and Ban Bang Sak (two dated palaeotsunamis) the database was insufficient to estimate local tsunami recurrence.

The regional scale: By linking the records of all study sites in southwest Thailand, a regional pattern of tsunami occurrence could be determined (fig. 11.2). By improving the reliability of events that continuously appear along the coast of the study area, the combined tsunami record of all Thai sites supports the recurrence interval of 500-600 years established for Phra Thong Island. The youngest predecessor of the IOT 2004 that took place 500-600 years ago is documented on Phra Thong, at Ban Bang Sak, and in a cave site at the coast of Krabi (Harper, 2005). The second palaeotsunami at ~1050 years ago is present on Phra Thong and at Pakarang, and the palaeotsunamis at ~1400 and ~1900 years ago left deposits on Phra Thong and at Ban Bang Sak.

The supra-regional scale: Since the impact of tsunamis that affect the coasts of the study area is not restricted to Thailand but may generate onshore deposits in areas as far as east Africa, other coastal areas around the Indian Ocean, especially within the Bay of Bengal, may yield evidence of the same tsunamis that are described in this study. The five palaeotsunamis that are documented in Thailand for the last 3000 years, especially the events that happened approximately 550, 1050 and 1400 years ago, are supported by evidence from north Sumatra (Monecke et al., 2008), east India (Rajendran et al., 2006, 2011; Nair et al., 2011), and Sri Lanka (Jackson, 2008; Ranasinghage et al., 2010). Additionally, the two youngest predecessors of the IOT 2004 seem to be contemporaneous with strong palaeo-earthquakes in the North-Sumatra-Andaman Zone at 1450 AD and 956 AD (Meltzner et al., 2010), where all tsunamis with impact on Thailand are triggered (see *Chapter 3.2*). While the correlation with records from India and north Sumatra generally supports the reliability of a recurrence interval of one strong tsunami every ~500 years, at least for the last 2500 years, lagoon records from Sri Lanka suggest higher recurrence intervals of 300-500 years between 4000 and 5000 BP and 200-300 years in the period 6000-7000 BP (Jackson, 2008; Ranasinghage et al., 2010). However, the higher number of palaeotsunamis on Sri Lanka can be explained by the fact that the island, different from Thailand, might be affected not only by tsunamis generated in the North-Sumatra-Andaman Zone but as well by tsunamis triggered along the Mentawai Segment (see *Chapter 3.2*) that is supposed to generate mega-ruptures with basin-wide tsunamis every ~200 years (the last one occurred in 1833 AD; Sieh et al., 2008).

→ *The application of optically stimulated luminescence and radiocarbon allows for precise and accurate dating of tsunami evidence identified in the study area. The correlation of local chronologies from spatially distinct sites enabled to estimate recurrence intervals for strong tsunamis with basin-wide impact.*

11.2.3 Magnitude and impact of prehistoric tsunamis

Hypothesis 3 – Tsunami deposits allow for the evaluation of magnitude and impact of past tsunamis in southwest Thailand.

<u>*Ad goals IV.1 and IV.2 – Holocene sea-level variations and coastal evolution*</u>

To deduce the magnitude and impact of tsunamis in the study area from their sedimentary imprints, boundary conditions for the time of impacts have been established for all relevant sites in form of the adjacent sea-level curves (*Chapter 7*) and palaeogeographical scenarios (*Chapter 8*).

Holocene sea levels. The sea-level curve for the study area is characterised by a mid-Holocene maximum of 2-3 m above present sea level at approximately 5500 cal BP and a gradual drop afterwards. However, for the last 3000 years, the time window of all palaeotsunamis identified in this study, sea level was less than 1 m above its present position. Thus, the differences to the present day situation were insignificant compared to the indeterminable diurnal tide-level variations in the order of 1-3 m.

Palaeogeography. In the course of long-term coastal evolution the study sites repeatedly experienced significant changes of local geomorphology and ecology which both might have influenced hydrodynamic processes during tsunami inundation, as well as the preservation of tsunami-laid deposits. (a) While the ecological conditions on Phra Thong Island prevailed constant during the last 3000 years, the position of the shoreline shifted westwards with an average velocity of 34 m per century since 5500 cal BP (with spatial and temporal variations of coastal progradation in a range of 20-45 m per century) and had to be considered for the interpretation of inundation distances. (b) At Ban Bang Sak, a similar geomorphology and ecology compared to the actual situation was reconstructed for the impact of event B, but the shoreline was several tens of meters further east and the ground surface up to 3 m lower than today. In contrast, events C inundated a much flatter coastal area, where flooding was not influenced by morphological structures such as beach ridges. (c) For the period 1000-1200 cal BP, when event B inundated Pakarang Cape, both morphology and palaeoecology were different from the present situation. The coastline was ~1km further east and after crossing the reef platform the tsunami wave had to cross a shallow lagoon that separated the reef from the mainland.

Ad goal IV.3 – Evaluating the impact of tsunamis on the coastal evolution of SW Thailand

The sedimentary record of southwest Thailand documents no lasting impact of tsunamis on coastal ecosystems and geomorphology, implying that long-term coastal evolution has not been influenced by catastrophic low-frequency events (*Chapter 9*). This is in accordance with observations after the IOT 2004 that document strong short-term impact on social and natural systems, but recovery of most morphological and ecological damage within <10 years.

Ad goal IV.4 – Estimating the magnitude of palaeotsunamis

The relative magnitudes of palaeotsunamis compared to the IOT 2004 have been reconstructed (i) on the basis of sedimentary properties, locally (*Chapter 10*), and (ii) by correlating contemporaneous but spatially distinct imprints of tsunamis and earthquakes within the Indian Ocean, and comparing the distributions with expected impact patterns of different tsunami scenarios.

(i) Hydrodynamics. For tsunami deposits from Ban Bang Sak, sedimentary properties were used to estimate hydrodynamic parameters and transport distances as indicators for the tsunami magnitude. Application of inverse sedimentation modelling revealed onshore flow velocities of 4.1-5.9 m/s and onshore flow depths of 5.5-7.0 m for the ~1450 AD tsunami, which is comparable to values of the IOT 2004 at the same location. Maximum transport distances and erosional depths deduced from offshore sediment sources point to transport dynamics comparable with the IOT 2004 for the ~1450 AD event and at least two of the events between 1180 and 2000 cal BP (erosive depth shallower than 45 m water depth), but much shallower source areas (beach) for another event between 1180 and 2000 cal BP.

(ii) Inundation width and impact radius. Correlation of spatially distinct evidence on a local scale allowed for reconstruction of inundation widths for palaeotsunamis on Phra Thong Island. In consideration of Holocene shifts in the shoreline position, minimum inundation distances of all palaeotsunamis have been at least 500-600 m. By considering the wider geographical context of the whole Bay of Bengal, most palaeotsunamis identified in this study, especially those of ~1450 AD, ~950 AD and ~550 AD, affected not only Thailand but as well areas in India, on Sri Lanka, north Sumatra and the Maldives (fig. 11.3). In combination with the distribution of contemporaneous palaeo-earthquakes, the reconstructed impact patterns can only be explained by events comparable to 2004, i.e. tsunamis triggered by ruptures of the North-Sumatra-Andaman Zone with magnitudes >M_w9. All other possible events are not capable to generate the observed distribution of tsunamites, uplift and subsidence (fig. 11.3).

Figure 11.3: *Spatial patterns of time-overlapping tsunami and earthquake evidence for the palaeotsunamis identified in the study area compared to the observed impact patterns of the IOT 2004 and tsunamis generated by partial ruptures of the North-Sumatra-Andaman Zone (Subarya et al., 2006; Bilham et al., 2005), as well as modelled impact patterns for tsunami generated by the biggest historical earthquakes in the Mentawai and North-Andaman-Myanmar Segments (Okal and Synolakis, 2008).*
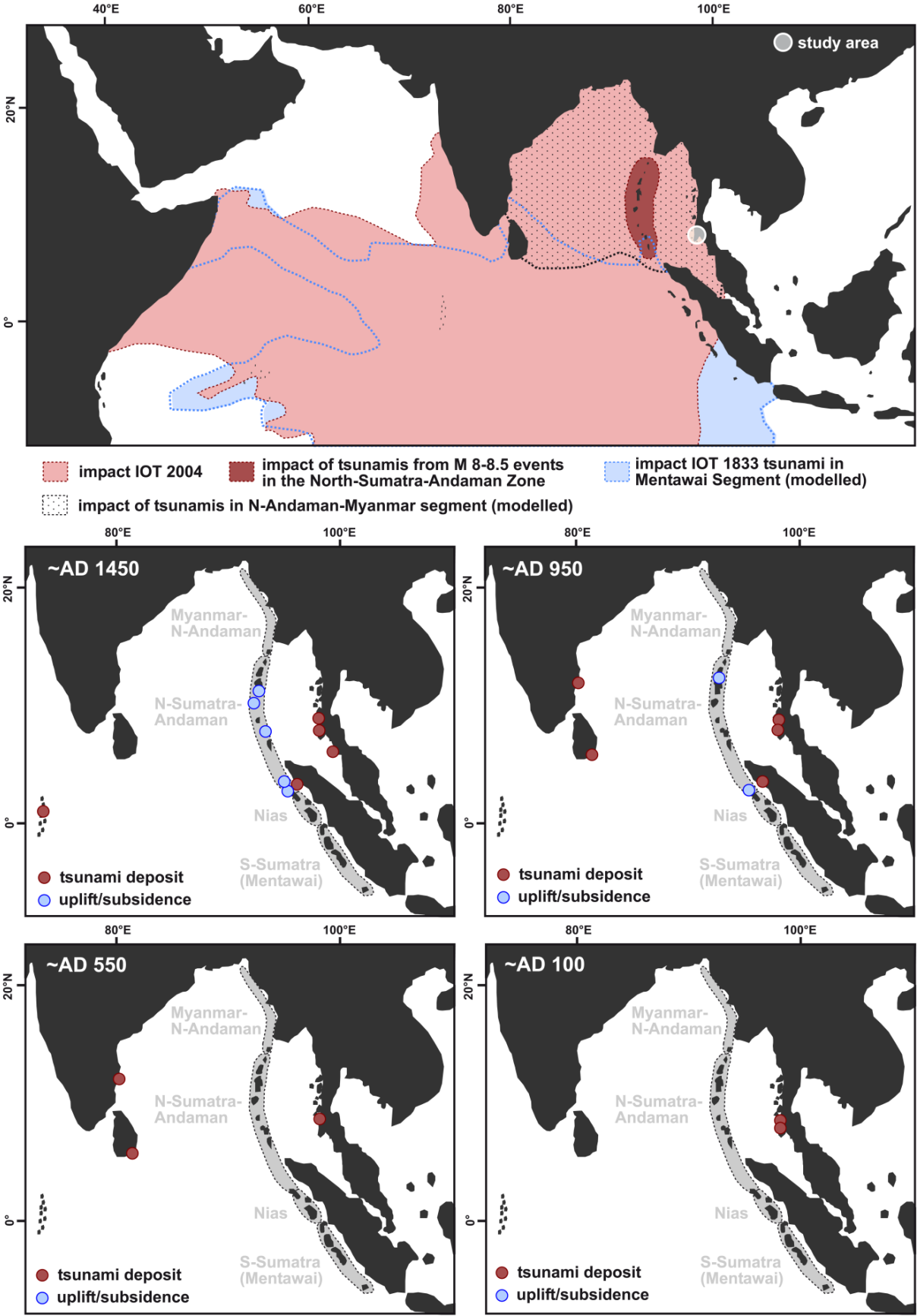
→ *Tsunami deposits in their sedimentary contexts were successfully used to demonstrate that tsunamis had no significant impact on the long-term evolution of coastal environments and geomorphology, although all documented palaeotsunamis had magnitudes comparable to the IOT 2004.*

11.2.4 Synthesis – Tsunami recurrence in the Bay of Bengal

Although even strong tsunamis had no long-term effect on the morphology and ecology of coastal systems in southwest Thailand, the IOT 2004 demonstrated the disastrous short-term impact that tsunamis may have on coastal communities and infrastructure. Therefore, the reconstructed recurrence interval of ~500 years for tsunamis with magnitudes comparable to 2004 is a valuable piece of information for tsunami risk assessment in Thailand. However, since tsunamis that affect the coast of Thailand with waves high enough to generate onshore deposits are invariably generated by mega-ruptures of the North-Sumatra-Andaman Zone, the recurrence interval of tsunamis in Thailand is equal to that of earthquakes with similar magnitude, i.e. ≥M_w9, and rupture geometry as in 2004. Tsunamis triggered by ruptures of this type have a basin-wide impact and are capable to cause damage and loss of life not only in Thailand but as well on Sumatra, on Sri Lanka, in India, on the Maldives and in east Africa. Therefore, the record of Thailand provides valuable information about tsunami recurrence in these countries as well. This is even more important, since the sedimentary archives of these regions (i) provide scarcely documented records for the period between 1000 and 4000 cal BP, and (ii) in the majority may store evidence of tsunamis from multiple sources, such as the North-Sumatra-Andaman Zone, the Mentawai Segment and possibly the Myanmar-North-Andaman Zone for Sri Lanka, resulting in an overlap of different recurrence intervals. Thus, correlation of other sites in the northern Indian Ocean with the Thai tsunami record will not only help to cover the scarcely documented period between 1000 and 2500 cal BP, but might as well enable to discriminate between tsunami signals from different source areas.

11.3 Assessment and mitigation of future tsunami risk

The IOT 2004 has demonstrated that southwest Thailand is a region exposed to an enormous tsunami hazard. Since then, coastal management strategies are aimed at the reduction of future tsunami risk for the potentially affected population (permanent residents, commuters, tourists) to a tolerable level. To achieve this, it is crucial to assess (i) the future tsunami risk and its critical tolerance value, and, if the level of tolerable risk is exceeded, (ii) possibilities and strategies to reduce it.

(i) Risk assessment. The tsunami risk of an area is quantitatively defined by the equation risk = hazard x vulnerability. The present day vulnerability (exposure, sensitivity and resilience)

of the Thai west coast has been analysed in numerable studies since 2004 (e.g. Willroth et al., 2011; Römer et al., 2012). However, the IOT 2004 gives only one example for the consequences of tsunamis in Thailand and is not necessarily equal in its size to potential future events. Since risk mitigation should be oriented on potential future events, for the determination of future tsunami risk, the implementation of geological evidence is not only important to evaluate the long-term hazard, i.e. the frequency and potential magnitudes of future events, but as well to estimate the vulnerability in case of tsunamis with magnitudes different from the IOT 2004. Taking all information into account, our investigations support the seismicity based calculations of Nadim and Glade (2006) that due to the low frequency of destructive tsunamis in Thailand the real tsunami risk, i.e. the scientifically calculated risk due to tsunamis, does not necessarily require mitigation measures within the next decades. However, even if real tsunami risk is on a tolerable level for the next century, due to the very high perceived risk, i.e. the risk that is perceived by the potentially affected population, immediate measures are expected to be done (Nadim and Glade, 2006). Since the economic and touristic development of the area is closely related to the perception of tsunami risk, reduction of perceived risk is a sufficient argument to justify immediate measures.

(ii) *Risk mitigation*. Generally, it is not possible to change the tsunami hazard of a region, but the consequences of tsunamis can be diminished by reducing the vulnerability of potentially affected regions. In this context, geological tsunami evidence can contribute (a) by deducing flooding areas of potential future tsunamis from past events, since these might be different from areas inundated by the IOT 2004. Flooding areas and inundation distances determined on the basis of tsunami deposits can be used to improve and evaluate risk maps generated by numerical inundation models. (b) By providing information about maximum flow conditions that have to be expected for potential future events, especially if these might be stronger than observed during the IOT 2004, additional input for the specifications of tsunami-secure construction in potential risk areas is available. The height of secure buildings has to be oriented on the maximum flow depth expected for future events, and expected flow velocities should be considered for purposes of building stability. (c) Eventually, learning from the past is an important factor for the build-up of public awareness and preparedness towards future tsunami risk. The identification of prehistoric tsunamis demonstrates that the IOT 2004 was not a unique event in Thailand. This awareness may strengthen the acceptance towards mitigation measures and, thus, can improve, among others, the reaction of coastal residents in cases of tsunami warnings and the quality of hazard management by local authorities and stakeholders.

References

Abbott, T.R., 1991. Seashells of southeast Asia, 145pp.

Ad-hoc-Arbeitsgruppe Boden der Staatlichen Geologischen Dienste und der Bundesanstalt für Geowissenschaften und Rohstoffe (Eds.), 2005. Bodenkundliche Kartieranleitung. Schweizerbart, Stuttgart.

Admiralty Tide Tables, 2003. Indian Ocean and south China Sea. Volume 3. Hydrographer to the Navy, Admiralty Hydrography Department, 357pp.

Aitken, M.J., 1998. An introduction to optical dating. Oxford University Press, 267pp.

Alam, E., Dominey-Howes, D., Chagué-Goff, C., Goff, J., 2012. Tsunamis of the northeast Indian Ocean with a particular focus on the Bay of Bengal region – a synthesis and review. Earth Science Reviews 114, 175-193.

Alcantara-Ayala, I., 2002. Geomorphology, natural hazards, vulnerability and prevention of natural disasters in developing countries. Geomorphology 47, 107-124.

Andrade, C., 1992. Tsunami generated forms in the Algarve barrier islands. Science of Tsunami Hazards 10, 21-34.

Apotsos, A., Gelfenbaum, G., Jaffe, B., 2012. Time-dependent onshore tsunami response. Coastal Engineering 64, 73-86.

Apotsos, A., Jaffe, B., Gelfenbaum, G., Elias, E., 2009. Modelling time-varying tsunami sediment deposition. Proceedings of Coastal Dynamics 2009: Impacts of human activities on dynamic coastal processes. World Scientific Publishing Corporation, 1-15.

Arnold, L.J., Roberts, R.G., 2009. Stochastic modelling of multi-grain equivalent dose (D_e) distributions: implications for OSL dating of sediment mixtures. Quaternary Geochronology 4, 204-230.

Atwater, B., Moore, A.L., 1992. A tsunami about 1000 years ago in Puget Sound, Washington. Science 258, 1614-1617.

Atwater, B.F., 1987. Evidence for great Holocene earthquakes along the outer coast of Washington State. Science 236, 942-944.

Bahlburg, H., Weiss, R., 2007. Sedimentology of the December 26, 2004, Sumatra tsunami deposits in eastern India (Tamil Nadu) and Kenya. International Journal of Earth Sciences (Geologische Rundschau) 96, 1195-1209.

Baker, R.G.V., Haworth, R.J., 2000. Smooth or oscillating late Holocene sea-level curve? Evidence from cross-regional statistical regressions of fixed biological indicators. Marine Geology 163, 353-365.

Baker, R.G.V., Haworth, R.J., Flood, P.G., 2001. Inter-tidal fixed indicators of former Holocene sea-levels in Australia: A summary of sites and a review of methods and models. Quaternary International 83-85, 257-273.

Ballarini, M., Wallinga, J., Murray, A.S., van Heteren, S., Oost, A.P., Bos, A.J.J., van Eijk, C.W.E., 2003. Optical dating of young coastal dunes on a decadal time scale. Quaternary Science Reviews 22, 1011-1017.

Ballarini, M., Wallinga, J., Wintle, A.G., Bos, A.J.J., 2007. A modified SAR protocol for optical dating of individual grains from young quartz samples. Radiation Measurements 42, 360-369.

Banerjee, D., Murray, A.S., Foster, I.D.L., 2001. Scilly Isles, UK: optical dating of a possible tsunami deposit from the 1755 Lisbon earthquake. Quaternary Science Reviews 20, 715-718.

Bard, E., Hamelin, B., Fairbanks, R., 1990. U-Th ages obtained by mass spectrometry in corals from Barbados: sea level during the past 130,000 years. Nature 346, 456-458.

Beck, R., Burger, D., Pfeffer, K.-H., 1995. Kleinere Arbeiten aus dem Geographischen Institut der Universität Tübingen. Laborskript 11.

Bell, R., Cowan, H., Dalziell, E., Evans, E., O'Leary, M., Rush, B., Yule, L., 2005. Survey of impacts on the Andaman coast, southern Thailand following the great Sumatra-Andaman earthquake and tsunami of December 26, 2004. Bulletin of the New Zealand Society of Earthquake Engineering 38(3), 123-148.

Bilham, R., Engdahl, E.R., Feldl, N., Satyabala, S.P., 2005. Partial and complete rupture of the Indo-Andaman plate boundary 1847–2004. Seismological Research Letters 76, 299-311.

Bird, E., 2008. Coastal Geomorphology. An Introduction. Second Edition, 411pp.

Bishop, P., Sanderson, D., Hansom, J., Chaimanee, N., 2005. Age-dating of tsunami deposits: lessons from the 26 December 2004 tsunami in Thailand. The Geographical Journal 171(4), 379-384.

Blott, S.J., Pye, K., 2001. GRADISTAT: a grain size distribution and statistics package for the analysis of unconsolidated sediments. Earth Surface Processes and Landforms 26, 1237-1248.

Bondevik, S., 2008. The sands of tsunami time. Nature 455, 1183-1184.

Borrero, J., 2005. Field survey of northern Sumatra and Banda Aceh, Indonesia after the tsunami and earthquake of 26 December 2004. Seismological Research Letters 76, 312-320.

Bourgeois, J., 2009. Geologic effects and records of tsunamis. In: Robinson, A.R., Bernard, E.N., eds. The Sea 15, 53-91.

Bozke, L., Kowalski, A., Szczuciński, W., Rachlewicz, G., Lorenc, S., Siepak, J., 2006. Assessment of mercury mobility and bioavailability by fractionation method in sediments from coastal zone inundated by the 26 December 2004 tsunami in Thailand. Environmental Geology 51, 527-536.

Bradley, S., Milne, G., Zong, Y., Horton, B., 2008. Modelling sea-level data from China and Malay-Thai Peninsula to infer Holocene eustatic sea-level change. American Geophysical Union, Fall Meeting 2008.

Briggs, R., Sieh, K., Meltzner, A., Natawidjaja, D., Galetzka, J., Suwargadi, B., Hsu, Y., Simons, M., Hananto, N., Suprihanto, I., Prayudi, D., Avouac, J., Prawirodjo, L., Bock, Y., 2006. Deformation and slip along the Sunda megathrust in the great 2005 Nias-Simeulue earthquake. Science 311, 1897-1901.

Brill, D., Brückner, H., Jankaew, K., Kelletat, D., Scheffers, A., Scheffers, S., 2011: Potential predecessors of the 2004 Indian Ocean Tsunami – sedimentary evidence of extreme wave events at Ban Bang Sak, SW Thailand. Sedimentary Geology 239, 146-161.

Brill, D., Klasen, N., Brückner, H., Jankaew, K., Scheffers, A., Kelletat, D., Scheffers, S., 2012a. OSL dating of tsunami deposits from Phra Thong Island, Thailand. Quaternary Geochronology 10, 224-229.

Brill, D., Klasen, N., Brückner, H., Jankaew, K., Kelletat, D., Scheffers, A., Scheffers, S., 2012b. Local inundation distances and regional tsunami recurrence in the Indian Ocean inferred from luminescence dating of sandy deposits in Thailand. Natural Hazards and Earth System Sciences 12, 2177-2192.

Brown, B.E., 2005. The fate of coral reefs in the Andaman Sea, eastern Indian Ocean following the Sumatran earthquake and tsunami, 26 December 2004. The Geographical Journal 171(4), 372-374.

Brown, B.E., Dunne, R.P., Chansang, H., 1996. Coral bleaching relative to elevated seawater temperature in the Andaman Sea (Indian Ocean) over the last 50 years. Coral Reefs 15, 151-152.

Brückner, H., Brill, D., 2009. Der Tsunami von 2004 – fünf Jahre danach. Geographische Rundschau 61(12), 4-10.

Brückner, H., Kelterbaum, D., Marunchak, O., Porotov, A., Vött, A., 2010. The Holocene sea level story since 7500 BP – Lessons from the Eastern Mediterranean, the Black and the Azov Seas. Quaternary International 225, 160-179.

Brückner, H., Müllenhoff, M., Gehrels, R., Herda, A., Knipping, M., Vött, A., 2006. From archipelago to floodplain – geographical and ecological changes in Miletus and its environs during the past six millennia (Western Anatolia, Turkey). Zeitschrift für Geomorphologie, Suppl. Vol. 142, 63-83.

Bruins, H.J., MacGillivray, J.A., Synolakis, C., Benjamini, Ch., Keller, J., Kisch, H., Klügel, A., van der Plicht, J., 2008. Geoarchaeological tsunami deposits at Palaikastro (Crete) and the Late Minoan IA eruption of Santorini. Journal of Archaeological Science 35, 191-212.

Brune, S., Babeyko, A.Y., Ladage, S., Sobolev, S.V., 2010. Landslide tsunami hazard in the Indonesian Sunda Arc. Natural Hazards and Earth System Sciences 10, 589-604.

Bryant, E. A., 2001. Tsunami. The underrated hazard. Cambridge University Press, 320pp.

Bulur, E., Bøtter-Jensen, L., Murray, A.S., 2000. Optically stimulated luminescence from quartz measured using linear modulation technique. Radiation Measurements 32, 407-411.

Calgaro, E., Lloyd, K., 2008. Sun, sea, sand and tsunami: examining disaster vulnerability in the tourism community of Khao Lak, Thailand. Singapore Journal of Tropical Geography 29, 288-306.

Camoin, G.F., Colonna, M., Montaggioni, L.F., Casanova, J., Faure, G., Thomassin, B.A., 1997. Holocene sea level changes and reef development in the southwestern Indian Ocean. Coral Reefs 16, 247-259.

Camoin, G.F., Montaggioni, F., Braithwaite, C.J.R., 2004. Late glacial to post glacial sea levels in the western Indian Ocean. Marine Geology 206, 119-146.

Cartwright, J., Nakamura, H., 2008. Tsunami: A history of the term and of scientific understanding of the phenomenon in Japanese and western culture. Notes and Records of the Royal Society 62, 151-166.

Chagué-Goff, C., 2010. Chemical signatures of palaeotsunamis: A forgotten proxy? Marine Geology 271, 67-71.

Chagué-Goff, C., Andrew, A., Szczuciński, W., Goff, J., Nishimura, Y., 2012. Geochemical signatures up to the maximum inundation of the 2011 Tohoku-oki tsunami – implications for the 869 AD Jogan and other palaeotsunamis. Sedimentary Geology, doi:10.1016/j.sedgeo.2012.05.021.

Chagué-Goff, C., Schneider, J., Goff, J., Dominey-Howes, D., Strotz, L., 2011. Expanding the proxy toolkit to help identify past events – Lessons from the 2004 Indian Ocean Tsunami and the 2009 South Pacific Tsunami. Earth-Science Reviews 107, 107-122.

Chansang, H., 1988. Coastal tin mining and marine pollution in Thailand. AMBIO 17, 223-228.

Chlieh, M., Avouac, J., Sieh, K., Natawidjaja, D., Galetzka, J., 2008. Heterogeneous coupling of the Sumatra megathrust constrained by geodetic and paleogeodetic measurements. Journal of Geophysical Research 113, 1-31.

Choowong, M., Ugai, H., Charoentitirat, T., Charusiri, P., Veerote, D., Daorerk, V., Songmuang, R., Ladachard, R., 2004. Holocene biostratigraphical records in coastal deposits from Sam Roi Yod National Park, Prachuap Khiri Khan, Western Thailand. The Natural History Journal of Chulalongkorn University 42, 1-18.

Choowong, M., Murakoshi, N., Hisada, K., Charusiri, P., Doarerk, V., Charoentitirat, T., Chutakositkanon, V., Jankaew, K., Kanjanapayont, P., 2007. Erosion and deposition by the 2004 Indian Ocean tsunami in Phuket and Phang-nga provinces, Thailand. Journal of Coastal Research 23, 1270-1276.

Choowong, M., Phantuwongraj, S., Charoentitirat, T., Chutakositkanon, V., Yumuang, S., Charusiri, P., 2008a. Beach recovery after 2004 Indian Ocean tsunami from Phang-nga, Thailand. Geomorphology 104, 134-142.

Choowong, M., Muratoshi, N., Hisada, K., Charoentitirat, T., Charusiri, P., Phantuwongraj, S., Wongkok, P., Choowong, A., Subsayjun, R., Chutakositkanon, V., Jankaew, K., Kanjanapayont, P., 2008b. Flow conditions of the 2004 Indian Ocean tsunami in Thailand, inferred from capping bedforms and sedimentary structures. Terra Nova 20, 141-149.

Choowong, M., Murakoshi, N., Hisada, K., Charusiri, P., Charoentitirat, T., Chutakositkanon, V., Jankaew, K., Kanjanapayont, P., Phantuwongraj, S., 2008c. 2004 Indian Ocean tsunami inflow and outflow at Phuket, Thailand. Marine Geology 248, 179-192.

Church, J.A., White, N.J., Aarup, T., Wilson, W.S., Woodworth, P., Domingues, C., Hunter, J., Lambeck, K., 2008. Understanding global sea levels: Past, present and future. Sustainable Science 3, 9-22.

Cisternas, M., Atwater, B.F., Torrejón, F., Sawai, Y., Machuca, G., Lagos, M., Eipert, A., Youlton, C., Salgado, I., Kamataki, T., Shishikura, M., Rajendran, C.P., Malik, J.K., Rizal, Y., Husni, M., 2005. Predecessors of the giant 1960 Chile earthquake. Nature 437, 404-407.

Cita, M.B., Camerlenghi, A., Kastens, K.A., McCoy, F.W., 1984. New findings of Bronze Age homogenites in the Ionian Sea: Geodynamic implications for the Mediterranean. Marine Geology 55, 47-62.

Clark, J.A., Farrell, W.E., Peltier, W.R., 1978. Global changes in post glacial sea level: a numerical calculation. Quaternary Research 9, 265-287.

CNN World, 2010. More than 2 million affected by earthquake, Chile's president says. Article from 27.02.2010. http://articles.cnn.com/2010-02-27/world/chile.quake_1_magnitude-haiti-quake-chilean-president-michelle-bachelet?_s=PM:WORLD; last access: 05.05.2012

Coates, M., 2008. A comparison of tidal assemblages on exposed and sheltered tropical and temperate rocky shores. Global Ecology and Biogeography Letters 7(2), 115-124.

Cochard, R., Ranamukhaarachchi, S., Shivakoti, G., Shipin, O., Edwards, P., Seeland, K., 2008. The 2004 tsunami in Aceh and southern Thailand: A review on coastal ecosystems, wave hazards and vulnerability. Perspectives in Plant Ecology, Evolution and Systematics 10, 3-40.

Costa, P.J., Andrade, C., Freitas, M.C., Oliveira, M.A., Lopes, V., Dawson, A.G., Moreno, J., Fatela, F., Jouanneau, J.M., 2012. A tsunami record in the sedimentary archive of the central Algarve coast, Portugal: Characterizing sediment, reconstructing sources and inundation paths. The Holocene 22, 899-914.

CRISP, Centre for Remote Imaging, Sensing and Processing. IKONOS satellite images from 13.01.2003 and 29.12.2004. University of Singapore.

Cummins, P.R., 2007. The potential for giant tsunamigenic earthquakes in the northern Bay of Bengal. Nature 449, 75-78.

Cunha, P., Buylaert, J.P., Murray, A.S., Andrade, C., Freitas, M.C., Fatela, F., Munha, J.M., Martins, A.A., Sugisaki, S., 2010. Optical dating of clastic deposits generated by an extreme marine coastal flood: the 1755 tsunami deposits in the Algarve (Portugal). Quaternary Geochronology 5, 329-335.

Cunningham, A.C., Wallinga, J., 2010. Selection of integration time intervals for quartz OSL decay curves. Quaternary Geochronology 5, 657-666.

Dahanayake, K., Kulasena, N., 2008. Recognition of diagnostic criteria for recent- and paleo-tsunami sediments from Sri Lanka. Marine Geology 254, 180-186.

Davies, H.L., Davies, J.M., Perembo, R.C.B., Lus, W.Y., 2003. The Aitape 1998 tsunami: Reconstructing the event from interviews and field mapping. Pure and Applied Geophysics 160, 1895-1922.

Dawson, A.G., 1994. Geomorphological effects of tsunami run-up and backwash. Geomorphology 10, 83-94.

Dawson, A.G., 1999. Linking tsunami deposits, submarine slides and offshore earthquakes. Quaternary International 60, 119-126.

Dawson, A.G., Stewart, I., 2007. Tsunami deposits in the geological record. Sedimentary Geology 200, 166-183.

Dawson, A.G., Long, D., Smith, D.E., 1988. The Storegga slides: Evidence from eastern Scotland for a possible tsunami. Marine Geology 82, 271-276.

Dawson, A., Hindson, R., Andrade, C., Freitas, C., Parish, R., Bateman, M., 1995. Tsunami sedimentation associated with the Lisbon earthquake of 1 November AD 1755: Boca do Rio, Algarve, Portugal. The Holocene 5, 209-215.

Dawson, S., Smith, D.E., Ruffman, A., Shi, S., 1996a. The diatom biostratigraphy of tsunami sediments: Examples from recent and Middle Holocene events. Physics and Chemistry of the Earth 21, 87-92.

Dawson, A,G., Shi, S., Dawson, S., Takahashi, T., Shuto, N., 1996b. Coastal sedimentation associated with the June 2nd and 3rd, 1994 tsunami in Rajegwesi, Java. Quaternary Science Reviews 15, 901-912.

Department of Marine and Coastal Resources, 2005. Rapid assessment of the tsunami impact on marine resources in the Andaman Sea. Thailand, 7-32.

Department of Mineral Resources, 2002. Proceedings of the symposium on geology of Thailand, October 26-30, 2002. Bangkok.

Department of Mineral Resources: http://www.dmr.go.th/main.php?filename=ActiveFault_Eng; last access: 10.09.2011

Devillers, B., Excoffon, P., Morhange, C., Bonnet, S., Bertoncello, F., 2007. Relative sea-level changes and coastal evolution at Forum Julii (Fréjus, Provence). Comptes Rendus Geosciences 339, 329-336.

Dheeradilok, P., 1995. Quaternary coastal morphology and deposition in Thailand. Quaternary International 26, 49-54.

Di Geronimo, I., Choowong, M., Phantuwongraj, S., 2009. Geomorphology and superficial bottom sediments of Khao Lak coastal area (SW Thailand). Polish Journal of Environmental Studies 18, 111-121.

Dominey-Howes, D., Cummins, P., Burbidge, D., 2007. Historic records of teletsunami in the Indian Ocean and insights from numerical modelling. Natural Hazards 42, 1-17.

Donato, S.V., Reinhardt, E.G., Boyce, J.I., Rothaus, R., Vosmer, T., 2008. Identifying tsunami deposits using bivalve shell taphonomy. Geology 36, 199-202.

Duller, G.A.T., 2004. Luminescence dating of Quaternary sediments: recent advances. Journal of Quaternary Science 19, 183-192.

Duller, G.A.T., 2008. Single-grain optical dating of Quaternary sediments: why aliquot size matters in luminescence dating. Boreas 37, 589-612.

Dura, T., Rubin, Ch., Kelsey, H., Horton, B.P., Hawkes, A., Vane, Ch., Daryono, M., Grand Pre, C., Ladinsky, T., Bradley, S., 2011. Stratigraphic record of Holocene coseismic subsidence, Padang, West Sumatra. Journal of Geophysical Research 116, 1-11.

Engel, M., Brückner, H., 2011. The identification of palaeo-tsunami deposits – a major challenge in coastal sedimentary research. In: Karius, V., Hadler, H., Deicke, M., von Eynatten, H., Brückner, H., Vött, A. (eds.), Dynamische Küsten – Grundlagen, Zusammenhänge und Auswirkungen im Spiegel angewandter Küstenforschung. Coastline Reports 17, 65-80.

Engel, M., Brückner, H., Wennrich, V., Scheffers, A., Kelletat, D., Vött, A., Schäbitz, F., Daut, G., Willershäuser, T., May, S.M., 2010. Coastal stratigraphies of eastern Bonaire (Netherlands Antilles): new insights into the palaeo-tsunami history of the southern Caribbean. Sedimentary Geology 231, 14-30.

Engel, M., Knipping, M., Brückner, H., Kiderlen, M. Kraft, J.C., Reconstructing middle to late Holocene palaeogeographies of the lower Messenian plain (southwestern Peloponnese, Greece): Coastline migration, vegetation history and sea level change. Palaeogeography, Palaeoclimatology, Palaeoecology 284, 257-270.

Engel, M., May, S.M., 2012. Bonaire's boulder fields revisited: evidence for Holocene tsunami impact on the Leeward Antilles. Quaternary Science Reviews, doi:10.1016/j.quascirev.2011.12.011.

Engelhart, S.E., Horton, B.P., David, H., Roberts, D.H., Bryant, C.L., Corbett, D.R., 2007. Mangrove pollen of Indonesia and its suitability as a sea-level indicator. Marine Geology 242, 65-81.

Feldens, P., Schwarzer, K., Szczucińsci, W., Stattegger, K., Sakuna, D., Somgpngchaiykul, P., 2009. Impact of 2004 tsunami on seafloor morphology and offshore sediments, Pakarang Cape, Thailand. Polish Journal of Environmental Studies 18, 63-68.

Fenton, C., Sutiwanich, C., 2005. Paleoseismic Investigation of the Ranong and Khlong Marui faults, Chumphon Province, Southern Thailand. American Geophysical Union, Fall Meeting 2005.

Fleming, K., Johnston, P., Zwartz, D., Yokoyama, Y., Lambeck, K., Chappell, J., 1998. Refining the eustatic sea-level curve since the last glacial maximum using far- and intermediate-field sites. Earth and Planetary Science Letters 163, 327-342.

Flierl, G.R., Robinson, A.R., 1972. Deadly surges in the Bay of Bengal: Dynamics and storm-tide tables. Nature 239, 213-215.

Folk, R.L., Ward, W.C., 1957. Brazos River bar: a study in the significance of grain size parameters. Journal of Sedimentary Petrology 27, 3-26.

Fritz, H.M., Blount, C.D., Thwin, S., Kyaw Thu, M., Chan, N., 2009a. Cyclone Nargis storm surge in Myanmar. Nature Geoscience 2, 448-449.

Fritz, H., Mohammed, F., Yoo, J., 2009b. Lituya Bay landslide impact generated mega-tsunami 50th anniversary. Pure and Applied Geophysics 166, 153-175.

Fujino, S., Naruse, H., Matsumoto, D., Jarupongsakul, T., Sphawajruksakul, A., Sakakura, N., 2009. Stratigraphic evidence for pre-2004 tsunamis in southwestern Thailand. Marine Geology 262, 25-28.

Fujino, S., Naruse, H., Matsumoto, D., Sakakura, N., Suphawajruksakul, A., Jarupongsakul, T., 2010. Detailed measurements of thickness and grain size of a widespread onshore tsunami deposit in Phang-nga Province, southwestern Thailand. Island Arc 19, 389-398.

Fujiwara, O., 2008. Bedforms and sedimentary structures characterizing tsunami deposits. In: Shiki, T., Tsuji, Y., Yamazaki, T. (eds.). Tsunamiites. Features and Implications, 51-62.

Fujiwara, O., Kamataki, T., 2008. Tsunami depositional processes reflecting the waveform in a small bay: Interpretation from the grain-size distribution and sedimentary structures. In: Shiki, T., Tsuji, Y., Yamazaki, T. (eds.). Tsunamiites. Features and Implications, 133-152.

Galbraith, R.F., Roberts, R.G., Laslett, G.M., Yoshida, H., Olley, J.M., 1999. Optical dating of single grains of quartz from Jinmium rock shelter, northern Australia. Part I: experimental design and statistical models. Archaeometry 41, 339-364.

Gehrels, W.R., 1999. Middle and late Holocene sea-level changes in eastern Maine reconstructed from foraminiferal saltmarsh stratigraphy and AMS ^{14}C dates on basal peat. Quaternary Research 52, 350-359.

Geist, E.L., Bilek, S., Arcas, D., Titov, V., 2006. Differences in tsunami generation between the December 26, 2004 and March 28, 2005 Sumatra earthquakes. Earth Planets Space 58, 185-193.

Gelfenbaum, G., Jaffe, B., 2003. Erosion and sedimentation from the 17 July, 1998 Papua New Guinea Tsunami. Pure and Applied Geophysics 160, 1969-1999.

Geyh, M., 2005. Handbuch der physikalischen und chemischen Altersbestimmung. Wissenschaftliche Buchgesellschaft Darmstadt. 211pp.

Geyh, M.A., Kudrass, H.-R., Streif, H., 1979. Sea-level changes during the late Pleistocene and Holocene in the Straits of Malacca. Nature 278, 441-443.

Giri, C., Zhu, Z., Tieszen, L., Singh, A., Gillette, S., Kelmelis, J., 2008. Mangrove forest distributions and dynamics (1975-2005) oft the tsunami-affected region of Asia. Journal of Biogeography 35, 519-528.

Goff, J., Chgué-Goff, C., Nichol, S., 2001. Palaeotsunami deposits: a New Zealand perspective. Sedimentary Geology 143, 1-6.

Goff, J., McFadgen, B., Chagué-Goff, C., 2004. Sedimentary differences between the 2002 Easter storm and the 15th-century Okoropunga tsunami, south-eastern North Island, New Zealand. Marine Geology 204, 235-250.

Goff, J., McFadgen, B., Chague-Goff, C., Nichol, S., 2012. Palaeotsunamis and their influence on Polynesian settlement. The Holocene, doi:10.1177/0959683612437873.

Gornitz, V., 2005. Natural Hazards. In: Schwartz, M.L. (ed.), Encyclopedia of Coastal Science, 678-684.

Goto, K., S.A. Chavanich, F. Imamura, P. Kunthasap, T. Matsui, K. Minoura, D. Sugawara, Yanagisawa, H., 2007. Distribution, origin and transport process of boulders deposited by the 2004 Indian Ocean tsunami at Pakarang Cape, Thailand. Sedimentary Geology 202, 821-837.

Goto, K., Imamura, F., Keerthi, N., Kunthasap, P., Matsui, T., Minoura, K., Ruangrassamee, A., Sugawara, D., Supharatid, S., 2008. Distribution and significance of the 2004 Indian Ocean tsunami deposits: Initial results from Thailand and Sri Lanka. In: Shiki, T., Tsuji, Y., Yamazaki, T. (eds.). Tsunamiites. Features and Implications, 105-122.

Goto, K., Okada, K., Imamura, F., 2009. Importance of the initial waveform and coastal profile for tsunami' transport of boulders. Polish Journal of Environmental Studies 18, 53-62.

Goto, K., Okada, K., Imamura, F., 2010a. Numerical analysis of boulder transport by the 2004 Indian Ocean tsunami at Pakarang Cape, Thailand. Marine Geology 268, 97-105.

Goto, K., Takahashi, J., Oie, T., Imamura, F., 2010b. Remarkable bathymetric change in the nearshore zone by the 2004 Indian Ocean tsunami: Kirinda Harbor, Sri Lanka. Geomorphology 127, 107-116.

Goto, K., Chagué-Goff, C., Fujino, S., Goff, J., Jaffe, B., Nishimura, Y., Richmond, B., Suguwara, D., Szczucińki, W., Tappin, D., Witter, R., Yulianto, E., 2011. New insights of tsunami hazard from the 2011 Tohoku-oki event. Marine Geology 290, 46-50.

Grand Pre, C.A., Horton, B., Kelsey, H., Rubin, C., Hawkes, A., Daryono, M., Rosenberg, G., Culver, S., 2012. Stratigraphic evidence for an early Holocene earthquake in Aceh, Indonesia. Quaternary Science Reviews, doi:10.1016/j.quascirev.2012.03.011.

Gupta, H. and Gahalaut, V., 2009. Is the northern Bay of Bengal tsunamigenic? Bulletin of Seismological Society of America 99, 3496-3501.

Hammer, Ø., Harper, D.A.T., Ryan, P.D., 2001. PAST: Paleontological statistics software package for education and data analysis. Palaeontologia Electronica 4, 1-9.

Hanebuth, T., Stattegger, K., Grootes, P.M., 2000. Rapid flooding of the Sunda Shelf: a late-Glacial sea-level record. Science 288, 1033-1035.

Harper, S.B., 2005. Bedded shell deposit at Ao Nang, Krabi Province, southern Thailand: a record of a prehistoric tsunami event or extreme storm event or neither. Abstract Volume of the Geological Society of America 37(7), Salt Lake City, Utah, USA, 75.

Hawkes, A.D., Bird, M., Cowie, S., Grundy-Warr, C., Horton, B.P., Tan Shau Hwai, A., Law, L., Macgregor, C., Nott, J., Eong Ong, J., Rigg, J., Robinson, R., Tan-Mullins, M., Tiong Sa, T., Yasin, Z., Wan Aik, L., 2007. Sediments deposited by the 2004 Indian Ocean Tsunami along the Malaysia–Thailand Peninsula. Marine Geology 242, 169-190.

Helal, M.A., Mehanna, M.S., 2008. Tsunamis from nature to physics. Chaos, Solitons and Fractals 36, 787-796.

Hesp, A.P., Hung, C.C., Hilton, M., Ming, C.L., Turner, M.I., 1998. A first tentative Holocene sea level curve for Singapore. Journal of Coastal Research 14, 308-314.

Hindson, R.A., Andrade, C., 1999. Sedimentation and hydrodynamic processes associated with the tsunami generated by the 1755 Lisbon earthquake. Quaternary International 56, 27-38.

Hori, K., Kuzumoto, R., Hirouchi, D., Umitsu, M., Janjirawuttikul, N., Patanakanog, B., 2007. Horizontal and vertical variation of 2004 Indian tsunami deposits: an example of two transects along the western coast of Thailand. Marine Geology 239, 163-172.

Horton, B.P., Larcombe, P., Woodroffe, S.A., Whittaker, J.E., Wright, M.R., Wynn, C., 2003. Contemporary foraminifera distributions of a mangrove environment, Great Barrier Reef coastline, Australia: implications for sea-level reconstructions. Marine Geology 198, 225-243.

Horton, B., Gibbard, P.L., Milne, G.M., Morley, R.J., Purintavaragul, C., Stargardt, J.M., 2005. Holocene sea levels and palaeoenvironments, Malay-Thai Peninsula, southeast Asia. The Holocene 15, 1199-1213.

Horton, B.P., Zong, Y., Hillier, C., Engelhardt, S., 2007. Diatoms from Indonesian mangroves and their suitability as sea-level indicators for tropical environments. Marine Micropaleontology 63, 155-168.

Horton, B.P., Sawai, Y., Hawkes, A.D., Witter, R.C., 2011. Sedimentology and paleontology of a tsunami deposit accompanying the great Chilean earthquake of February 2010. Marine Micropaleontology 79, 132-138.

Huntley, D., Clague, J., 1996. Optical dating of tsunami-laid sands. Quaternary Research 46, 127-140.

Imamura, F., Goto, K., Ohkubo, S., 2008. A numerical model of the transport of a boulder by tsunami. Journal of Geophysical Research 113, C01008, 1-12.

India Meteorological Department, 2007. Cyclone eAtlas. Tracks of cyclones and depressions over North Indian Ocean 1891-2007.

IOC, 2008. The great waves. Revised edition. Paris, 16pp.

IPCC, 2007. Climate change 2007: Impacts, adaptation and vulnerability. Contribution of working group II to the fourth assessment report of the Intergovernmental Panel on Climate Change, Cambridge University Press, Cambridge, UK, 315-356.

IPCC, 2012. Managing the risks of extreme events and disasters to advance climate change adaptation. A special report of working groups I and II of the Intergovernmental Panel on Climate Change. Cambridge University Press, Cambridge, UK, and New York, NY, USA, 582pp.

Islam, M.S., Tooley, M.J., 1999. Coastal and sea-level changes during the Holocene in Bangladesh. Quaternary International 55, 61-75.

Jackson, K.L., 2008. Paleotsunami history recorded in Holocene coastal lagoon sediments, southeastern Sri Lanka. Master thesis at the University of Miami. Open Access Theses. Paper 171. http://scholarlyrepository.miami.edu/oa_theses/171.

Jackson, K.L., Eberli, G.P., Rankey, E.C., Amelung, F., Moore, A.L., 2008. High recurrence rate of paleotsunamis in southeastern Sri Lanka. Abstract Volume of the Eos Trans. AGU Fall Meeting, San Francisco, USA.

Jaffe, B., Buckley, M., Richmond, B., Strotz, L., Etienne, S., Clark, K., Watt, S., Gelfenbaum, G., Goff, J., 2011. Flow speed estimated by inverse modelling of sandy sediment deposited by the 29 September 2009 tsunami near Satitoa, east Upolu, Samoa. Earth-Science Reviews 107, 23-37.

Jaffe, B.E., Gelfenbaum, G., 2007. A simple model for calculating tsunami flow speed from tsunami deposits. Sedimentary Geology 200, 347-361.

Jagodzínski, R., Sternal, B., Szczuciński, W., Lorenc, S., 2009. Heavy minerals in 2004 tsunami deposits on Kho Khao Island, Thailand. Polish Journal of Environmental Studies 18, 103-110.

Jankaew, K., Atwater, B.F., Sawai, Y., Choowong, M., Charoentitirat, T., Martin, M.E., Prendergast, A., 2008. Medieval forewarning of the 2004 Indian Ocean tsunami in Thailand. Nature 455, 1228-1231.

Jankaew, K., Martin, M. E., Sawai, Y., Prendergast, A., 2011. Sand sheets on a beach-ridge plain in Thailand: Identification and dating of tsunami deposits in a far-field tropical setting. in: Mörner, N.A., (ed.). The Tsunami Threat – Research and Technology, 299-324.

Jintasaeranee, P., Weinrebe, W., Klaucke, I., Snidvongs, A., Krastel, S., Winkelmann, D., 2008. Hydroacoustic mapping oft the Andaman Sea shelf break, Thailand – indications for slope failures and gas venting. American Geophysical Union, Fall Meeting 2008.

Joint Typhoon Warning Center, 1989. Tropical Cyclone Report 1989.

Kanamori, H., Rivera, L., Lee, W., 2010. Historical seismograms for unravelling a mysterious earthquake: The 1907 Sumatra Earthquake. Geophysical Journal International 181, 358-374.

Kayanne, H., Ikeda, Y., Echigo, T., Shishikura, M., Kamataki, T., Satake, K., Malik, J. N., Basir, S. R., Chakrabortty, K. G., Roy, A., 2007. Coseismic and postseismic creep in the Andaman Islands associated with the 2004 Sumatra-Andaman earthquake. Geophysical Research Letters 34, L01310, 1-4.

Kelletat, D., 1997. Mediterranean coastal biogeomorphology: Processes, forms, and sea-level indicators. In: Briand, F., Maldonado, A., (eds). Transformations and evolution of the Mediterranean coastline. CIESM Science Series n°3 (Commission Internationale pour l'Exploration Scientifique de la mer Méditerranée). Bulletin de L'Institut océanographique, Monaco, numéro special 18, 209-226.

Kelletat, D., 2005. Notches. In: Schwartz, M., (ed.). Encyclopedia of Coastal Science. Springer, 728-730.

Kelletat, D., Scheffers, S. R., Scheffers, A., 2007. Field signatures of the SE-Asian mega-tsunami along the west coast of Thailand compared to Holocene paleo-tsunami from the Atlantic region. Pure and Applied Geophysics 164, 413-431.

Kelterbaum, D., Brückner, H., Dikarev, V., Gerhard, S., Pint, A., Porotov, A., Zin'ko, V., 2012. Palaeogeographic changes at Lake Chokrak on the Kerch Peninsula, Ukraine, during the Mid- and Late-Holocene. Geoarchaeology 27, 206-219.

Kench, P.S., Nichol, S.L., Smithers, S.G., McLean, R.F., Brander, R.W., 2008. Tsunami as agents of geomorphic change in mid-ocean reef islands. Geomorphology 95, 361-383.

Kendall, M., Paterson, G., Aryuthaka, Ch., Nimsantijaroen, S., Kongkaeow, W., Whanpetch, N., 2006. Impact of the 2004 tsunami on intertidal sediment and rocky shore assemblages in Ranong and Phangnga provinces, Thailand. Phuket Marine Biological Center Research Bulletin 67, 63-75.

Khan, A.A., 2012. Seismogenic sources in the Bay of Bengal vis-à-vis potential for tsunami generation and its impact in the northern Bay of Bengal. Natural Hazards 61, 1127-1141.

Kortekaas, S., Dawson, A.G., 2007. Distinguishing tsunami and storm deposits: an example from Martinhal, SW Portugal. Sedimentary Geology 200, 208-221.

Korup, O., Clague, J.J., 2009. Natural hazards, extreme events, and mountain topography. Quaternary Science Reviews 28, 977-990.

Kotwicki, L., Szczuciński, W., 2006. Meiofaunal assemblages and sediment characteristics of sandy beaches on the west coast of Thailand after the 2004 tsunami event. Phuket Marine Biological Center Research Bulletin 67, 39-47.

Kozak, L., Niedzielski, P., Szczuciński, W., 2008. The methodology and results of determination of inorganic arsenic species in mobile fractions of tsunami deposits by a hyphenated technique of HPLC-HGAAS. International Journal of Environmental Chemistry 88, 989-1003.

Kraft, J.C., Rapp, G., Kayan, I., Luce, J., 2003. Harbor areas at ancient Troy: Sedimentology and geomorphology complement Homer's Iliad. Geology 31, 163-166.

Krastel, S., 2011. RV Chakratong Tongyai Fahrtbericht / Cruise Report: MASS-III Morphodynamics and Slope Stability of the Andaman Sea Shelf Break (Thailand), Phuket - Phuket (Thailand), 11.01. - 24.01.2011. In: IFM-GEOMAR Report 43, doi: 10.3289/IFM-GEOMAR_REP_43_2011.

Krastel, S., Schmincke, H.-U., Jacobs, C., Rihm, R., Le Bas, T., Alibes, B., 2001. Submarine landslides around the Canary Islands. Journal of Geophysical Research 106, 3977-3997.

Kulig, G., 2005. Erstellung einer Auswertesoftware zur Altersbestimmung mittels Lumineszenzverfahren unter spezieller Berücksichtigung des Einflusses radioaktiver Ungleichgewichte in der 238-U-Zerfallsreihe. Bakkalaureusarbeit Network Computing, TU Freiberg.

Kumar, K.A., Achyuthan, H., 2006. A record of palaeo-tsunami in the Indian Ocean. Marine Geodesy 29, 253-263.

Kundu, B., Gahalaut, V.K., 2010. An investigation into the seismic potential oft the Irrawaddy Region, Northern Sunda Arc. Bulletin of the Seismological Society of America 100, 891-895.

Kunz, A., Frechen, M., Ramesh, R., Urban, B., 2010. Revealing the coastal event-history of the Andaman Islands (Bay of Bengal) during the Holocene using radiocarbon and OSL dating. International Journal of Earth Science (Geologische Rundschau) 99, 1741-1761.

Laborel, J., Laborel-Deguen, F., 1994. Biological indicators of relative sea-level variations and of co-seismic displacements in the Mediterranean region. Journal of Coastal Research 10, 395-415.

Laborel, J., Laborel-Deguen, F., 1996. Biological indicators of Holocene sea-level and climatic variations on rocky coasts of tropical and subtropical regions. Quaternary International 31, 53-60.

Laborel, J., Laborel-Deguen, F., 2005. Sea-level indicators, biologic. In: Schwartz, M.L., (ed.). Encyclopedia of Coastal Science, 833-834.

Lambeck, K., Chappell, J., 2001. Sea level change through the last glacial cycle. Science 292, 679-686.

Latter, J.H., 1981. Tsunamis of volcanic origin: Summary of causes, with particular reference to Krakatoa 1883. Bulletin of Volcanology 44, 467-490.

Lau, A.Y.A., Switzer, A.D., Dominey-Howes, D., Aitchison, J.C., Zong, Y., 2010. Written records of historical tsunamis in the northeastern South China Sea – challenges associated with developing an integrated database. Natural Hazards and Earth System Sciences 10, 1793-1806.

Lay, T., Kanamori, H., Ammon, C.J., Nettles, M., Ward, S.N., Aster, R.C., Beck, A.L., Bilek, S.L., Brudzinski, M.R., Butler, R., Deshon, H.R., Ekström, G., Satake, K., Sipkin, S., 2005. The great Sumatra–Andaman earthquake of 26 December 2004. Science 308, 1127-1133.

Liew, S., Gupta, A., Wong, P., Kwoh, L.K., 2010. Recovery from a large tsunami mapped over time: The Aceh coast, Sumatra. Geomorphology 114, 520-529.

Liu, P., Lynett, P., Fernando, H., Jaffe, B., Fritz, H., Higman, B., Morton, R., Goff, J., Synolakis, C., 2005. Observations by the international tsunami survey team in Sri Lanka. Science 308, 1595.

Loeblich, A.R., Tappan, H., 1987. Foraminiferal genera and their classification. New York, 2 volumes, 1182pp.

Loeblich, A.R., Tappan, H., 1994. Foraminifera of the Sahul Shelf and Timor Sea. Cushman Foundation for Foraminiferal Research, Special Publication 31.

Long, D., Smith, D.E., Dawson, A.G., 1989. A Holocene tsunami deposit in eastern Scotland. Journal of Quaternary Science 4, 61-66.

Løvholt, F., Bungum, H., Harbitz, C.B., Glimsdal, S., Lindholm, C.D., Pedersen, G., 2006. Earthquake related tsunami hazard along the western coast of Thailand. Natural Hazards and Earth System Science 6, 979-997.

Løvholt, F., Glimsdal, S., Harbitz, C., Zamora, N., Nadim, F., Peduzzi, P., Dao, H., Smebye, H., 2012. Tsunami hazard and exposure on the global scale. Earth-Science Reviews 110, 58-73.

MacInnes, B., Bourgeois, J., Pinegina, T., Kravchunovskaya, E., 2009. Tsunami geomorphology: Erosion and deposition from the 15 November 2006 Kuril Island tsunami. Geology 37, 995-998.

Madsen, A.T., Murray, A.S., Andersen, T.J., Pejrup, M., Breuning-Madsen, H., 2005. Optically stimulated luminescence dating of young estuarine sediments; a comparison with ^{210}Pb and ^{137}Cs dating. Marine Geology 214, 251-268.

Malik, J., Banerjee, C., Shishikura, M., 2010. Paleo-tsunami and land-level change evidence from the west coast of South Andaman, Andaman Nicobar Island, India. EGU General Assembly, Geophysical Research Abstracts Volume 12.

Malik, J.N., Shishikura, M., Echigo, T., Ikeda, Y., Satake, K., Kayanne, H., Sawai, Y., Murty, C.V.R., Dishit, O., 2011. Geologic evidence for two pre-2004 earthquakes during recent centuries near Port Blair, South Andaman Island, India. Geology 39, 559-562.

Mamo, B., Strotz, L., Dominey-Howes, D., 2009. Tsunami sediments and their foraminiferal assemblages. Earth-Science Reviews 96, 263-278.

Mastronuzzi, G., Brückner, H., Sansò, P., Vött, A., (Eds.), 2010. Tsunami fingerprints in different archives – Sediments, dynamics and modelling approaches, Proceedings of the 2nd International Tsunami Field Symposium in Ostuni (Italy) and Lefkada (Greece). Zeitschrift für Geomorphologie (Annals of Geomorphology), N. F., 54, suppl. 3.

Mastronuzzi, G., Sansò, P., 2000. Boulders transport by catastrophic waves along the Ionian coast of Apulia (southern Italy). Marine Geology 170, 93-103.

Mastronuzzi, G., Sansò, P., 2004. Large boulder accumulations by extreme waves along the Adriatic coast of southern Apulia (Italy). Quaternary International 120, 173-184.

Matsutomi, H., et al., 2005. The December 26, 2004 Sumatra earthquake tsunami, tsunami field survey around Phuket, Thailand. http://www.drs.dpri.kyoto-u.ac.jp/Sumatra/Thailand/phuket_survey_e.html.

May, S.M., 2010. Sedimentological, geomorphological and geochronological studies on Holocene tsunamis in the Lefkada – Preveza area (NW Greece) and their implications for coastal evolution. Dissertation, Universität zu Köln, http://kups.ub.uni-koeln.de/id/eprint/3189.

May, S.M., Vött, A., Brückner, H., Grapmayer, R., Handl, M., Wennrich, V., 2012. The Lefkada barrier and beachrock system (NW Greece) – Controls on coastal evolution and the significance of extreme wave events. Geomorphology 139-140, 330-347.

May, S.M., Vött, A., Brückner, H., Smedile, A., in press. The Gyra washover fan in the Lefkada Lagoon, NW Greece – possible evidence of the 365 AD Crete earthquake and tsunami. Earth Planets Space.

McCloskey, J., Antonioli, A., Piatanesi, A., Sieh, K., Steacy, S., Nalbant, S., Cocco, M., Giunchi, C., Huang, J., Dunlop, P., 2008. Tsunami threat in the Indian Ocean from future megathrust earthquake west of Sumatra. Earth and Planetary Science Letters 265, 61-81.

Meltzner, A.J, Sieh, K., Chiang, H.-W., Shen, C.-C., Suwargadi, B.W., Natawidjaja, D.H., Philibosian, B.E., Briggs, R.W., Galetzka, J., 2010. Coral evidence for earthquake recurrence and an AD 1390-1455 cluster at the south end of the 2004 Aceh-Andaman rupture. Journal of Geophysical Research 115, B10402, 1-46.

Meltzner, A.J., Sieh, K., Abrams, M., Agnew, D.C., Hudnut, K.W., Avouac, J.P., Natawidjaja, D.H., 2006. Uplift and subsidence associated with the great Aceh-Andaman earthquake of 2004. Journal of Geophysical Research 111, B02407, 1-8.

Milne, G.A., Gehrels, W.R., Hughes, C.W., Tamisiea, M.E., 2009. Identifying the causes of sea-level change. Nature Geoscience 2, 471-478.

Minoura, K., Nakaya, S., Uchida, M., 1994. Tsunami deposits in a lacustrine sequence of the Sanriku coast, northeast Japan. Sedimentary Geology 89, 25-31.

Minoura, K., Imamura, F., Kuran, U., Nakamura, T., Papadopoulos, G., Takahashi, T., Yalciner, A.C., 2000. Discovery of Minoan tsunami deposits. Geology 28, 59-62.

Minoura, K., Imamura, F., Sugawara, D., Kono, Y., Iwashita, T., 2001. The 869 Jogan tsunami deposit and recurrence interval of large-scale tsunami on the Pacific coast of northeast Japan. Journal of Natural Disaster Science 23, 83-88.

Mitrovica, J.X., Peltier, W.R., 1991. On postglacial geoid subsidence over the equatorial oceans. Journal of Geophysical Research 96, 2053-2071.

Mitrovica, J.X., Milne, G.A., 2002. On the origin of late Holocene sea-level highstands within equatorial ocean basins. Quaternary Science Reviews 21, 2179-2190.

Mitrovica. J.X., Vermeersen, L.L.A., 2002. Glacial isostatic adjustment and the earth system: sea level, crustal deformation, gravity and rotation. Washington (D.C.), American Geophysical Union.

Monecke, K., Finger, W., Klarer, D., Kongko, W., McAdoo, B.G., Moore, A.L., Sudrajat, S.U., 2008. A 1,000-year sediment record of tsunami recurrence in northern Sumatra. Nature 455, 1232-1234.

Montaggioni, L.F., 2005. History of Indo-Pacific coral reef systems since the last glaciation: Development patterns and controlling factors. Earth-Science Reviews 71, 1-75.

Moore, A.L., 2000. Landward fining in onshore gravel as evidence for a late Pleistocene tsunami on Molokai, Hawaii. Geology 28, 247-250.

Moore, A., Nishimura, Y., Gelfenbaum, G., Kamataki, T., Triyono, R., 2006. Sedimentary deposits of the 26 December 2004 tsunami on the northwest coast of Aceh, Indonesia. Earth Planets Space 58, 253-258.

Moore, A.L., McAdoo, B.G., Ruffman, A., 2007. Landward fining from multiple sources in a sand sheet deposited by the 1929 Grand Banks tsunami, Newfoundland. Sedimentary Geology 200, 336-346.

Moore, A., Goff, J., McAdoo, B., Fritz, H., Gusman, A., Kalligeris, N., Kalsum, K., Susanto, A., Suteja, D., Synolakis, C., 2011. Sedimentary Deposits from the 17 July 2006 Western Java Tsunami, Indonesia: Use of Grain Size Analyses to Assess Tsunami Flow Depth, Speed, and Traction Carpet Characteristics. Pure and Applied Geophysics 168, 1951-1961.

Morhange, C., Laborel, J., Hesnard, A., 2001. Changes of relative sea level during the past 5000 years in the ancient harbor of Marseilles, Southern France. Palaeogeography, Palaeoclimatology, Palaeoecology 166, 319-329.

Mörner, N.A., 2007. Sea level changes and tsunamis environmental stress and migration overseas: the case of the Maldives and Sri Lanka. Internationales Asienforum 38, 353-374.

Morton, R., Gelfenbaum, G., Jaffe, B.E., 2007. Physical criteria for distinguishing sandy tsunami and storm deposits using modern examples. Sedimentary Geology 200, 184-207.

Morton, R., Goff, J.R., Nichol, S., 2008. Hydrodynamic implications of textural trends in sand deposits of the 2004 tsunami in Sri Lanka. Sedimentary Geology 207, 56-64.

Murari, M.K., Achyuthan, H., Singhvi, A.K., 2007. Luminescence studies on the sediments laid down by the December 2004 tsunami event: prospects for the dating of paleotsunamis and for the estimation of sediment fluxes. Current Science 92, 367-371.

Murnane, R., Liu, K.-B., 2004. Hurricanes and typhoons. Past, present, and future. New York. 461pp.

Murray, A.S., Wintle, A.G., 2000. Luminescence dating of quartz using an improved single aliquot regenerative-dose protocol. Radiation Measurements 32, 57-73.

Murray, A.S., Wintle, A.G., 2003. The single aliquot regenerative dose protocol: potential for improvements in reliability. Radiation Measurements 37, 377-381.

Murty, T.S., Rafiq, M., 1991. A tentative list of tsunamis of the north Indian Ocean. Natural Hazards 4, 81–83.

Murty, T.S., Flather, R.A., 2004. Impact of storm surges in the Bay of Bengal. Journal of Coastal Research 12, 149-161.

Murty, T.S., Flather, R.A., Henry, R.F., 1986. The storm surge problem in the Bay of Bengal. Progress in Oceanography 16, 195-233.

Nadim, F., Glade, T., 2006. On tsunami risk assessment for the west coast of Thailand. ECI Conference on Geohazards, paper 28.

Nagendra, R., Kamalak Kannan, B.V., Sajith, C., Sen, G., Reddy, A.N., Srinivasalu, S., 2005. A record of foraminiferal assemblage in tsunami sediments along Nagappattinam coast. Current Science 89, 1947-1952.

Nair, R., Murari, M., Lakshmi, V., Buynevich, I., Goble, R., Srinivasan, P., Murthy, S., Trivedi, D., Kandpal, S., Hussain, S., Sengupta, D., Singhvi, A., 2011. Subsurface signatures and timing of extreme wave events along the southeast Indian coast. Journal of Earth System Sciences 120, 873-883.

Nanayama, F., Satake, K., Furukawa, R., Shimokawa, K., Atwater, B.F., Shigeno, K., Yamaki, S., 2003. Unusually large earthquakes inferred from tsunami deposits along the Kuril trench. Nature 424, 660-663.

Nanayama, F., Shigeno, K., 2006. Inflow and outflow facies from the 1993 tsunami in southwest Hokkaido. Sedimentary Geology 187, 139-58.

Nanayama, F., Shigeno, K., Satake, K., Shimokawa, K., Koitabashi, S., Miyasaka, S., Ishii, M., 2000. Sedimentary differences between the 1993 Hokkaido nansei-oki tsunami and the 1959 Miyakojima typhoon at Taisei, southwestern Hokkaido, northern Japan. Sedimentary Geology 135, 255-264.

Narayana, A.C., 2011. Tectonic geomorphology, tsunamis and environmental hazards: reference to Andaman-Nicobar Islands. Natural Hazards 57, 65-82.

Naruse, H., Fujino, S., Suphawajruksakul, A., Jarupongsakul, T., 2010. Features and formation processes of multiple deposition layers from the 2004 Indian Ocean tsunami at Ban Nam Khem, southern Thailand. Island Arc 19, 399-411.

Neubauer, N.-P., Brill, D., Brückner, H., Kelletat, D., Scheffers, S., Vött, A., 2011. 5000 Jahre Tsunami-Geschichte am Kap Pakarang (Thailand). Coastline Reports 17, 81-89.

Newcomb, K.R., McCann, W.R., 1987. Seismic history and seismotectonics oft the Sunda Arc. Journal of Geophysical Research 92, 421-439.

Nichol, S.L., Goff, J.R., Devoy, R., Chagué-Goff, C., Hayward, B., James, I., 2007. Lagoon subsidence and tsunami on the West Coast of New Zealand. Sedimentary Geology 200, 248-262.

Nichol, S.L., Chagué-Goff, C., Goff, J., Horrocks, M., McFadgen, B.G., Strotz, L.C., 2010. Geomorphology and accommodation space as limiting factors on tsunami deposition: Chatham Island, southwest Pacific Ocean. Sedimentary Geology 229, 41-52.

Nielsen, A., Murray, A.S., Pejrup, M., Elberling, B., 2006. Optically stimulated luminescence dating of a Holocene beach ridge plain in northern Jutland, Denmark. Quaternary Geochronology 1, 305-312.

Nishimura, Y., Miyaji, N., 1995. Tsunami deposits from the 1993 southwest Hokkaido earthquake and the 1640 Hokkaido Komagatake eruption, Northern Japan. Pure and Applied Geophysics 144, 719-733.

Nott, J., 2003. Waves, coastal boulder deposits and the importance of the pre-transport setting. Earth and Planetary Science Letters 210, 269-276.

Okal, E.A., Synolakis, C.E., 2008. Far-field tsunami hazard from mega-thrust earthquakes in the Indian Ocean. Geophysical Journal International 172, 995-1015.

Ortiz, M., Bilham, R., 2003. Source area and rupture parameters of the 31 December 1881 Mw 7.9 Car Nicobar earthquake estimated from tsunamis recorded in the Bay of Bengal. Journal of Geophysical Research 108, 2215.

Osborne, A.R., Burch, T.L., 1980. Internal solitons in the Andaman Sea. Science 208, 451-460.

Otvos, E.G., 2000. Beach ridges – definitions and significance. Geomorphology 32, 83-108.

Papadopoulos, G., Caputo, R., McAdoo, B., Pavlides, S., Karastathis, V., Fokaefs, A., Orfanogiannaki, K., Valkaniotis, S., 2006. The large tsunami of 26 December 2004: Field observations and eyewitnesses accounts from Sri Lanka, Maldives Islands and Thailand. Earth Planets Space 58, 233-241.

Papadopoulos, G., Imamura, F., 2001. A proposal for a new tsunami intensity scale. ITS Proceedings 5, 569-577.

Pari, Y., Ramana Murthy, M.V., Jaya Kumar, S., Subramanian, B.R., Ramachandran, S., 2008. Morphological changes at Vellar estuary, India – impact of the December 2004 tsunami. Journal of Environmental Management 89, 45-57.

Paris, R., Wassmer, P., Sartohadi, J., Lavigne, F., Barthomeuf, B., Desgages, E., Grancher, D., Baumert, P., Vautier, F., Brunstein, D., Gomez, C., 2009. Tsunamis as geomorphic crises: lessons from the December 26, 2004 tsunami in Lhok Nga, West Banda Aceh (Sumatra, Indonesia). Geomorphology 104, 59-72.

Paris, R., Fournier, J., Poizot, E., Etienne, S., Morin, J., Lavigne, F., Wassmer, P., 2010. Boulder and fine sediment transport and deposition by the 2004 tsunami in Lhok Nga (western Banda Aceh, Sumatra, Indonesia): A coupled offshore-onshore model. Marine Geology 268, 43-54.

Patwardhan, A., Sharma, U., 2005. Improving the methodology for assessing natural hazard impacts. Global and Planetary Change 47, 253-265.

Peltier, W.R., 1999. Global sea level rise and glacial isostatic adjustment. Global and Planetary Change 20, 93-123.

Peltier, W.R., 2002. On eustatic sea level history: Last glacial maximum to Holocene. Quaternary Science Reviews 21, 377-396.

Peters, R., Jaffe, B.E., 2010. Identification of tsunami deposits in the geologic record: developing criteria using recent tsunami deposits. U.S. Geological Survey Open-File Report, 39pp.

Peterson, C., Cruikshank, K., Schlichting, R., Braunsten, S., 2010. Distal run-up records of latest Holocene paleotsunami inundation in alluvial flood plains: Neskowin and Beaver Creek, Oregon, Central Cascadia Margin, West Coast U.S.A. Journal of Coastal Research 26, 622-634.

Peterson, C., Carver, G., Cruikshank, K., Abramson, H., Garrison-Laney, C., Dengler, L, 2011. Evaluation of the use of paleotsunami deposits to reconstruct inundation distance and run-up heights associated with prehistoric inundation events, Crescent City, southern Cascadia margin. Earth Surface Processes and Landforms 36, 967-980.

Phantuwongraj, S., Choowong, M., 2011. Tsunamis versus storm deposits from Thailand. Natural Hazards 63, 31-50.

Pielke, R.J., Pielke, R.S., 1997. Hurricanes: Their nature and impacts on society. Chichester.

Pilarczyk, J.E., Reinhardt, E.G., 2012. Testing foraminiferal taphonomy as a tsunami indicator in a shallow arid system lagoon: Sur, Sultanate of Oman. Marine Geology 295-298, 128-136.

Pinegina, T.K., Bourgeois, J., 2001. Historical and paleo-tsunami deposits on Kamchatka, Russia; long-term chronologies and long-distance correlations. Natural Hazards and Earth System Sciences 1, 177-185.

Pinegina, T., Bourgeois, J., Bazanova, L., Melekestsev, I., Braitseva, O., 2003. A millennialscale record of Holocene tsunamis on the Kronotskiy Bay coast, Kamchatka, Russia. Quaternary Research 59, 36-57.

Pirazzoli, P.A., 1991. World Atlas of Holocene sea-level changes. Elsevier Oceanography Series 58, 300pp.

Pirazzoli, P.A., 2005. Sea-level indicators, geomorphic. In: Schwartz, M.L., (ed.). Encyclopedia of Coastal Science, 836-838.

Prendergast, A., Cupper, M. L., Jankaew, K., Sawai, Y., 2012. Indian Ocean tsunami recurrence from optical dating of tsunami sand sheets in Thailand. Marine Geology 295-298, 20-27.

Preusser, F., Degering, D., Fuchs, M., Hilgers, A., Kadereit, A., Klasen, N., Krbetschek, M., Richter, D., Spencer, J., 2008. Luminescence dating: basics, methods and applications. Quaternary Science Journal (Eiszeitalter und Gegenwart) 57, 95-149.

Prichard, D., Dickinson, L., 2008. Modelling the sedimentary signature of long waves on coasts: implications for tsunami reconstruction. Sedimentary Geology 206, 42-57.

Priest, G., Goldfinger, Ch., Wang, K., Witter, R., Zhang, Y., Baptista, A., 2010. Confidence levels for tsunami-inundation limits in northern Oregon inferred from a 10,000-year history of great earthquakes at the Cascadia subduction zone. Natural Hazards 54, 27-73.

Rajendran, C.P., Rajendran, K., Machado, T., Satyamurthy, T., Aravazhi, P., Jaiswal, M., 2006. Evidence of ancient sea surges at the Mamallapuram coast of India and implications for previous Indian Ocean tsunami events. Current Science 91, 1242-1247.

Rajendran, C.P., Rajendran, K., Srinivasalu, S., Andrade, V., Aravazhi, P., Sanwal, J., 2011. Geoarchaeological evidence of a Chola-Period tsunami from an ancient port at Kaveripattinam on the southeastern coast of India. Geoarchaeology 26, 867-887.

Rajendran, K., Rajendran, C.P., Earnest, A., Ravi Prasad, G.V., Dutta, K., Ray, D.K., Anu, R., 2008. Age estimates of coastal terraces in the Andaman and Nicobar Islands and their tectonic implications. Tectonophysics 455, 53-60.

Ranasinghage, P.N., Ortiz, J.D., Moore, A.L., Siriwardana, C., McAdoo, B.G., 2010. Signatures of paleo-coastal hazards in back-barrier environments of eastern and southeastern Sri Lanka. Abstract volume of the AGU Fall Meeting, San Francisco, USA.

Rasser, M.W., Riegl, B., 2002. Holocene coral reef rubble and its binding agents. Coral Reefs 21, 57-72.

Rastogi, B.K., Jaiswal, R.K., 2006. A catalog of tsunamis in the Indian Ocean. Science of Tsunami Hazards 25, 128-143.

Reimer, P.J., Baillie, M.G.L., Bard, E., Bayliss, A., Beck, J.W., Blackwell, P.G., Bronk Ramsey, C., Buck, C.E., Burr, G.S., Edwards, R.L., Friedrich, M., Grootes, P.M., Guilderson, T.P., Hajdas, I., Heaton, T.J., Hogg, A.G., Hughen, K.A., Kaiser, K.F., Kromer, B., McCormac, F.G., Manning, S.W., Reimer, R.W., Richards, D.A., Southon, J.R., Talamo, S., Turney, C.S.M., van der Plicht, J., Weyhenmeyer, C.E., 2009. IntCal09 and Marine09 radiocarbon age calibration curves, 0–50,000 years cal BP. Radiocarbon 51, 1111-1150.

Rhodes, B., Tuttle, M., Horton, B., Doner, L., Kelsey, H., Nelson, A., Cisternas, M., 2006. Paleotsunami research. EOS 87, 205-206.

Rhodes, B., Kirby, M.E., Jankaew, K. Choowong, M., 2011. Evidence for a mid-Holocene tsunami deposit along the Andaman coast of Thailand preserved in a mangrove environment. Marine Geology 282, 255-267.

Rhodes, E.J., Bailey, R.M., 1997. The effect of thermal transfer on the zeroing of the luminescence of quartz from recent glaciofluvial sediments. Quaternary Science Reviews 16, 291-298.

Richmond, B.M., Jaffe, B.E., Gelfenbaum, G., Morton, R.A., 2006. Geologic impacts of the 2004 Indian Ocean tsunami on Indonesia, Sri Lanka, and the Maldives. Zeitschrift für Geomorphologie 146, 235-251.

Richmond, B., Buckley, M., Etienne, S., Chagué-Goff, C., Clark, K., Goff, J., Dominey-Howes, D., Strotz, L., 2011. Deposits, flow characteristics, and landscape change resulting from the September 2009 south Pacific tsunami in the Samoan islands. Earth-Science Reviews 107, 38-51.

Roberts, H., Plater, A.J., 2006. Reconstruction of Holocene foreland progradation using optically stimulated luminescence (OSL) dating: an example from Dungeness, UK. The Holocene 17, 495-505.

Rodnight, H., 2008. How many equivalent dose values are needed to obtain a reproducible distribution? Ancient TL 26, 3-9.

Rodolfo, K.S., 1969. Sediments of the Andaman Basin, northeastern Indian Ocean. Marine Geology 7, 371-402.

Rohling, E.J., Grant, K., Hemleben, C., Siddal, M., Hoogakker, B., Bolshaw, M., Kocera, M., 2008. High rates of sea-level rise during the last interglacial period. Nature Geocsience 1, 38-42.

Rosetto, T., Peiris, A., Pomonis, A., Wilkinson, S.M, Del Re, D., Koo, R., Gallocher, S., 2007. The Indian Ocean tsunami of December 26, 2004: observations in Sri Lanka and Thailand. Natural Hazards 42, 105-124.

Römer, H., Willroth, P., Kaiser, G., Vafeidis, A., Ludwig, R., Sterr, H., Revilla Diez, J., 2012. Potential of remote sensing techniques for tsunami hazard and vulnerability analysis – a case study from Phang-nga province, Thailand. Natural Hazards and Earth Sysetm Science 12, 2103-2126.

Ruiz, F., Abad, M., Caceres, L.M., Vidal, J.R., Carretero, M.I., Pozo, M., Gonzalez-Delgado, M.L., 2010. Ostracods as tsunami tracers in Holocene sequences. Quaternary Research 73, 130-135.

Sakuna, D., Szczuciński, W., Feldens, P., Schwarzer, K., Khokiattiwong, S., accepted. Sedimentary deposits left by the 2004 Indian Ocean tsunami on the inner continental shelf offshore of Khao Lak, Andaman Sea (Thailand). Earth Planets Space.

Satake, K., Atwater, B., 2007. Long-term perspectives on giant earthquakes and tsunamis at subduction zones. Annual Reviews of Earth and Planetary Science 35, 349-374.

Satake, K., Aung, T., Sawai, Y., Okamura, Y., Win, K., Swe, W., Swe, C., Swe, T.L., Tun, S.T., Soe, M.M., Oo, T.Z., Zaw, S.H., 2006. Tsunami heights and damage along the Myanmar coast from the December 2004 Sumatra-Andaman earthquake. Earth Planets Space 58, 243-152.

Sawai, Y., Jankaew, K., Martin, M. E., Prendergast, A., Choowong, M., Charoentitirat, T., 2009. Diatom assemblages in tsunami deposits associated with the 2004 Indian Ocean tsunami at Phra Thong Island, Thailand. Marine Micropaleontology 73, 70-79.

Scheffers, A., Kelletat, D., 2003. Sedimentologic and geomorphologic tsunami imprints worldwide – a review. Earth-Science Reviews 63, 83-92.

Scheffers, A., Kelletat, D., 2005. Tsunami relics in the coastal landscape west of Lisbon, Portugal. Science of Tsunami Hazards 23, 3-16.

Scheffers, A., Kelletat, D., Vött, A., May, S.M., Scheffers, S., 2008. Late Holocene tsunami traces on the western and southern coastlines of the Peloponnesus (Greece). Earth and Planetary Science Letters 269, 271-279.

Scheffers, A., Brill, D., Kelletat, D., Brückner, H., Scheffers, S., Fox, K., 2012a. Holocene sea levels along the Andaman Sea coast of Thailand. The Holocene 22, 1162-1173.

Scheffers, A., Engel, M., Scheffers, S., Squire, P., Kelletat, D., 2012b. Beach ridge systems – Archives for Holocene coastal events? Progress in Physical Geography 36, 5-37.

Scheffers, A., Scheffers, S., Squire, P., 2012c. Trimlines as evidence for palaeo-tsunamis. Natural Hazards 63, 165-179.

Scheffers, S.R., Haviser, J., Browne, T., Scheffers, A., 2009. Tsunamis, hurricanes, the demise of coral reefs and shifts in prehistoric human populations in the Caribbean. Quaternary International 195, 69-87.

Scheffers, S., Brill, D., Brückner, H., Kelletat, D., Vött, A., 2010. A tsunami proxy from Indian Ocean corals. The 4th Thai-German Scientific Conference "Ocean Geosciences, Marine Ecology and Engineering for Natural Hazard Management and Sustainable Use of Marine Resources", 27-29 February 2010, Bangkok, Thailand.

Scheucher, L., Vortisch, W., 2011. Sedimentological and geomorphological effects of the Sumatra-Andaman Tsunami in the area of Khao Lak, southern Thailand. Environmental Earth Sciences 63, 785-796.

Schulte, P., Alegret, L., Arenillas, I., Arz, J., Barton, P., Bown, P., Bralower, T., Christeson, G., Laeys, P., Cockell, Ch., Collins, G., Deutsch, A., Goldin, T., Goto, K., Grajales-Nishimura, J., Grieve, R., Gulick, S., Johnson, K., Kiessling, W., Koeberl, Ch., Kring, D., MacLeod, K., Matsui, T., Melosh, J., Montanari, A., Morgan, J., Neal, C., Nichols, D., Norris, R., Pierazzo, E., Ravizza, G., Rebolledo-Vieyra, M., Reimold, W., Robin, E., Salge, T., Speijer, R., Sweet, A., Urrutia-Fucugauchi, J., Vajda, V., Whalen, M., Willumsen, P., 2010. The Chicxulub Asteroid Impact and Mass Extinction at the Cretaceous-Paleogene Boundary. Science 327, 1214-1218.

Scoffin, T.P., le Tissier, M.D.A., 1998. Late Holocene sea level and reef flat progradation, Phuket, south Thailand. Coral Reefs 17, 273-276.

Scott, D.B., Medioli, F.S., 2005. Sea-level indicators – biological in depositional sequences. In: Schwartz, M.L., (ed.). Encyclopedia of Coastal Science. Springer, 835-835.

Shah-hosseini, M., Morhange, C., Naderi Beni, A., Marriner, N., Lahijani, H., Hamzeh, M., Sabatier, F., 2011. Coastal boulders as evidence for high-energy waves on the Iranian coast of Makran. Marine Geology 290, 17-28.

Shanmugam, G., 2006. The tsunamite problem. Journal of Sedimentary Research 76, 718-730.

Shanmugam, G., 2012. Process-sedimentological challenges in distinguishing paleo-tsunami deposits. Natural Hazards 63, 5-30.

Shen, B.W., Tao, W.K., Lau, W.K., Atlas, R., 2010. Predicting tropical cyclogenesis with a global mesoscale model: Hierarchical multiscale interactions during the formation of tropical cyclone Nargis (2008). Journal of Geophysical Research 115, doi:10.1029/2009JD013140.

Shi, S., Dawson, A.G., Smith, D., 1995. Coastal sedimentation associated with the December 12th, 1992 Tsunami in Flores, Indonesia. Pure and Applied Geophysics 144, 525-536.

Shiki, T., Yamazaki, T., 2008. The term "Tsunamiite". In: Shiki, T., Tsuji, Y., Yamazaki, T. (eds.). Tsunamiites. Features and Implications, 5-7.

Sibuet, J.-C., Rangin, C., Le Pichon, X., Singh, S., Cattaneo, A., Graindorge, D., Klingelhoefer, F., Lin, Y. L., Malod, J., Maury, T., Schneider, J. L., Sultan, N., Umber, M., Yamaguchi, H., 2007. 26th December 2004 great Sumatra–Andaman earthquake: Co-seismic and post-seismic motions in northern Sumatra. Earth and Planetary Science Letters 263, 88-103.

Sieh, K., 2006. Sumatran megathrust earthquakes: from science to saving lives. Philosophical Transactions of the Royal Society of America 364, 1947-1963.

Sieh, K., Natawidjaja, D.H., Meltzner, A.J., Shen, Ch., Cheng, H., Li, K., Suwargadi, B.W., Galetzka, J., Philibosian, B., Edwards, R.L., 2008. Earthquake supercycles inferred from the sea-level changes recorded in the corals of West Sumatra. Science 322, 1674-1678.

Singh, O.P., Ali Khan, T.M., Rahman, M.S., 2000. Changes in the frequency of tropical cyclones over the North Indian Ocean. Meteorology and Atmospheric Physics 75, 11-20.

Sinsakul, S., 1992. Evidence of Quaternary sea level changes in the coastal areas of Thailand: a review. Journal of Southeast Asian Earth Sciences 7, 23-37.

Sinsakul, S., 2000. Late Quaternary geology of the Lower Central Plain, Thailand. Journal of Asian Earth Sciences 18, 415-426.

Sinsakul, S., Sonsuk, M., Hasting, P.J., 1985. Holocene sea levels in Thailand: evidence and basis for interpretation. Journal of Geological Society Thailand 8, 1-12.

Small, C., Gornitz, V., Cohen, J.E., 2000. Coastal hazards and the global distribution of human population. Environmental Geosciences 7, 3-12.

Smedile, A., De Martini, P.M., Pantosti, D., Bellucci, L., Del Carlo, P., Gasperini, L., Pirrotta, C., Polonia, A., Boschi, E., 2011. Possible tsunami signatures from an integrated study in the Augusta Bay offshore (Eastern Sicily – Italy). Marine Geology 281, 1-13.

Smith, D.E., Foster, I.D.L., Long, D., Shi, S., 2007. Reconstructing the pattern and depth of flow onshore in a paleotsunami from associated deposits. Sedimentary Geology 200, 362-371.

Soloviev, S.L., Solovieva, O.N., Go, C.N., Kim, K.S., Shchetnikov, N.A., 2000. Tsunamis in the Mediterranean Sea 2000 B.C.-2000 A.D. Dordrecht. 243pp.

Som, S.K., Shivgotra, V., Saha, A., 2009. Coral microatoll as geodetic tool in North Andaman and Little Andaman, India. Journal of Earth System Sciences 118, 157-162.

Soulsby, R.L., Smith, D.E., Ruffman, A., 2007. Reconstructing tsunami run-up from sedimentary characteristics – a simple mathematical model. Coastal Sediments '07(2), 1075-1088.

Southon, J., Kashgarian, M., Fontugne, M., Metivier, B., Yim, W.W.S., 2002. Marine reservoir corrections for the Indian Ocean and southeast Asia. Radiocarbon 44, 167-180.

Spiegel-Online, 2012. 34 Meter hohe Wellen könnten Japan treffen. Article from 01.04.2012. http://www.spiegel.de/wissenschaft/natur/0,1518,825048,00.html; last access: 05.05.2012.

Spiske, M., Bahlburg, H., 2011. A quasi-experimental setting of coarse clast transport by the 2010 Chile tsunami (Bucalemu, Central Chile). Marine Geology 289, 72-85.

Spiske, M., Weiss, R., Bahlburg, H., Roskosch, J., Amijaya, H., 2010. The TsuSedMod inversion model applied to the deposits of the 2004 Sumatra and 2006 Java tsunami and implications for estimating flow parameters of paleo-tsunami. Sedimentary Geology 224, 29-37.

Srinivasalu, S., Thangadurai, N., Switzer, A.D., Ram Mohan, V., Ayyamperumal, T., 2007. Erosion and sedimentation in Kalpakkam (N Tamil Nadu, India) from the 26th December 2004 tsunami. Marine Geology 240, 65–75.

Srinivasalu, S., Thangadurai, N., Jonathan, M.P., Armstrong-Altrin, J.S., Ayyamperumal, T., Ram-Mohan, V., 2008. Evaluation of trace-metal enrichments from the 26 December 2004 tsunami sediments along the southeast coast of India. Environmental Geology 53, 1711-1721.

Srisutam, C., Wagner, J.-F., 2010. Tsunami sediment characteristics at the Thai Andaman coast. Pure and Applied Geophysics 167, 215-232.

Stein, S., Okal, E.A., 2007. Ultra long period seismic study of the December 2004 Indian Ocean earthquake and implications for regional tectonics and the subduction process. Bulletin of the Seismological Society of America 97, 279–295.

Stephenson, T.A., Stephenson, A., 1949. The universal features of zonation between tide- marks on rocky coasts. Journal of Ecology 37, 289-305.

Stokes, S., 1992. Optical dating of young (modern) sediments using quartz: results from a selection of depositional environments. Quaternary Science Reviews 11, 153-159.

Subarya, C., Chlieh, M., Prawirodirdjo, L., Avouac, J.P., Bock, Y., Sieh, K., Meltzner, A.J., Natawidjaja, D.H., McCaffery, R., 2006. Plate-boundary deformation associated with the great Sumatra–Andaman earthquake. Nature 440, 46–51.

Sugawara, D., Minoura, K., Imamura, F., 2008. Tsunamis and tsunami sedimentology. In: Shiki, T., Tsuji, Y., Yamazaki, T. (eds.). Tsunamiites. Features and Implications, 9-49.

Sugawara, D., Minoura, K., Nemoto, N., Tsukawaki, S., Goto, K., Imamura, F., 2009. Foraminiferal evidence of submarine sediment transport and deposition by backwash during the 2004 Indian Ocean tsunami. Island Arc 18, 513-525.

Switzer, A.D., Jones, B.G., 2008. Large-scale overwash sedimentation in a freshwater lagoon from the southeast Australian coast: sea-level change, tsunami or exceptionally large storm? The Holocene 18, 787–803.

Switzer, A.D., Pucillo, K., Haredy, R.A., Jones, B.G., Bryant, E.A., 2005. Sea level, storm or tsunami: enigmatic sand sheet deposits in a sheltered coastal embayment from southeastern New South Wales, Australia. Journal of Coastal Research 21, 655–663.

Switzer, A.D., Srinivasalu, S., Thangadurai, N., Ram Mohan, V., 2012. Bedding structures in Indian tsunami deposits provide clues to the dynamics of tsunami inundation. Geological Society of London 361, 61-77.

Synolakis, C., Bardet, J.-P., Borrero, J., Davies, H., Okal, E., Silver, E., Sweet, S., Tappin, D., 2002. The slump origin of the 1998 Papua New Guinea tsunami. Proceedings of the Royal Society of London 458, 763-789.

Szczuciński, W., 2010. Post-depositional changes of sedimentological and geochemical monitoring. Abstract Volume of the 3rd International Tsunami Field Symposium. Sendai, Japan, 189–190.

Szczuciński, W., 2012. The post-depositional changes of the onshore 2004 tsunami deposits on the Andaman Sea coast of Thailand. Natural Hazards 60, 115-133.

Szczuciński, W., Niedzielski, P., Rachlewicz, G., Sobczynski, T., Ziola, A., Kowalski, A., Lorenc, S., Siepak, J., 2005. Contamination of tsunami sediments in a coastal zone inundated by the 26 December 2004 tsunami in Thailand. Environmental Geology 49, 321-331.

Szczuciński, W., Chaimanee, N., Niedzielski, P., Rachlewicz, G., Saisuttichai, D., Tepsuwan, T., Lorenc, S., Siepak, J., 2006. Environmental and geological impacts of the 26 December 2004 Tsunami in coastal zone of Thailand – overview of short and long-term effects. Polish Journal of Environmental Studies 15, 793–810.

Szczuciński, W., Niedzielski, P., Kozak, L., Frankowski, M., Ziola, A., Lorenc, S., 2007. Effects of rainy season on mobilization of contaminants from tsunami deposits left in a coastal zone of Thailand by the 26 December 2004 tsunami. Environmental Geology 53, 253–264.

Tanabe, S., Saito, Y., Sato, Y., Suzuki, Y., Sinsakul, S., Tiyapairach, S., Chaimanee, N., 2003. Stratigraphy and Holocene evolution of the mud-dominated Chao Phraya delta, Thailand. Quaternary Science Reviews 22, 789-807.

Tanner, W., 1995. Origin of beach ridges and swales. Marine Geology 129, 149-161.

Tantanasiriwong, R., 1978. An illustrated checklist of marine shelled gastropods from Phuket Island, adjacent mainland and offshore islands, western peninsular Thailand. Phuket Marine Biological Center Research Bulletin 21.

Taylor, M., Stone, G., 1996. Beach-ridges: a review. Journal of Coastal Research 12, 612-621.

Titov, V., Rabinovich, A.B., Mofjeld, H.O., Thomson, R.E., Gonzalez, F.I., 2005. The global reach of the 26 December 2004 Sumatra tsunami. Science 309, 2045-2048.

Tjia, H.D., 1996. Sea-level changes in the tectonically stable Malay–Thai Peninsula. Quaternary International 31, 95-101.

Tomanek, L., Helmuth, B., 2002. Physiological ecology of rocky intertidal organisms: a synergy of concepts. Integrative and Comparative Biology 42, 771-775.

Trisirisatayawong, I., Naeije, M., Simons, W., Fenoglio-Marc, L., 2011. Sea level change in the Gulf of Thailand from GPS-corrected tide gauge data and multi-satellite altimetry. Global and Planetary Change 76, 137-151.

Tsuji, Y., Namegaya, Y., Matsumotu, H., Iwasaki, S., Kanbua, W., Sriwichai, M., Meesuk, V., 2006. The 2004 Indian tsunami in Thailand: Surveyed runup heights and tide gauge records. Earth Planets Space 58, 223-232.

Tuttle, M.P., Ruffman, A., Anderson, T., Jeter, H., 2004. Distinguishing tsunami from storm deposits in eastern North America: the 1929 Grand Banks Tsunami versus the 1991 Halloween Storm. Seismological Research Letters 75, 117-131.

Uchida, J., Fujiwara, O., Hasegawa, S., Kamataki, T., 2010. Sources and depositional processes of tsunami deposits: Analysis using foraminiferal tests and hydrodynamic verification. Island Arc 19, 427-442.

Umitsu, M., Tanavud, Ch., Patanakanog, B., 2007. Effects of landforms on tsunami flow in the plains of Banda Aceh, Indonesia, and Nam Khem, Thailand. Marine Geology 242, 141-153.

UN Department of Humanitarian Affairs, 1989. Thailand Typhoon Gay 1989. UN Situation Report, 2304.

UNESCO, 2007. Tsunami risk assessment and mitigation for the Indian Ocean: knowing your tsunami risk – and what to do about it. IOC Manual and Guides No. 52, Paris.

Van de Plassche, O. (ed.), 1986. Sea-level research: A manual for the collection and evaluation of data. Norwich, 618pp.

Vött, A., Brückner, H., 2006. Versunkene Häfen im Mittelmeerraum. Geographische Rundschau 58, 12-20.

Vött, A., Brückner, H., Schriever, A., Luther, J., Handl, M., van der Borg, K., 2006. Holocene palaeogeographies oft the Palairos coastal plain (Akarnania, Northwest Greece) and their geoarchaeological implications. Geoarchaeology 21, 649-664.

Vött, A., Schriever, A., Handl, M., Brückner, H., 2007. Holocene palaeogeographies oft the Eastern Acheloos River delta and the lagoon of Etoliko (NW Greece). Journal of Coastal Research 23, 1042-1066.

Vött, A., Brückner, H., May, M., Lang, F., Herd, R., Brockmüller, S., 2008. Strong tsunami impact on the Bay of Aghios Nikolaos and its environs (NW Greece) during Classical–Hellenistic times. Quaternary International 181, 105-122.

Vött, A., Brückner, H., Brockmüller, S., Handl, M., May, S.M., Gaki-Papanastassiou, K., Herd, R., Lang, F., Maroukian, H., Nelle, O., Papanastassiou, D., 2009. Traces of Holocene tsunamis across the sound of Lefkada, NW Greece. Global and Planetary Change 66, 112-128.

Wallinga, J., 2002. On the detection of OSL age overestimation using single-aliquot techniques. Geochronometria 21, 17-26.

Wang, P., Horwitz, M.H., 2007. Erosional and depositional characteristics of regional overwash deposits caused by multiple hurricanes. Sedimentology 54, 545–564.

Watkinson, I., Elders, C., Hall, R., 2008. The kinematic history of the Khlong Marui and Ranong Faults, southern Thailand. Journal of Structural Geology 30, 1554–1571.

Weiss, R., Bahlburg, H., 2006. A note on the preservation of offshore tsunami deposits. Journal of Sedimentary Research 76, 1267-1273.

Weiss, R., Fritz, H., Wünnemann, K., 2009. Hybrid modelling oft the mega-tsunami runup in Lituya Bay after half a century. Geophysical Research Letters 36, 1-6.

Willroth, P., Revilla Diez, J., Arunotai, N., 2011. Modelling the economic vulnerability of households in the Phang-Nga province (Thailand) to natural disasters. Natural Hazards 58, 753-769.

Wintle, A.G., Murray, A.S., 2006. A review of quartz optically stimulated luminescence characteristics and their relevance in single-aliquot regeneration dating protocols. Radiation Measurements 41, 369-391.

Witter, R., Zhang, Y., Priest, G., 2008. Reconstructing hydrodynamic flow parameters of the 1700 tsunami at Ecola Creek, Cannon Beach, Oregon. US Geological Survey. Final Technical Report. 59pp.

Wong, P., 2009. Impacts and recovery from a large tsunami: Coasts of Aceh. Polish Journal of Environmental Studies 18, 5-16.

Woodroffe, C.D., 2005. Late Quaternary sea-level highstands in the central and eastern Indian Ocean: A review. Global and Planetary Change 49, 121-138.

Woodroffe, S.A., 2009. Testing models of mid to late Holocene sea-level change, North Queensland, Australia. Quaternary Science Reviews 28, 2474-2488.

Woodroffe, S.A., Horton, B.P., 2005. Late and post-glacial sea level changes of the Indo-Pacific: a review. Journal of Asian Earth Science 5, 29-43.

WoRMS, 2012. Foraminifera. [http://www.marinespecies.org/aphia.php?p=taxdetails&id=1410;2012-09-13].

Yanagisawa, H., Koshimura, S., Goto, K., Miyagi, T., Imamura, F., Ruangrassamee, A., Tanavud, C., 2009. The reduction effects of mangrove forest on a tsunami based on field surveys at Pakarang Cape, Thailand and numerical analysis. Estuarine, Coastal and Shelf Science 81, 27-37.

Yawsangratt, S., Szczuciński, W., Chaimanee, N., Jagodzinski, R., Lorenc, S., Chatprasert, S., Saisuttichai, D., Tepsuwan, T., 2009. Depositional effects of 2004 tsunami and hypothetical paleotsunami near Thap Lamu Navy Base in Phang Nga Province, Thailand. Polish Journal of Environmental Studies 18, 17-23.

Yawsangratt, S., Szczuciński, W., Chaimanee, N., Chatprasert, S., Majewski, W., Lorenc, S., 2011. Evidence of probable palaeotsunami deposits on Kho Khao Island, Phnag Nga Province, Thailand. Natural Hazards 63, 151-163.

Yu, K.-F., Zhao, J.-X., Done, T., Chen, T.-G., 2009. Microatoll record for large century-scale sea-level fluctuations in the mid-Holocene. Quaternary Research 71, 354-360.

Ziegler, A.D., Wong, P.P., Grundy-Warr, C., 2009. Still vulnerable to killer tsunamis. Science 326, 1188-1189.

Zong, Y., 2004. Mid-Holocene sea-level highstand along the southeast coast of China. Quaternary International 117, 55-67.

Appendix 1

Additional sediment records from the west coast of Thailand – stratigraphical results from locations without evidence of palaeotsunamis.

Location of study sites

Besides the three locations investigated in detail in *Chapters 4-10*, seven additional sites were visited during field work in December 2008, including sandy coastal plains on Ko Ra, on Ko Kho Khao and at Bang Niang, mangroves and lagoons on Phuket, as well as karst depressions in the Phang-nga Bay (fig. S1). However, first explorations of geoarchives at these sites did not reveal promising evidence for detailed palaeotsunami research.
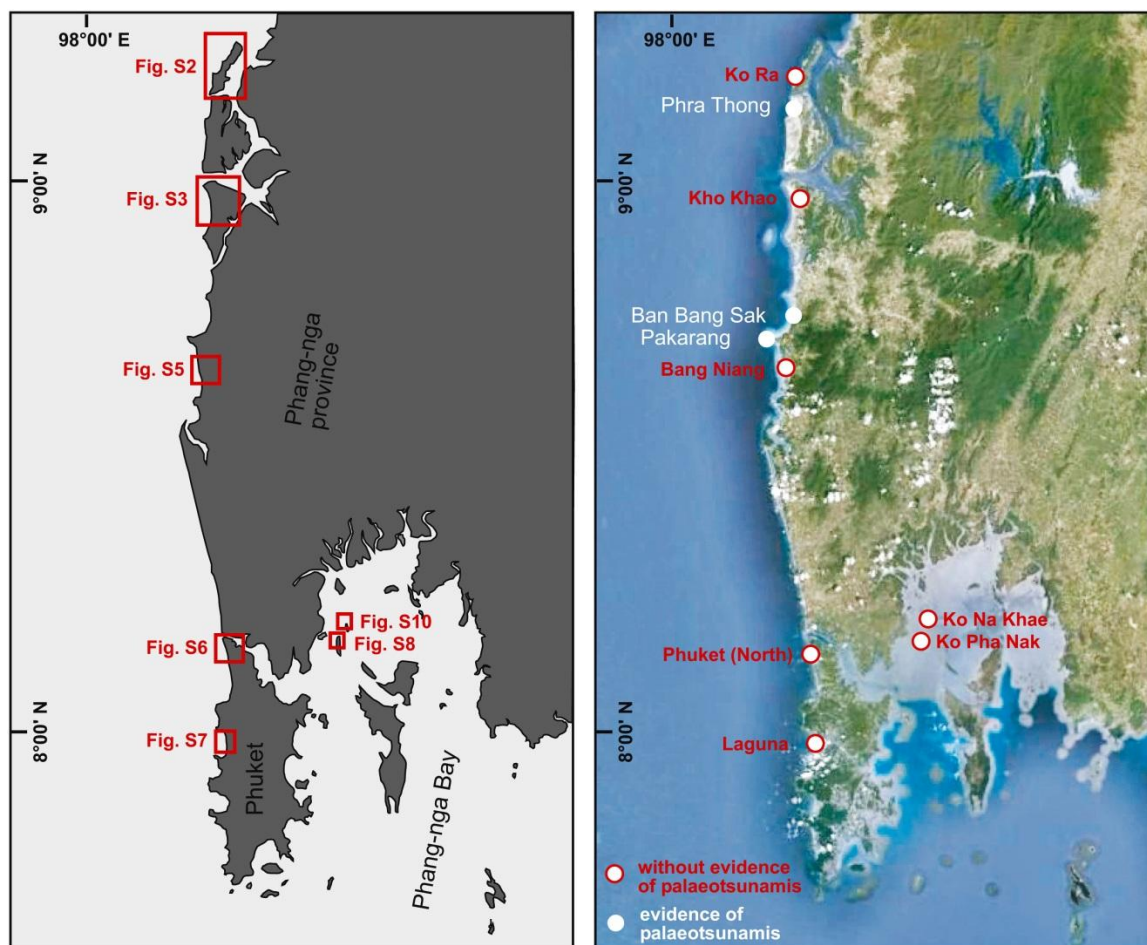
Figure S1: Geographical position of study sites without clear evidence of palaeotsunamis. Left: Google Earth image, 2012.
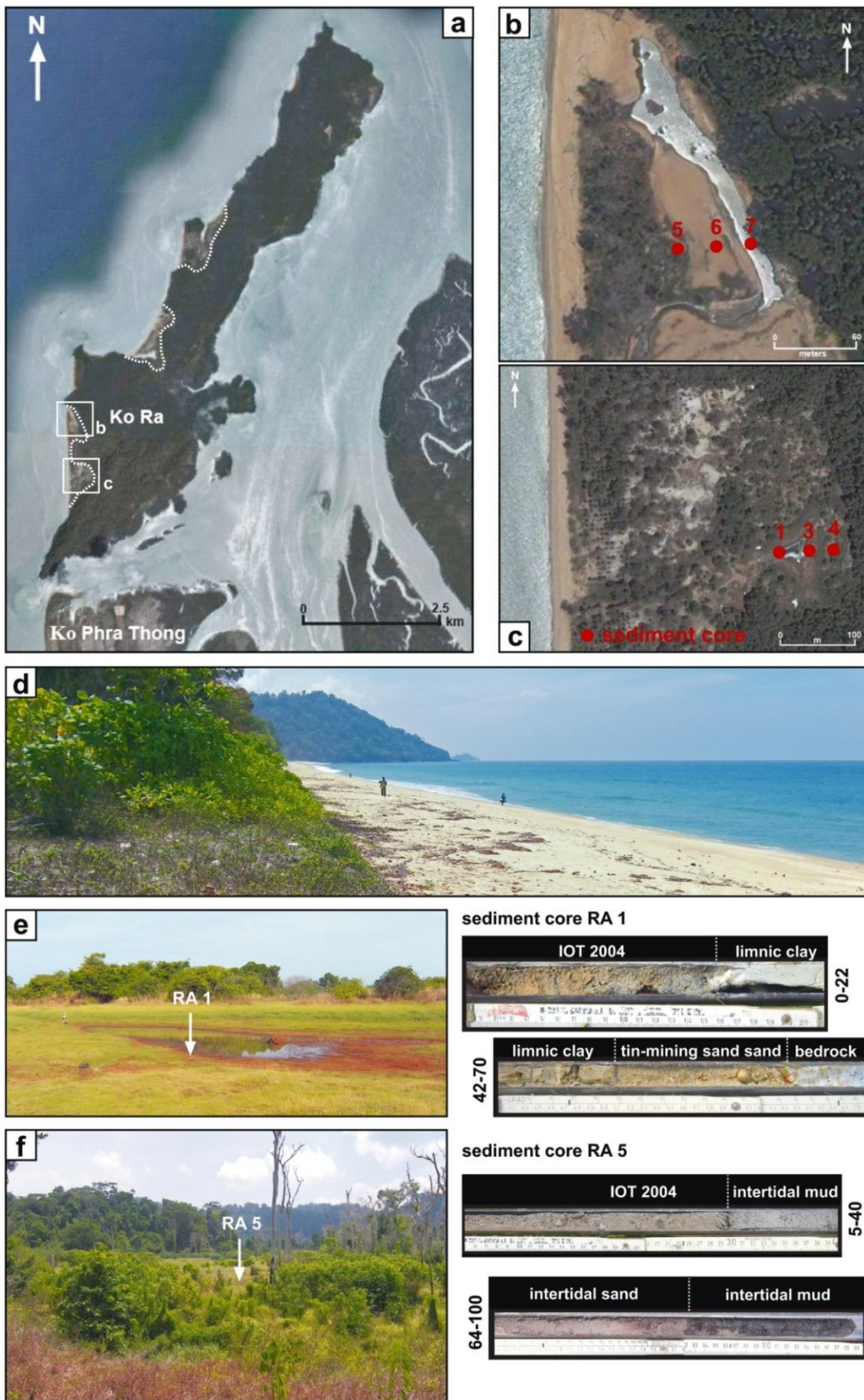
Figure S2: *Geographical overview (a-c: Google Earth, 2012) and sediment stratigraphy (e-f) of Ko Ra.*

Ko Ra – coastal plain

Ko Ra is the island directly to the north of Ko Phra Thong, separated only by a 250 m wide tidal channel (fig. S2a). In contrast to Ko Phra Thong, the island Ra is mainly build up by Tertiary, metamorphic rocks that form a nearly 100 m high, north-south running mountain range. Holocene sediments occur only at the western coast of the island, where they form narrow pocket beaches that are bordered to the east by steep slopes of the pre-Holocene bedrock. Due to tin-mining activity the coastal sediments are intensively disturbed, locally. Since the low lying areas along the western coast were flooded by high tsunami waves in 2004, the island was visited in March 2010 and explored for potential evidence of prehistoric tsunamis. For this, a total of seven Pürckhauer cores (RA 1-7) with lengths of 1 m each were taken in the coastal plain at the southern end of the island (fig. S2).

Cores RA 1-4 were taken at the eastern margin of the southern part of the coastal plain. The sediment cores originate from shallow, water-filled depressions in the undulating topography and document a succession of weathered bedrock below 0.60-0.70 m b.s. (decalcified clay with weathered rock fragments), littoral sand (well washed, yellow sand with pebbles), fine-grained pond deposits (homogeneous, white mud), and the sand sheet of the IOT 2004 that was hardly recognisable in 2010 (fig. S2e). In cores RA 5-7, taken in the northern part of the coastal plain next to the inlet of a small river and separated from the sea by a 3 m high beach ridge, the sand sheet of the IOT covers organic rich marsh deposits and intertidal mud. Within the exploration range of 1 m the base of the intertidal deposits could not be reached (fig. S2f).

Apart from the deposit of the IOT 2004 that covers most parts of the low lying coastal area, no evidence of older tsunami inundations was found. In the southern part of the investigated area, where bedrock was already present in depths of less than 1 m, restricted accommodation space and disturbance of the thin Holocene sediment cover by tin mining seem to be responsible for the absence of prehistoric tsunami deposits. In contrast, a possible archive for predecessors of the IOT 2004 could exist within the muddy sediments along the river inlet in the northern section of the plain. However, the limited core depth of only 1 m did not allow for exploration of the whole sediment succession to evaluate this hypothesis.

Kho Khao Island – sandy beach-ridge plain

The island Kho Khao is separated by narrow tidal channels from Phra Thong Island in the north and the mainland in the east (fig. S1). It extends 16 km from north to south and up to 7 km in east-west direction. Similar to Phra Thong, Kho Khao Island is composed mainly of Quaternary sediments. Pre-Quaternary rocks outcrop only at its northern spit, where they form a c. 90 m high mountain ridge. The exposed western part of the island is generally dominated

by a sandy, grass covered ridge plain with shallow swales, while the sheltered eastern coast is dominated by mangroves and tidal channels. The IOT 2004 inundated the exposed coastal plain to a distance of more than 1 km from the shoreline and caused heavy erosion of the beach, resulting in shoreline retreat and erosive scarps with uprooted trees.
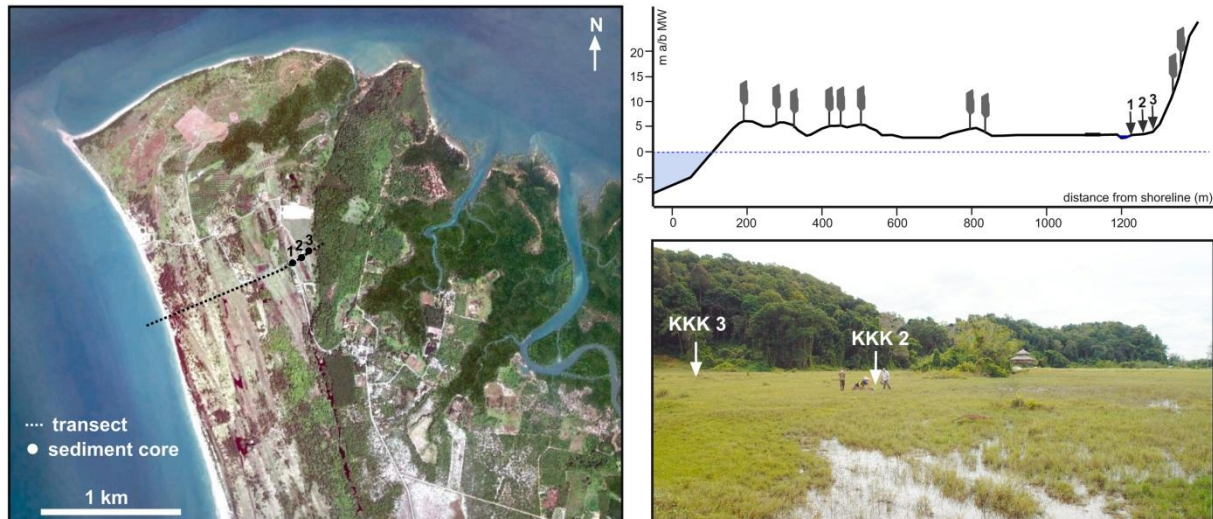

Figure S3: *Position of sediment cores from Kho Khao Island. Left: Google Earth image, 2012.*

In December 2008 three vibra corings, reaching depths of 3-4 m b.s., were performed more than 1200 m east of the shoreline at the northern spit of the island, where the coastal plain is limited by the steep slope of the pre-Quaternary bedrock (fig. S3). All sediment cores originate from the elongated, swampy depression of a coast-parallel swale that was sampled along a west-east transect (KKK 1 – KKK 2 – KKK 3). Core **KKK 1** starts with grey, carbonate-rich fine sand with abundant mica and fragments of *Cerastoderma glaucum* (unit II – shallow marine) from 3.00 to 1.63 m b.s. Above follows greyish-brown, decalcified medium to coarse sand with fine gravel (unit III – littoral). Eventually, the normally graded sand layer of the IOT 2004, documented from 0.50 to 0.30 m b.s., is covered by organic mud (unit IVa – coastal swamp). Core **KKK 2** shows a similar succession of deposits but reaches the pre-Holocene bedrock (unit Ia – yellowish, decalcified, stiff clay with weathered rock fragments) within the coring depth at 3.37 m b.s. Above follow deposits of unit II (shallow marine) from 3.37-1.56 m b.s., unit III (littoral) from 1.56-0.29 m b.s. and the IOT 2004 deposit on top. In core **KKK 3** (fig. S4) the pre-Holocene bedrock (unit Ia) is already reached in a depth of 2.90 m below surface. Above unit II (shallow marine), between 2.90 and 1.27 m b.s., white, decalcified clayey silt that was deposited in a limnic milieu (unit IVb) is documented. The succession is terminated by the sand sheet of the IOT 2004 that forms an erosive contact with the limnic mud below, and the brown organic mud (unit IVa) of the recent swampy environment on top.

sediment core KKK 3

Figure S4: Photograph of sediment core KKK 3.

In all three cores evidence of tsunamis older than 2004 is absent. On the one hand the sandy background sedimentation could mask possible evidence of palaeotsunamis (in KKK 1 and KKK 2 even the IOT 2004 deposit could hardly be distinguished in 2008). On the other hand the shallow topography did not allow for the formation of preservative archives under natural conditions, since low-energy environments with sedimentation of limnic mud (KKK 3) are the result of more recent tin-mining activity. However, suitable archives might exist further south on the island, where a potential palaeotsunami deposit was documented by Yawsangratt et al. (2012).

Ban Bang Niang – coastal plain

Ban Bang Niang is located in the central section of the Khao Lak coastal plain, an area today dominated by artificial structures and drained by a small river. Therefore, a clear topography-based discrimination into ridges and swales is not possible anymore. In December 2008 two vibra cores were taken in a distance of 1200 m from the shoreline, close to the eastern limit of the coastal plain. The place got famous for a police boat that was transported inland for more than 1 km by the IOT 2004 (fig. S5).

A 1.20 m deep profile cut by the river shows that the upper part of the sediment succession is dominated by fluvial deposition and the impact of the IOT 2004 (fig. S5). Sediment core **BBN 1**, taken directly next to it, reached intensively weathered alluvial deposits from the early Holocene or Pleistocene (unit Ib) at 6.70 m below surface. The transgressive sequence above (unit II.2) is strongly influenced by the input of river load in form of subangular gravel. Between 4.68 and 1.90 m b.s., grey mud with occasional marine shells indicates sheltered marine sedimentation (unit II.2). The stratigraphy is terminated by stratified alluvial deposits (unit IVc) and the IOT 2004 layer at 0.42-0.11 m b.s. that contains large amounts of litter and construction debris. In core **BBN 2**, taken several meters further east, the pre-transgressive substrate starts already at 3.40 m b.s. in the form of weathered alluvial gravel. Above, marine deposits with strong fluvial and colluvial influence, indicated by angular gravel and the scarcity of marine fossils, are documented. Fluvial sediments above 2.44 m b.s. terminate the succession.
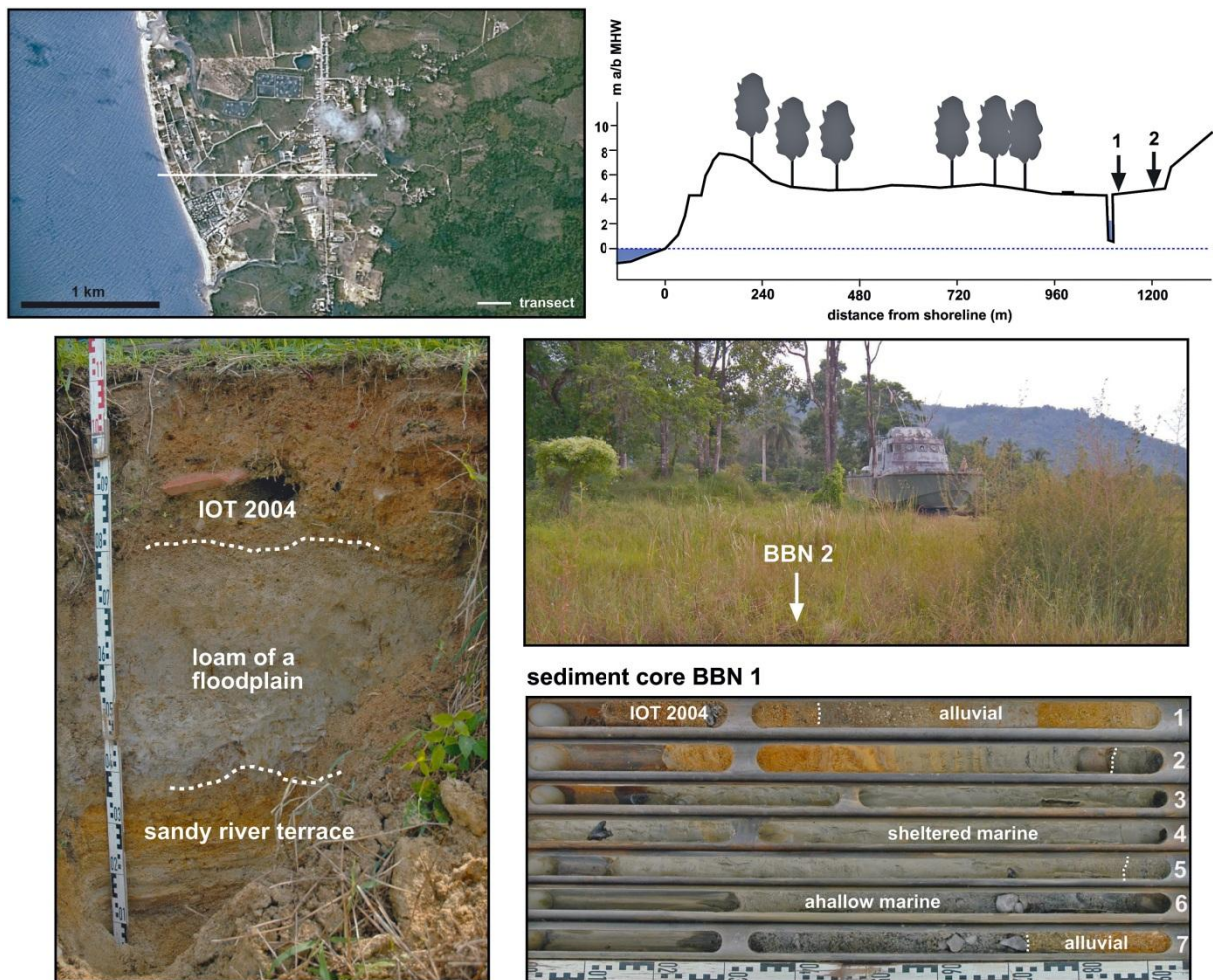
Figure S5: *Location of coring sites (top left: Google Earth image, 2012; top right: GPS transect marked in the satellite image) and stratigraphy of coastal sediments at Ban Bang Niang.*

The sediment archives documented in BBN 1 and 2 are not suited to preserve evidence of palaeotsunamis. The sediment dynamics of the river environment, with repeated cycles of deposition and erosion due to channel shifting, and the overall sandy background sedimentation hinder preservation and identification of potential palaeotsunamites.

North Phuket – mangrove forest

Two push cores of 70 cm length were analysed from the mangrove area at the northern spit of Phuket (fig. S6). Here, the mangrove forests at the sheltered eastern side of the island are separated from the exposed west coast solely by a 50 m wide and 4 m high beach ridge. Core **PHU 2a/1** reveals an alternation of dark brown, sandy peat and greyish brown sand (fig. S6). Although they have no sharp contacts, the layers are clearly discriminated by organic content and granulometry. While the organic-rich units are interpreted as in-situ sedimentation in the mangrove forest, the sandy parts seem to reflect input of material from the westward beach ridge. The uppermost sand unit at 0-10 cm b.s. might be deposited by the IOT 2004, but the

genesis of the other sand strata remains unclear. Since the whole succession, based on a radio-carbon-dated piece of bark, is younger than 4-299 years, the frequency of the sand sheets is too high to be the result of prehistoric tsunamis. In a second core several meters away, due to bioturbation, no stratification could be recognised at all.
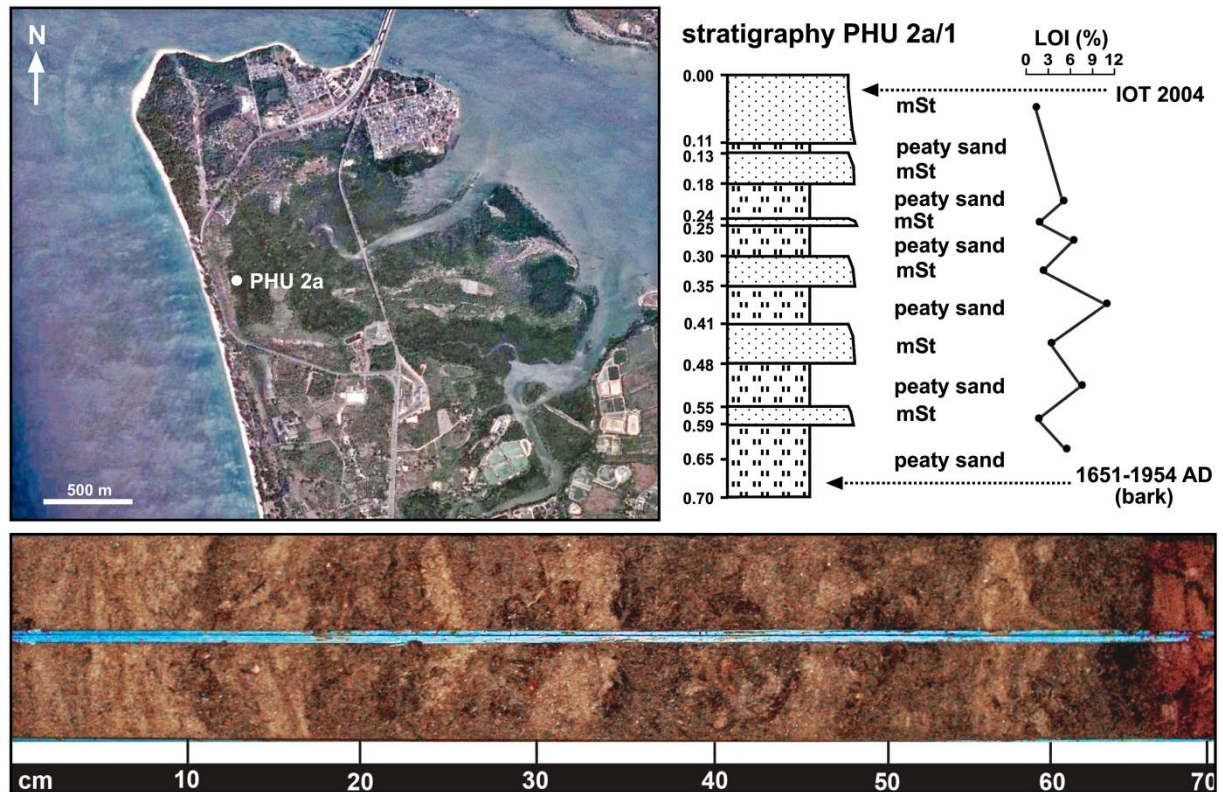
Figure S6: *Location of coring sites (Google Earth image, 2012) and stratigraphy of sediments (core PHU 2a/1) in the mangrove area of northern Phuket.*

Phuket Laguna – artificial lagoon

Phuket Laguna is an artificial lagoon at Bang Tao Beach, Phuket, and nowadays part of a tourist resort (fig. S7). It is separated from the sea by a 100 m wide sand barrier. Push cores were taken next to the sandy barrier (LAG 1c) and in the central part of the lagoon (LAG 1a). The 70 cm long core **LAG 1a** is composed of brown lagoonal mud that is interrupted only by a sandy layer of the IOT 2004 (fig. S7). Core **LAG 1c** documents littoral sand with marine shell fragments down to a depth of 2.70 m b.s. Although the central part of the lagoon due to the fine-grained background sedimentation provides a valuable archive for tsunami deposits in general, the young age of the water body limits this function to events that took place within the last century.

stratigraphy LAG 1a
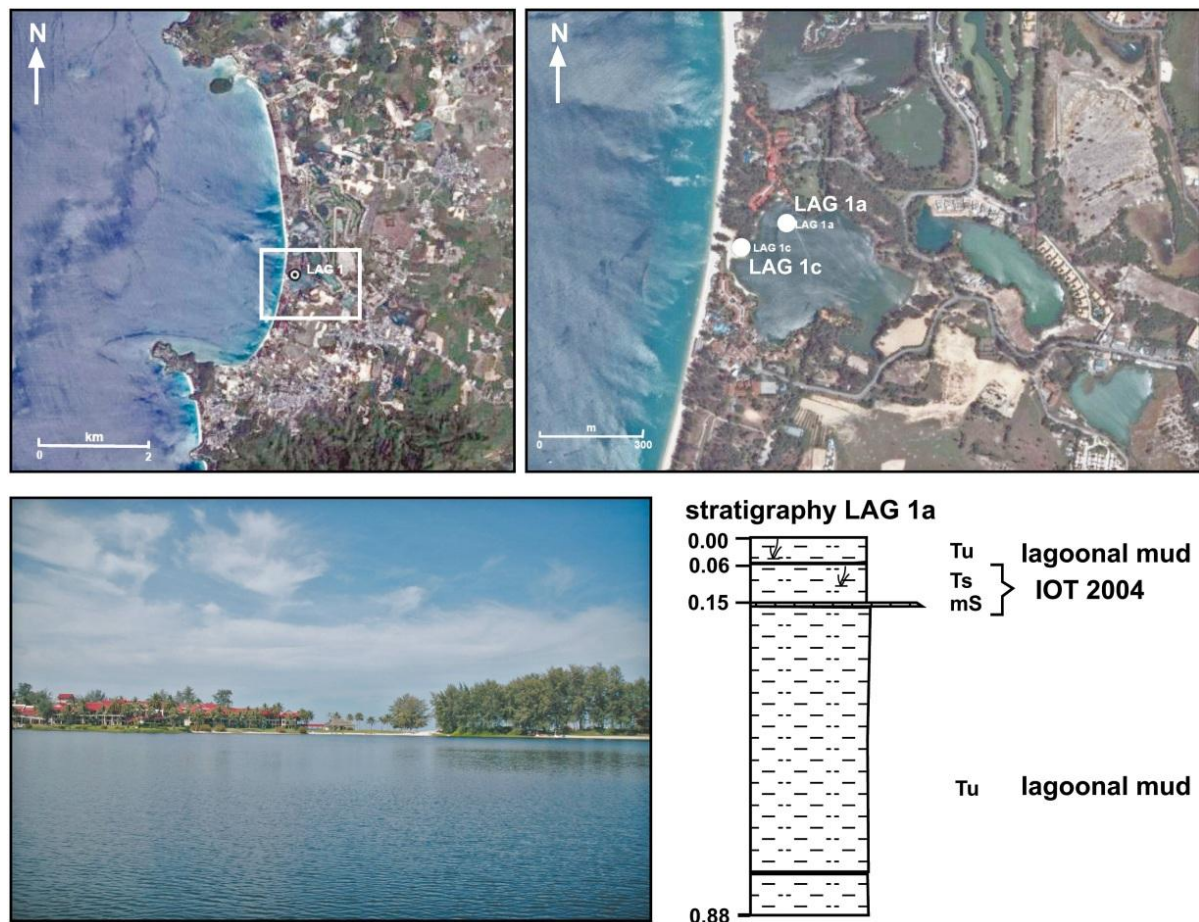
Figure S7: Location of coring sites (Google Earth images, 2012) and stratigraphy of sediments at Phuket Laguna.

Ko Pha Nak – water-filled karst depression

On the tower-karst island Pha Nak an approximately 2 m long sediment core was retrieved from a flooded karst depression in a water depth of 2 m. The shallow embayment is surrounded by steep limestone walls at three sides and opened to the sea only in the north (fig. S8). Core **KPN 1** is composed of silty mud with shell valves interrupted by layers of clayey sand with coral and rock oyster (*Saccostrea cucullata*) fragments at 1.39-1.18, 1.00-0.97, 0.81-0.78, 0.61-0.59 and the last 0.53 m below surface (fig. S9). While the silty units are interpreted as in-situ sedimentation in the sheltered embayment, the genesis of the sandy layers is still unclear. Since the IOT 2004 had only minor effects in this part of the Bay of Bengal, it is unlikely that the uppermost sand layer – normally graded, 50 cm thick, brown – is related to this event. Furthermore, the whole sediment succession below that layer is older than 4500 years, with the lowermost three sand layers radiocarbon dated to 3935-3363 cal BC, 3498-3109 cal BC, and older 2623-2473 cal BC. Therefore, the deposits might rather be connected to the Holocene sea-level maximum at 5500 cal BP than to the impacts of tsunamis.
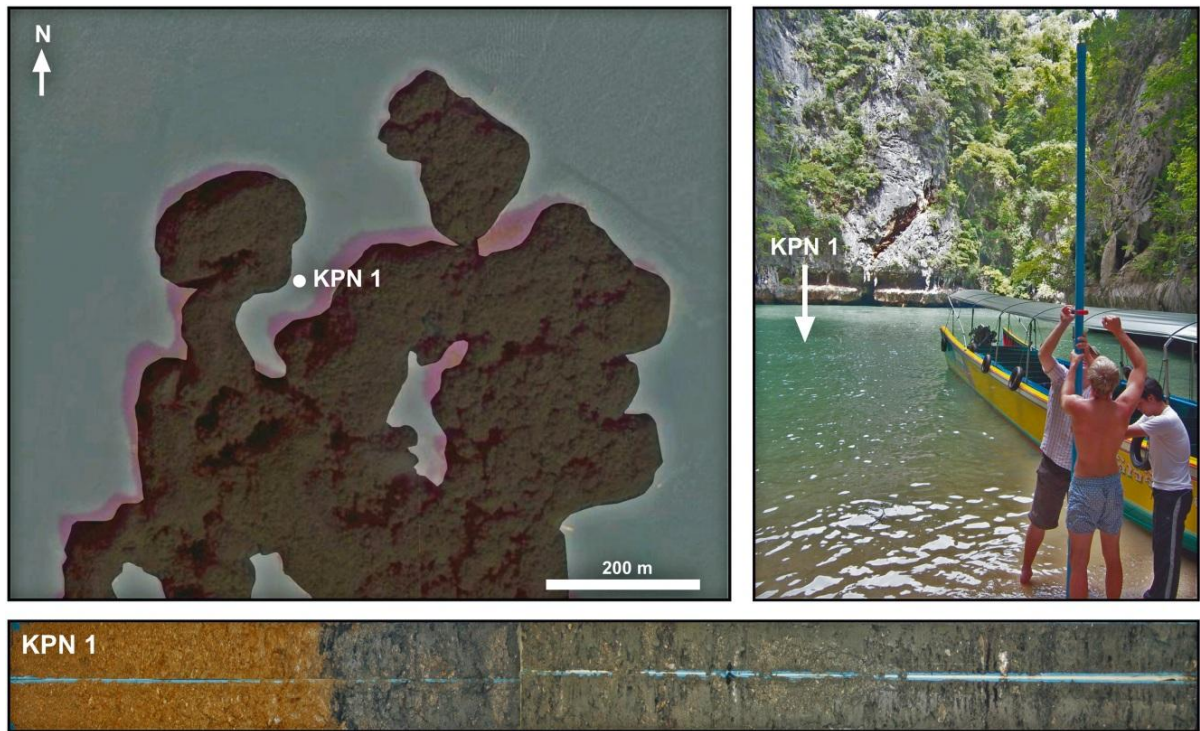
Figure S8: *Ko Pha Nak. Location of coring site (Google Earth image, 2012) and photograph of sediment core KPN 1.*
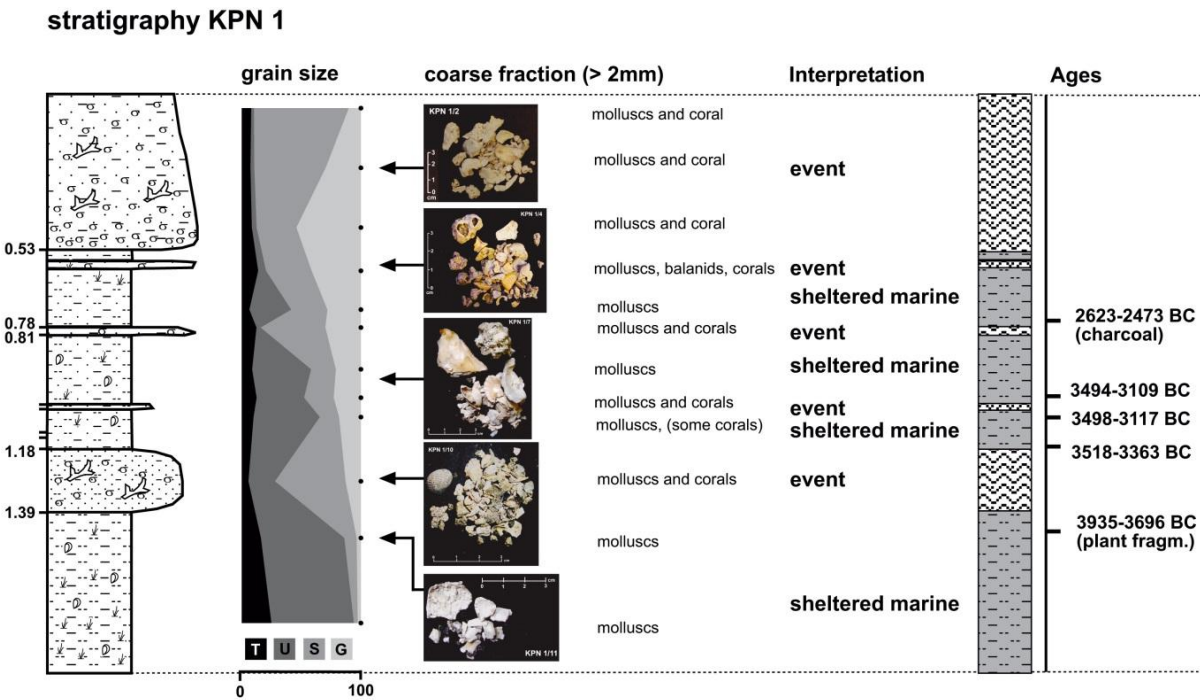
Figure S9: *Stratigraphy of core KPN 1. All ages are calibrated 2-sigma radiocarbon data.*

Ko Na Khae – terrestrial karst sinkhole

On Ko Na Khae, the sediment succession within a terrestrial karst sinkhole that is separated from the sea by a 10 m wide and 3 m high beach barrier was analysed. The depression is limited by steep limestone walls on three sides and opened to the sea only in the southwest (fig. S10). Two push cores (**KNK 1** and **KNK 2**) of 40 cm length revealed yellowish-brown, decalcified clay without any stratification mixed with angular fragments of rock oysters (*Saccostrea cucullata*) in the lower part of the cores. While the clayey substrate reflects the residual of intensively weathered limestone, the oyster fragments are indicative for marine flooding of the sinkhole. However, this flooding might be rather due to the elevated sea level during the mid-Holocene sea-level maximum (Scheffers et al., 2012) than due to flooding by tsunamis.
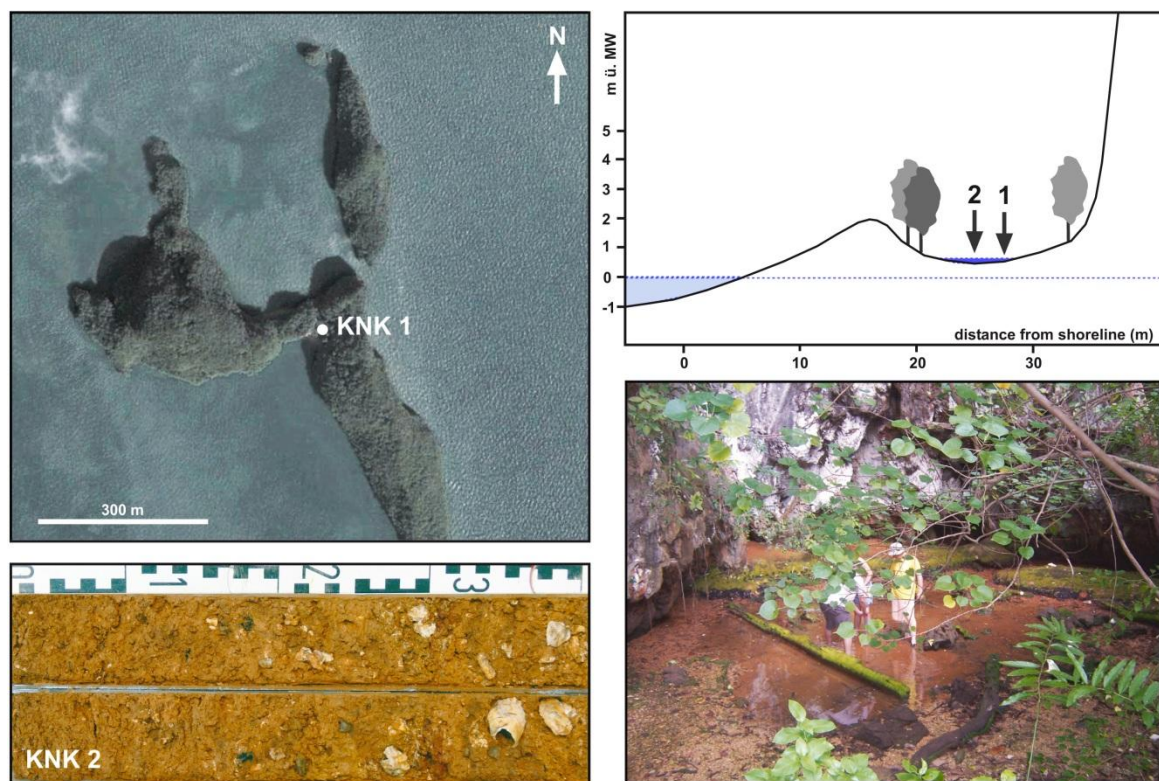
Figure S10: Ko Na Khae. Location (top left: Google Earth image, 2012; top right: topographic profile through the sink hole) and stratigraphical evidence of core KNK 2.

Appendix 2

Coastal evolution of Southwest Thailand during the Holocene – implications for site-specific occurrence of palaeotsunami deposits[5]
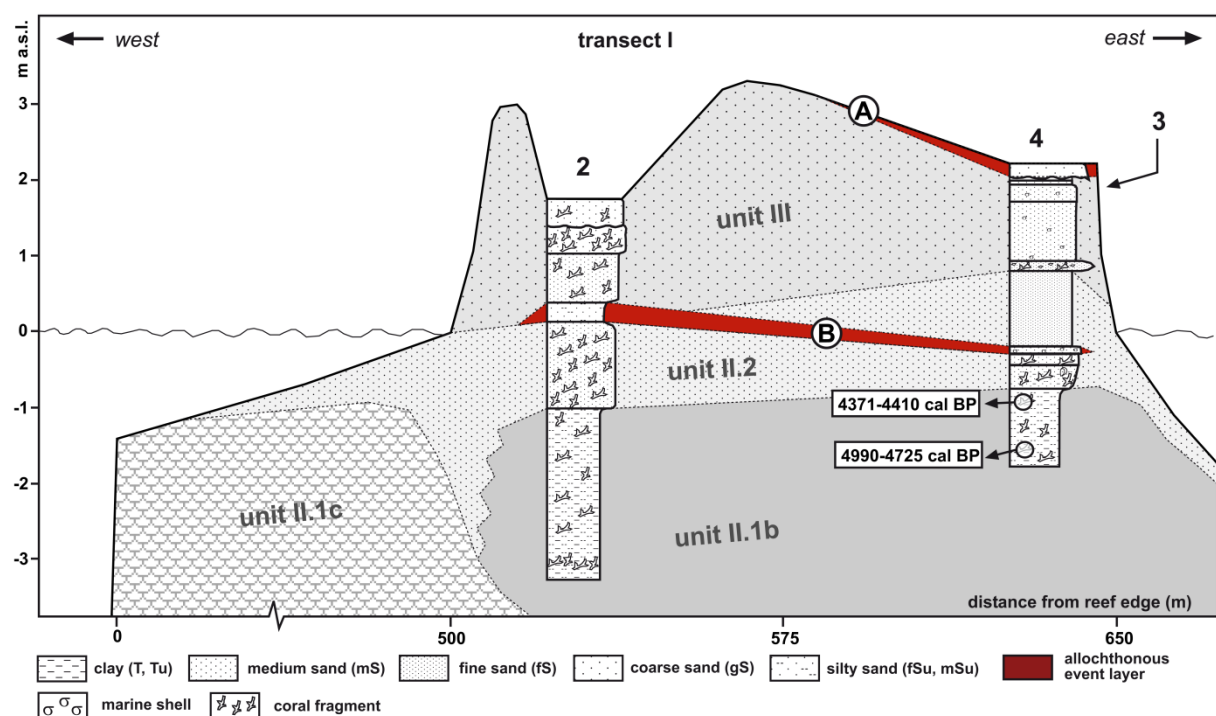
Figure S11*: Stratigraphical cross section through the sediment succession of Pakarang Cape along transect I.*
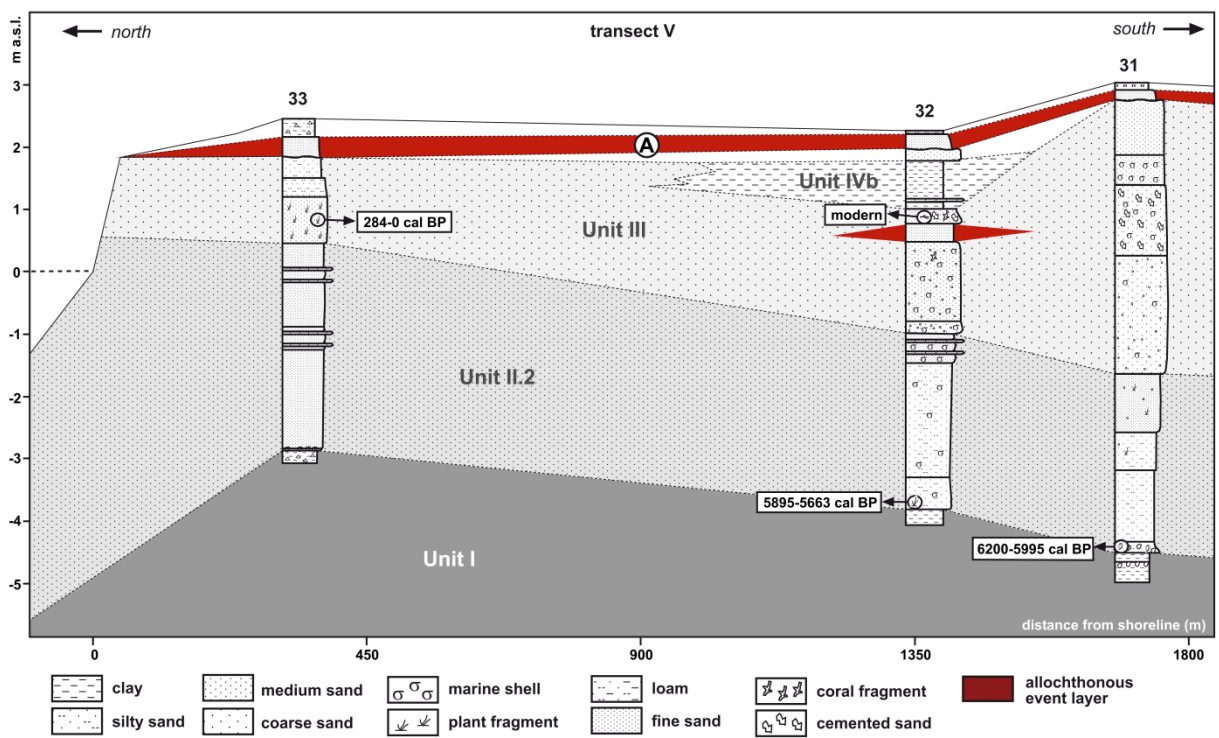
---

[5] Supplement material for Chapter 8.
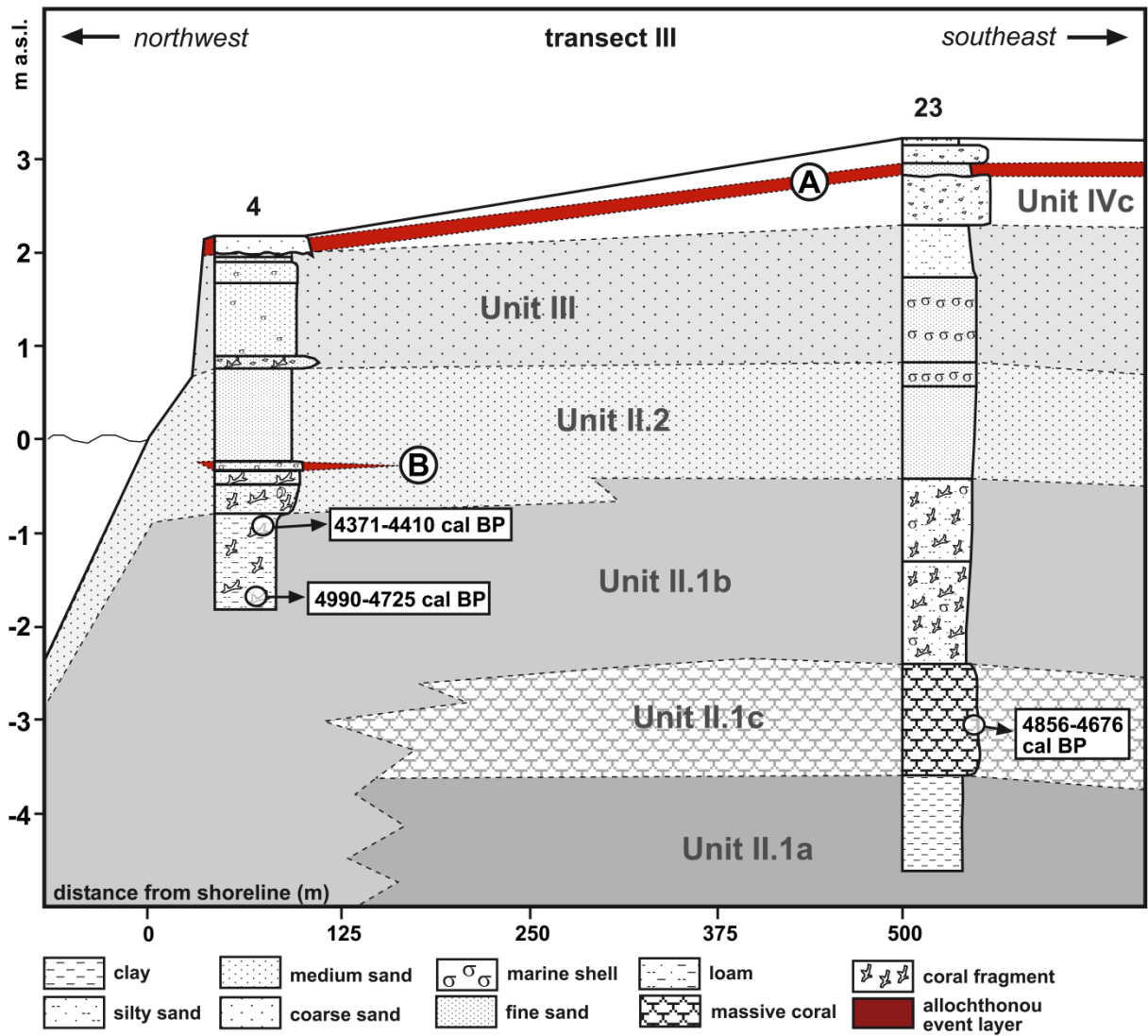
Figure S12*: Stratigraphical cross section through the sediment succession of Pakarang Cape along transect III.*
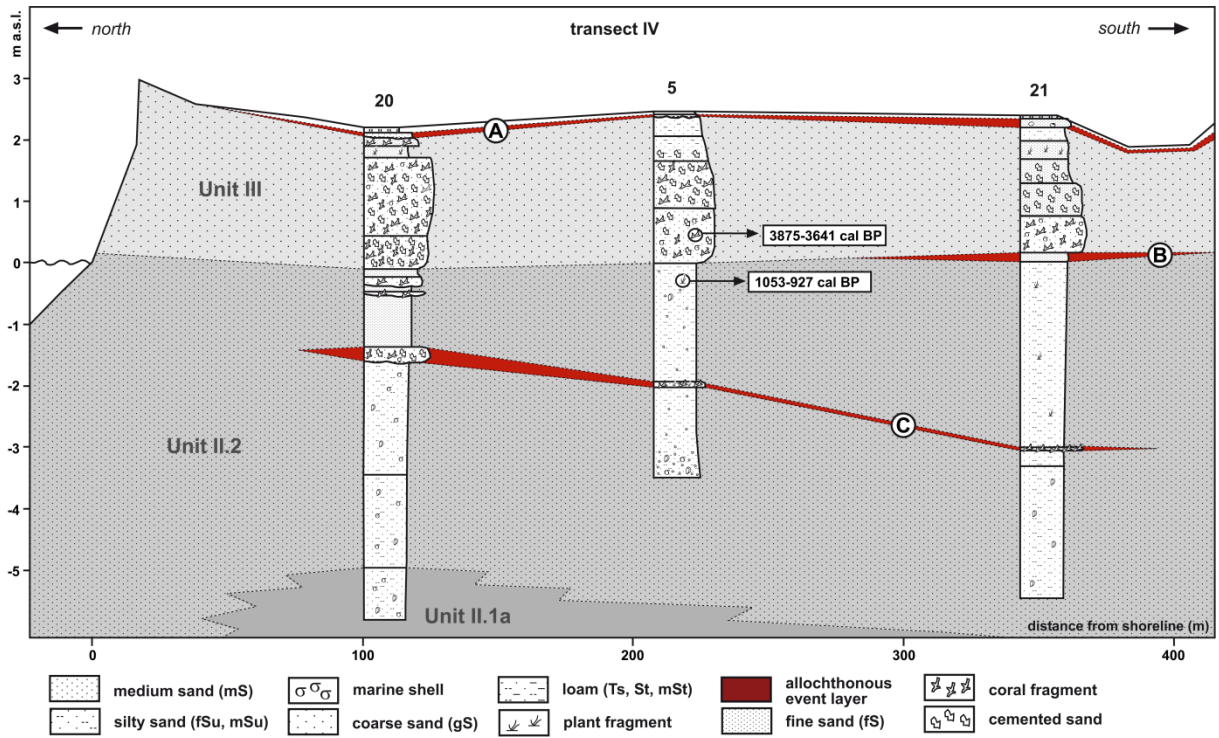
Figure S13: *Stratigraphical cross section through the coastal sediment succession of Pakarang Cape along transect IV*

Figure S14: *Stratigraphical cross section through the coastal sediment succession of Pakarang Cape along transect V.*
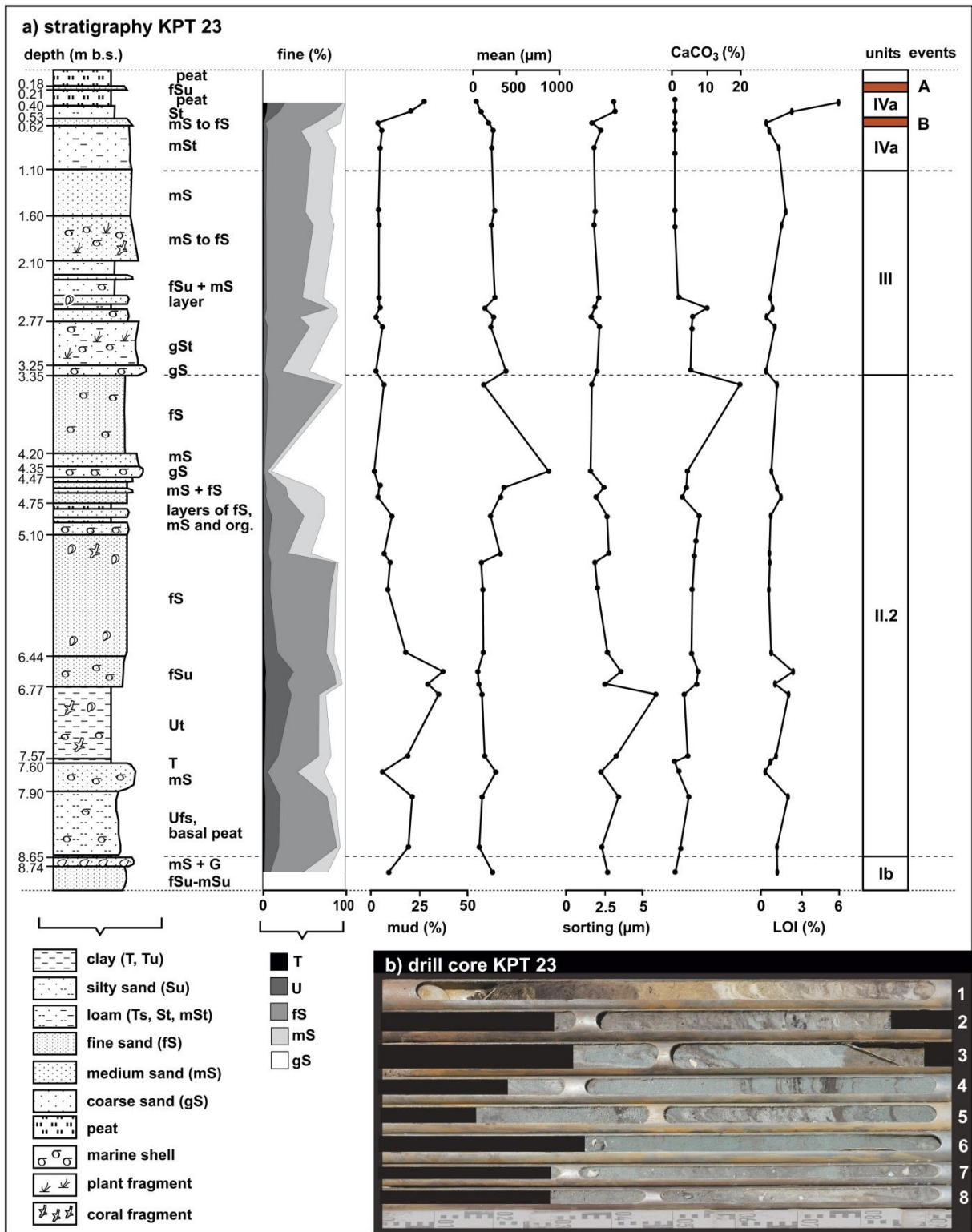
Figure S15: *Stratigraphy of sediment core KPT 23 as an example for the site-specific characteristics of sedimentary units on Phra Thong Island.*
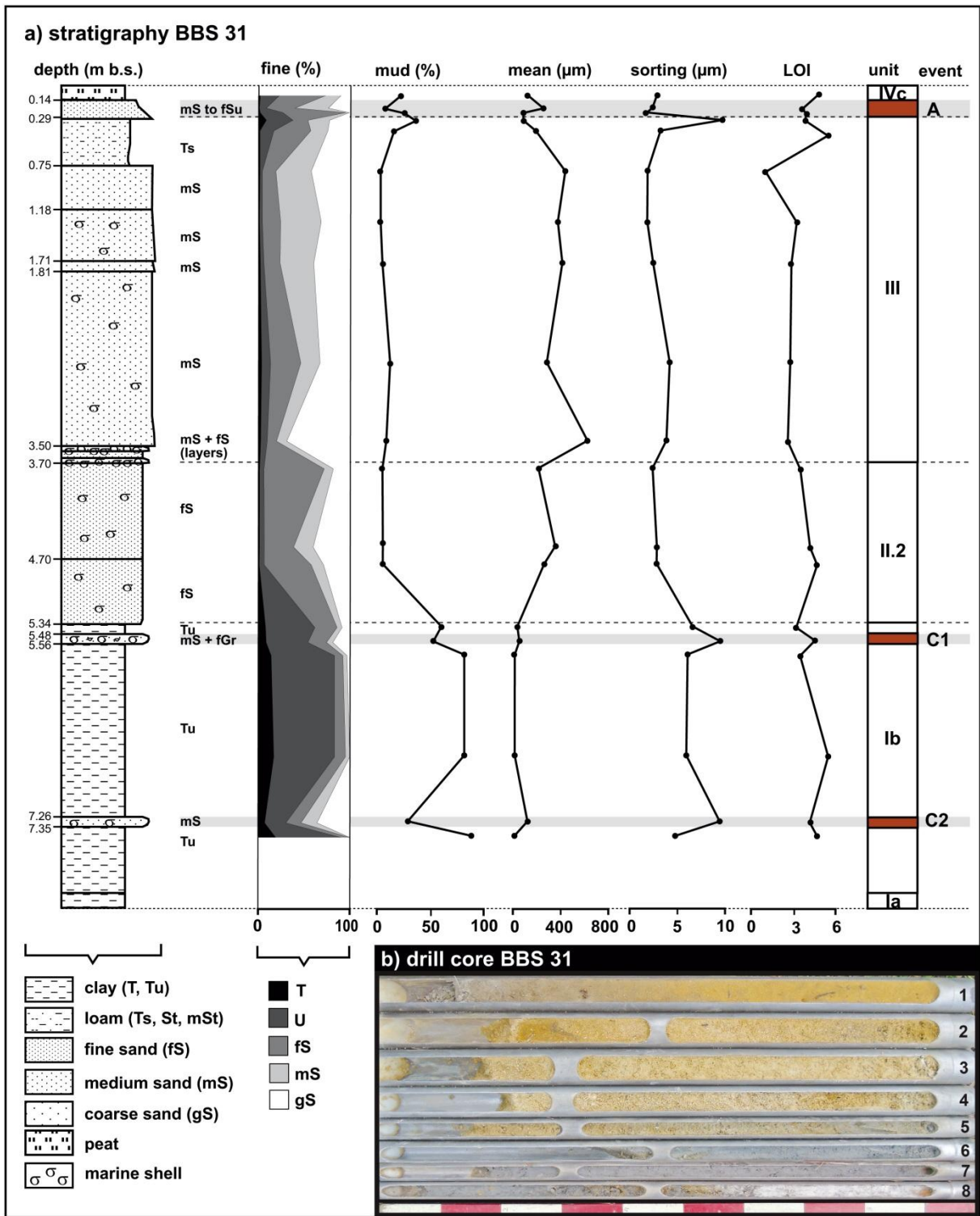
Figure S16*: Stratigraphy of sediment core BBS 31 as an example for the site-specific characteristics of sedimentary units at Ban Bang Sak.*

Appendix 3

Supplementary material for Chapter 10: Assessing sediment transport and hydrodynamic parameters in tsunami waves using onshore deposits from Thailand [6]
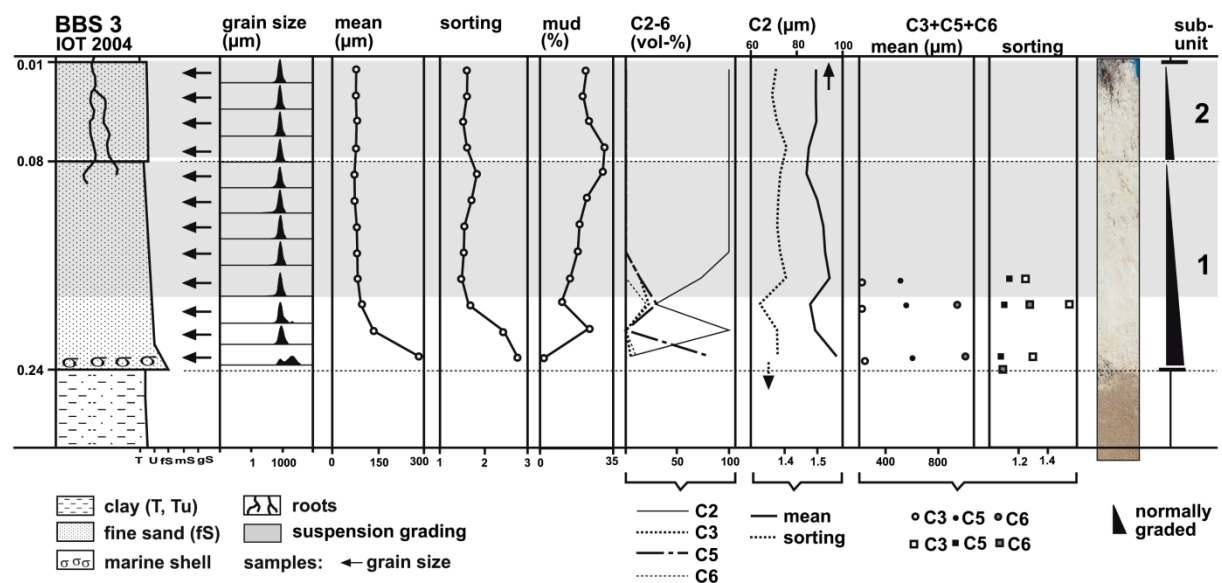
Figure S17: *Sedimentary structure of the IOT 2004 deposit in core BBS 3.*
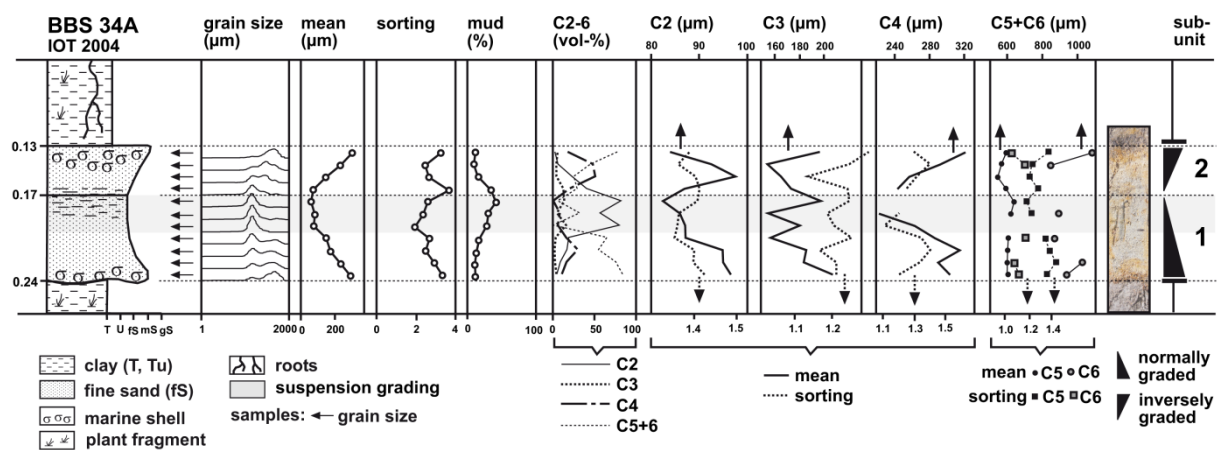
Figure S18: *Sedimentary structure of the IOT 2004 deposit in core BBS 34.*

---

[6] Supplement material for Chapter 10.
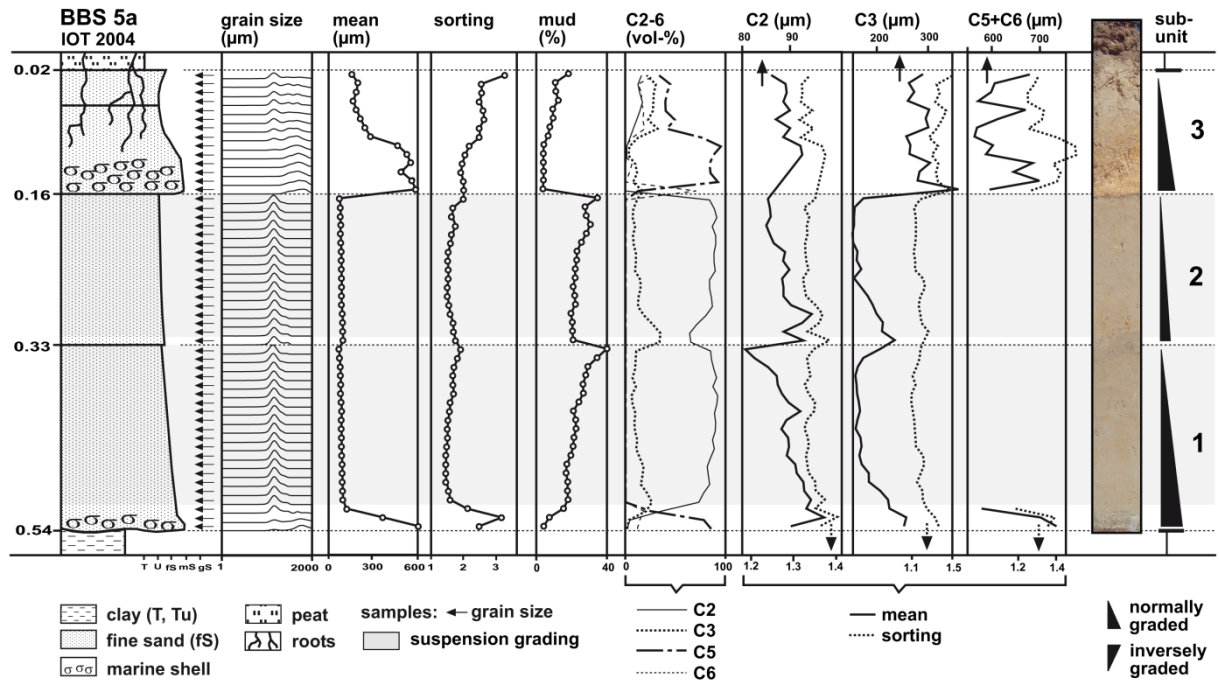
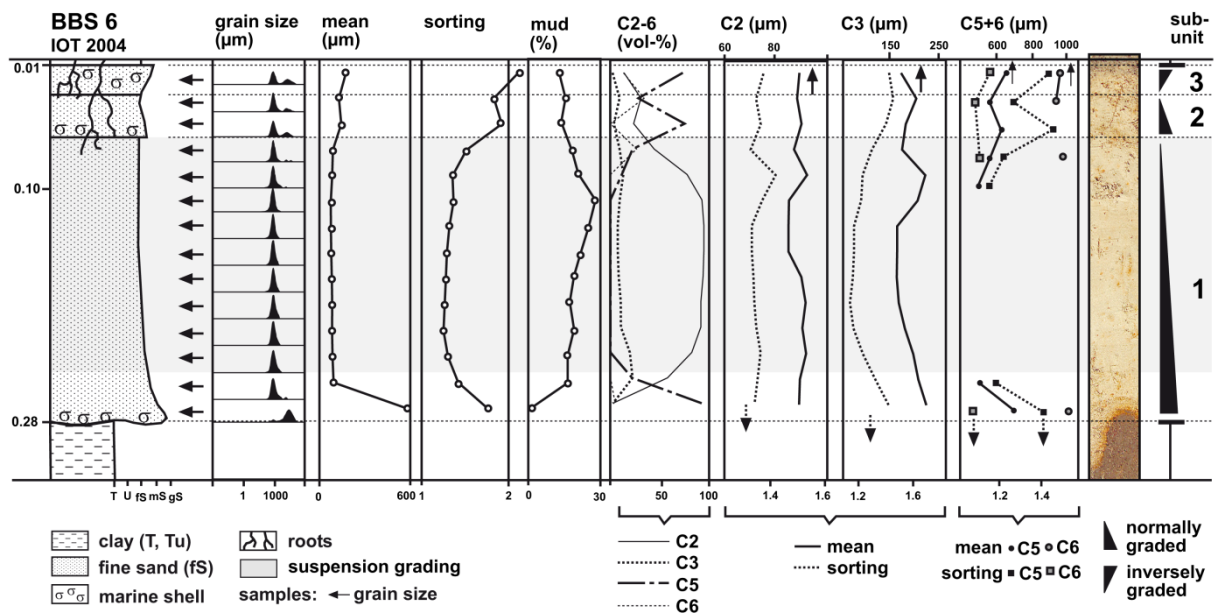*Figure S19: Sedimentary structure of the IOT 2004 deposit in core BBS 5a.*

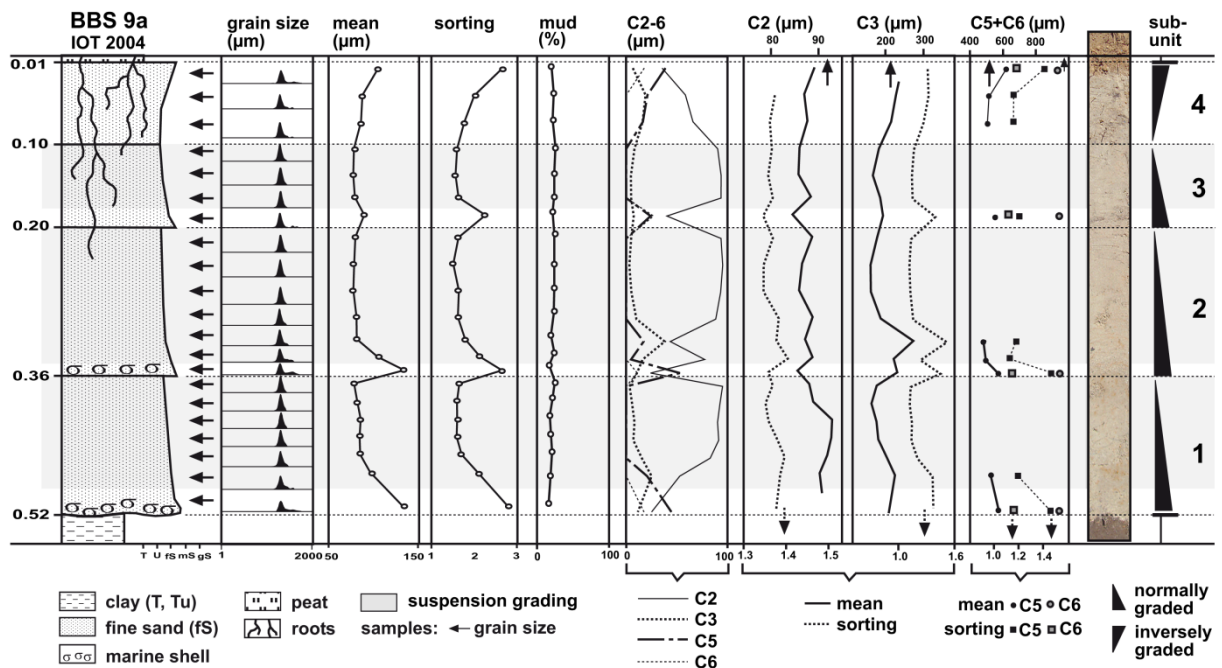*Figure S20: Sedimentary structure of the IOT 2004 deposit in core BBS 6.*

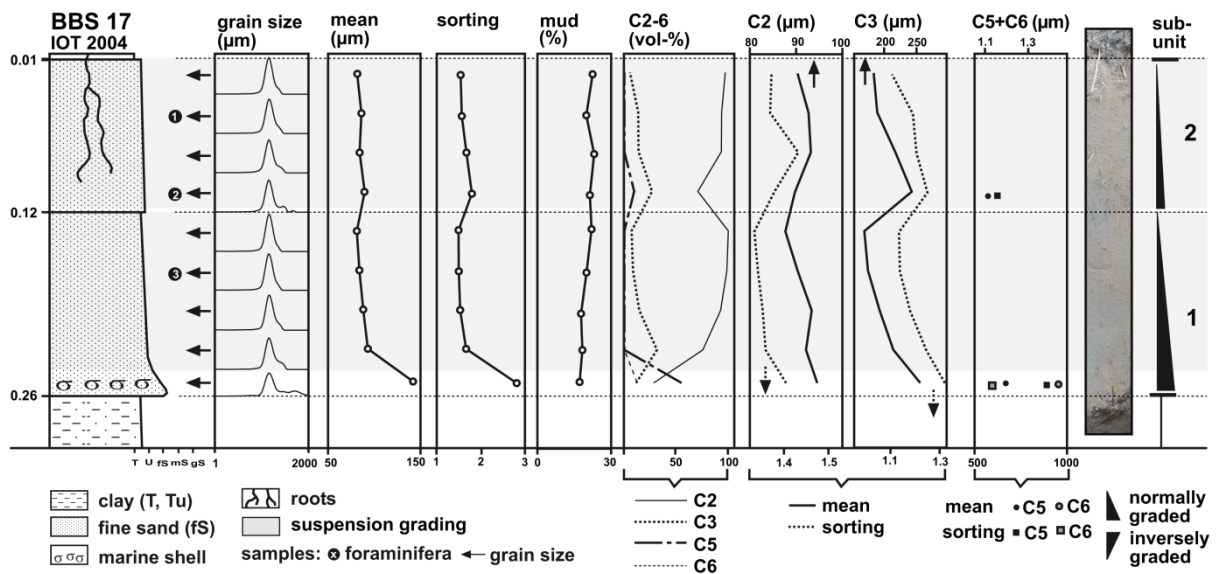*Figure S21: Sedimentary structure of the IOT 2004 deposit in core BBS 9a.*

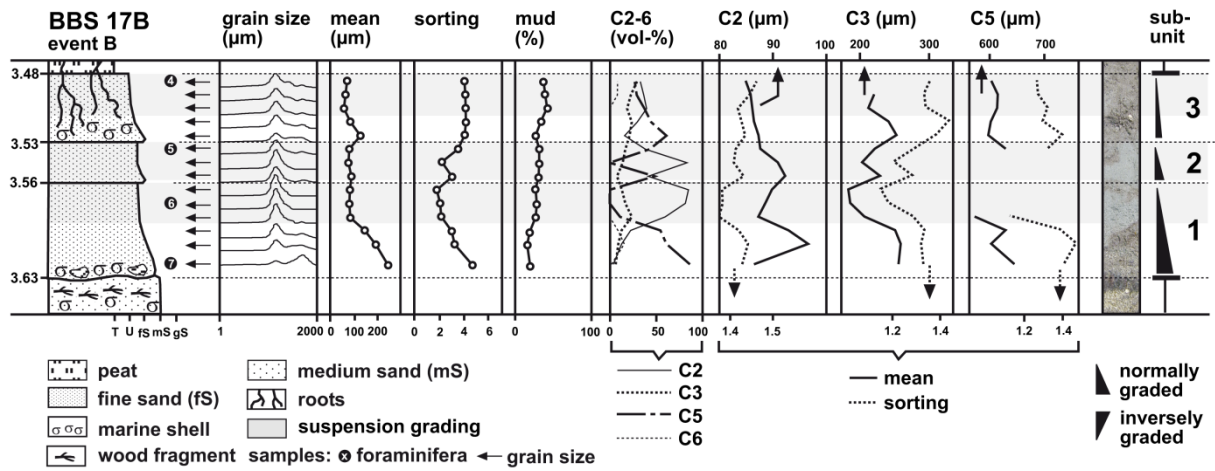*Figure S22: Sedimentary structure of the IOT 2004 deposit in core BBS 17.*

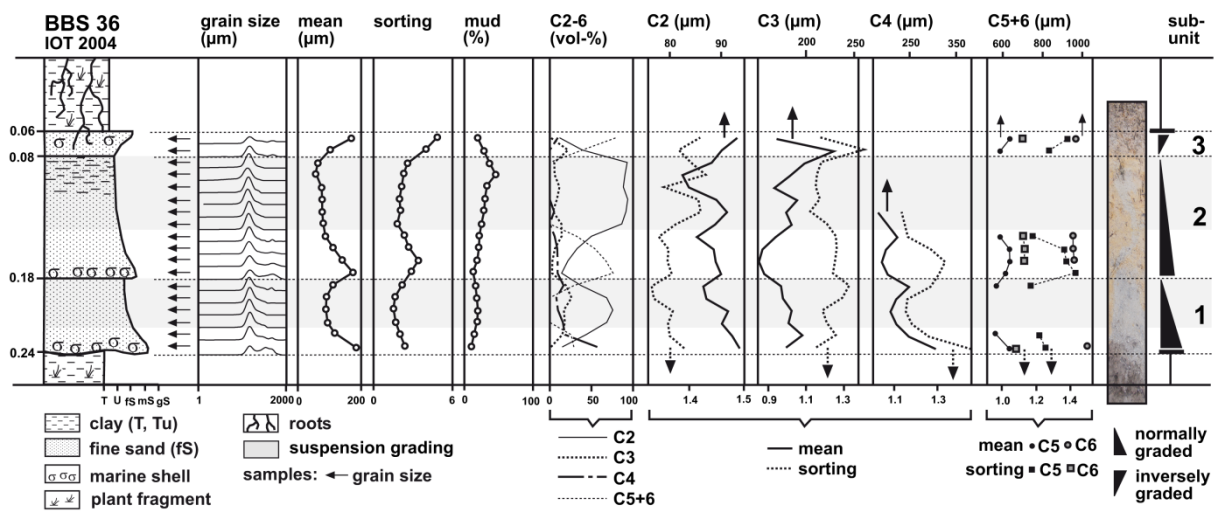*Figure S23*: *Sedimentary structure of event layer B in core BBS 17.*

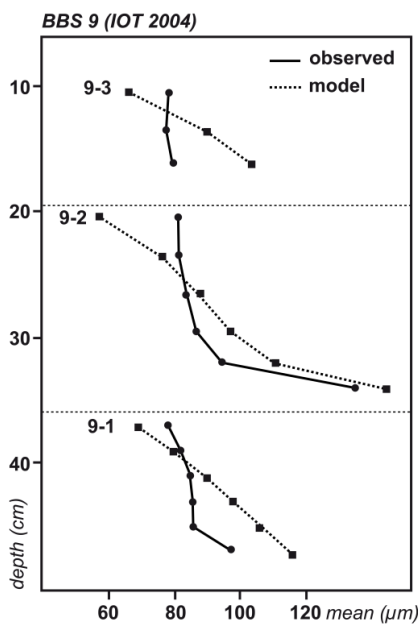*Figure S24*: *Sedimentary structure of the IOT 2004 deposit in core BBS 36.*
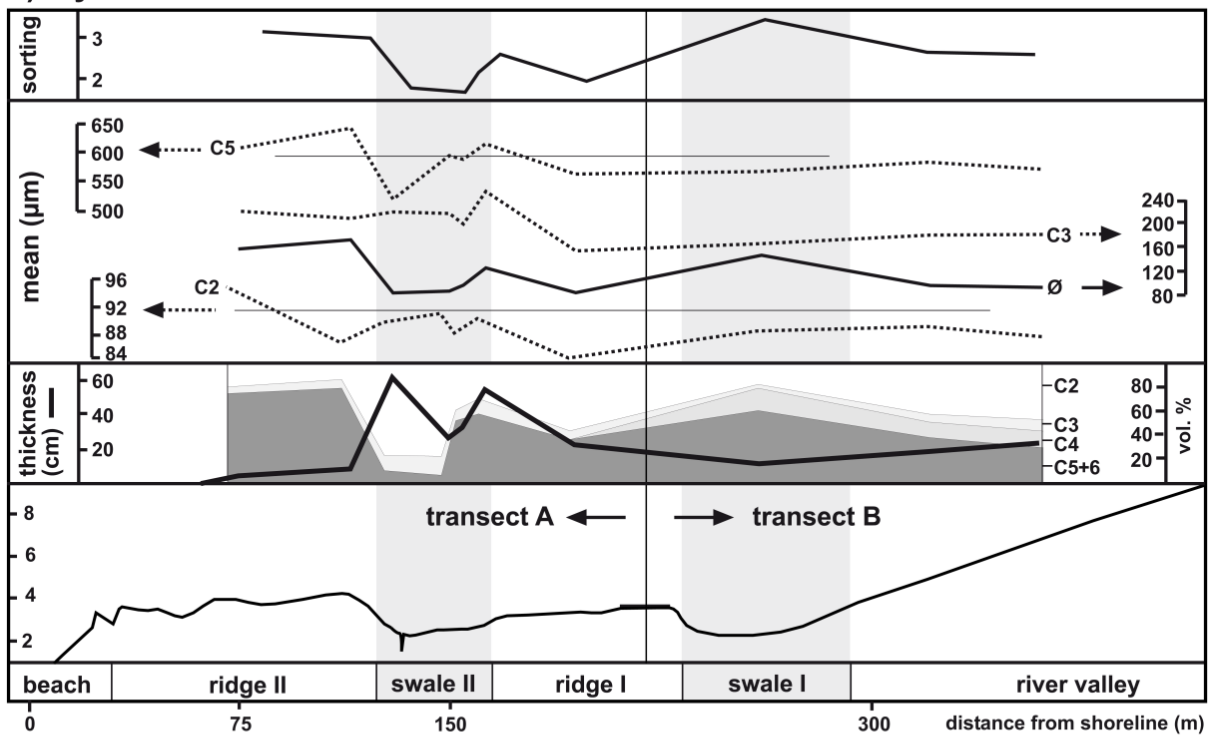

Figure S25: *Modelled versus observed grading in the IOT 2004 deposit of BBS 9.*

207

a) layer A

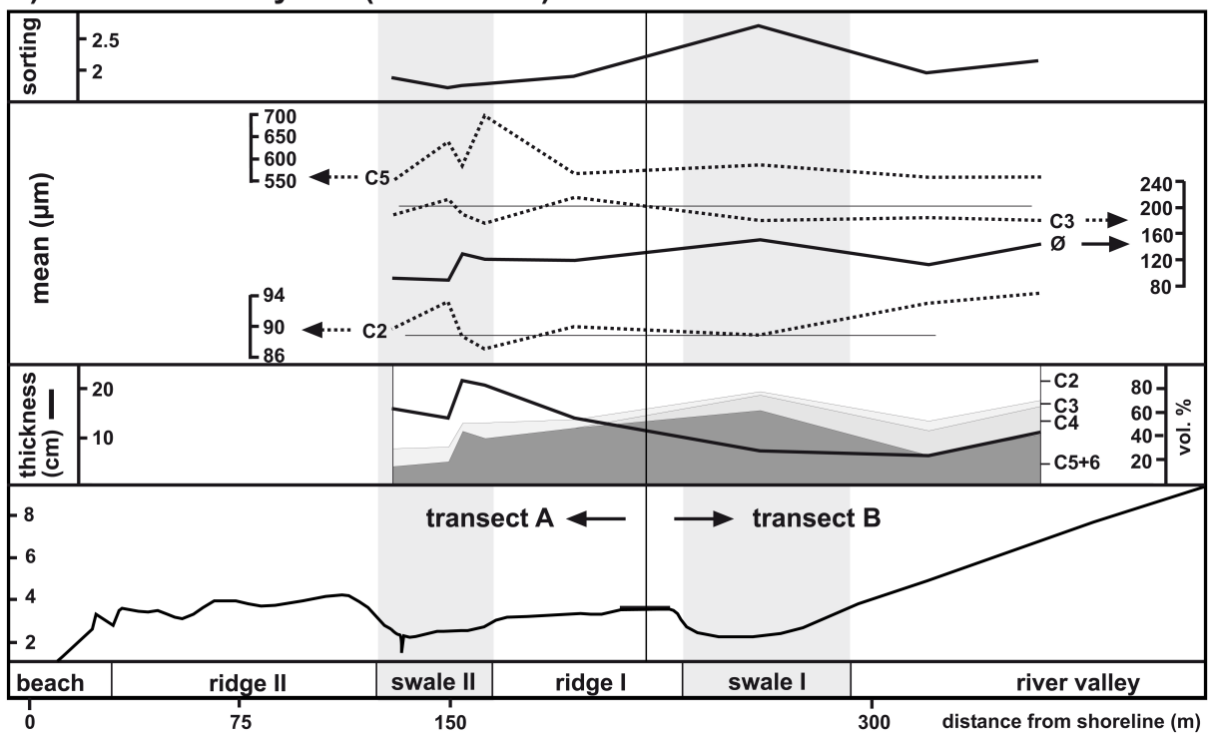## b) subunit 1 of layer A (first inflow)

Figure S26*: Lateral grain-size trends in (a) the complete layer of the IOT 2004, and (b) its first inflow unit (subunit 1).*

Table S1: *Taxonomy and ecology of all identified foraminifera.*

Agglutinella arenata (Said, 1949)	*Globigerinella* sp.
Alveolinella quoii (Orbigny, 1826)	*Globigerinoides trilobus* (Reuss, 1850)
Ammonia convexa Collins, 1958	*Globigerinoides* sp.
Ammonia parkinsoniana (Orbigny, 1839)	*Guttulina yamazaki* Cushman & Ozawa, 1930
Ammonia tepida (Cushman, 1926)	*Hanzawaia grossepunctata* (Earland, 1934)
Ammonia sp.	*Haplophragmoides* sp.
Amphicoryna hirsuta f. *sublineata* (Brady, 1884)	*Haynesina depressula simplex* (Cushman, 1933)
Amphistegina lessonii Orbigny, 1843	*Haynesina* sp.
Amphistegina papillosa Said, 1949	*Homotrema rubra* (Lamarck, 1816)
Amphistegina radiata (Fichtel & Moll, 1798)	*Lachlanella* sp.
Amphistegina lobifera Larsen, 1976	*Lagena* sp.
Amphistegina sp.	*Lenticulina* sp.
Anomalinulla glabrata (Cushman, 1924)	*Lobatula lobatula* (Walker & Jakob, 1798)
Assilina ammonoides (Gronovius, 1781)	*Loxostomina* sp.
Asterorotalia gaimardi (Orbigny, 1826)	*Millettiana millettii* (Heron-Allen & Earland, 1915)
Asterorotalia sp.	*Neoconorbina terquemi* (Rzehak, 1888)
Aubignyna sp.	*Neoconorbina* sp.
Baggina sp.	*Nonion subturgidum* (Cushman, 1924)
Bolivina persiensis Lutze, 1974	*Nonionella* sp.
Bolivina robusta Brady, 1881	*Neorotalia calcar* (d`Orbigny, 1839)
Borelis sp.	*Ophthalmidium circularis* (Chapman, 1915)
Bulimina sp.	*Orbulina universa* Orbigny, 1839
Cancris auriculus (Fichtel & Moll, 1798)	*Pararotalia domontayi* McCulloch, 1977
Cancris carinatus (Millett, 1904)	*Pararotalia nipponica* Asano, 1936
Caribeanella ogiensis (Matsunaga, 1954)	*Pararotalia venusta* (Brady, 1884)
Cassidelina sp.	*Pararotalia* sp.
Cellanthus craticulatum (Fichtel and Moll)	*Peneroplis pertusus* (Forskal, 1775)
Challengerella persica Billman, Hottinger & Oesterle, 1980	*Peneroplis planatus* (Fichtel & Moll, 1798)
Cibicides praecinctus (Karrer, 1868)	*Planogypsina acervalis* (Brady, 1884)
Cibicides pseudolobatulus Perelis & Reiss, 1975	*Planulina floridana* (Cushman, 1919)
Cibicides refulgens Montfort, 1808	*Poroeponides lateralis* (Terquem, 1878)
Cibicides sp.	*Pseudomassilina australis* (Cushman, 1932)
	Pseudotriloculina granulocostata (Germeraad, 1946)
Cibicidoides subhaidingerii (Parr, 1950)	
Clavulina sp.	*Pygmaeoseistron islandicum* (R.W. Jones, 1984)
Conorbina sp.	*Pyramidula* sp.
Cornuloculina inconstans (Brady, 1879)	*Pyramidulina pauciloculata* (Cushman, 1917)
Cribroelphidium gerthi (Voorthuysen, 1957)	*Quinqueloculina cuvieriana* d`Orbigny, 1839
Cribroelphidium incertum (Williamson, 1858)	*Quinqueloculina philippinensis* Cushman, 1921
Cribroelphidium williamsoni (Haynes, 1976)	*Quinqueloculina seminula* (Linnaeus, 1758)
Cylindroclavulina sp.	*Quinqueloculina tubilocula* Zheng, 1979
Cymbaloporetta bradyi (Cushman, 1924)	*Quinqueloculina* spp.
Discogypsina vesicularis (Parker & Jones, 1860)	*Reussella* sp.
Discorbinella sp.	*Rosalina* spp.
Discorbinoides minogasiformis (Ujiie, 1992)	*Rupertianella rupertiana* (Brady, 1881)
Elphidium advenum (Cushman, 1922)	*Sagrinella convallaria* (Millett, 1900)
Elphidium advenum limbatum (Chapman, 1907)	*Spirrilina* sp.
Elphidium crispum (Linnaeus, 1758)	*Spiroloculina* sp.
Elphidium fichtellianum (Orbigny, 1846)	*Spiroplectammina* sp.
Elphidium hispidulum Cushman, 1936	*Sorites variabilis* Lacroix, 1941
Elphidium neosimplex McCulloch, 1977	*Textularia* sp.
Elphidium striatopunctatum (Fichtel & Moll, 1798)	*Triloculina tricarinata* Orbigny, 1826
Elphidium spp.	*Triloculina* spp.
Eponides sp.	*Trochammina inflata* (Montagu, 1808)
Fissurina sp.	*Uvigerina* sp.
Flintinoides labiosa (Orbigny, 1839)	*Vertebralina striata* Orbigny, 1826
Globigerina sp.	

Appendix 4

Summaries of articles published in German

Brückner, H., <u>Brill, D.</u>, 2009. Der Tsunami von 2004 – fünf Jahre danach. Geographische Rundschau 61(12), 4-10.

On December 26, 2004 a disastrous tsunami caused great damage and loss of life in coastal areas around the Indian Ocean. The catastrophe aroused readiness for immediate aid and assistance from all over the world, leading to a rehabilitation of many of the stricken coastal zones. However, the speed and extent of the measures during the five years after the event differed a lot in the affected countries. Besides reconstructing the destroyed areas, measures for improved protection from future extreme events were taken. All of these efforts will be successful only if the local coastal population continues to be aware of future tsunami risk.

Neubauer, N.-P., <u>Brill, D.</u>, Brückner, H., Kelletat, D., Scheffers, S., Vött, A., 2011. 5000 Jahre Tsunami-Geschichte am Kap Pakarang (Thailand). Coastline Reports 17, 81-89.

The 2004 Indian Ocean Tsunami (IOT), generated by an exceptionally strong rupture of the Sunda Arc, devastated vast coastal areas all around the Indian Ocean. Besides killing > 230,000 people and massively destroying human infrastructure its impact became particularly noticeable by erosion and deposition of coastal sediments. Since historical tsunami records are rare in the countries around the Indian Ocean, this geological evidence is of great importance to identify similar events which may have occurred in the past. We studied depositional features of the IOT at Cape Pakarang (SW Thailand) and used them as a reference for potential palaeoevents in the sedimentary record. Amongst others the 2004 tsunami left a sheet of sand commonly several centimetres thick in the coastal plain and dislocated boulders of up to 20 t. For the impact of potential palaeotsunamis we found two indicators: (1) the sediments of the coastal plain were sampled by means of vibra coring. We identified two allochthonous event layers, a homogeneous sand cap embedded in the deposits of a lagoon and a sheet of coral fragments, surrounded by shallow marine sand. For both, radiocarbon dating suggests an age of ca. 1100 cal BP. Due to correlation with contemporaneous palaeotsunami evidence from Northern Sumatra, India and Sri Lanka, the two event layers are interpreted as deposits of an 1100 year old palaeotsunami. (2) Dating 10 coral boulders on the reef platform produced ^{14}C-age estimates between 4500 and 5300 cal BP, with two clusters at 5200 and 4700 cal BP. Additionally, all coral fragments from sediment cores revealed similar ages. Thus, the contempo-

raneous death of the dated corals point to the impact of two palaeoevents at 5200 and 4700 cal BP, which destroyed large parts of the former reef.

Erklärung

Ich versichere, dass ich die von mir vorgelegte Dissertation selbständig angefertigt, die benutzten Quellen und Hilfsmittel vollständig angegeben und die Stellen der Arbeit – einschließlich Tabellen, Karten und Abbildungen –, die anderen Werken im Wortlaut oder dem Sinn nach entnommen sind, in jedem Einzelfall als Entlehnung kenntlich gemacht habe; dass diese Dissertation noch keiner anderen Fakultät oder Universität zur Prüfung vorgelegen hat; dass sie – abgesehen von unten angegebenen Teilpublikationen – noch nicht veröffentlicht worden ist sowie, dass ich eine solche Veröffentlichung vor Abschluss des Promotionsverfahrens nicht vornehmen werde. Die Bestimmungen dieser Promotionsordnung sind mir bekannt. Die von mir vorgelegte Dissertation ist von Univ. Prof. Dr. Helmut Brückner betreut worden.

Nachfolgend genannte Teilpublikationen liegen vor:

- Brückner, H., Brill, D., 2009. Der Tsunami von 2004 – fünf Jahre danach. Geographische Rundschau 61(12), 4-10.

- Neubauer, N.-P., Brill, D., Brückner, H., Kelletat, D., Scheffers, S., Vött, A., 2011. 5000 Jahre Tsunami-Geschichte am Kap Pakarang (Thailand). Coastline Reports 17, 81-89.

- Brill, D., Brückner, H., Jankaew, K., Kelletat, D., Scheffers, A. and Scheffers, S., 2011: Potential predecessors of the 2004 Indian Ocean Tsunami – sedimentary evidence of extreme wave events at Ban Bang Sak, SW Thailand. Sedimentary Geology 239, 146-161.

- Jankaew, K., Brill, D., Martin, M.E., Sawai, Y., 2011. Distribution and sedimentary characteristics of tsunami deposits on Phra Thong Island, Thailand. 2nd INQUA-IGCP-567 International Workshop on Active Tectonics, Earthquake Geology, Archaeology and Engineering, Corinth, Greece (2011), 99-101.

- Brill, D., Klasen, N., Brückner, H., Jankaew, K., Scheffers, A., Kelletat, D., Scheffers, S., 2012. OSL dating of tsunami deposits from Phra Thong Island, Thailand. Quaternary Geochronology 10, 224-229.

- Brill, D., Klasen, N., Brückner, H., Jankaew, K., Kelletat, D., Scheffers, A., Scheffers, S., 2012. Local inundation distances and regional tsunami recurrence in the Indian Ocean inferred from luminescence dating of sandy deposits in Thailand. Natural Hazards and Earth System Sciences 12, 2177-2192.

- Scheffers, A., Brill, D., Kelletat, D., Brückner, H., Scheffers, S., Fox, K., 2012. Holocene sea levels along the Andaman Sea Coast of Thailand. The Holocene 22, 1162-1173.

Köln, den 14.09.2012   _____
                                    (Dominik Brill)

Curriculum vitae

Name:	**Dominik Brill**
Geburtsdatum:	**7. Juni 1983**
Geburtsort:	**Fulda**
Nationalität:	**deutsch**
Anschrift:	**Krieler Str. 83, 50935 Köln**

Ausbildung

Universität zu Köln: 2011-2012

- Seit Mai 2011: Promotionsstudiengang Geographie

Philipps-Universität Marburg: 2004-2011

- 2009-2011: Promotionsstudiengang Geographie
  (Januar 2010 bis April 2011: Promotionsstipendium der Philipps-Universität Marburg)
- Dezember 2008: Diplom in Geographie („mit Auszeichnung")
- April 2006: Vordiplom in Geographie
- Studium der Geographie mit den Nebenfächern Geologie und Botanik

Schulbildung: 1990-2003

- 1994-2003: Gymnasium Winfriedschule Fulda, Abitur
- 1990-1994: Grundschule Bad Salzschlirf

Berufliche Erfahrung

Universität zu Köln: 2011-2012

- wissenschaftlicher Mitarbeiter und Doktorand
- Forschungsschwerpunkt: Paläotsunamis in Thailand

Philipps-Universität Marburg: 2009-2011

- wissenschaftlicher Mitarbeiter und Doktorand
- Forschungsschwerpunkt: Paläotsunamis in Thailand
- Lehre: Unterseminar „Geomorphologie und Bodengeographie"

Philipps-Universität Marburg: 2006-2008

- Studentische Hilfskraft
- Praktika: Regierungspräsidium Gießen (Regionalplanung, Naturschutz), RegioConsult

Ersatzdienst (Tomesa Klinik): 2003-2004